Publ. Astron. Obs. Belgrade No. 76 (2003), 11 - 17 *Invited lecture*

LINE BROADENING RESEARCH IN TUNISIA : HISTORY, PRESENT STATE AND INTERNATIONAL COLLABORATION

N. BEN NESSIB

Groupe de Recherche en Physique Atomique et Astrophysique
E–mail: nebil.bennessib@planet.tn

Abstract. We present a review and analysis of the results of spectral line shapes investigation in Tunisia since 1970 up to 2003.

1. INTRODUCTION

Now, in my country there are 300 000 students and 13 000 teachers at the 7 universities of Tunisia. The number of active researchers is 10 000 and the budget of the high school ministry makes 7% of the government total budget. The older institution is the Science Faculty of Tunis, it was built in 1968. Most teachers prepared their thesis in France and returned to Tunisia. Each one has a different subject in his research study: Raman effect, electronic microscopy, molecular physics, atomic physics, nuclear physics, semiconductors, . . .

The father of atomic physics in Tunisia is Professor Taoufik BEN MENA, he worked on instrumental spectroscopy in the Aimée Cotton laboratory of the University of Orsay Paris-Sud. After him Mrs Zeineb BEN AHMED-BEN OSMAN worked on the Zeeman effect and M. Mohamed MILADI worked on the electronic structure of the molecule NO in the same laboratory. After these three works, two other works were done at the University of Jussieu-Paris VI: the work on atomic broadening by M. Mohamed SASSI and on molecular broadening by Mrs Zohra BEN LAKHDAR-AKROUT.

Since the first paper on line broadening by Tunisians (Sassi *et al.*, 1970) up to now, more than 30 publications concerning line shapes investigations have been published. In these published works, various problems from this research field have been considered.

First theoretical investigations of Tunisians have been done by Professor Mohamed SASSI from 1970 up to 1975. They concern Stark broadening of non hydrogenic emitters and particulary the study of overlapping lines done specially with M. Claude DEUTSCH at the University of Paris VI. When SASSI returned to Tunisia, he formed a research group with M. Hédi BELAKRMI in the Ecole Normale Supérieur of Bardo. They studied particulary the ion dynamic effects and microfield distributions depending on time. In 1982, M. SASSI joined the Faculté des Sciences de Tunis with his

student H. BELAKRMI. He took, a new student for the thesis, M. Nébil BEN NESSIB and proposed to him the study of strong collisions. After N. BEN NESSIB read the paper of BASSALO, CATANNI and WALDER in 1983 he tried to generalize their work on overlapping lines. So he generalized the convergent theory to overlapping lines, with application to the HeI 4471Å line. This research group dispersed 1988.

First experimental investigations of Tunisians have been done by Professor Zohra AKROUT-BEN LAKHDAR. They concern the shape of molecular spectrum : mercury 2537 Å line perturbed by noble gases. The work was done in the laboratory of LENNIER, in Paris from 1975 up to 1978. When she returned to Tunisia, she formed a research group with two students M. Abdelbari MEJRI and M. Youssef MAJDI who presented their thesis on the Faculté des Sciences de Tunis.

After his thesis in 1988, N. BEN NESSIB joined the BEN LAKHDAR research group and founded the "Laboratoire de Physique Atomique et Moléculaire" cooperating especially with the NGUYEN Hoe research group of the University of Paris VI. In four years, he worked on theoretical formalisms of Stark broadening and published 4 papers about quantum formalism of Stark broadening using the Coulomb-Born Oppenheimer approximation of calculating the scattering matrix. Miss Neila TERZI joined the "Laboratoire de Physique Atomique et Moléculaire". She worked on radial integrals and calculated Stark broadening of infrared helium lines (Terzi *et al.*, 1998).

In the same group, M. Mohamed Abdelbari MEJRI studied the hydrogenic spectral lines in hot and dense plasma, particulary the shift of hydrogenic-like ion lines due to electron collisions which are treated by including all effects due to monopole, dipole and quadripole interactions between radiator and perturbing electrons. He published with NGUYEN and BEN LAKHDAR a work in the Europeen Journal of Physics D(Eur. J. Phys. D., 1998).

The laboratory of Professor BEN LAKHDAR became "Laboratoire de Physique Atomique, Moléculaire et Applications" since 2000. The research in atomic physics is oriented toward the experimental study of a plasma induced in water by a stabilized arc at atmospheric pressure.

2. HISTORY

2. 1. SASSI'S WORK: OVERLAPPING LINES

In the work in 1970, SASSI et al. proposed, for LiI 2P-4D and 2P-4F lines, the use of the intensity ratio of the forbidden and permitted components or from the wavelength separation of their intensity maxima. They showed that the 2P-4D permitted line is shifted towards the red while the 2P-4F forbidden line is shifted towards the violet. Thus, the line separation becomes very sensitive to the electron concentration variation. This is also true of the relative intensity of the two lines.

In the work of SASSI and COULAUD (J. Phys. B, 1972)they study the ionic profiles in the region of the forbidden component of CsI (6G-5D). It is shown that limiting the number of perturbing levels to those with the same principal quantum number introduces negligible errors in the peak separation between the allowed and forbidden lines but may affect the profile in the region of the forbidden component. In the case of CsI 6G-5D, this limitation contributes to overestimate the maximum intensity of the forbidden component and reduces the intensity between the allowed and the forbidden lines.

He contributed in the expressions of the generalized width and shift functions $A(z)$ and $B(z)$ defined with the second-order time integral of the electron-collision operator of partially degenerate lines (Phys. Rev., 1972).

The generalized impact theory of Stark broadening of overlapping lines in plasma, with the nonmarkovian and ion dynamic effects is treated in Annals of Physics 1994 and 1975.

He studies particulary the evolution of the ratio of the forbidden and allowed line maximum and the wavelength distance between the two components with the temperature and the electron density.

2. 2. BEN LAKHDAR'S WORK: MOLECULAR BROADENING

Mrs Zohra BEN LAKHDAR-AKROUT performed her research in the laboratory of Professor LENNUIER in the University of Pierre and Marie Curie Paris VI. She studied the absorption spectral profile of the line 2537 Å for the mercury perturbed by noble gases.

In her first work (J. Physique, 1976), she measured the absorption coefficient of mixtures of mercury-krypton and mercury-xenon vapors in the range 120-7500Ghz about the line center. At low frequency, she shows the existence of an anisotropy in the interaction potential between the $\mathrm{Hg}(3_1^P)$ and the perturber. This anisotropy has been observed both for the attractive side (Van der Waals terms) and the repulsive one. For high frequencies, the absorption profile shows successive peaks (blue satellites) which can be attributed to bound pairs. The near wing, although far from the impact approximation domain cannot be interpreted by pure quasistatic theory. Taking into account the significant movement of the perturber with respect to the active atom during the interaction period she suggests that wing can be attributed to the attractive potential branches.

In her second work (J. Physique, 1978) about the same line profile of Hg (2537 Å), she gives the same interpretation of experimental data when the perturber is argon and not krypton and xenon as in the first work. Comparison with the results obtained by other authors shows the need to question the meaning of the empirical expression proposed for the representation of interaction-potentials. In the second part of this second work, she studies the theoretical expressions which describe these potentials and in particular she consider the computation of the dipole-induced dipole coefficient of $\mathrm{Hg}(6^1S_0)$ and $\mathrm{Hg}(6^3P_1)$ interacting with rare gases. In the third part, she treats the case of heavy gases. It is shown that it is possible, in some cases, to interpret the coefficients deduced from experimental data as differences between dipole-induced dipole interaction coefficients.

In 1996, N. BEN NESSIB et al. present a work about theoretical calculation of Stark broadening of neutral oxygen lines (Physica Scripta, 1996). Concerning collisions of neutral atoms with electrons, the impact approximation is always valid in the physical conditions of stellar atmospheres and of laboratory experiments. Concerning collisions of neutral atoms with ions, the impact approximation is most often valid in the physical conditions of hot stellar atmospheres where the density is weak (10^{10} to 10^{14} cm^{-3}) and where the ion perturbers are light protons and He^+ ions. In laboratory experiments, the density is higher (10^{16} -10^{17} cm^{-3}) and the perturbers are heavier (Ar^+ for instance). Thus the validity condition of the impact approximation has to be checked for each line and conditions (Temperature and density). If the

impact approximation is valid, then we have input the TOPbase (Opacity Project) sophisticated atomic structure data into the Sahal-Bréchot's computer code to calculate widths and shifts of spectral lines. But when the impact approximation breaks down, the quasistatic approximation has to be used. The quasistatic profiles for isolated lines provided by Griem are computed with quadratic interactions only. However, the quadrupolar interactions may be unnegligible. The quasistatic profile for quadrupolar interactions has been obtained by Sahal-Bréchot in 1991 and exist in her computer code. Still the quasistatic quadratic ion broadening parameter A, which is a measure of the relative importance of ion broadening has been calculated by Griem using a simplified Coulomb approximation for the atomic structure. So we have also computed the quasistatic ion parameter broadening A with the TOPbase atomic structure and compared to the A-value of Griem. The difference with Griem's values is about 20 per cent, except for the 5330 Å line, where the difference exceeds 50 per cent. On the whole, our results are in better agreement with experiments than the calculations by Griem, especially for the widths where the agreement can attain a few percent. We show that our results are improved with the use of TOPbase, and the calculation of the quasistatic ion parameter broadening , especially for the widths. These calculations are extended to infrared helium lines by TERZI (A& A suppl., 1998) and we are doing the same kind of calculations for ionic emitters (MAHMOUDI, 2003).

In the work of TERZI *et al.* (1998), they have calculated Stark widths and shifts for six infrared lines of helium arising from highly excited levels. In this work, they have checked several criteria as the validity condition of the perturbation theory, impact or quasistatic approximation, isolated or overlapping line, . . .

Dr. N. BEN NESSIB studied the semiclassical collisional functions in a non ideal plasma (A& A, 1997). He obtained new analytic expressions of the non adiabatic semiclassical collisional functions which generalize the $A(z)$ and $a(z)$ standard ones to a strongly non ideal plasma by using the Coulomb cutoff potential. He present the correlated collision functions for transition probability A_0^c, $A_\pm^c$ and A_2^c and for total cross-sections a_0^c, $a_\pm^c$ and a_2^c.

Dr. M.A. MEJRI studied broadening of hydrogenic-like ion lines due to electron collision in dense and hot plasmas (Eur. Phys. J. D., 1998). These collisions are treated by including all effects due to monopole, dipole and quadrupole interactions between radiator and electron perturbers. The latter follows exact hyperbolic trajectories with a possible penetrating part inside atomic orbits. Applications are to the Paschen lines alpha and beta.

3. PRESENT STATE

Line broadening research is developed now, particulary in two research groups:

3. 1. TUNIS GROUP

In the new laboratory "Laboratoire de Physique Atomique, Moléculaire et Applications", there is a division of plasma physics where the aim of the work is the study of water plasma and pollution in water by spectroscopic investigations (the work is particulary done by Mrs N. TERZI and some new students in the laboratory). A cooperation is particulary established, in this field with Professor Guy TAIEB from Orsay University. The alkaline dusts in water are the major elements studied. The study of the arc plasma is another interesting work of Y. MAJDI and N. TERZI.

3. 2. BIZERTE GROUP

In the frame of the semiclassical approach, investigations of the applicability of different theories have been carried out.

The theory for multiply charged ions has been improved.

The work on a new quantum mechanical approach to the Stark broadening has been carried out with a thesis of M. Haykel ELABIDI. Research on Stark broadening of multiply charged ions was developed and new quantum calculations for the electron-impact broadening in intermediate coupling is in progress.

With another student, Miss Hédia BEN CHAOUACHA, the development of semiclassical collisional functions in a strongly correlated plasma is going on. We generalize the functions $A(z)$ and $a(z)$ to the case of non Coulomb potential as the cut-off potential, with one correction term and the ion sphere potential, with two correction terms.

We study also the singly ionized emitters as CII, NII and OII with the semiclassical formalism. This is the subject of the thesis of M. Walid MAHMOUDI. In this research field, we calculate widths and shifts of ionized atoms with the impact and quasistatic approximation as done for neutral emitter by BEN NESSIB et al. (Physica Scripta, 1996).

New approaches, especially convenient for quick calculations of a large number of lines have been developed, a new formalism where we show the temperature dependence is developed and application to neutral helium and magnesium spectral lines is in progress. This is the subject of the thesis of Miss Besma ZMERLI.

Working on microfield distributions, is one of the axes of the research group. This is at the limit of the line broadening but it just gives a complementary information on the interactions in a plasma. A new thesis on microfield distributions in low, medium and high correlated plasma is the subject of M. Belhassen TRABELSI. The work is at the beginning but we found new expressions especially for low and medium correlated plasma.

4. INTERNATIONAL COLLABORATION

4. 1. FRENCH COLLABORATION

The principal cooperation is with Dr. Sylvie SAHAL-BRECHOT from the LERMA (Laboratoire d'Etude du Rayonnement et de la Matière en Astrophysique), Paris-Meudon Observatory. This cooperation started with the works of Ben Nessib and after that with Terzi. Mrs SAHAL-BRECHOT is considered in Tunisia as a very important personality with her scientific and human qualities.

The Tunis research group collaborates also with Toulouse research group the " Centre de physique des plasmas et de leurs applications de Toulouse" and with the "Laboratoire de Photophysique moléculaire", Université Paris-Sud, Orsay.

The Bizerte research group collaborates also with the LUTH (Laboratoire de l'Univers et de ses théories) of the Paris-Meudon Observatory. This cooperation is particulary maintained with Mrs Marguerite CORNILLE and M. Jacques DUBAU. The cooperation consist in the study of atomic and collisional data of multicharged ions. This new research axis permits us to elaborate new quantum formalism for Stark broadening in intermediate coupling and ab initio semiclassical spectral line broadening.

The Tunis research group collaborates with Professor Nikola KONJEVIĆ from the Institute of Physics in Belgrade. He visited Tunisia several times, gave lectures there and offered ideas for equipments and new experimental setup.

The Bizerte research group collaborates with Dr. Milan DIMITRIJEVIĆ from the Belgrade Observatory. The work on the four time ionized silicon opens a new method for calculating. This new method of calculating can be used for elements whose spectrum is poorly known and it is not possible to obtain a sufficiently complete set of experimental atomic energy levels needed for adequate semiclassical perturbation calculations. The energy levels are then calculated using the general purpose atomic structure code SUPERSTRUCTURE developed at the University College in London.

Cooperation of the Bizerte group is also maintained with KONJEVIĆ for the study, experimentally and theoretically of isoelectronic sequences. We started with the carbon isoelectronic sequence and found some discrepancy between semiclassical prediction and experimental results for some transitions.

A new cooperation will start with Professor Stevan DJENIŽE and Dr Vladimir MILOSAVLJEVIĆ from the Faculty of Physics, University of Belgrade. This research concerns transition probabilities in multicharged ions as N IV, N V, Ar IV and Ar V and other ions. We have powerful theoretical methods for calculating this parameters and in Belgrade they can obtain this parameter by using the relative line intensity ratio. The collaboration is then immediate.

5. CONCLUSIONS

More than 30 years of line broadening studies by Tunisian researchers, four generations have passed, more than 30 works on this field have been executed. This is not too much, but just enough to say that line broadening in Tunisia has a favorable terrain to be developed.

The scientific research does not distinguish between races, religions and nationalities, it stands above all. We try to do the best and we are open to any cooperation.

References

Bel Akremi, H.: 1987, Effet Stark dépendant du temps et raies partiellement dégénérées, thèse de spécialité, Université de Tunis, April 1987.

Ben Lakhdar, Z., Perrin, D., Lennuier, R.: 1976, Etude expérimentale des railes de la raie 2537 Å du mercure perturbée par le krypton et le xénon, *J. Physique* **37**, 831.

Ben Lakhdar, Z., Perrin, D., Lennuier, R.: 1978, Sur les potentiels d'interaction Hg(6^1S_0) ou Hg(6^3P_1)-gaz rares, *J. Physique* **39**, 137.

Ben Lakhdar, Z.: 1978, Etude du profil spectral d'absorption de la raie 2537 Å du mercure perturbé par les gaz rares, Université Pierre et Marie Curie Parie VI, September 1978.

Ben Lakhdar, Z., Ben Nessib, N.: 1991, Collision width function in a correlated plasma, *Spectral Line Shapes* **5**, 88.

Ben Nessib, N.: 1988, " Elargissement des raies partiellement dégénérées. Application à l'hélium neutre ", thèse de spécialité, Université de Tunis, January 1988.

Ben Nessib, N., Ben Lakhdar, Z., Nguyen H., Arranz, J.P.: 1994, Modélisation de l'élargissement Stark dans les lasers X, *Ann. Phys.* **C1**, 45.

Ben Nessib, N., Sahal-Bréchot, S., Ben Lakhdar, Z.: 1996, Stark Broadening of Neutral Oxygen Neutral Lines in the Impact and Quasistatic Approximation, *Physica Scripta* **54**, 608.

Ben Nessib, N., Sahal-Bréchot, S., Ben Lakhdar, Z.: 1997, Semiclassical Stark Broadening Calculations of Neutral Oxygen Lines, *Spectral Line Shapes* **9**, 117.
Ben Nessib, N., Ben Lakhdar, Z., Sahal-Bréchot, S.: 1997, Semiclassical collisional functions in a non ideal plasma, *Astronnomy and Astrophysics* **324**, 799.
Ben Nessib, N.: 1997, Contributions à l'élargissement spectral dans un plasma d'atomes complexes ", thèse d'Etat, Université de Tunis II, May 1997.
Chapelle, J., Coulaud, G., Deutsch, C., Diatta, C., Sassi, M.: 1971,*J. Phys. Fr. Supp.* **C5b**, 151.
Coulaud, G., Deutsch, C., Sassi, M.: 1971, Contributed papers to the Tenth Conference on Phenomena in Ionized Gases, Oxford, 378.
Deutsch, C., Sassi, M., Coulaud, G.: 1972, Off-Diagonal matrix elements in the Stark-broadening theory of neutral lines in plasmas, *Phys. Rev.* **A6**, 2484.
Deutsch, C., Sassi, M., Coulaud, G.: 1974, Stark broadening of the overlapping 4471.48 Å HeI line in a plasma, *Ann. Phys.* **83**, 1.
Dimitrijević, M.S., Ben Nessib, N.: 1991, Simple convergent formula for estimating Stark widths of neutral atom lines, *Spectral Line Shapes* **5**, 605.
Dimitrijević, M.S., Ben Lakhdar, Z., Ben Nessib, N.: 1993, Simple convergent formula for estimating stark widths and shifts for neutral and ionic lines, Proceeding of the I.C.S.L.S., ed. Nova.
Mejri, M.A., Nguyen, H., Ben Lakhdar, Z.: 1998,Shifts of one-electron ion lines from interactions with electrons in hot and dense plasma, *Eur. Phys. J. D* **4**, 125
Mejri, M.A.: 1987, Etude théorique de l'élargissement des raies hydrogénoïdes émises par un plasma. Application à la raie $P_\alpha$de l'hélium II., thèse de spécialité, Université de Tunis, June 1987.
Nguyen, H., Arranz, J.P., Ben Lakhdar, Z., Ben Nessib, N.: 1993, Atomic structure of Li-like ions in hot and dense plasmas, Proceeding of the I.C.S.L.S., ed. Nova.
Nguyen, H., Arranz, J.P., Ben Lakhdar, Z., Ben Nessib, N.: 1995, Broadening of Li-like ions in hot and dense plasmas, *Spectral Line Shapes* **8**, 213.
Perrin, D.J., Benlakhdar, Z., Jeanett, J.C., Lennuier, R.: 1982, Experimental shape of the 253.7nm mercury line perturbed by the light noble gases (Fr.), *J. Phys. E* **43**, 45.
Sassi, M.: 1972, , *J. Quant. Spectrosc. Radiat. Transfer* **12**, 75.
Sassi, M., Coulaud, G.: 1972, Calculated ionic profiles in the region of the forbidden component CsI (6G-5D), *J. Phys. B.* **5**, L35.
Sassi, M., Herman, L., Coulaud, G.: 1970, Relative intensities and relative shifts of the 2P-4F and 2P-4D LiI lines as a function of electron concentration, *Phys. Lett.* **32A**, 549.
Sassi, M.: 1974, Contributions à l'étude de l'Elargissement des raies partiellement dégénérées. Application à la raie 4471 Åde l'hélium neutre ", thèse d'Etat, Université Paris VI.
Sassi, M., Deutsch, C., Coulaud, G.: 1975, Stark broadening of the overlapping 4471.48 Å HeI line in a plasma II. Nonmarkovian and ion dynamic effects, *Ann. Phys.* **89**, 274.
Sayer, B., Wang, R., Jeannet, J.C., Sassi, M.: 1971, Absorption measurements of quadrupole transition probabilities 6S-nD in caesium vapour, *J. Phys. B* **4**, L20.
Terzi, N., Sahal-Bréchot, S, Ben Lakhdar, Z.: 1998, Stark profiles of infrared helium lines, *Astronomy and Astrophysics Supplement* **133**, 229.
Terzi, N.: 1999, Etude théorique et expérimentale de l'élargissement Stark de profils de raies de l'hélium neutre. Application astrophysique, 15 June 1999.

Publ. Astron. Obs. Belgrade No. 76 (2003), 19-23 *Invited lecture*

AN ALTERNATIVE APPROACH TO DATA PROCESSING

SRĐAN BUKVIĆ

Faculty of Physics, University of Belgrade, Studentski Trg 12-16, Belgrade, Serbia
E-mail: ebukvic@ff.bg.ac.yu

Abstract. We present a new form of merit function which measures an agreement between large number of data and a model function with the particular choice of parameters. We demonstrate the efficiency of introduced merit function on the common problem of finding base line of the spectrum. Also, we discuss efficiency of existing minimization algorithms in discrete topography which is concomitant to proposed merit function in general case.

1. INTRODUCTION

In the past two decades experimental technique was moved from analog to digital domain. Consequently, the amount of data acquired in experiments has increased significantly requiring reliable automated algorithms for data processing. A frequent task in data processing is to find best parameters of some model function, in the sense of the "best fit", related to the particular data set. It is common practice to use the least-squares as a merit function for various data fittings. Unfortunately, the measurement process is not free of errors which cause that some experimental points are occasionally just way off. Also, data of interest are frequently spoiled by small amount of points due to some undesirable process which can not be avoided. This can easily turn the least-squares into nonsense. To overcome these problems various robust techniques have been proposed.

In astrophysics and physics a prominent example which requires the rough approach is the task of spectrum baseline and continuum estimation. In Gabel *et al.* (2002) is in details described the complex procedure of continuum estimation in the presence of superimposed spectral lines. It is shown that a prior knowledge of spectral line positions is necessary for continuum estimation. Moreover, the described procedure assumes that parts of recorded signal, taken for continuum estimation, are not spoiled by unknown spectral lines of low intensity. In general case it is difficult to satisfy all requirements necessary for reliable continuum estimation. Here, spectrum lines act as an undesirable feature of the signal and the points belonging to the spectral lines can be considered as outliers.

The intention of this paper is to introduce a simple and efficient method for rough estimations, insensitive to outlying points. Proposed method is suitable for large data sets only, i.e. it can not replace least-squares for data sets containing just a few points.

2. MERIT FUNCTION

Consider a particular data set of x_i 's and y_i 's (i=1, 2, .. n) and a model function $y(x; a_1, a_2, \ldots a_m)$ depending on x and some parameters $a_1, \ldots a_m$. Let's define quantity d in the following way. At a distance $y(x_i; a_1, a_2, \ldots a_m) - y_i < d$ we will say that the point (x_i, y_i) is *close* to the model function $y(x_i; a_1, a_2, \ldots a_m)$ for given set of parameters $\{a\}$. If so put f_i =1, otherwise f_i=0. Now we will define quantity χ:

$$\chi = n - \sum_{i=1}^{n} f_i \qquad (1)$$

The purpose of χ is to be used as a merit function. Thus, we will search for a set of parameters $\{a\}$ for which the merit function χ has a minimum in respect to the chosen value d. In other words, we will search for set of parameters $\{a\}$ for which the maximal number of data points will be *close* to the model function, i.e. the model function will closely resemble the data in respect to d.

The explained approach will be termed Close Points Concept (CPC). The aim of the CPC is to quantify our ability to recognize trace-like set of points as a line and, at the same time, to ignore outlying points. The distance d defines what will be 'close' and which points will be disregarded. A straightforward way to apply CPC is to incorporate merit function (1) in some of the existing minimization algorithms.

3. ESTIMATION OF THE SPECTRUM BASE LINE

First we will consider most common and most simple case of a spectrum when the base line is supposed to be horizontal i.e. parallel to the y axis. This is justified when a narrow range of the spectrum is recorded. In such a case we can avoid the use of the merit function in general form (1) and explicit use of a minimization algorithm.

Suppose that the spectrum contains n points obtained by means of k bit linear A/D converter. It means that spectrum intensity in each point is expressed via one of q=2^k different levels of the A/D converter. In order to obtain the base line we will make an auxiliary histogram consisting of exactly 2^k bins, each bin corresponding to the one of 2^k values of the A/D converter. We will proceed as follows: starting with the point 1 we incerese the content of bin y_1 by 1, similarly for point 2 content of bin y_2 is also incresed by 1 and so on, up to the last point n. Finally, each bin will contain the number of occurrences of appropriate level of the A/D converter within chosen part of the spectrum. It will be assumed that obtained histogram has just one maximum, i.e. bin j has a maximal count, see Fig. 1. It is obvious that the line y_b =j is a base line of the spectrum in respect to the merit function (1). In this case the distance d, which is used to distinguish "close" and "far" points, was set to be one half of the A/D converter step. Also, the search for the best y was done within discrete set of values defined by the A/D converter. The proposed procedure is extremely simple and works successfully practically with any spectrum or spectrum like signals (Djeniže and Bukvić 2001, Spasojevic *et al.* 1996)

It is of interest to estimate discrimination level, parts of the signal above this level will be considered as spectral lines, everything below discrimination level will be considered as a noise. The key assumption is that the signal below the spectrum base line originates only due to noise of any kind which is present in the system, while the signal

above the base line consists of a useful signal spoiled by the noise. It is a matter of choice how to represent the noise distribution which is present in our histogram below spectrum base line, however one standard deviation (σ) appears as a most common manner. Accordingly we can take the value σ as a discrimination and $y_d=j+\sigma$ as a discrimination level, see Fig. 1.

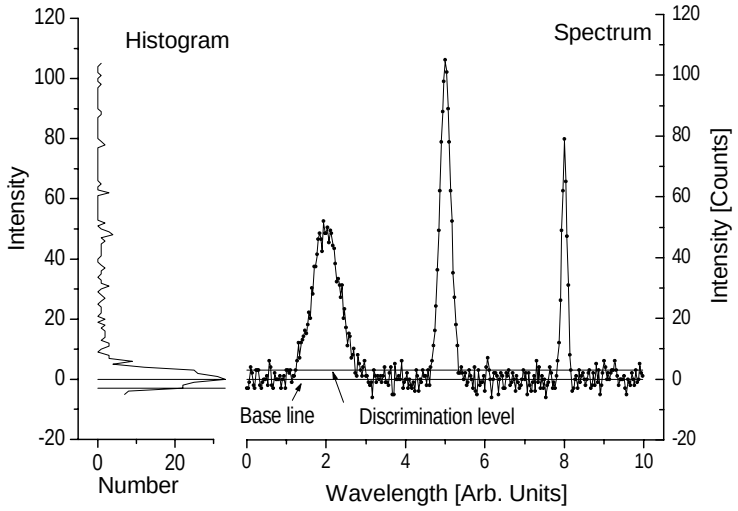

Fig. 1: Spectrum base line estimated by CPC approach. See text for details.

The purpose of our second example is to demonstrate the potentials of the CPC in numerically more complex situation with explicit use of the merit function (1) and appropriate minimization algorithm. To control the numerical process we will consider an artificial set of data generated according to the following relation:

$$y = P_1 + P_2 + P_3 + B \tag{2}$$

where peaks P_1, P_2, P_3 have the same, Gaussian, form:

$$P_i = a_i \exp\left[\frac{(x-c_i)^2}{d_i^2}\right]$$

and B is a broad line also of the Gaussian form which mimics a nonlinear base line:

$$B = a_b \exp\left[\frac{(x-c_b)^2}{d_b^2}\right] + b$$

In Fig. 2 is shown a graph generated by function (2) with the following coefficients:

a_1=5, c_1=20, d_1=10; a_2=1, c_2=30, d_2=12; a_3=1, c_3=70, d_3=10
a_b=1, c_b=50, d_b=1000, b=0

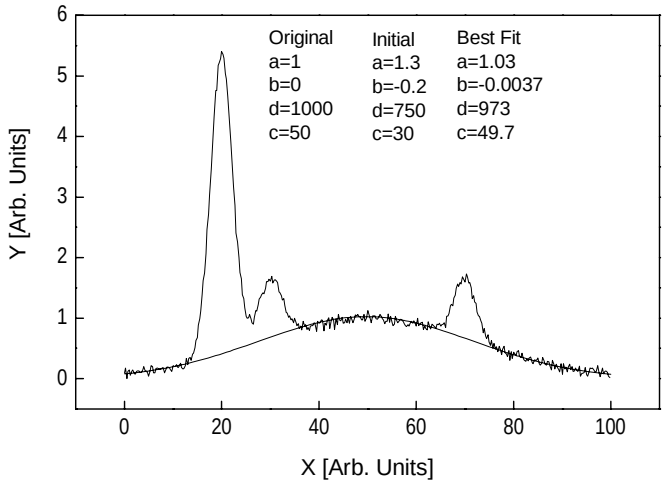

Fig. 2: Non linear base line of the spectrum estimated by CPC approach. See text for details.

Each point is randomized with normally distributed errors in order to simulate a noise concomitant to experimental data. Our intention is to obtain coefficients a_b, c_b, d_b, and b for the function B using the *whole data set* relying on the Close Points Concept. In other words we will fit our data to the function B considering sharp peaks P_1, P_2, and P_3 just as a deviation (outliers) of the main flow of the data given by term B. This task requires minimization of the merit function (1) by some of existing algorithms. We have chosen downhill simplex method (Press *et al.* 1988) applied in the routine AMOEBA, as the most suitable.

In Fig. 2 is shown the graph of the function B for parameters found by fitting for distance d set to 0.1. The best fit values are: a_b=1.03, c_b=49.7, d_b973, b=-0.0037. One can notice that these values are reasonably close to the original ones. Initial values for AMOEBA algorithm were: a_b=1.3, c_b=30, d_b=750, b=-0.2.

4. DISCUSSION

Initially we will discuss the influence of the distance d on the results. As it has been explained the role of d is to discriminate close and far points. If data are obtained by A/D converter and data set contains over a thousand points it is most simple to accept one step of A/D converter as a reasonable value for d. For data sets with several hundred points the distance d is most suitable to be slightly less than the magnitude of the noise present in the

system. A very low *d* value can cause that just a few points, or no one, are close to the model function making any algorithm unusable. Similarly, too high value for *d* can cause that all points become close to the model function for too broad range of parameters making the result useless. Generally, the distance *d* should be similar to the width of the line we are going to fit. Such a value provides sufficient number of close points in the sense of CPC.

An important feature of the CPC is that topography of a multidimensional space defined by (1) is not smooth; rather it is stepwise, discrete, topography. On the contrary, practically all minimization algorithms are supposed to be used in smooth, continual space. Some of them, however, work in stepwise topography, and we have applied downhill simplex method as a most rough one. Due to discrete nature of the topography, the choice of initial guess is more difficult then usual. Too bad choice can cause that no one experimental point is close to the model function moving initial point into completely flat region of the multidimensional space where not any minimization algorithm can work. Also, the usual problem of finding just a local minimum is more emphasized here due to discrete nature of the merit function (1). For very large data set the merit function becomes pseudo continual which facilitates the use of standard algorithms. But, for small number of points the discrete nature of (1) make it useless in the sense of finding the best fit. It is interesting to relate this feature to our ability to recognize trace which is consisting of many points as a line, while just a few points are very difficult to be thought of as a line.

A few words more about uncertainties concomitant to the parameters obtained by fitting. Unfortunately this problem is related to the non statistical approach of the CPC. Namely, we suppose that outliers *are not* distributed according to the Gaussian model, therefore, we can not apply standard procedures to estimate uncertainties of the best fit parameters. AMOEBA minimization algorithm is suitable because it is not based on the assumption of normally distributed errors and, consequently, it does not produce uncertainties for the best fit parameters.

5. CONCLUSION

We have introduced a new form of merit function (1) based on close points concept suitable for problems where rough approach is necessary. The efficiency has been shown on two typical examples of the introduced merit function. In the first example, which is related to the common problem of finding spectrum base line, we have explained a simple numerical procedure avoiding explicit use of the merit function (1) and appropriate minimization algorithm. In the second example a standard minimization algorithm has been used to fit artificially generated data to the nonlinear function of the Gauss type over which three sharp peaks were superimposed. Comparing original and values obtained by fitting we have demonstrated the potentials of CPC. Also, we have discussed the influence of introduced parameter *d* and possible problems related to the discrete character of merit function (1). Finally, we would like to emphasize the necessity for appropriate minimization algorithm developed for the use in discrete space.

References

Gabel, J.R., Crenshaw, D.M., *et al.*: 2003, *Apstrophys. J.*, **583**, 178.

Spasojević, Dj., Bukvić, S., Milošević, S., Stanley, E.: 1996, *Phys. Rev. E*, **54**, 2531.

Djeniže, S., Bukvić, S.: 2001, *Astron. Astrophys.*, **365**, 252.

Press, W.H., Flannery, B.P., Teukolsky, S.A., Vetterling, W.T.: 1988, *Num. Rec.*, Cambridge University Press, Cambridge.

Publ. Astron. Obs. Belgrade No. 76 (2003), 25 *Invited lecture*

EMISSION AND ABSORPTION LINE PROFILES FROM SUPERNOVA ENVELOPES

I.J. DANZIGER

Osservatorio Astronomico di Trieste,
Via G.B. Tiepolo 11, 34131 Trieste, Italy

Abstract. A supernova ejects a massive envelope with ballistic velocities approximately one tenth the speed of light or more. In the early "photospheric" phase one sees either normal very broadened absorption lines or P Cygni lines only a fraction of which are uncontaminated by line blending. Emission lines in the "nebular" phase are more amenable to interpretation. In some cases lines are also seen formed in the circumstellar material blown from the star prior to the explosion of the supernova. The absorption lines in the photospheric phase have been used to map the velocity structure, the mass of material above the photosphere and the stratification of various elements in the envelope. Emission lines especially when the envelope is optically thin, allow one to probe velocity structure, the distribution of important elements such as oxygen, and even the distribution of the radioactive species such as Ni^{56} which are the source of heating and excitation, and also the total mass of elements that are emitting those lines. Emission line profiles have proved to be clear indicators of the formation and presence of dust in supernova envelopes. A study of line profiles of gas in the circumstellar material provides estimates of mass loss rates, total masses and estimates of progenitor star mass.

Invited lecture

THE INFLUENCE OF SOME NON-SYMMETRIC ION-ATOM RADIATIVE COLLISIONS ON THE OPACITY OF STAR ATMOSPHERES

LJ.M. IGNJATOVIĆ, A.A. MIHAJLOV

Institute of Physics, P.O. Box 57, 11001 Belgrade,
Serbia and Montenegro

Abstract. The ion-atom radiative collisions, as a factor which influences the optical characteristics of star atmospheres, were considered in several previous papers. It was shown that the most ignificant role is played by the processes of radiative charge exchange and photoassociative processes in $H^+ + H$ and $He^+ + He$ collisions. However, the star atmospheres are the example of chemically heterogeneous plasmas par exelence, hence the main task of this work is to investigate some of non-symmetrical radiative ion-atom collisional processes, which may occur in such plasmas. The influence of absorption processes in $He + H^+$ and $H + Na^+$ collisions on the opacity of solar photosphere, as well as the influence of $He + H^+$ on the opacity of some of DB white dwarfs, will be presented in this work.

Publ. Astron. Obs. Belgrade No. 76 (2003), 25 *Invited lecture*

EMISSION AND ABSORPTION LINE PROFILES FROM SUPERNOVA ENVELOPES

I.J. DANZIGER

Osservatorio Astronomico di Trieste,
Via G.B. Tiepolo 11, 34131 Trieste, Italy

Abstract. A supernova ejects a massive envelope with ballistic velocities approximately one tenth the speed of light or more. In the early "photospheric" phase one sees either normal very broadened absorption lines or P Cygni lines only a fraction of which are uncontaminated by line blending. Emission lines in the "nebular" phase are more amenable to interpretation. In some cases lines are also seen formed in the circumstellar material blown from the star prior to the explosion of the supernova. The absorption lines in the photospheric phase have been used to map the velocity structure, the mass of material above the photosphere and the stratification of various elements in the envelope. Emission lines especially when the envelope is optically thin, allow one to probe velocity structure, the distribution of important elements such as oxygen, and even the distribution of the radioactive species such as Ni^{56} which are the source of heating and excitation, and also the total mass of elements that are emitting those lines. Emission line profiles have proved to be clear indicators of the formation and presence of dust in supernova envelopes. A study of line profiles of gas in the circumstellar material provides estimates of mass loss rates, total masses and estimates of progenitor star mass.

Invited lecture

THE INFLUENCE OF SOME NON-SYMMETRIC ION-ATOM RADIATIVE COLLISIONS ON THE OPACITY OF STAR ATMOSPHERES

LJ.M. IGNJATOVIĆ, A.A. MIHAJLOV

Institute of Physics, P.O. Box 57, 11001 Belgrade,
Serbia and Montenegro

Abstract. The ion-atom radiative collisions, as a factor which influences the optical characteristics of star atmospheres, were considered in several previous papers. It was shown that the most ignificant role is played by the processes of radiative charge exchange and photoassociative processes in $H^+ + H$ and $He^+ + He$ collisions. However, the star atmospheres are the example of chemically heterogeneous plasmas par exelence, hence the main task of this work is to investigate some of non-symmetrical radiative ion-atom collisional processes, which may occur in such plasmas. The influence of absorption processes in $He + H^+$ and $H + Na^+$ collisions on the opacity of solar photosphere, as well as the influence of $He + H^+$ on the opacity of some of DB white dwarfs, will be presented in this work.

Publ. Astron. Obs. Belgrade No. 76 (2003), 26 *Invited lecture*

PHOENIX - THE WAY FORWARD IN MODELLING OF STELLAR ATMOSPHERES

DARKO JEVREMOVIĆ

Astronomical Observatory,
Vogina 7, 11160 Belgrade, Serbia and Montenegro

Abstract. We briefly describe the current version of the general stellar atmosphere code PHOENIX. We then present some illustrative results from the modelling of chromospheres of cool stars, supernovae and iradiated giant planets. Good fits to observations can be obtained, when account is taken for spherically symmetric, line-blanketed, static or expanding atmospheres. We conclude with an outline of developements and features which we intend to include in the PHOENIX in the next few years and their significance to future stellar atmosphere modelling.

Publ. Astron. Obs. Belgrade No. 76 (2003), 27-42 *Invited lecture*

THE COMPLEX STRUCTURE OF THE Mg II REGIONS OF 40 BeV STARS

E. LYRATZI, E. DANEZIS, M. STATHOPOULOU, E. THEODOSSIOU, D. NIKOLAIDIS, C. DRAKOPOULOS, A. SOULIKIAS

University of Athens, School of Physics, Department of Astrophysics, Astronomy and Mechanics, Panepistimiopolis, Zografos 157 84, Athens – Greece
E-mail: edanezis@cc.uoa.gr

Abstract. In this paper we present a study of the UV Mg II resonance lines in 40 BeV stars' spectra. We used the model proposed by Danezis *et al.* (2002b, 2003). This model is based on the idea of independent density layers in the regions where the spectral lines that present SACs (DACs) are created. We calculated the apparent rotation (V_{rot}) and expansion/contraction velocities (V_{exp}) of these density regions, as well as their ξ value, which is an expression of the optical depth. We also present the relation among these parameters and their evolution with the spectral subtype.

1. INTRODUCTION

The definitive characteristics of the emission early type stars are the peculiar emission-absorption features in their spectra. In order to explain this phenomenon, first Struve (1931, 1942) developed a model, which accepts that the emission and/or absorption features are formed in an extended low-density equatorial envelope surrounding a rapidly rotating B star. This model implies small radial velocity fields in the shell but large rotational velocities throughout much of the disk or shell. In Be stars, the Balmer series in the optical range and the UV Mg II resonance lines present strong emission lines.

The Mg II resonance lines λλ 2795.523, 2802.698 Å arise from the transition $3s^2S$ - $3p^2P^0$. As the energy difference between the two levels is quite large (4.5 eV), the Mg II spectral lines are sensitive to Non-LTE effects (Underhill, 1970) and thus to the structure of the stellar atmosphere and its radiation field (Lamers *et al.* 1973). As a result, the study of the Mg II resonance lines in the spectra of early type stars is a significant tool for the study of the structure of the stellar atmospheres.

Mihalas (1972) used a model atom which gave a good fit to the observed equivalent widths of the λ 4481 Å line of Mg II on the range from O6 through B5 stars.

Hubert (1973) studied the optical spectra of eight Be stars and concluded the emission to be reinforced or disappeared, depending on the stars' phase (B or Be). Besides, during the star's transition from B to Be and from Be to B, the lines are stronger. Five of the studied stars, while in emission, keep their absorbing envelope.

Lamers *et al.* (1973) found that, in B stars, the equivalent width of the Mg II lines, which lies between the values 1 to 4.5 Å, does not really depend on the temperature. They studied the spectra of the Be stars κ CMa (B2Ve) and κ Dra (B7e) and found that the Mg II lines are about 0.6 times weaker than those of normal stars and that βMon (B3e), which is a classical shell star, presents Mg II lines with normal strength. They suggested that this behavior is due to the absorption lines being partially filled in with emission. They also

found that the blended lines (mainly VII, CrII, FeII and TiII) contribute less than 25 per cent to the observed equivalent widths. In order to explain the observed equivalent widths in B1-B2 stars, in terms of microturbulence, they suggested a velocity of about 15 km/s, which exceeds the value derived from the optical spectrum (4 to 5 km/s) by quite a large factor. However, as the UV Mg II lines and the lines at 4481 Å, in the optical range, are formed at about the same optical depth, in early B stars, they should present the same microturbulent velocity.

Collins (1974) indicated that rotation may affect the measured equivalent widths of certain lines in the sense that higher rotation will increase the line strengths.

Underhill (1975) observed sharp components of the ions NII, CII and Mg II in the spectrum of HD 58350 and attributed the one velocity of 230 km/s to a gas cloud accelerated from the star and moving rapidly out of the star and the other velocity of about 25 km/s to a moving circumstellar shell.

Gurzadyan (1975) studied the Mg II resonance lines in the spectra of 51 relatively faint stars with spectral types from B1 to K5 and found that there is an empirical relationship between the equivalent width and the spectral type of the star. In the types B1 to K0 the Mg II lines are in absorption, while in some cases the Mg II lines present a wide absorption with a weak emission in the center. In the faint B stars the equivalent widths of the Mg II lines are small and mainly due to the interstellar component, while in the bright B stars they sometimes appear larger than the theoretically predicted values. He concluded the doublet to be more or less stable for a given spectral type.

Snijders and Lamers (1975) considered that the Mg II lines are sensitive to non-LTE effects and to the structure of the stellar atmosphere and its radiation field and that the interstellar Mg II resonance lines in the UV are usually strong in the spectra of early O and B stars. They calculated the equivalent widths and line profiles of the Mg II resonance lines at λλ 2795.523, 2802.698 Å, of their subordinate lines at λλ 2790.768, 2797.989 Å, as well as of the doublet at 4481 Å in the spectra of early type stars. They found that in stars later than B2 the observed and predicted (considering LTE) equivalent widths agreed reasonably, while the stars of types earlier than B3 showed lines stronger than predicted. They also found that microturbulence adds to the width of the line cores by a factor 1.3-1.5 for main-sequence stars and by a factor 2-3 for supergiants.

According to Kondo *et al.* (1975) "the Mg II features are of considerable interest for studies of both the interstellar medium and the structure of stellar atmospheres, where these lines may involve a significant part of the energy in some regions of the atmosphere". They studied the relation between the existence of emission cores at the bottom of the strong absorption lines and the existence of a chromosphere for stars of early to intermediate type. They suggested that, for the early type stars, the main question about the chromosphere is the physical problem of the energy source, meaning "whether the concept of acoustic waves, generated in a convection zone and growing into shock waves to heat a chromosphere, is relevant, or whether other mechanisms dominate". They used a synthetic spectrum to fit the Mg II absorption lines of the observed spectra, in order to have a quantitative evaluation of the lines' strength. This procedure was based on the idea that the absorption lines can be approximated by a Gaussian formula and did not include the possible emission and the interstellar absorption, for which, in some cases they used additional absorption functions. In this way they determined the equivalent widths and the full widths at half-depth for the Mg II resonance lines at λλ 2795.523, 2802.698 Å, as well as for their subordinate lines at λλ 2790.768, 2797.989 Å. The values they measured were in good agreement with those determined theoretically. They suggested that, in the spectral range from B2 to B6, the Mg II equivalent widths might be used as an indicator of

luminosity. They also proposed that there exists a correlation of the equivalent width with Vsini. For the spectral region between O8 and B8 stars, they found emission features in the spectra of the earliest and latest spectral types. They attributed this phenomenon to "chromospheres being minimal at intermediate B type as a result of cross-over of different physical mechanisms for early and late-type stars".

Kondo *et al.* (1976a) considered that the Mg II doublet is a great tool for studying stellar chromospheres. They suggested that the chromospheric emission, if it exists, could imply the presence of a positive outward temperature gradient in the outer regions of the stellar atmospheres. The observational evidence for the existence of chomospheres in B stars is mainly the weak emission features at the bottom of the absorption lines of the resonance doublet at λλ 2795.523, 2802.698 Å. However, the weak emission at the bottom of the doublet's lines is strongly affected, even obliterated sometimes, by the quite pronounced interstellar absorption lines. They proposed that "the existence of an intervening spectral type of minimum chromospheric activities could imply an additional heating mechanism (other than acoustic heating from a convection zone) for the massive stars. In the case of a greatly extended atmosphere, the Mg II emission might not be a definite evidence of a chromosphere, as emission from regions outside the line of sight could overpower the usual effect that a cool gas will absorb more radiation in a spectrum line than it emits".

Kondo *et al.* (1976b) pointed out that it is difficult to determine the range of early spectral types, where the chromospheric emission disappears, as the circumstellar and interstellar Mg II emission lines may affect the determination of spectral type at which the emission disappears. They proposed that there is probably a difference among luminosity classes. They found that the shell absorption gets stronger from intermediate to late B stars and suggested that "it might be due to the rising temperature in the gaseous shell which converts Mg II to Mg III and to the weakening of the outward-driving mechanisms of the atmosphere". In early B type supergiants, the Mg II doublet consists of the photospheric resonance lines with superposed interstellar resonance absorption lines. The intermediate B supergiants present a value of about 100 km/s for the velocity of the escaping shell, maybe due to the transition from acoustic heating to radiation pressure.

Morgan *et al.* (1977) studied the Mg II resonance lines of γ Cas and ζ Tau and detected "significant absorption features" shortward of each resonance absorption, which they attribute to "additional absorption within the stars' extended atmosphere". They concluded that the Mg II resonance lines of ζ Tau were not formed in the same layer as their subordinate lines. They remark: "The strong subordinate lines are formed exterior to the regions where the bulk of the visible stellar spectrum is formed and interior to the portions of the circumstellar disk where the visible shell lines are formed". Finally, for ζTau, they calculated an outward velocity of 60-120 km/s from near the stellar surface layers all the way to the outer edge of the shell.

Kondo *et al.* (1977) calculated the equivalent widths of the Mg II resonance lines in the spectra of O to F stars and found that they increase from early to late B subtypes. They report that, while the emission in early type stars may arise from the star's chromosphere, when a binary system is concerned, the emission may be due to high-temperature plasma flowing in the system rather than to chromosphere of the primary star.

Marlborough *et al.* (1978) pointed out that the UV spectra of Be stars are very complex and contain many shell absorption lines which usually have velocity shifts. On the other hand, the emission lines are not usually present, probably due to the insufficient extent and/or density of the circumstellar envelope. They detected Mg II emission in four spectra of γCas (taken in the time interval from November 1974 to November 1976), which

presented differences in position and strength. They tested three classes of Be star models proposed for the emission, in order to explain the spectra of γCas: a) the single-star models invoking detached rings of material responsible for the emission features (Struve 1931, McLaughlin 1961, Albert and Huang 1974, Huang 1977), b) models of binary systems, where a late-type companion loses material to form the observed extended atmosphere of a Be star (Kriz and Harmanec 1975, Harmanec and Kriz 1976), and c) single-star models in which the emission lines arise in the dense regions of a stellar wind (Poeckert and Marlborough 1978). All the three models failed to explain the observational data of γCas. Thus, they proposed an extension of the stellar-wind model, in which the terminal speed of the wind depends on the distance from the equatorial plane. At low distances the terminal wind speed is low, while at larger distances it is significantly higher. Turbulence due to differential rotation near the equatorial plane is responsible for the production of a coronal layer at larger distances above and below the equatorial plane. According to this model the observed optical and UV emission lines arise in the inner regions of the wind.

Slettebak and Snow (1978), in their study on γCas, suggested that since the Mg II resonance lines are very narrow, they cannot be photospheric but of circumstellar or, more probably, interstellar origin. They detected a narrow emission component shifted about 0.7 Å to the red of each Mg II line center, which corresponds to a velocity of 85 km/s.

De Jager *et al.* (1979) studied the spectra of 33 stars of all spectral types. They found variable mass loss from late B supergiants, due to "occasional stellar "puffs" superposed on a more or less regular wind". In the spectrum of the B8 star βOri, the Mg II resonance lines are shifted by -190 km/s. This fact indicates that "there are concentrations of low-ionization species in the stellar wind as a result of the occurrence of significant density variations". The Be and shell stars presented very strong and sharp resonance lines. The noninterstellar component was significantly shifted toward long wavelengths, suggesting that a new infall of shell material was occurring at the time of the observation (Delplace and van der Hucht 1978).

Lamers *et al.* (1980) studied the spectra of 9 Ap, Bp, Be, Bn and shell stars and found that the Mg II lines of Be stars are weaker than in normal stars and that the Bp, Bn and shell stars present normal Mg II lines.

Bruhweiler *et al.* (1982) studying the UV Mg II resonance lines in the spectra of the Be stars γCas, φPer and υCyg, proposed that the Mg II emission is a normal phenomenon in Be stars, since it appears in all the studied spectra. The Mg II absorption is shifted with respect to the emission by 5-10 km/s. Thus, a part of the absorption lines must originate from a slowly expanding circumstellar shell and another is expected to be of interstellar origin. They propose that the emission, which must originate in a region of low ionization and low expansion velocities, is due to a Bowen (1947) mechanism driven by Lyβ, since the widths of the Balmer and Mg II emission are comparable. Thus, the Mg II emission must originate in the same physical region as the hydrogen recombination spectrum.

Danezis (1984, 1986) and Danezis *et al.* (1991) studied the UV spectra of the gaseous envelope of AX Mon taken by the IUE satellite and noted that the absorption lines of many ionization potential ions (including Mg II), not only of those presenting PCygni profile, are accompanied by two strong absorption components of the same ion and the same wavelength, shifted shortward at different Δλ. This means that the regions where these spectral lines are created are not continuous, but they are formed by a number of independent density layers of matter. These layers of matter can rotate and move with different apparent velocities of the order of 10 km/s, -75 km/s and -260 km/s.

The existence of satellite components in the UV spectrum of AX Mon has been detected also by Sahade *et al.* (1984) and Sahade and Brandi (1985). For the Mg II

absorption components, they found velocities between the values of -200 and 250 km/s. Also, Hutsemekers (1985), in the UV spectrum of another Be star, HD 50138, noticed a number of satellite components that accompanied the main spectral lines.

Laskarides *et al.* (1992) observed one more satellite component in the spectral lines of ions with low ionization potential in the absorption UV spectrum of AX Mon, lying at the red side of the main lines. The existence of these spectral lines has been proposed by Doazan (1982). This fact indicates contraction of the outer layers of the gaseous envelope.

Cidale (1998) adopted a model for the Be stars' atmospheres, in order to compute the Mg II line profiles. This model is called "chromospheric-wind model" and suggests that the atmosphere consists of a classical photosphere, an expanding high-temperature chromosphere and a cool envelope. This model accepts that the Mg II lines arise from a nonrotating and spherically expanding medium. They sometimes appear as pure absorption and sometimes they display emission wings and absorption cores (Dachs 1980, Doazan *et al.* 1991). The lines present PCygni profiles or blueshifted variable absorption components in the velocity range of -50 to -200 km/s. There is no relation between the emission and the spectral type or Vsini. However, the lines' profiles depend on the temperature structure and on the velocity and mass-density distributions. Particularly, the velocity law defines the profiles shape and the extension of the line-forming regions. High velocity gradients yield extended regions, which give rise to resonance lines with double absorption components or PCygni profiles. In this case the blueshifted component reveals the velocity of the most external layers, generally located in the cool envelope. She proposed that the undisplaced component originates in the photosphere, while the blueshifted component and the emission arise from the outer regions. The emission, which is related to the existence of a chromosphere, is very faint or does not exist at all in the early subtypes. It strengthens in the intermediate subtypes and appears quite prominent by the time the late subtypes are reached, indicating the presence of a chromosphere.

Finally, Danezis *et al.* (2002a) studied the Mg II resonance lines in the spectra of 21 BeV stars. They attributed many of the peculiarities occurring to these lines to the existence of Satellite Absorption Components (SACs). In order to study all the lines presenting SACs, they proposed a model for the structure of the regions where the spectral lines that present SACs are created (Danezis *et al.*, 2002b, 2003). Based on this model, they studied the variation of the apparent rotation (V_{rot}) and expansion/contraction velocities (V_{exp}) of the density regions where the Mg II resonance lines (λλ 2795.523, 2802.698 Å) are formed for a series of 21 Be V stars of all the spectral subtypes.

In this paper we apply the proposed by Danezis *et al.* (2003) model to 40 BeV stars, in order to calculate the apparent rotation and expansion/contraction velocities and the ξ values of the density regions where the UV Mg II resonance lines are created.

2. DATA

The data we used are the Mg II resonance lines of 40 Be V stars. The stars' spectrograms have been taken with IUE satellite and their spectral types have been taken by the SIMBAD database (Centre de Donnees Astronomiques de Strasbourg (CDS), Strasbourg, France). Our data are presented in Table 1.

Table 1					
Star	**Spectral Type**	**Camera**	**Star**	**Spectral Type**	**Camera**
HD 206773	B0 V : pe	Lwr 14808	HD 191610	B2.5 V e	Lwr 07342
HD 200310	B1 V e	Lwr 09544	HD 60855	B2/B3 V	Lwp 15477
HD 212571	B1 V e	Lwr 05948	HD 25940	B3 V e	Lwr 05950
HD 44458	B1 V pe	Lwp 30173	HD 45725	B3 V e	Lwp 10041
HD 200120	B1.5 V nne	Lwr 11035	HD 183362	B3 V e	Lwp 11044
HD 36576	B 2 IV-V e	Lwp 14029	HD 208057	B3 V e	Lwp 29221
HD 32991	B2 V e	Lwr 11426	HD 205637	B3 V : p	Lwr 05947
HD 58050	B2 V e	Lwr 14810	HD 217543	B3 V pe	Lwp 13326
HD 164284	B2 V e	Lwr 11038	HD 22192	B5 V e	Lwr 09071
HD 41335	B2 V ne	Lwr 07384	HD 217891	B6 V e	Lwr 09069
HD 52721	B2 V ne	Lwp 05462	HD 138749	B6 V nne	Lwr 07858
HD 58343	B2 V ne	Lwr 07363	HD 6811	B7 V e	Lwr 09070
HD 148184	B2 V ne	Lwr 06744	HD 192044	B7 V e	Lwp 08135
HD 202904	B2 V ne	Lwr 07343	HD 210129	B7 V ne	Lwp 23173
HD 65079	B2 V ne…	Lwp 30119	HD 47054	B8 V e	Lwp 13074
HD 28497	B2 V : ne	Lwr 07337	HD 58715	B8 V e	Lwp 10104
HD 45995	B2 V nne	Lwr 08648	HD 183914	B8 V e	Lwr 04609
HD 10516	B2 V pe	Lwr 07335	HD 23552	B8 V ne	Lwr 08744
HD 32343	B2.5 V e	Lwr 05890	HD 185037	B8 V ne	Lwp 08136
HD 65875	B2.5 V e	Lwr 05616	HD 199218	B8 V nne	Lwp 09903

3. SPECTRAL ANALYSIS OF THE Mg II RESONANCE LINES IN THE UV SPECTRA OF 40 Be V STARS

Figures and diagrams

In Figs. 1 and 2 we present the Mg II lines' fittings of 9 BeV stars together with the normal B star's HD 30836 Mg II profile, in order to indicate the blended lines and the intense appearance of the SACs. The heavy line presents the observed spectral line's profile and the thin one the model's fit. The differences between the observed spectrum and its fit are sometimes hard to see, as we have accomplished the best fit. The dashed lines indicate the laboratory wavelengths of the Mg II resonance lines at λλ 2795.523, 2802.697 Å.

By the model's best fit of the Mg II resonance lines of 40 BeV stars, we calculated the apparent rotation (V_{roti}) and expansion/contraction (V_{expi}) velocities of each one of the absorption and the emission components of the lines. We have also calculated the values of ξ_i for each line. By the study of the interstellar lines we calculated a systematical error which leads to a displacement of about +98±18 km/s. This displacement is clearly seen in Figs. 1 and 2. Our results have undergone the appropriate corrections and appear in diagrams 1 to 14.

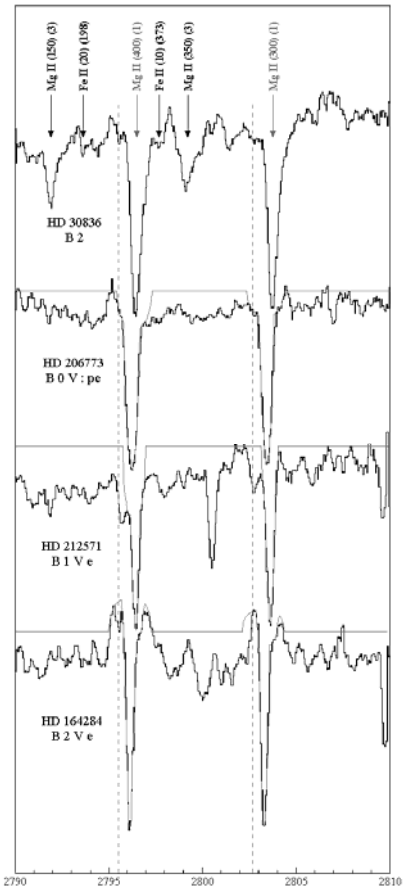

Fig. 1

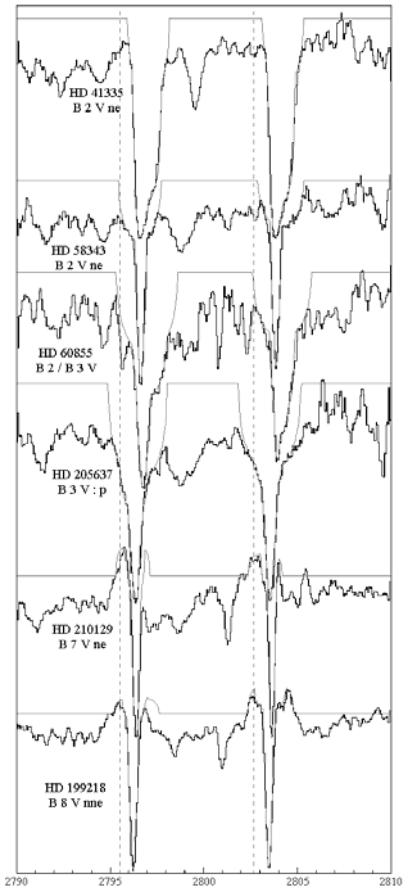

Fig. 2

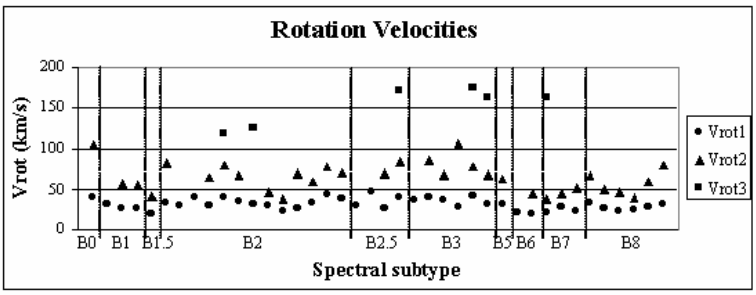

Diagram 1: Apparent rotation velocities of all the SACs as a function of the spectral subtype. The rotation velocity presents a uniform fluctuation, which we could not accept as accidental. Three rotation velocity groups are presented with the mean values of 31 km/s, 64 km/s and 153 km/s. These groups are presented separately in diagrams 3-5.

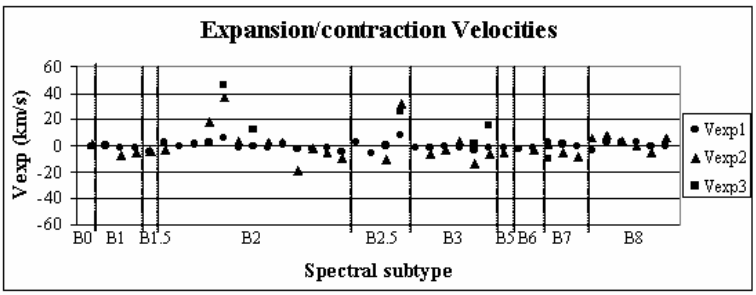

Diagram 2: Expansion/contraction velocities of all the SACs as a function of the spectral subtype. The values of the expansion/contraction velocities of all the SACs lie in a narrow range between -18 km/s and +18 km/s and present two maxima of +42 km/s and +29 km/s, which correspond to stars with spectral subtypes B2 and B2/B3, respectively.

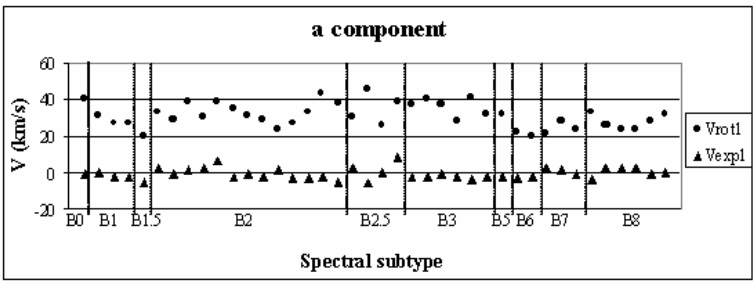

Diagram 3: Apparent rotation and expansion/contraction velocities of the first SAC as a function of the spectral subtype. As one can see, the first SAC's rotation and expansion/contraction velocities present a uniform fluctuation around the values of 31 km/s and -1 km/s respectively.

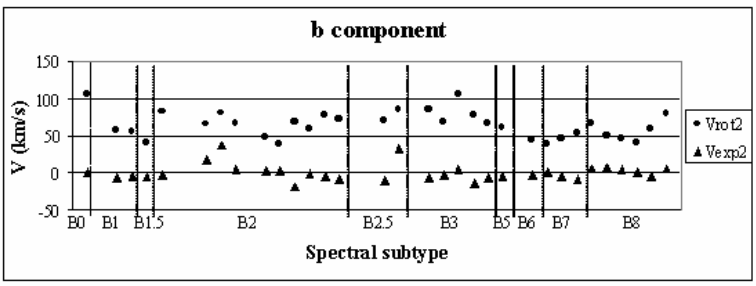

Diagram 4: Apparent rotation and expansion/contraction velocities of the second SAC as a function of the spectral subtype. A less intense uniform fluctuation is also presented in the second SAC's rotation and expansion/contraction velocities around the values of 64 km/s and 0 km/s respectively.

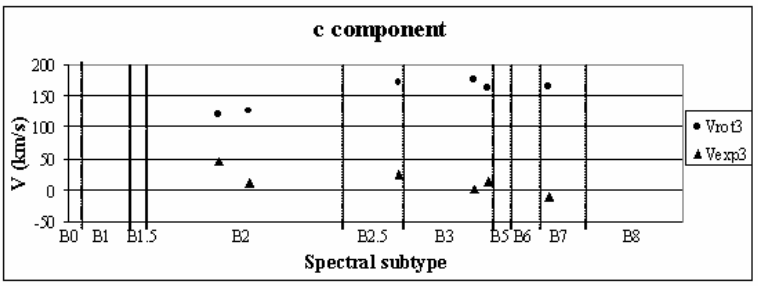

Diagram 5: Apparent rotation and expansion/contraction velocities of the third SAC as a function of the spectral subtype. A slight increase is observed in the rotation velocity of the third SAC around the value of 153 km/s, whereas the respective expansion velocity presents a slight decrease around the value of +15 km/s.

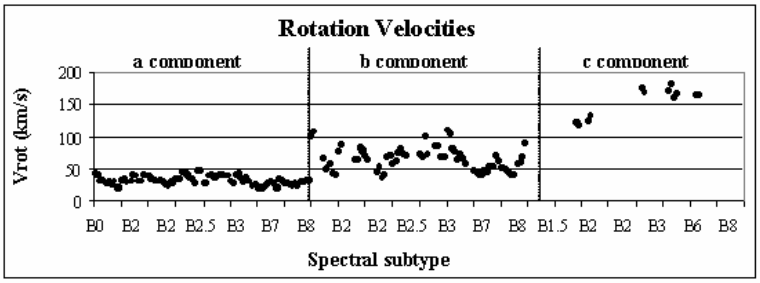

Diagram 6: Apparent rotation velocities of all the SACs as a function of the spectral subtype (presented separately). The rotation velocity of the first SAC presents a small dispersion around the value of 31 km/s whereas in the case of the second SAC the dispersion increases around the greater value of 64 km/s. The third SAC's rotation velocity increases more and presents a greater dispersion around the value of 153 km/s.

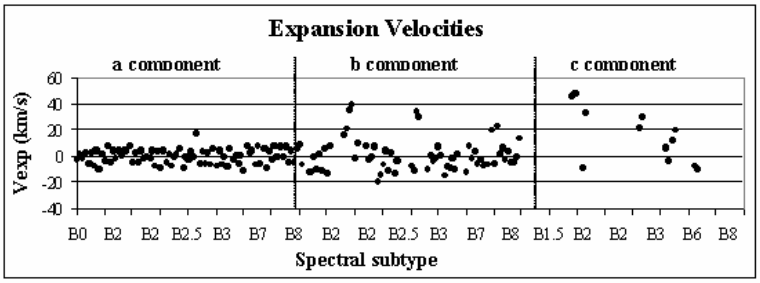

Diagram 7: Apparent expansion/contraction velocities of all the SACs as a function of the spectral subtype (presented separately). As in the case of the rotation velocity, the expansion/contraction velocities of the first, second and third SAC present increasing dispersion around the values of -1 km/s, 0 km/s and +15 km/s, respectively.

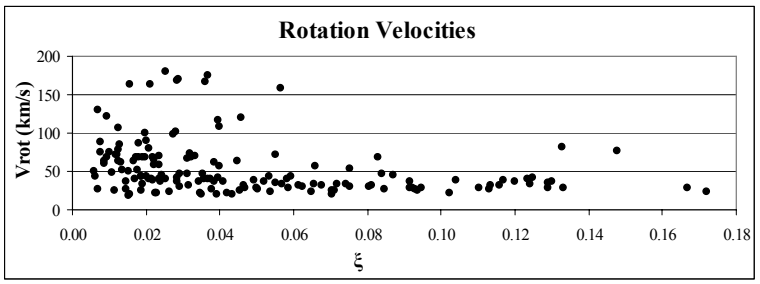

Diagram 8: Apparent rotation velocities of all the SACs as a function of the respective value of ξ. For small values ξ the rotation velocity lies in the range of 16 to 100 km/s. As the ξ value increases the rotation velocity's values lie in a smaller range between 20 and 82 km/s. The points referring to greater rotation velocity values (between 102 and 180 km/s) correspond to the third SAC which presents small values of ξ (between 0.007 and 0.057).

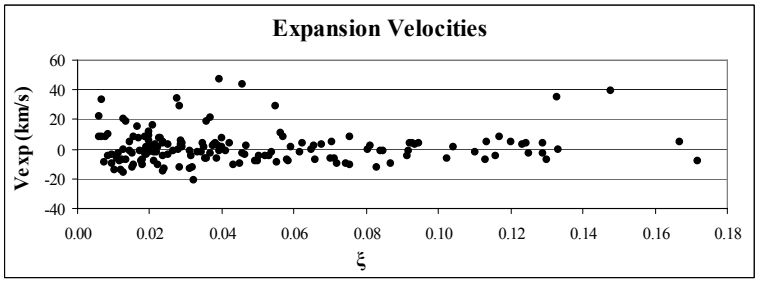

Diagram 9: Expansion/contraction velocities of all the SACs as a function of the respective ξ value. For small ξ values the expansion/contraction velocity lies in the range of -21 to +47 km/s. As the ξ value increases the expansion/contraction velocity's values lie in a smaller range between -12 and +8 km/s. The points referring to greater values of expansion/ contraction velocities (between +20 and +47 km/s) correspond to the second and third SAC.

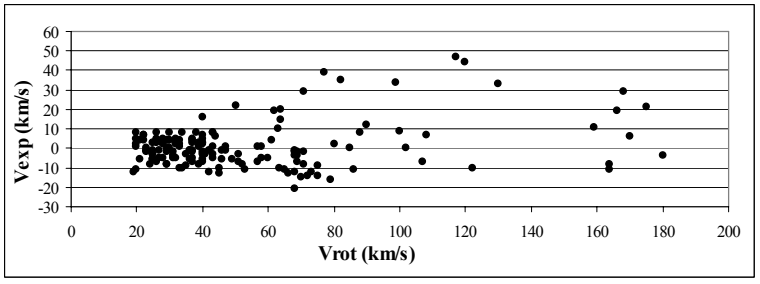

Diagram 10: Expansion/contraction velocities of all the SACs as a function of the respective apparent rotation velocities. For small values of the rotation velocity, between 16 and 66 km/s, the values of the expansion/contraction velocity lie in a small range between -11 and +22 km/s. As the rotation velocity increases, the expansion/contraction velocity presents greater dispersion and its values, which lie between -21 and +47 km/s, seem to gather into two branches around 0 and +35 km/s.

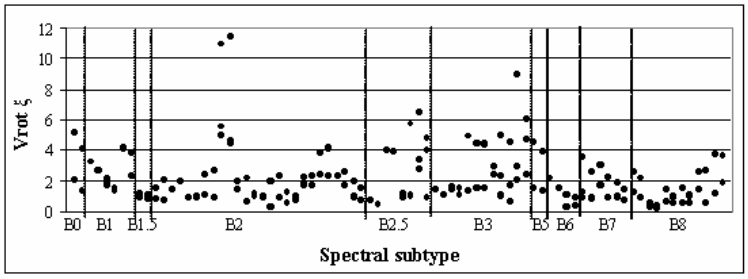

Diagram 11: Values of the product of ξ and the apparent rotation velocities (V_{rot}) as a function of the spectral subtype.

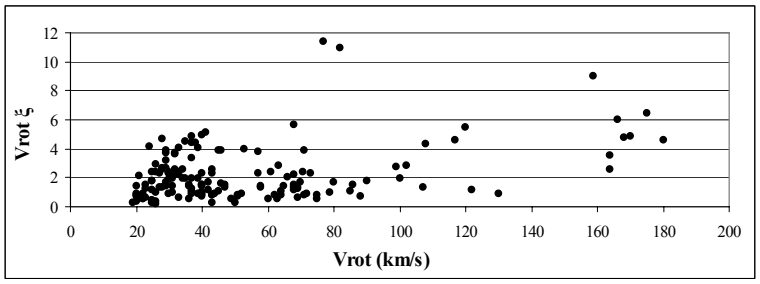

Diagram 12: Values of the product of ξ and the apparent rotation velocities (V_{rot}) as a function of the apparent rotation velocities.

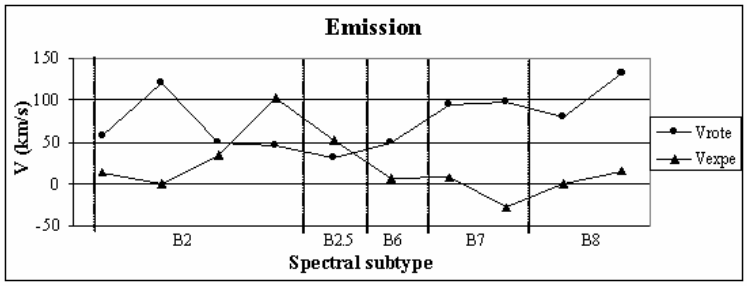

Diagram 13: Apparent rotation and expansion/contraction velocities of the emission component as a function of the spectral subtype.

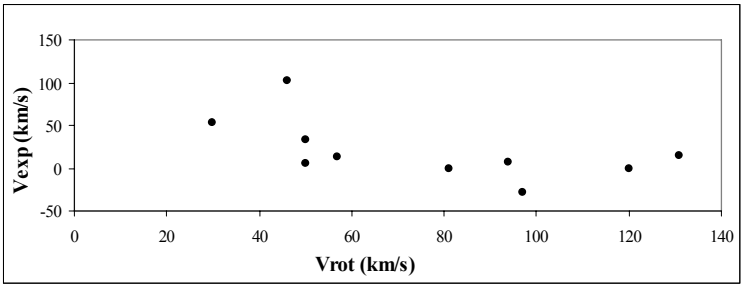

Diagram 14: Expansion/contraction velocities of the emission component as a function of the respective apparent rotation velocities. As the values of the rotation velocity increase, the values of the expansion/contraction velocity decrease.

4. CONCLUSIONS

1. By applying the proposed by Danezis *et al.* (2002b, 2003), model we are able to reproduce, with great accuracy, the profiles of the Mg II doublet of the 40 BeV stars we studied. This means that the coronal model allowing the existence of successive, independent density shells of matter represents accurately the structure of the Mg II region of the Be stars. This result verifies the proposition of de Jager *et al.* (1979) that "there are concentrations of low-ionization species in the stellar wind as a result of the occurrence of significant density variations", as well as the fact that there are "significant absorption features" shortward of each resonance absorption, which, according to Morgan *et al.* (1977) are attributed to "additional absorption within the stars' extended atmosphere". These "significant absorption features" are the Satellite Absorption Components (SACs) that appear in the spectra of the early type stars. Danezis *et al.* (2003) explained that the peculiar phenomena observed in the spectra of Oe and Be stars, such as the SACs, are due to independent density regions in the stars' environment. Such regions may be structures that cover all or a significant part of the stellar disk (shells, blobs, puffs, bubbles) (Underhill 1975, de Jager *et al.* 1979, Henrichs 1984, Underhill and Fahey 1984, Bates and Halliwell 1986, Grady *et al.* 1987, Lamers *et al.* 1988, Waldron *et al.* 1992, Cranmer and Owocki 1996, Rivinious *et al.* 1997, Kaper *et al.* 1996, 1997, 1999, Markova 2000), interaction of fast and slow wind components, CIRs, structures due to magnetic fields or spiral streams as a result of the star's rotation (Underhill and Fahey 1984, Mullan 1984a,b 1986, Prinja and Howarth 1988, Cranmer and Owocki 1996, Fullerton *et al.* 1997, Kaper *et al.* 1996, 1997, 1999, Cranmer *et al.* 2000).
2. The SACs phenomenon appears to be a classical one for the Be stars. From the present study, we observe that all the 40 Be V stars present SACs, though, they are not presented as intensively as they are in the case of the Be III stars, such as HD 144 or HD 45910 (paper II), where the SACs appear as discrete lines. In the case of the Be V stars, the relatively small values of the expansion/contraction velocities result in the SACs being blended among them as well as with the main spectral line, making it difficult for the observer to detect them.
3. In Figs. 1 and 2, in Table 2 and in diagram 1 one can see that all the studied stars present discernible or indiscernible SACs of the Mg II resonance lines. The indiscernible SACs appear in the spectra of the stars with spectral subtypes B0-B1, B4-B6 and B8. This is due to the fact that the SACs of the Mg II resonance lines in the

spectra of the stars of these spectral subtypes present similar radial velocities. In this case, we can separate these lines by the systematic differentiations of the apparent rotation velocities and the values of ξ_i. The SACs of the Mg II resonance lines are more discernible in the spectra of the stars with spectral subtypes B2-B3 and B7, as they present quite different radial shifts. In this case the density regions' apparent rotation velocities present greater values.

4. The regions where the Mg II resonance lines are created present three velocity groups, which do not appear, though, in all the 40 Be V stars we studied in this paper. All of the studied stars present the SAC with rotation velocity of the order of 31±7 km/s. The SAC with rotation velocity of the order of 64±18 km/s appears in most of the stars except in a B1, a B2, two B2.5, a B3 and a B6 star. These two SACs present an almost zero expansion/contraction velocity. The third rotation velocity group of the order of 153±24 km/s presents expansion/contraction velocity of the order of +15 km/s. This SAC appears in some stars of spectral subtypes B2-B3 and B7. All the above means that the Mg II doublet is more or less stable for a given spectral type as Gurzadyan (1975) proposed. In diagram 2 one can see that the values of the expansion/contraction velocity of all the SACs lie in a narrow range between -18 km/s and +18 km/s and present two maxima of +42 km/s and +29 km/s, which correspond to stars with spectral subtypes B2 and B2/B3, respectively. In diagrams 1-3, 6 and 7 one can see that the apparent rotation and expansion/contraction velocities of the first SAC present a uniform fluctuation in a narrow range around the values 31 km/s and -1 km/s, respectively. The same phenomenon is presented in the second SAC (diagrams 1, 2, 4, 6 and 7), where the apparent rotation and expansion/contraction velocities fluctuate around the values 64 km/s and 0 km/s, respectively and present greater dispersion than the one presented in the values of the first SAC. The third SAC (diagrams 5, 6 and 7) presents greater values of rotation and expansion/contraction velocity, which lie in wider ranges between 102 km/s and 180 km/s and-10 km/s and +47 km/s, respectively. The rotation velocity values of the third SAC increase slightly, around the value of 153 km/s, while the respective expansion/contraction velocity values decrease slightly, around the value of +15 km/s. In diagram 10 we present the relation between the expansion/contraction velocity and the apparent rotation velocity. We observe that, as the apparent rotation increases, the expansion/contraction velocity increases too and presents a greater dispersion, while its values gather into two branches.
5. In diagrams 8 and 9 one can see the variation of the apparent rotation and expansion/contraction velocity with ξ, respectively. For small values of ξ the two velocities lie in a wide range, while by the increase of ξ the velocities' range becomes narrower. In diagrams 11 and 12 we present $V_{rot}\xi$ as function of the spectral subtype and the apparent rotation velocity, respectively. As the product of the rotation velocity and the values of ξ ($V_{rot}\xi$) is an evaluation of the absorbed energy, we would like to extract some first conclusions about the variation of the absorbed energy with the spectral subtype and the apparent rotation velocity, as well as to verify other researchers' conclusions. Gurzadyan (1975) concluded that there existed an empirical relationship between the equivalent width and the spectral type of the star, while Kondo *et al.* (1977) concluded that the equivalent widths were increasing from early to late B subtypes. According to diagram 11, for the Be V stars, $V_{rot}\xi$ is more or less stable with the spectral subtype, presenting a fluctuation. In diagram 12 one can see that $V_{rot}\xi$ increases as the values of the apparent rotation velocity increase, meaning that there exists a correlation of the equivalent width with Vsini (Kondo *et al.* 1975). More conclusions about the energy will be presented in a forthcoming paper (paper II).

6. The stars that present emission are of spectral types B2, B6, B7 and B8 (diagram 13). This means that the emission appears in the spectra of the earliest and latest spectral subtypes of the Be V stars (Kondo *et al.* 1975). The expansion/contraction velocity of the emission component decreases as the rotation velocity increases. The emission component presents positive or negative expansion velocities. The calculated values correspond to the regions where the emission component is created (strings, blobs, puffs, bubbles), and not to a uniform region around the star. This means that the emission region may approach or move away from the observer and its different position and motion around the star is responsible of whether this value is positive or negative. In diagrams 13 and 14 one can see that, as the apparent rotation velocity increases, the expansion/contraction velocity decreases in contrast with the relation of the two velocities of the absorption components. At this point, we would like to point out that the emission component is blended with absorption lines of other ions, making difficult the evaluation of the apparent rotation and expansion/contraction velocity. As a result the calculated values present greater statistical error than the absorption components.
7. Until now, the main idea of the Mg II doublet was that the resonance lines were created in a specific region in the star's atmosphere and consisted of an absorption feature and a possible emission feature. Based on this idea, the equivalent width was calculated supposing that the whole absorption feature represents one absorption line, the rotation velocity was calculated by the width of the blue edge and the expansion velocity was calculated by the line shift, supposing that the deepest point of the feature corresponds to the wavelength at which the absorption appears. As we have already mentioned, according to the model presented by Danezis *et al.* (2002b, 2003), the Mg II resonance lines consist in a main absorption line accompanied by a number of SACs and a possible emission line. Thus, the above mentioned ways of the equivalent width and the rotation and expansion/contraction velocities' calculation can not be taken for granted. This fact can be explained, if we accept the existence of density regions (blobs, puffs, strings, bubbles) in the cool envelope. In this way we do not have to accept that the Mg II resonance lines are created in regions lying behind and in front of the corona, where the temperature is higher than the one needed for the creation of the Mg II ions. Finally, we could accept that in the cool envelope, around the density regions (blobs, puffs, strings, bubbles), there may exist sub-regions with similar structure, which give rise to narrow and faint absorption lines.
8. At this point we would like to point out that the calculated values of the apparent rotation and expansion/contraction velocities correspond to the regions, where the Satellite Absorption Components (SACs) are created, and not to the star. Specifically, these values correspond to the density regions (blobs, puffs, bubbles) which result when streams of matter are twisted and form strings that produce blobs, puffs or bubbles.It is important to make clear that the observed fluctuations of the apparent rotation and expansion/contraction velocities correspond to the regions where the SACs are created (strings, blobs, puffs, bubbles) and do not refer to a uniform shell around the star. Specifically, the calculated velocities correspond to the rotation of the region around itself and not around the star.
9. Finally, we would like to point out that a part of the measured apparent rotation velocity must be attributed to the expansion of the studied region. As it is known, the star ejects mass with a specific radial velocity. The stream of matter is twisted, forming density regions such as interaction of fast and slow wind components, corrotating interaction regions (CIRs), structures due to magnetic fields or spiral streams as a result

of the star's rotation (Underhill and Fahey 1984, Mullan 1984ab, 1986, Prinja and Howarth 1988, Cranmer and Owocki 1996, Fullerton *et al.* 1997, Kaper *et al.* 1996, 1997, 1999, Cranmer *et al.* 2000)). This means that hydrodynamic and magnetic forces take effect as centripetal forces, resulting in the outward moving matter twisting and moving around the star. As a result, a part of the outward velocity is measured as rotation velocity. This motion of the matter is responsible for the formation of high density regions (shells, blobs, puffs, spiral streams), which, either are spherically symmetric around the star, or appear to the observer as spherically symmetric (Danezis *et al.* 2003).

Acknowledgements. Dr. Danezis, E. Dr. Theodossiou E. and Lyratzi E. would like to thank Dr. M.S. Dimitrijević, former Director of the Astronomical Observatory of Belgrade for his help and comments. This research project is proceeding at the University of Athens, Department of Astrophysics - Astronomy and Mechanics, under the financial support of the Special Account for Research Grants, for which we thank very much.

References

Albert, E., Huang, S.S.: 1974, *Astrophys. J.*, **189**, 479.
Bates, B., Halliwell, D.R.: 1986, *Mon. Not. Roy. Astron. Soc.*, **223**, 673.
Bowen, I.S.: 1947, *Publ. Astron. Soc. Pacific*, **59**, 196.
Bruhweiler, F.C., Morgan, T.H., van der Hucht, K.A.: 1982, *Astrophys. J.*, **262**, 675.
Cidale, L.S.: 1998, *Astrophys. J.*, **502**, 824.
Collins, G.W.: 1974, *Astrophys. J.*, **191**, 157.
Cranmer, S.R., Owocki, S.P.: 1996, *Astrophys. J.*, **462**, 469.
Cranmer, S.R., Smith, M.A., Robinson, R.D.: 2000, *Astrophys. J.*, **537**, 433.
Dachs, J.: 1980, *ESA SP*-**157**, 139.
Danezis, E.: 1984, *The nature of Be stars, PhD Thesis*, University of Athens.
Danezis, E.: 1986, *IAU, Colloq. No 92, Physics of Be Stars*, Cambridge University Press.
Danezis, E., Theodossiou, E., Laskarides, P.G.: 1991, A*strophys. J. Suppl. Series*, **179**, 111.
Danezis, E., Lyratzi, E., Nikolaidis, D., Theodossiou, E., Stathopoulou, M., Christou, G., Soulikias, A.: 2002a, The complex structure of Mg II regions in the gaseous envelope of Be V stars *Proceedings of the IAU Symposium 210: Modeling of stellar atmospheres*, June 17 21, 2002, Uppsala, Sweden.
Danezis, E., Nikolaidis, D., Lyratzi, E., Stathopoulou, M., Theodossiou, E., Kosionidis, A., Drakopoulos, C., Christou, G., Koutsouris, P.: 2002b, A new model of density layers of matter in the expanding gaseous envelope of Oe and Be stars. *Proceedings of the IAU Symposium 210: Modeling of stellar atmospheres*, June 17 21, 2002, Uppsala, Sweden.
Danezis, E., Nikolaidis, D., Lyratzi, V., Stathopoulou, M., Theodossiou, E., Kosionidis, A., Drakopoulos, C., Christou G., Koutsouris, P.: 2003, *Astrophys. J. Suppl. Series*, **284**, Issue 4 (in press).
de Jager, C., Kondo, Y., Hoekstra, R., van der Hucht, K.A., Kamperman, T.M., Lamers, H.J.G.L.M., Modisette, J.L., Morgan, T.H.: 1979, *Astrophys. J.*, **230**, 534.
Delplace, A.M., van der Hucht, K.A.: 1978, *Astron. Astrophys.*, **67**, 399.
Doazan, V.: 1982, *B Stars with and without emission lines, NASA SP*-**456**.
Doazan, V., Sedmak, G., Barylak, M., Rusconi, L.: 1991, *A Be Star Atlas of Far UV and Optical High-Resolution Spectra (ESA SP*-**1147**, Paris: ESA Sci. Publ.).
Fullerton, A.W., Massa, D.L., Prinja, R.K., Owocki, S.P., Cranmer, S.R.: 1997, *Astron. Astrophys.*, **327**, 699.

Grady, C.A., Sonneborn, G., Chi-chao Wu, Henrichs, H.F.: 1987, *Astrophys. J. Suppl. Series*, **65**, 673.
Gurzadyan, G., A.: 1975, *Publ. Astron. Soc. Pacific*, **87**, 289.
Harmanec, P., Kriz, S.: 1976, in *IAU Symposium No 70, Be and Shell Stars*, ed. A. Slettebak (Dordrecht: Reidel), p. 385.
Henrichs, H.F.: 1984, *Proc. 4th European IUE Conf., ESA SSSP*-**218**, p.43, eds Rolfe, E., Battrick, B., Rome.
Huang, S.S.: 1977, *Astrophys. J.*, **212**, 123.
Hubert, H.: 1973, *Astron. Astrophys. Suppl. Series*, **9**, 133.
Hutsemekers, D.: 1985, *Astron. Astrophys. Suppl. Series*, **60**, 373.
Kaper, L., Henrichs, H.F., Nichols, J.S., Snoek, L.C., Volten, H., Zwarthoed, G.A.A.: 1996, *Astron. Astrophys. Suppl. Series*, **116**, 257.
Kaper, L.Henrichs, H.G., Fullerton, A.W., Ando, H., Bjorkman, K.S., Gies D.R., Hirata, R., Dambe, E., McDavid, D., Nichols, J.S.: 1997, *Astron. Astrophys.*, **327**, 281.
Kaper, L., Henrichs, H.F., Nichols, J.S., Telting, J.H.: 1999, *Astron. Astrophys.*, **344**, 231.
Kondo, Y., Modisette, J.L., Wolf, G.W.: 1975, *Astrophys. J.*, **199**, 110.
Kondo, Y., Modosette, J.L., Dufour, R.J., Whaley, R.S.: 1976a, *Astrophys. J.*, **206**, 163.
Kondo, Y., Morgan, T.H., Modosette, J.L.: 1976b, *Astrophys. J.*, **209**, 489.
Kondo, Y., Morgan, T.H., Modosette, J.L.: 1977, *Publ. Astron. Soc. Pacific*, **89**, 675.
Kriz, S., Harmanec, P.: 1975, *Bull. Astron. Inst. Czech*, **26**, 55.
Lamers, H.J.G.L.M., van der Hucht, K.A., Snijders, M.A.J., Sakhibullin, N.: 1973, *Astron. Astrophys.*, **25**, 105.
Lamers, H.J.G.L.M., Faraggiana, R., Burger, M.: 1980, *Astron. Astrophys.*, **82**, 48.
Lamers, H.J.G.L.M., Snow, T.P., de Jager, C., Langerwerf, A.: 1988, *Astrophys. J.*, **325**, 342.
Laskarides, P.G., Danezis, E., Theodossiou, E.: 1992, *Astrophys. J. Suppl. Series*, **179**, 13.
Markova, N.: 2000, *Astron. Astrophys. Suppl. Series*, **144**, 391.
Marlborough, J.M., Snow, T.P., Slettebak, A.: 1978, *Astrophys. J.*, **224**, 157.
McLaughlin, D.B.: 1961, *J. Roy. Astron. Soc. Canada*, **55**, 13 and 73.
Mihalas, D.: 1972, *Astrophys. J.*, **177**, 115.
Morgan, T.H., Kondo, Y., Modisette, J.L.: 1977, *Astrophys. J.*, **216**, 457.
Mullan, D.J.: 1984a, *Astrophys. J.*, **283**, 303.
Mullan, D.J.: 1984b, *Astrophys. J.*, **284**, 769.
Mullan, D.J.: 1986 *Astron. Astrophys.*, **165**, 157.
Poeckert, R., Marlborough, J.M.: 1978, *Astrophys. J.*, **220**, 940.
Prinja, R.K., Howarth, I.D.: 1988, *Mon. Not. Roy. Astron. Soc.*, **233**, 123.
Rivinius, Th., Stahl, O., Wolf, B., Kaufer, A., Gäng, Th., Gummersbach, C.A., Jankovics, I., Kovács, J., Mandel, H., Peitz.J., Szeifert, Th., Lamers, H.J.G.L.M.: 1997 *Astron. Astrophys.*, **318**, 819.
Sahade, J., Brandi, E., Fontela, J.M.: 1984, *Astron. Astrophys. Suppl. Series*, **56**, 17.
Sahade, J., Brandi, E.: 1985, *Rev. Mex.* **10**, 229.
Slettebak, A., Snow, T.P.: 1978, *Astrophys. J. Lett.*, **224**, L127.
Snijders, M.A.J., Lamers, H.J.G.L.M.: 1975, *Astron. Astrophys.*, **41**, 245.
Struve, O.: 1931, *Astrophys. J.*, **74**, 225.
Struve, O.: 1942, *Astrophys. J.*, **95**, 134.
Underhill, A.B.: 1970, in *Spectral Line Formation in Steady State Extended Atmospheres*, Ed. H.G. Groth and P. Wellman, Nat. Bureau of Standards, Washington, p. 3.
Underhill, A.B.: 1975, *Astrophys. J.*, **199**, 693.
Underhill, A.B., Fahey, R.P.: 1984, *Astrophys. J.*, **280**, 712.
Waldron, W.L., Klein, L., Altner B.: 1992, *ASP Conf. Series*, **22**, 181.

Publ. Astron. Obs. Belgrade No. 76 (2003), 43-44 *Invited lecture*

NON-THERMAL VELOCITY DISTRIBUTION FUNCTIONS IN THE INTERPLANETARY MEDIUM : ON THEIR ORIGIN AND CONSEQUENCES FOR THE SOLAR WIND ACCELERATION

M. MAKSIMOVIĆ

LESIA & CNRS, Paris Observatory, France
E-mail: Milan.Maksimovic@obspm.fr

Abstract. Non-thermal electron and ion velocity distribution is permanently observed in the solar wind. The exact origins of such departures from equilibrium Maxwell-Boltzmann distributions remain unclear. It is however believed that the rarity of Coulomb collisions in most of the extended corona and solar wind play a crucial role in the mechanisms which produce and/or maintain such distributions. In this lecture, we will summarize the various observations of those distributions and discuss their possible coronal origin and role in the Solar Wind acceleration processes.

Since the historical work by Parker (1958), numerous sophisticated models of the solar wind have been developed. The different acceleration mechanisms, the origin of the high-speed solar wind as well as the associated problem of the coronal heating have been recently reviewed in a full and comprehensive way by Cranmer (2002). However all the solar wind properties are still far from being well understood. The reason of this difficulty is that the solar wind is neither a collision-dominated medium nor a collisionless one. The Knudsen number K_n, which is defined as the ratio of the particle mean free path and the density scale height, is close to unity at the earth orbit. This means, that neither the hydrodynamic approach nor the pure collisionless one (also called exospheric) are fully appropriate to model solar wind expansion and explain its observed properties.

The classical fluid approach is applicable for the extreme regime where $K_n << 1$ which means that the medium is collision-dominated. In this case, the particle velocity distribution functions (VDFs) are Maxwellians as the medium is assumed to be at local thermodynamic equilibirum. The Euler or Navier-Stokes approximations are applicable resulting in a description of a thermally driven wind out of the hot solar corona. The problem with this approach is that the particle VDFs might well not be Maxwellians at the base of the solar wind. There is an increasing number of both theoretical (Vinas *et al.* 2000, Leubner 2002) and observational evidences (Esser & Edgard 2000) which tend to show that non thermal VDFs can develop and exist in the high corona or even in the transition region. The existence of such distributions could easily be understood through the fact that in a plasma the particle free paths increase rapidly with speed. As a consequence, high energy tails could naturally develop in the weakly collisional corona and solar wind acceleration region. Indeed, it is well known that the solar wind electron VDFs permanently exhibit non thermal tails that can be modelled by a classical halo Maxwellian population (Feldman *et al.* 1975) or by the power law part of a generalized Lorentzian or Kappa function

(Maksimovic *et al.* 1997b). In the frame of the fluid approach, which cannot explain the existence of suprathermal tails, the effect of non thermal VDFs on solar wind acceleration can be understood through the increase of the heat flux (Holweg *et al.* 1978, Olbert 1981).

Another way of taking into account the possible effects of coronal non thermal particle distributions is to adopt a kinetic approach. Among the various kinetic approaches for the solar wind, the simplest one is probably the exospheric one, which totally neglects binary collisions between particles over an altitude called the exobase. The first solar wind model of this type has been developed by Chamberlain (1960) by analogy to the evaporation of planetary atmospheres. This first exospheric model has resulted in a solar breeze, assuming that the radial expansion of the solar corona results from the thermal evaporation of the hot coronal protons out of the gravitational field of the Sun. The small solar wind speeds resulting are due to the use of the Pannekoek-Rosseland electrostatic potential which is based on the contradictory assumption of a hydrostatic equilibrium. The real electric potential is higher than the former one, assuming the quasi-neutrality of the plasma and a zero electric current. Models using this latter correction (Lemaire & Scherer 1971, Jockers 1970) have reproduced supersonic wind speeds, although not sufficent for explaining the high speed values of the fast wind.

More recently, Maksimovic *et al.* (1997a) have modelled the solar wind using the assumption that the velocity distribution function of the electrons in the corona, is a non-Maxwellian one, e.g. a generalized Lorentzian or Kappa function. Such non-Maxwellian functions containing suprathermal tails result in a higher electrostatic potential needed for zero charge and current, and therefore in larger terminal bulk speeds. This model yields a rather good description of main features of the solar wind giving densities and temperatures within the ranges observed at 1 AU. Its main advantage is the prediction of high speeds without unreasonably large coronal temperatures and without additional heating of the outer region of the corona, as needed in hydrodynamic models to achieve the same solar wind speed. More generally, the main advantage of exospheric models is that they exhibit clearly a driving mechanism for the solar wind, in this case the interplanetary electrostatic potential involving the only assumption of the VDF at the exobase.

In this lecture, we will review briefly the various solar wind models, summarize the relevant observations and discuss the possible processes for the Solar Wind acceleration.

References

Chamberlain, J.W.: 1960, *Astrophys. J.*, **131**, 47.
Cranmer, S.R.: 2002, *Space Sciences Rev.*, **101**, 229.
Esser, R., Edgar, R.J.: 2000, *Astrophys. J. Lett.* , **532**, L71.
Feldman, W.C., *et al.*: 1975, *J. Geophys. Research*, **80**, 4181.
Hollweg, J.V.: 1978, *Rev. Geophys. Space Phys.*, **16**, 689.
Jockers, K. : 1970, *Astron. Astrophys.*, **6**, 219.
Lemaire, J., and Scherer, M.: 1971, *J. Geophys. Research*, **76**, 7479.
Leubner, M.P.: 2002, *Astrophys. Space Sci.*, **282**, 573.
Maksimovic, M., Pierrard, V., Lemaire, J.F.: 1997a, *Astron. Astrophys.*, **324**, 725.
Maksimovic, M., Pierrard, V., Riley, P: 1997b, *Geophys. Research Lett.*, **24**, 1151.
Olbert, S.: 1981, *ESA SP-161*, 135.
Parker, E.N.: 1958, *Astrophys. J.*, **128**, 664.
Vinas, A.F., Wong, H.K., Klimas, A.J.: 2000, *Astrophys. J.*, **528**, 509.

Publ. Astron. Obs. Belgrade No. 76 (2003), 45 *Invited lecture*

MODELLING OF THE OPTICAL SPECTRUM OF ABSORPTION FOR THE NON IDEAL HYDROGEN OR QUASI-HYDROGEN PLASMA WITHIN CUT-OFF COULOMB POTENTIAL APPROXIMATION

A.A. MIHAJLOV, N.M. SAKAN

Institute of Physics, P.O. Box 57, 11001 Belgrade, Serbia and Montenegro

Abstract. The determination of optical as well as the transport characteristics of the highly ionized gaseous plasma in general always needs to take into account the effect of the inter-plasma electro-statical screening. The importance of the mentioned effect grows significantly with the enlargement of the gaseous plasma non-ideality, and becomes the most important factor in the case of extremely non ideal plasma. In this work is presented the method which enables us to take into account the effects of inter-plasma electro-statical screening in a rather direct manner. This is made possible with the application of the approximation where the electron scattering on the ions within the plasma is described by the cut-off Coulomb potential. The similar approximation was used before for the calculation of the transport characteristics of the highly ionized gaseous plasma. Here, the same approximation is used for the determination of the bound-free and free-free absorption coefficients of fully ionized hydrogen or quasi hydrogen gaseous plasma within the areas of electron densities and temperatures: $1 \cdot 10^{18} < Ne < 1 \cdot 10^{20}$ cm^{-3} and $15000 < T < 25000$ K.

Publ. Astron. Obs. Belgrade No. 76 (2003), 47 - 63 *Invited lecture*

ELECTRON AND ION CONTRIBUTIONS TO THE STARK BROADENING IN THE He I SPECTRUM

V. MILOSAVLJEVIĆ

Faculty of Physics, University of Belgrade, P.O.B. 368, Belgrade, Serbia
E–mail: vladimir@ff.bg.ac.yu

Abstract. Stark broadening parameters of seven (388.86, 447.15, 471.32, 501.56, 587.56, 667.82 and 706.52 nm) He I spectral line profiles have been measured at electron densities and electron temperatures between 0.3×10^{22} and 8.2×10^{22} m^{-3} and 8 000 and 33 000 K, respectively. He I spectral line profiles have been measured in plasmas created in five various discharge conditions using a linear, low–pressure, pulsed arc as an optically thin plasma source operated in a helium–nitrogen–oxygen gas mixture. The influence of electrons and ions to above mention He I spectral line shapes has been studied in this work. On the basis of the observed asymmetry of the line profiles, their ion broadening parameters (A) caused by influence of the ion microfield on the line broadening mechanism and also by the influence of the ion dynamic effect (D) on the line shape, the A and D parameters have been obtained. They represent the first data obtained experimentally by the use of the line profile deconvolution procedure. Stronger influence of the ion contribution to these He I line shapes has been found than the semiclassical theoretical approximation provides. This can be important for plasma modeling or diagnostics.

Also, on the basis of the precisely recorded He I line profiles the basic plasma parameters i.e. electron temperature (T) and electron density (N) have been obtained using the new line deconvolution procedure. The plasma parameters have been also measured using independent experimental diagnostical techniques. Excellent agreement was found among the two sets of the obtained parameters. This enables the deconvolution procedure to be recomended for plasma diagnostical purposes, especially in astrophysics where direct measurements of the plasma parameters (T and N) are not possible.

1. INTRODUCTION

Spectral line shapes represent important sources of information about the physical conditions in the place of birth of the radiation, especially since the launching of the Hubble space telescope. Many theoretical and experimental works have been devoted to the line shape investigations (Griem, 1964, 1974, 1997; Lesage and Fuhr, 1999; Konjević et al., 2002; NIST, 2003 and references therein). Among them a significant number is dedicated to the neutral helium (He I) spectral lines. Namely, after hydrogen, helium is the most abundant element in the universe. Helium atoms and ions are present in many kinds of cosmic light sources and their radiation is very useful for plasma diagnostical and modeling purposes. In spite of this special role have the 388.86 nm (2s ^{3}S$_1$ - 3p ^{3}P$^0_{2,1,0}$ transition), 447.15 nm (2p ^{3}P$^0_{2,1}$ - 4d

$^3D_{3,2,1}$ transition), 471.32 nm (2p $^3P^0_{2,1}$ - 4s $^3S_1$ transition), 501.56 nm (2s $^1S_0$ - 3p $^1P^0_1$ transition), 587.56 nm (2p $^3P^0_{2,1}$ - 3d $^3D_{3,2,1}$ transition), 667.82 nm (2p $^1P^0_1$ - 3d $^1D_2$ transition) and 706.52 nm He I (2p $^3P^0_{2,1}$ - 3s $^3S_1$ transition) neutral helium (He I) spectral lines. Recently, these lines have been used in various investigations of the radiation emitted by cosmic light sources like: white dwarfs, variables, supergiants and galaxies (Rupke et al., 2002; Bergeron and Liebert, 2002; Peimbert et al., 2002; Thuan et al., 2002; Bresolin et al., 2002; Benjamin et al., 2002; Drissen et al., 2001; Cuesta and Phillips, 2000). Also, Benjamin et al. (2002) have used some of these lines to investigate the radiative transfer effects for a spherically symmetric nebula with no systematic velocity gradients. Izotov et al. (2001) used some of these lines to derive the ^{4}He abundance in the Metal-deficient Blue Compact Dwarf Galaxies Tol 1214-277 and Tol 65[1], too. Special role has the 667.82 nm line, which is in the work by Harvin et al. (2002) used to investigate the physical properties of the Massive Compact Binary in the Triple Star System HD 36486 (δ Orionis A). The 587.56 nm spectral line has been used by Labrosse and Gouttebroze (2001) to estimate the formation of the helium spectrum in solar quiescent prominences and, also, by Muglach and Schmidt (2001) to determine the height and dynamics of the quiet solar chromosphere at the limb. The 706.52 nm line was used for various astrophysical investigations (see Branch et al., 2002; Fransson et al., 2002; Vázquez et al., 2002; Webb et al., 2002). Therefore, the use of these He I spectral lines for diagnostical purposes in astrophysics implies the knowledge of their line profile characteristics.

In plasmas with electron densities (N) higher than $10^{21}\,\mathrm{m}^{-3}$, where the Stark effect begins to play an important role by the He I spectral lines broadening, the knowledge of the Stark broadening characteristics is necessary. A significant number of theoretical and experimental studies are devoted to the He I Stark FWHM (full-width at half intensity maximum, W) investigations (Lesage and Fuhr, 1999 and references therein). The aim of this work is to present measured Stark broadening parameters of the mentioned He I spectral lines at (8 000 - 33 000) K electron temperatures (T) and at electron densities of (0.3 - 8.2)$\times 10^{22}\mathrm{m}^{-3}$. The T-values used are typical of many cosmic light sources. Using a deconvolution procedure, described in Milosavljević and Poparić (2001) and already applied in the case of some He I, Ne I, Ar I and Kr I lines (Milosavljević and Djeniže, 2002abc, 2003ab), on the basis of the observed line profile asymmetry, the characteristics of the ion contribution to the total Stark FWHM (W_t) expressed in term of the ion contribution parameter (A) and ion–dynamic effect (D) (Griem, 1974; Bassalo et al., 1982; Barnard et al., 1974) have been obtained. The separate electron (W_e) and ion (W_i) contributions to the total Stark width (W_t) of the He I spectral line have also been obtained. As an optically thin plasma source we have used the linear, low-pressure, pulsed arc operated in five various discharge conditions. The W_t, W_e, W_i and A values have been compared to all available theoretical and experimental Stark broadening parameters.

On the basis of the precisely recorded He I line shapes, the basic plasma parameters i.e. electron temperature (T^D) and electron density (N^D) have also been obtained. To the knowledge of this author, the results of the T and N values are the first published data obtained directly from the line deconvolution procedure. Plasma parameters have been also measured (T^{exp} and N^{exp}) using independent, well–known, experimental diagnostical techniques. Excellent agreement was found among the two sets of the obtained parameters (T^D and T^{exp}; and N^D and N^{exp}) making it justified to

recommend our deconvolution procedure for plasma diagnostical purposes, especially in astrophysics where direct measurements of the plasma parameters (T and N) are not possible.

2. THEORETICAL BACKGROUND

The total line Stark FWHM (W_t) is given as

$$W_t = W_e + W_i, \tag{1}$$

where W_e and W_i are the electron and ion contributions, respectively. For a non–hydrogenic, isolated neutral atom line the ion broadening is not negligible and the line profiles are described by an asymmetric K function (see Eq. (6) in Chapter 3 and in Milosavljević and Poparić, 2001). The total Stark width (W_t) may be calculated (Griem, 1974; Kelleher, 1981; Barnard et al., 1974) from the equation:

$$W_t \approx W_e[1 + 1.75AD(1 - 0.75R)], \tag{2}$$

$$\text{where} \qquad R = \sqrt[6]{\frac{36 \cdot \pi \cdot e^6 \cdot N}{(kT)^3}}, \tag{3}$$

is the ratio of the mean ion separation to the Debye length. N and T represent electron density and temperature, respectively. A is the quasi–static ion broadening parameter (see Eq. (224) in Griem, 1974) and D is a coefficient of the ion-dynamic contribution with the established criterion:

$$D = \frac{1.36}{1.75 \cdot (1 - 0.75 \cdot R)} \cdot B^{-1/3} \qquad \text{for} \qquad B < (\frac{1.36}{1.75 \cdot (1 - 0.75 \cdot R)})^3;$$

$$\text{or} \qquad D = 1 \qquad \text{for} \qquad B \geq (\frac{1.36}{1.75 \cdot (1 - 0.75 \cdot R)})^3, \tag{4}$$

$$\text{where} \qquad B = A^{1/3} \cdot \frac{4.03 \cdot 10^{-7} \cdot W_e[nm]}{(\lambda[nm])^2} \cdot (N[m^{-3}])^{2/3} \cdot \sqrt{\frac{\mu}{T_g[K]}} < 1; \tag{5}$$

is the factor with atom-ion perturber reduced mass μ (in amu) and gas temperature T_g. When D = 1 the influence of the ion–dynamic is negligible and the line shape is treated using the quasi–static ion approximation. From Eqs. (1-6) it is possible to obtain the plasma parameters (N and T) and the line broadening characteristics (W_t, W_e, W_i, A and D). One can see that the ion contribution, expressed in terms of the A and D parameters directly determines the ion width (W_i) component in the total Stark width (Eqs. (1) and (2)).

3. NUMERICAL PROCEDURE FOR DECONVOLUTION

The proposed functions for various line shapes, Eq. (6) are of the integral form and include several parameters. Some of these parameters can be determined in separate experiments, but not all of them. Furthermore, it is impossible to find an analytical solution for the integrals and methods of numerical integration have to be applied. This procedure, combined with the simultaneous fitting of several free parameters, causes the deconvolution to be an extremely difficult task and requires a number of computer supported mathematical techniques. Particular problems are the questions of convergence and reliability of the deconvolution procedure, which are tightly connected with the quality of experimental data.

$$K(\lambda) = K_o + K_{\max} \int_{-\infty}^{\infty} exp(-t^2) \cdot$$

$$[\int_0^{\infty} \frac{\mathrm{H_R}(\beta)}{1 + (2\frac{\lambda - \lambda_o - \frac{W_G}{2\sqrt{\ln 2}} \cdot t}{W_e} - \alpha \cdot \beta^2)^2} \cdot d\beta] \cdot dt. \qquad (6)$$

Here K_o is the baseline (offset) and $K_{\max}$ is the maximum of intensity (intensity for λ=λ_o) (Milosavljević and Poparić, 2001). $H_R(\beta)$ is an electric microfield strength distribution function of normalized field strength β=F/F_o, where F_o is the Holtsmark field strength. A (α=$A^{4/3}$) is the static ion broadening parameter and is a measure of the relative importance of ion and electron broadenings. R is the ratio of the mean distance between the ions to the Debye radius (see Eq. 3), i.e. the Debye shielding parameter and W_e is the electron width (FWHM) in the $j_{A,R}$ profile (Griem, 1974).

For the purpose of deconvolution iteration process we need to know the value of K (Eq. (6)) as a function of λ for every group of parameters (K_{max}, λ_o, W_e, W_G, R, A). W_G is defined in Eq.(2.3) in Milosavljević and Poparić (2001). The used numerical procedure for the solution of Eq. (6) is described in earlier publications Milosavljević and Poparić (2001), Milosavljević (2001) and Milosavljević et al. (2002abc). It should be noted that the application of a deconvolution and fitting method requires some assumptions or prior knowledge about plasma condition. Accordingly, for each emitter ionization stage one needs to know the electric microfield distribution, in order to fit the K functions. In the cases of quasi–static or quasi–static and dynamic broadening, our fitting procedure gives the electron impact width (W_e), static ion broadening parameter (A) and, finally dynamic ion broadening parameter (D).

4. EXPERIMENT

The modified version of the linear low–pressure pulsed arc (Milosavljević et al., 2002abc; Milosavljević, 2001; Milosavljević et al., 2000, 2001; Djeniže et al., 1998, 2001, 2002ab) has been used as a plasma source. A pulsed discharge was driven in a pyrex discharge tube at different inner diameters and plasma lengths. Various dimensions of the discharge tube offer the possibility of the electron temperature variation in a wide range. The working gas was helium - nitrogen - oxygen mixture (90% He + 8% N_2 + 2% O_2). The used tube geometry and corresponding discharge conditions are presented in Table. 1.

Table 1: Various discharge conditions. C-bank capacity (in μF), U-bank voltage (in kV), H-plasma length (in cm), Φ-tube diameter (in mm), P-filling pressure (in Pa). N^{exp} (in $10^{22}m^{-3}$) and T^{exp} (in 10^3K) denotes measured electron density and temperature, respectively, obtained at a 25^{th} μs for index 1 and at a 120^{th} μs for index 2 after the beginning of the discharge when the line profiles were analyzed. N_1^D (in $10^{22}m^{-3}$) and T_1^D (in 10^3K) are values obtained using line deconvolution procedure at a 25^{th} μs.

Exp.	C	U	H	Φ	P	N_1^{exp}	N_1^D	N_2^{exp}	T_1^{exp}	T_1^D	T_2^{exp}
a	8	4.5	6.2	5	267	6.1	5.4	0.7	33.0	31.4	16.0
b_1	14	4.2	14.0	25	267	8.2	7.5	0.9	31.5	30.5	14.5
b_2	14	3.4	14.0	25	267	6.7	6.9	0.8	30.0	30.2	14.0
b_3	14	2.6	14.0	25	267	4.4	4.0	0.3	28.0	27.1	12.5
b_4	14	1.5	7.2	5	133	5.0	4.9	0.6	18.0	17.6	8.0

Spectroscopic observation of spectral lines was made end-on along the axis of the discharge tube.

The line profiles were recorded by a step-by-step technique using a photomultiplier (EMI 9789 QB and EMI 9659B) and a grating spectrograph (Zeiss PGS-2, reciprocal linear dispersion 0.73 nm/mm in the first order) system. The instrumental FWHM of 8 pm was obtained by using narrow spectral lines emitted by the hollow cathode discharge. The spectrograph exit slit (10 μm) with the calibrated photomultipliers was micrometrically traversed along the spectral plane in small wavelength steps (7.3 pm). The averaged photomultiplier signal (five shots in each position) was digitized using an oscilloscope, interfaced to a computer. A sample output, is shown in Figs. 1 and 2.

Plasma reproducibility was monitored by the He I (501.5 nm, 388.8 nm and 587.6 nm) lines radiation and, also, by the discharge current using Rogowski coil signal (it was found to be within $\pm$5%).

The used deconvolution procedure in its details is described in Milosavljević and Poparić (2001) and Milosavljević (2001) and, briefly in Chapter 3. The measured profiles were convoluted due to the convolutions of the Lorentzian Stark and Gaussian profiles caused by Doppler and instrumental broadenings (Griem, 1974). Van der Waals and resonance broadenings (Griem, 1974) were estimated to be smaller by more than an order of magnitude in comparison to Stark, Doppler and instrumental broadenings. The deconvolution procedure was computed using the least Chi–square function (see Chapter 3).

The plasma parameters were determined using standard diagnostics methods. Thus, the electron temperature was determined from the ratios of the relative line intensities of four N III spectral lines (409.74 nm, 410.34 nm, 463.42 nm and 464.06 nm) to the 463.05 nm N II spectral line with an estimated error of $\pm$10 %, assuming the existence of the LTE (Griem, 1974). All the necessary atomic data have been taken from NIST (2003) and Glenzer et al. (1994). The electron density decay was measured using a well-known single wavelength He–Ne laser interferometer technique for the 632.8 nm transition with an estimated error of $\pm$9%. The experimental elec-

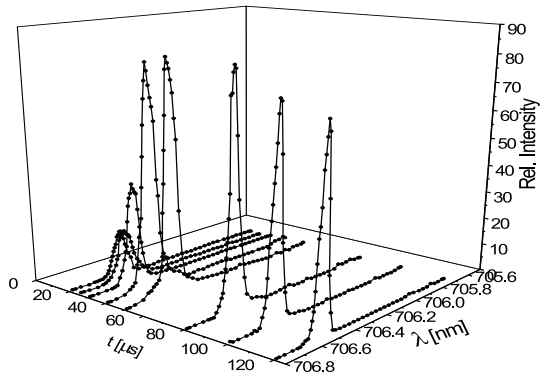

Fig. 1: Temporal evolution of the 706.52 nm He I line profile recorded under discharge conditions C=14μF and U=1.5 kV (see Table 1).

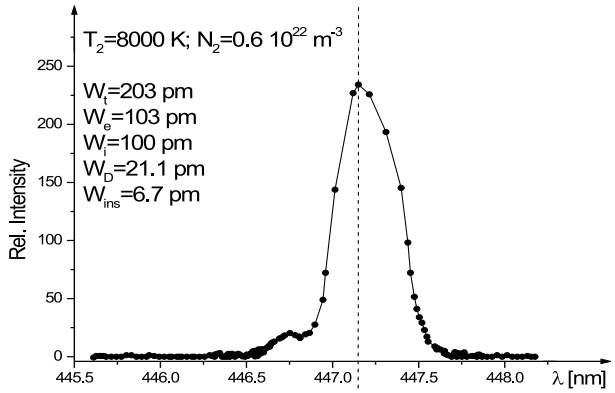

Fig. 2: Recorded profile of the 447.15 nm line at a given T and N. $W_{\rm t}$, $W_{\rm e}$, $W_{\rm i}$, $W_{\rm D}$, $W_{\rm ins}$, represents total, electron and ion Stark width, Doppler and instrumental width, respectively.

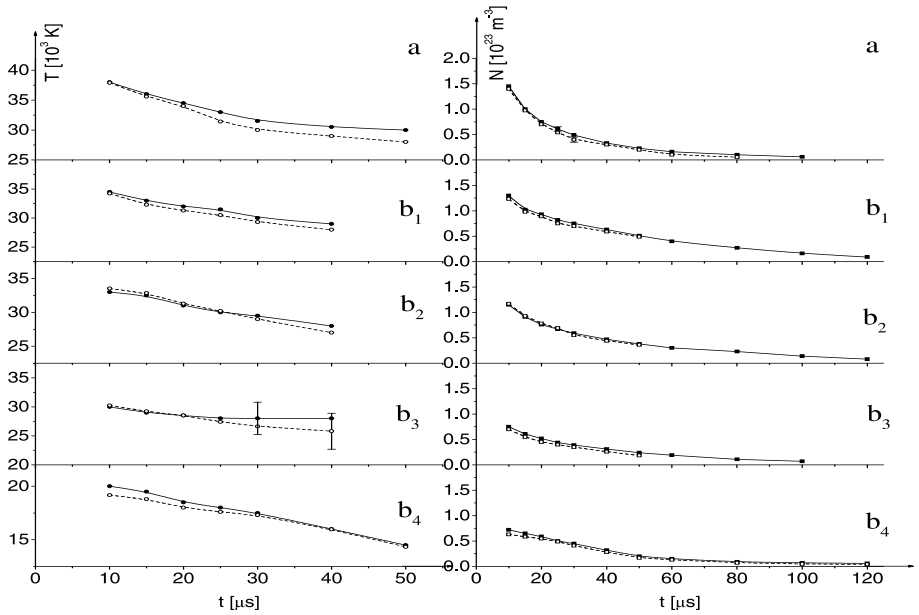

Fig. 3: Electron temperature (T) and density (N) decays. Full lines represent measured data using independent experimental techniques. Dashed lines represent plasma parameters obtained using our line deconvolution procedure in various plasmas (see Table 1). Error bars, indicated only in the case of the greatest disagreement (T in b_3), represent estimated accuracies of the measurements ($\pm 10\%$) and deconvolutions ($\pm 12\%$).

tron densities (N^{exp}) and temperatures (T^{exp}), obtained at the moment when the line profiles were analyzed, are presented in Table 1 together with the N^D and T^D values obtained from deconvolution procedures.

5. RESULTS AND DISCUSSION

The measured N^{exp} and T^{exp} decays are presented in Fig. 3 together with the N^D and T^D values obtained using the line profile deconvolution procedure, as an example for the 706.52 nm He I line. One can conclude that the agreement among N^{exp} and N^D values is excellent (within 4% on the average in the investigated five plasmas). This fact confirms the homogeneity of plasmas in the linear part of our light source (Fig. 1 in Djeniže et al., 1998). In the case of the electron temperature the situation is similar but the agreement among the two sets of the electron temperature decays is poorer. This can be explained taking into account the nature of the applied method of the measurement of the electron temperature. Namely, it should be remarked that the uncertainty of the used experimental method (Saha equation) depends on the existence of the LTE during the plasma decay. Existence of the LTE is estimated in the phases of the plasma decay when the electron concentration fulfills the criterion of the existence of the LTE (Griem, 1974, 1997). In our experiment N II and N III energy level (used in the Saha equation) populations remain in the LTE up to 50 μs after the beginning of the discharge (in all experiments). After this moment the Saha equation gives unreliable results. Within the experimental accuracy ($\pm$10%) of the electron temperature measurements and the uncertainties ($\pm$12%) of the T^D values obtained using the line deconvolution procedure, the T^{exp} and T^D values mutually agree up to 50 μs after the beginning of the discharge confirming our estimations about the existence of the LTE. This statement also confirms the homogeneity of the created plasmas.

The plasma broadening parameters (W_t, W_e, W_i, A, D) obtained by our deconvolution procedure of the recorded line profiles at a measured N and T values are presented in Tables 2 and 3 together with other authors' results. Various theoretical (G, BCW, DSB) predictions of the W_e, W_i, and A are also given. By the normalization of the A^G and A^{BCW} values to our electron density the well known $N^{1/4}$ numerical factor (Griem, 1974) was used.

In order to make the comparison among measured (W_t^{exp}) and calculated (W_t^{th}) total (electron + ion) width values easier, the W_t^{exp}/W_t^{th} dependence on the electron temperature is presented graphically in Figs. 4 - 10 for the investigated lines.

The W_t^G (Griem, 1974) and W_t^{BCW} (Bassalo et al., 1982) values are calculated using Eq. (226) from Griem (1974) with the W_e and A values predicted by the G (Griem, 1974) and BCW (Bassalo et al., 1982) theoretical approaches, respectively. The W_t^{exp}/W_t^{th} ratios related to the Dimitrijević and Sahal – Bréchot (1990) data have been calculated only for our experimental values. Namely, for the W_i^{DSB} calculations it is necessary to know the helium ion concentration connected to the plasma composition. We have performed this for our discharge conditions only.

It turns out that our W_e^{exp} and W_i^{exp} are the first separated experimental electron and ion Stark width data obtained by using the deconvolution procedure (Milosavljević and Poparić, 2001). The broadening parameter (W_t^{exp}) represents the first measured value at electron densities higher than 10^{22} m^{-3}. W_e^{exp} data are smaller than the G, BCW and DSB approximations yield for the three investigated lines (388.86,

Table 2: Line Broadening characteristics. Measured: total Stark FWHM (W_t^{exp} in pm within ±12% accuracy), electron and ion (He^+) Stark widths (W_e^{exp} and W_i^{exp} in pm within ±12% accuracy), quasistatic ion broadening parameter (A^{exp}, dimensionless within ±15% accuracy) and ion dynamic coefficient (D^{exp}, dimensionless within ±20% accuracy) at measured electron temperatures (T^{exp} in 10^3 K) and electron densities (N^{exp} in $10^{22}m^{-3}$). Ref presents: Tw, this work; RS, Roder and Stampa (1964); K, Kelleher (1981); SK, Solwitsch and Kusch (1979); B, Berg et al. (1962); W, Wulff (1958); Ku, Kusch (1971); KK, Kobilarov et al. (1989); Gr, Griem et al. (1962); ES, Einfeld and Sauerbrey (1976); C, Chaing et al. (1977); L, Lincke (1964); GJ, Greig and Jones (1970); BR, Bötticher et al. (1963); P, Pérez et al. (1991); M, Mijatović et al. (1995); MS, Mazing and Slemzin (1973); PL, Purić et al. (1970); BG, Büscher et al. (1995); Ga, Gauthier et al. (1981); VK, Vujičić and Kobilarov (1988). The indexes G, BCW and DSB denote theoretical data taken from Griem (1974), Bassalo et al. (1982) and Dimitrijević and Sahal – Bréchot (1990), respectively at a given T and N. The wavelengths (i.e. 5876, 6678 and 4472) are given in 10^{-10} m.

T^{exp}	N^{exp}	W_t^{exp}	W_e^{exp}	W_i^{exp}	A^{exp}	D^{exp}	Ref.	W_e^G	W_e^{BCW}	W_e^{DSB}	W_i^{DSB}	A^G	A^{BCW}
							5876						
33.0	6.1	210	172	38	0.163	1.46	Tw	215	156	183	42	0.093	0.118
31.5	8.2	268	218	50	0.176	1.40	Tw	289	213	246	55	0.100	0.127
30.0	6.7	218	179	39	0.167	1.46	Tw	237	175	201	45	0.095	0.120
28.0	4.4	151	126	25	0.150	1.57	Tw	155	117	132	29	0.086	0.108
18.0	5.0	150	126	24	0.156	1.60	Tw	176	134	150	31	0.088	0.108
20.9	1.03	39					K						
45.0	15.9	550					B						
31.0	5.4	200					KK						
16.5	1.7				0.05*		RS						
3.70	2.25	91					PL						
52.0	10.2	3160					BG						
							6678						
33.0	6.1	481	298	183	0.459	1.18	Tw	397	345	358	170	0.282	0.309
31.5	8.2	628	370	258	0.498	1.12	Tw	533	467	502	226	0.300	0.328
30.0	6.7	512	315	197	0.474	1.17	Tw	439	389	402	181	0.282	0.306
28.0	4.4	337	216	121	0.420	1.27	Tw	290	257	266	117	0.252	0.265
18.0	5.0	361	240	121	0.413	1.26	Tw	358	323	323	124	0.249	0.271
20.9	1.03	98					K						
30.1	3.2	231					P						
19.3	0.25	22					M						
20.0	10.0	960					Ga						
26.0	7.1	620					VK						
							4472						
16.0	0.7	237	106	131	0.917	1.0	Tw	162	150	140	113	0.636	0.668
14.5	0.9	316	145	171	0.911	1.0	Tw	212	200	185	142	0.668	0.704
14.0	0.8	258	120	138	0.883	1.0	Tw	190	180	165	125	0.642	0.675
12.5	0.3	101	48	53	0.806	1.03	Tw	73	69	63	45	0.491	0.517
8.0	0.6	203	103	100	0.825	1.0	Tw	155	147	134	82	0.554	0.574
20.9	1.03	109					K						
20.0	13	4500					B						

Table 3: Same as in Table 2. The wavelengths (i.e. 3889, 5016, 7065 and 4713) are given in 10^{-10} m.

T^{exp}	N^{exp}	W_t^{exp}	W_e^{exp}	W_i^{exp}	A^{exp}	D^{exp}	Ref.	W_e^G	W_e^{BCW}	W_e^{DSB}	W_i^{DSB}	A^G	A^{BCW}
							3889						
33.0	6.1	139	110	29	0.196	1.26	Tw	143	120	116	28	0.105	0.119
31.5	8.2	185	145	40	0.212	1.19	Tw	192	162	155	37	0.113	0.128
30.0	6.7	149	118	31	0.202	1.25	Tw	157	132	126	30	0.108	0.122
28.0	4.4	96	78	18	0.181	1.37	Tw	103	87	82	15	0.097	0.110
18.0	5.0	103	83	20	0.190	1.37	Tw	116	97	90	21	0.101	0.114
15.0	0.72				0.04*		RS						
20.9	1.03	24					K						
20.0	6.7	170					SK						
26.0	15.0	450					B						
30.0	3.2	73					W						
18.0	0.8	33					Ku						
36.0	6.1	151					KK						
30.0	2.7	74					Gr						
							5016						
33.0	6.1	452	279	173	0.460	1.0	Tw	384	354	336	134	0.277	0.293
31.5	8.2	602	365	237	0.496	1.0	Tw	518	481	453	179	0.295	0.314
30.0	6.7	481	294	187	0.486	1.0	Tw	427	395	372	145	0.279	0.296
28.0	4.4	312	198	114	0.433	1.08	Tw	282	262	246	95	0.249	0.265
18.0	5.0	332	218	114	0.427	1.07	Tw	340	315	289	100	0.252	0.263
14.1	0.38				0.14*		RS						
20.9	1.03	85					K						
20.0	6.7	54					SK						
24.0	16.5	1300					B						
30.0	3.2	190					W						
26.0	4.6	75					Ku						
30.0	2.3	182					Gr						
38.0	3.6	290					ES						
17.4	10.5	960					C						
22.7	9.3	720					L						
25.0	2.7	277					GJ						
16.9	2.0	160					BR						
30.15	3.23	237					P						
23.6	0.59	47					M						
							7065						
33.0	6.1	281	234	47	0.148	1.51	Tw	307	273	224	46	0.082	0.089
31.5	8.2	372	307	65	0.160	1.42	Tw	411	361	298	58	0.089	0.099
30.0	6.7	300	250	50	0.152	1.49	Tw	333	292	241	51	0.085	0.094
28.0	4.4	190	161	29	0.136	1.65	Tw	217	190	156	29	0.077	0.085
18.0	5.0	211	179	32	0.145	1.62	Tw	232	203	171	26	0.083	0.092
20.9	1.03	47			0.031*	2.33*	K						
21.4	0.34	17					M						
22.7	0.45	22					M						
23.6	0.59	29					M						
34.8	1.0	51					MS						
							4713						
33.0	6.1	542	371	171	0.343	1.0	Tw	554	483	398	95	0.146	0.162
31.5	8.2	713	481	232	0.368	1.0	Tw	740	648	533	125	0.157	0.175
30.0	6.7	595	407	188	0.352	1.0	Tw	603	528	430	99	0.150	0.166
28.0	4.4	372	261	111	0.317	1.0	Tw	394	341	281	65	0.136	0.151
18.0	5.0	403	286	117	0.335	1.0	Tw	428	370	319	69	0.142	0.161
16.5	1.7				0.20*		RS						
20.9	1.03	96					K						
20.0	13.0	1400					B						
30.0	2.6	300					Gr						
22.7	9.3	91					L						
30.2	3.23	295					P						
19.3	0.25	23					M						

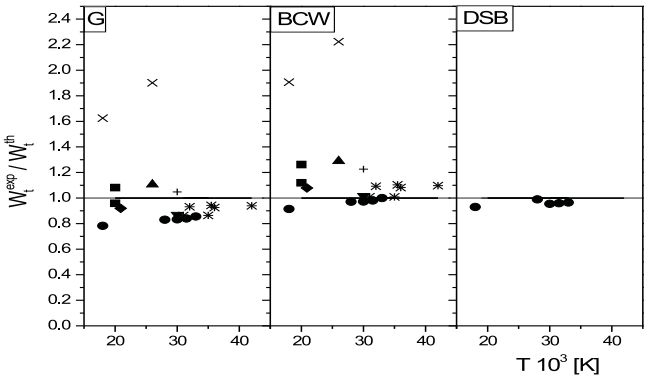

Fig. 4: Ratios of the experimental total Stark FWHM (W_t^{exp}) to the various theoretical (W_t^{th}) predictions vs. electron temperature for the He I 388.86 nm line. •, +, ♦, ■, ▲, ▼, × and ∗ represent our experimental data and those from Griem et al. (1962), Kelleher (1981), Solwitsch and Kusch (1979), Berg et al. (1962), Wulff (1958), Kusch (1971) and Kobilarov et al. (1989), respectively. G, BCW and DSB represent the ratios related to the theories taken from Griem (1974), Bassalo et al. (1982) and Dimitrijević and Sahal – Bréchot (1990), respectively.

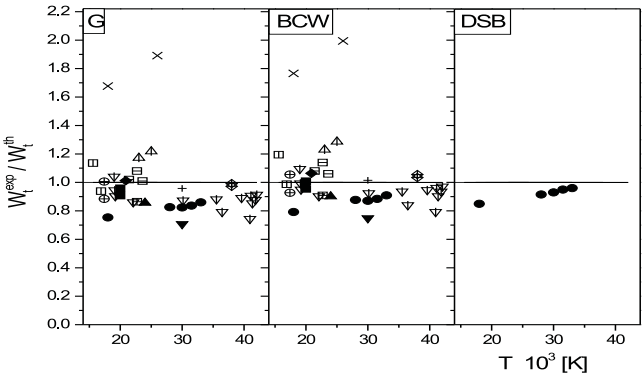

Fig. 5: Ratios of the experimental total Stark FWHM (W_t^{exp}) to the various theoretical (W_t^{th}) predictions vs. electron temperature for the 501.56 nm He I line. •, +, ♦, ■, ▲, ▼, ×, ⌖, ⊕, ⊞, ⧋, ⧈, ⧩ and ⊟ represent our experimental data and those from Griem et al. (1962), Kelleher (1981), Solwitsch and Kusch (1979), Berg et al. (1962), Wulff (1958), Kusch (1971), Einfeld and Sauerbrey (1976), Chaing et al. (1977), Lincke (1964), Greig and Jones (1970), Bötticher et al. (1963), Pérez et al. (1991) and Mijatović et al. (1995), respectively. G, BCW and DSB represent the ratios related to the theories taken from Griem (1974), Bassalo et al. (1982) and Dimitrijević and Sahal – Bréchot (1990), respectively.

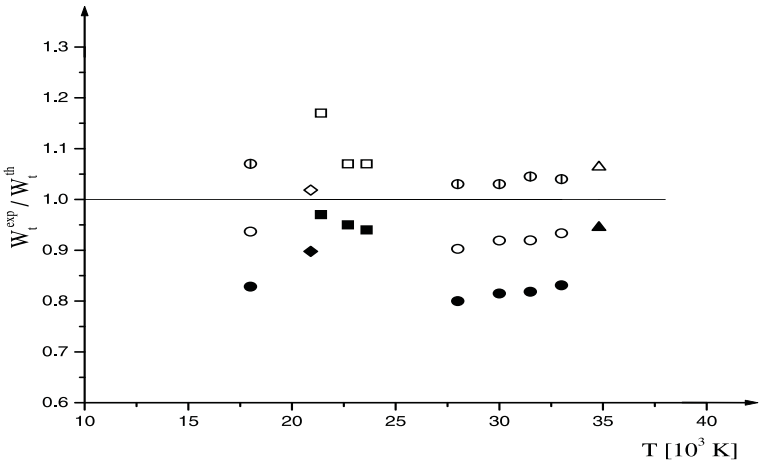

Fig. 6: Ratios of the experimental total Stark FWHM (W_t^{exp}) to the various theoretical (W_t^{th}) predictions vs. electron temperature for the He I 706.52 nm line. Circle, diamond, triangle and square represent our experimental data and those from Kelleher (1981), Mazing and Slemzin (1973) and Mijatović et al. (1995), respectively. Filled, empty and half divided symbols represent the ratios related to the theories taken from Griem (1974), Bassalo et al. (1982) and Dimitrijević and Sahal – Bréchot (1990), respectively.

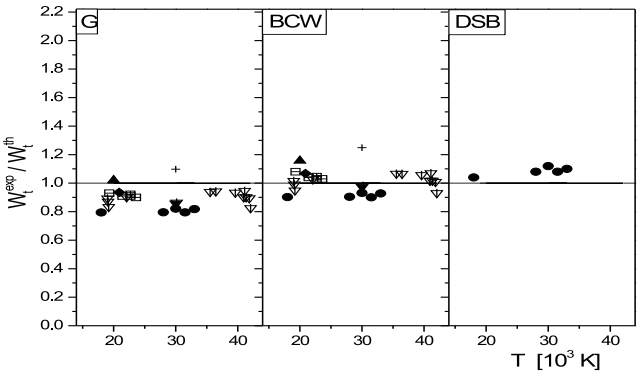

Fig. 7: Ratios of the experimental total Stark FWHM (W_t^{exp}) to the various theoretical (W_t^{th}) predictions vs. electron temperature for the He I 471.32 nm line. •, +, ♦, ▲, ▼, ⊞, ⍒ and ⊟ represent our experimental data and those from Griem et al. (1962), Kelleher (1981), Berg et al. (1962), Wulff (1958), Lincke (1964), Pérez et al. (1991) and Mijatović et al. (1995), respectively. G, BCW and DSB represent the ratios related to the theories taken from Griem (1974), Bassalo et al. (1982) and Dimitrijević and Sahal – Bréchot (1990), respectively.

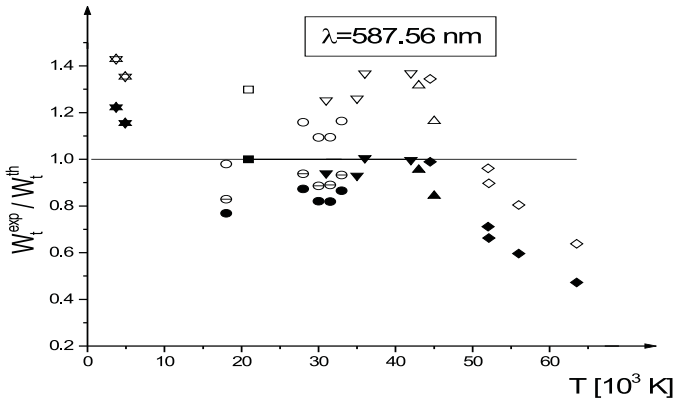

Fig. 8: Ratios of the experimental total Stark FWHM (W_t^{exp}) to the various theoretical (W_t^{th}) predictions vs. electron temperature for the He I λ= 587.56 nm. ◯, ♢, ∇, △, □ and ✡ represent our experimental data and those from Büscher et al. (1995), Kobilarov et al. (1989), Berg et al. (1962), Kelleher (1981), and Purić et al. (1970), respectively. Filled, empty and half divided symbols represent the ratios related to the theories taken from Griem (1974), Bassalo et al. (1982) and Dimitrijević and Sahal – Bréchot (1990), respectively.

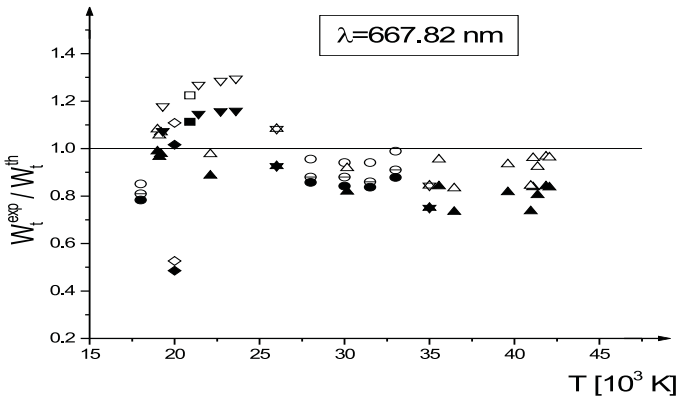

Fig. 9: Ratios of the experimental total Stark FWHM (W_t^{exp}) to the various theoretical (W_t^{th}) predictions vs. electron temperature for the He I λ= 667.82 nm. ◯, ♢, ∇, △, □ and ✡ represent our experimental data and those from Gauthier et al. (1981), Mijatović et al. (1995), Pérez et al. (1991), Kelleher (1981), and Vujičić and Kobilarov (1988), respectively. Filled, empty and half divided symbols represent the ratios related to the theories taken from Griem (1974), Bassalo et al. (1982) and Dimitrijević and Sahal – Bréchot (1990), respectively.

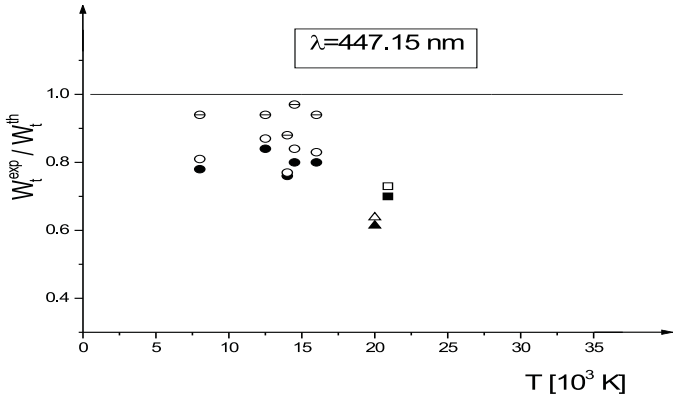

Fig. 10: Ratios of the experimental total Stark FWHM ($W_{\rm t}^{\rm exp}$) to the various theoretical ($W_{\rm t}^{\rm th}$) predictions vs. electron temperature for the He I λ= 447.15 nm. ◯, △ and □ represent our experimental data and those from Berg et al. (1962) and Kelleher (1981), respectively. Filled, empty and half divided symbols represent the ratios related to the theories taken from Griem (1974), Bassalo et al. (1982) and Dimitrijević and Sahal – Bréchot (1990), respectively.

501.56 and 471.32 nm). The highest disagreement was found with the 501.56 nm line. It this case W_e^{exp} lie 27% below W_e^G and about 20% below W_e^{BCW} and W_e^{DSB} values. Approximations BCW and DSB yield smaller W_e values than the G approximation. In the case of the 388.86 nm line the W_e^{exp} and W_e^{DSB} values show a tolerable mutual agreement (within ±16%). They are in excellent agreement (within ±4%) with W_e^{DSB} and (within ±8%) with W_i^{DSB} (Dimitrijević and Sahal – Bréchot, 1990) values for the 706.52 nm spectral line. Theoretical W_e^G (Griem, 1974) and W_e^{BCW} (Bassalo et al., 1982) values are higher than ours by about 33% and 17% (on the average), respectively, for this line. The $W_{\rm e}^{\rm exp}$ results are smaller than the G approximation for the other three investigated lines (447.15, 587.56 and 667.82 nm). The greatest disagreement was found for the 447.15 nm line. It amounts to about 53%. The other two approximations (BCW and DSB), in the case of the 667.82 nm and 447.15 nm lines, yield smaller $W_{\rm e}$ values than the G approximation, but they are also higher than ours. For the 587.56 nm line the $W_{\rm e}^{\rm exp}$, $W_{\rm e}^{\rm BCW}$ and $W_{\rm e}^{\rm DSB}$ values show a reasonable mutual agreement (within ±12% experimental accuracy). This indicated that the $W_{\rm e}$ values calculated by Freudenstein and Cooper (1978) and Dimitrijević and Konjević (1986), for the 667.82 nm line, exceed all other $W_{\rm e}$ data presented in Table 2.

By the inspection of Figs. 4–10 one can conclude that Griem's (1974) W_t values lie above most of the experimental values and also above BCW and DSB theoretical data. This is well evident in the case of the 471.32 nm line (see Fig. 7). Theoretical W_t values presented by Bassalo et al. (1982) lie about 10% - 15% below Griem's values. The W_t values ($W_e + W_i$) presented by Dimitrijević and Sahal – Bréchot (1990) agree with the (W_t^{exp}) within 3% - 10% (on the average) with the best agreement in the case of the 388.86 nm line (see Fig. 4). It should be pointed out that experimental

W_t^{exp} values are smaller than the G, BCW and DSB theories yield in the case of the 501.56 nm spectral line at electron temperatures higher than 25000 K (see Fig. 5). Experimental total half–widths of the 706.52 nm, including ours, agree well (within ± 10%) with calculated values from Bassalo et al. (1982). Our W_t^{exp} agree excellently with W_t^{DSB} from Dimitrijević and Sahal – Bréchot (1990) (see Figure 6). It turns out that our W_i^{exp}/W_t^{exp} (16% on the average) agree exellently with W_i^{DSB}/W_t^{DSB} (also 16% on the average) theoretical values (Dimitrijević and Sahal – Bréchot, 1990) for the 706.52 nm spectral line. This is clear in the case of the 667.82 nm line at higher electron temperatures (see Fig. 9). Theoretical W_t values presented by Bassalo et al. (1982) lie about 10% - 30% below Griem's values. The W_t values ($W_e + W_i$) presented by Dimitrijević and Sahal – Bréchot (1990) agree with ours (W_t^{exp}) to within 3% – 18% with the best agreement for the 447.15 nm line (see Fig. 10).

This constitutes evident contribution of the ion influence to the line broadening due to the quasi–static ion and ion–dynamic effects. The A^{exp} values are the first data obtained directly by the use of the line deconvolution procedure. They are higher than the G and BCW approaches provide at about: 87% and 67% (for 388.86 nm line), 135% and 110% (for 471.32 nm line), 70% and 61% (for 501.56 nm line), respectively. It has been found that the ion dynamic effect, expressed due to the D coefficient is negligible ($D \simeq 1$) by our plasma parameters and plasma composition for the 471.32 nm and 501.56 nm lines. In the case of the 388.86 nm line the ion dynamic effect is relatively small ($D \simeq 1.3$). It should be pointed out that we have found good agreement between our W_i^{exp}/W_t^{exp} and theoretical W_i^{DSB}/W_t^{DSB} (Dimitrijević and Sahal – Bréchot, 1990) ratio values only in the case of the 388.86 nm (within 10%, on the average). This agreement is within estimated experimental accuracies (± 12%) of the W_i^{exp} and W_t^{exp} values. In the case of the 471.32 nm and 501.56 nm lines, we have found W_i^{exp}/W_t^{exp} values that overvalue W_i^{DSB}/W_t^{DSB} data by about 65% and 35%, respectively. One can conclude that the ion contribution to the total line width plays a more important role than the G, BCW and DSB approximations provide, especially in the case of the 471.32 nm and 501.56 nm lines. The quasi–static ion effect is higher than the G (Griem, 1974) and BCW (Bassalo et al., 1982) approaches estimate by about 70% and 50%, respectively, for 706,52 nm. Besides, it has also been found that the ion–dynamic effect plays an important role concerning this line. This effect multiplies the quasi–static ion influence about 1.5 times with our plasma parameters and composition and show increasing tendency at lower electron densities confirming the theoretical (Griem, 1974; Barnard et al., 1974) estimations. The A are higher than what the G and BCW approaches yield by about: 75% and 38% (for the 587.56 nm line), 40% and 34% (for the 667.82 nm line), 31% and 28% (for the 447.15 nm line), respectively. Furthermore, it has been found that the ion dynamic effect multiplies the quasi–static ion contribution by about 1.5 for the 587.56 nm line and 1.2 for the 667.82 nm line. For the 447.15 nm line the ion dynamic effect is negligible (D=1). It should be pointed out that we have found good agreement between our W_i^{exp}/W_t^{exp} and theoretical W_i^{DSB}/W_t^{DSB} (Dimitrijević and Sahal – Bréchot, 1990) ratio values. These are: 18.5% (18.0%), 37.5% (30.5%) and 53% (44%) for the 587.56 nm, 667.82 nm and 447.15 nm lines, respectively. As can be seen, this agreement is within the estimated experimental accuracies (± 12%) of the W_i^{exp} and W_t^{exp} values for the 587.56 667.82 nm and 447.15 nm lines. It may be concluded that the ion contribution to the total line width increases with the upper-level energy of the transition and plays a

more important role than what the G and BCW approximations provide.

It turns out that the A^{exp} values, obtained by Roder and Stampa (1964) and Kelleher (1981), presented with asterisk in Tables 2 and 3, represent the line asymmetry factors obtained at the line half intensity maximum. These are smaller than our A^{exp} values.

6. CONCLUSION

Using line deconvolution procedure (Milosavljević and Poparić, 2001; Milosavljević, 2001) one obtained, on the basis of the precisely recorded He I spectral line profiles, their Stark broadening parameters: W_t, W_e, W_i, A and D and the main plasma parameters (N and T). One finds that the ion contribution to the line profiles plays much more important role than the semiclassical (Griem, 1974; Bassalo et al., 1982) theoretical approximation does which must be taken into account when using these He I lines to plasma diagnostical purposes according to the estimations made the semiclassical perturbation formalism (Dimitrijević and Sahal – Bréchot, 1990).

Acknowledgments. This work is a part of the project "Determination of the atomic parameters on the basis of the spectral line profiles" supported by the Ministry of Science, Technologies and Development of the Republic of Serbia.

References

Barnard, A.J., Cooper, J., Smith, E.W.: 1974, *J. Quant. Spectrosc. Radiat. Transfer*, **14**, 1025.
Bassalo, J.M., Cattani, M., Walder, V.S.: 1982, *J. Quant. Spectrosc. Radiat. Transfer*, **28**, 75.
Benjamin, R.A, Skillman, E.D., Smits, D.S.: 2002, *Astrophys. J.*, **569**, 288.
Berg, H.F., Ali, A.W., Lincke, R., Griem, H.R.: 1962, *Phys. Rev.*, **125**, 199.
Bergeron, P., Liebert, J.: 2002, *Astrophys. J.*, **566**, 1091.
Bötticher, W., Roder, O., Wobig, K.H.: 1963, *Z. Phys.*, **175**, 480.
Branch, D., et al.: 2002, *Astrophys. J.*, **566**, 1005.
Bresolin, F., Gieren, W., Kudritzki, R.-P., Pietvzyński, G., Przybilla, N.: 2002, *Astrophys. J.*, **567**, 277.
Büscher, S., Glenzer, S., Wrubel, Th., Kunze, H.-J.: 1995, *J. Quant. Spectrosc. Radiat. Transfer*, **54**, 73.
Chaing, W.T., Murphy, D.P., Chen, Y.G., Griem, H.R.: 1977, *Z. Naturforsch.*, **32a**, 818.
Cuesta, L., Phillips, J.P.: 2000, *Astrophys. J.*, **543**, 754.
Dimitrijević, M.S., Konjević, N.: 1986, *Astron. Astrophys.*, **163**, 297.
Dimitrijević, M.S., Sahal−Bréchot, S.: 1990, *Astron. Astrophys. Suppl. Ser.*, **82**, 519.
Djeniže, S., Milosavljević, V., Srećković, A.: 1998, *J. Quant. Spectrosc. Radiat. Transfer*, **59**, 71.
Djeniže, S., Milosavljević, V., Dimitrijević, M.S.: 2002a, *Astron. Astrophys.*, **382**, 359.
Djeniže, S., Srećković, A., Bukvić, S.: 2002b, *Eur. Phys. J. D.*, **20**, 11.
Djeniže, S., Bukvić, S.: 2001, *Astron. Astrophys.*, **365**, 252.
Drissen, L., et al.: 2001, *Astrophys. J.*, **546**, 484.
Einfeld, D., Sauerbrey, G.: 1976, *Z. Naturforsch.*, **31a**, 310.
Fransson, C., et al., : 2002, *Astrophys. J.*, **572**, 350.
Freudenstein, S.A., Cooper, J.: 1978, *Astrophys. J.*, **224**, 1079.
Gauthier, J.C., Geindre, J.P., Goldbach, C., Grandjouan, N., Mazure, A., Nollez, G.: 1981, *J. Phys. B*, **14**, 2099.
Glenzer, S., Kunze, H.J., Musielok, J., Kim, Y.K., Wiese, W.L. : 1994, *Phys. Rev. A*, **49**, 221.

Greig, J.R., Jones, L.A.: 1970, *Phys. Rev. A*, **1**, 1261.
Griem, H.R.: 1964, *Plasma Spectroscopy*, McGraw-Hill Book Company, New York.
Griem, H.R.: 1974, *Spectral Line Broadening by Plasmas*, Acad. Press, New York.
Griem, H.R.: 1997, *Principles of Plasma Spectroscopy*, Univ. Press, Cambridge.
Griem, R.H., Baranger, M., Kolb, A.C., Oertel, G.: 1962, *Phys. Rev.*, **125**, 177.
Harvin, J.A., Gies, D.R., Bagnuolo, W.G.Jr., Penny, L.R., Thaller, M.L.: 2002, *Astrophys. J.*, **565**, 1216.
Izotov, Y.I., Chaffee, F.H., Green, R.F.: 2001, *Astrophys. J.*, **562**, 727.
Kelleher, D.E.: 1981, *J. Quant. Spectrosc. Radiat. Transfer*, **25**, 191.
Kobilarov, R., Konjević, N., Popović, M.V.: 1989, *Phys. Rev. A*, **40**, 3871.
Konjević, N., Lesage, A., Fuhr, J.R., Wiese, W.L.: 2002, *J. Phys. Chem. Ref. Data*, **31**, 819.
Kusch, H.J.: 1971, *Z. Naturforsch.*, **26a**, 1970.
Labrosse, N., Gouttebroze, P.: 2001, *Astron. Astrophys.*, **380**, 323.
Lesage, A., Fuhr, J.R.: 1999, *Bibliography on Atomic Line Shapes and Shifts (April 1992 through June 1999)*, Observatoire de Paris
Lincke, R.: 1964, *PhD Thesis*, (unpublished), University of Maryland.
Mazing, M.A., Slemzin, V.A.: 1973, *Sov. Phys. Lebedev Inst. Rep.*, **4**, 42.
Mijatović, Z., Konjević, N., Ivković, M., Kobilarov, R.: 1995, *Phys. Rev. E*, **51**, 4891.
Milosavljević, V.: 2001, *PhD Thesis*, (unpublished), University of Belgrade, Faculty of Physics, Belgrade.
Milosavljević, V., Dimitrijević, M.S., Djeniže, S.: 2001, *Astrophys. J. Supp.*, **135**, 115.
Milosavljević, V., Djeniže, S., Dimitrijević, M.S., Popović, L.Č.: 2000, *Phys. Rev. E*, **62**, 4137.
Milosavljević, V., Djeniže, S.: 2002a, *Astron. Astrophys.*, **393**, 721.
Milosavljević, V., Djeniže, S.: 2002b, *New Astron.*, **(7/8)**, 543.
Milosavljević, V., Djeniže, S.: 2002c, *Phys. Lett. A*, **305/1-2**, 70.
Milosavljević, V., Djeniže, S.: 2003a, *Astron. Astrophys.*, **398**, 1179.
Milosavljević, V., Djeniže, S.: 2003b, *Eur. Phys. J. D.*, **in press**, .
Milosavljević, V., Poparić, G.: 2001, *Phys. Rev. E*, **63**, 036404.
Muglach, K., Schmidt, W.: 2001, *Astron. Astrophys.*, **379**, 592.
NIST : 2003, *Atomic Spectra Data Base Lines*, http://physics.nist.gov
Peimbert, A., Peimbert, M., Luridiana, V.: 2002, *Astrophys. J.*, **565**, 668.
Pérez, C., de la Rosa, I., de Frutos, A.M., Mar, S.: 1991, *Phys. Rev. A*, **44**, 6785.
Purić, J., Labat, J., Ćirković, Lj., Konjević, N.: 1970, *Fizika*, **2**, 67.
Roder, O., Stampa, A.: 1964, *Z. Physik*, **178**, 348.
Rupke, D.S., Veilleux, S., Sanders, D.B.: 2002, *Astrophys. J.*, **570**, 588.
Soltwisch, H., Kusch, H.J.: 1979, *Z. Naturforsch.*, **34a**, 300.
Thuan, T.X., Lecavelier des Etangs A., Izotov, Y.: 2002, *Astrophys. J.*, **565**, 941.
Vázquez, R., et al., : 2002, *Astrophys. J.*, **576**, 860.
Vujičić, B.T., Kobilarov, R.: 1988, *9th Int. Conf. Spect. Line Shapes*, Contributed papers, A18, Nicholos Copernicos University press, Torun Poland.
Webb, N.A., Naylor, T., Jeffries, R.D.: 2002, *Astrophys. J.*, **568**, L45.
Wulff, H.: 1958, *Z. Phys.*, **150**, 614.

Publ. Astron. Obs. Belgrade No. 76 (2003), 65 - 74 *Invited lecture*

ON THE CHEMICAL COMPOSITION OF THE MILKY-WAY OBJECTS

S. NINKOVIĆ

Astronomical Observatory, Volgina 7, 11000 Belgrade, Yugoslavia
E–mail: sninkovic@aob.aob.bg.ac.yu

Abstract. A review of the chemical composition of our Galaxy - the Milky Way - is presented. In addition to the well-known facts, such as dominance of hydrogen and helium over the heavy elements, etc, it should be emphasized that undoubtedly there is a correlation between the fraction of the heavy elements and the spatial distribution. On the other hand, though it seems possible, the existence of a negative gradient (decrease) in the mean metal fraction, for any subsystem of the Milky Way, is still uncertain. From this may arise additioinal complications concerning, say, the age-metallicity relation.

1. INTRODUCTION

It is clear that the first concepts and ideas concerning the "constituents of our world" belong to remote past. Since the scope of the present article is rather limited, a, practically, unavoidable historical review can be started by mentioning the discoveries of the XVIII century which laid the foundation to the modern chemistry: works of Lomonosov, Priestly, Lavoisier and others. In the following century - the XIX - the very modern concept of atoms and molecules (Dalton) is already mature. As very well known, the former ones appear as the smallest quantities of what is known as a *chemical element*, whereas the latter ones have the same meaning for what is known as a *compound*. The middle of the XIX century is the time of coming into use of the chemical symbols and chemical formulae. With it, even some organic compounds had become known.

Thus the role of the elements was already clear, it remained to find an *order* among them. This was done by D. Mendeleev who introduced a grouping of chemical elements taking into account their chemical properties and increasing atomic weight - nowadays referred to as *the periodic table*. In the periodic table each element is characterised by two numbers - the atomic number and the atomic weight. They were explained by the physics of the XX century: since the main part of each atom is its nucleus, the former number is equal to that of protons in the nucleus, whereas the latter one is equal to the total number of particles (protons and neutrons). According to this interpretation the essence of a chemical element is the nucleus of its atom (more precisely the nucleus of a given atomic number, one should also think of isotopes), once it was formed, it just remains to add the electron shell and we have a chemical

element since any quantity of a chemical element is a mere ensemble of its atoms. This standpoint has been fully confirmed by the modern nuclear physics - the phenomena of radioactivity, fission, fusion and finally the production of artificial nuclei (elements) in a laboratory.

2. CHEMISTRY AND ASTROPHYSICS: COSMICAL EVIDENCE CONCERNING CHEMICAL ELEMENTS

Though at first glance it may seem far from chemistry, astrophysics has given an important contribution to the history of chemical elements. It has explained how the elements (nuclei of their atoms) were formed. The stars, those distant celestial light sources, are in reality factories of chemical elements. Probably the story of compounds has also its origins in the universe, perhaps life, itself, originated somewhere far from the Earth. These are, of course, intriguing questions, but their consideration is beyond the scope of the present article. The first thing to be indicated here concerns the observational evidence of the chemical composition of stars and celestial bodies.

No doubt, there are two ways of obtaining evidence on the chemical composition of celestial bodies: the direct way by using the meteoritic material and the indirect way based on astronomical observations. Trimble (1996) in her review paper mentions works from the late XIX century where the meteoritic material was studied. On the other hand, it is very well known that in the early XIX century the dark lines present in the solar spectrum and also, in the spectra of other stars, were indicated by Fraunhofer. The further progress in physics in the same century (works of Doppler, Kirchhof, Bunsen, Stephan, Boltzmann, etc) enabled a correct interpretation of stellar spectra. It became possible to determine the physical conditions in the stellar photospheres and atmospheres and also, the presence and abundances of various chemical elements (in recent times the same was archived for the case of compounds). The possibilities of modern instruments allow the obtaining of very fine spectra and thanks to the progress in quantum mechanics detailed calculations for the purpose of giving their explanations are now performable.

The first important result of these studies is that *qualitatively* there is no difference in the chemical composition of the Earth and beyond it. In other words the same non-artificial 92 elements have been found on both the Earth and celestial bodies. It may be noticed for curiousity that helium was first discovered on the Sun, to be confirmed on the Earth afterwards.

The second important result is that *quantitatively* the chemical compositions of the Earth and nearby celestial bodies (in particular, the Moon and the terrestrial planets) on the one side and for, say, the stars, including the Sun too, on the other side, are very different. Since the subject of the present paper concerns the chemical composition throughout our own Galaxy, the Milky Way (in further text MW), there is no need to mention the chemical composition of other classes of objects (e.g. comets); it is sufficient to say that the chemical composition of the Jupiter-like planets is like that of stars.

3. ELEMENTAL ABUNDANCES IN THE MILKY WAY

During the first half of the XX century spectra of many stars were treated and in this way became available to further analyses. Some of the important moments

in the history of obtaining first elemental abundances for stars of MW are related in Trimble's (1996) review. Therefore, any interested reader is referred to it. Here, only an important plot will be presented (Fig. 1). What can be noticed from it is a few strong peaks. The first one concerns the two least massive atomic nuclei - proton and alpha-particle. The other ones are less prominent, but their existence obtains a full explanation in branches of modern astrophysics, such as, above all nucleosynthesis.

As the principal conclusion it will be said that the chemical composition of the Milky-Way stars is dominated by hydrogen and helium. In addition, the former, as the element with smallest atomic weight, is also dominant in the interstellar matter and the situation is practically the same in other galaxies. Therefore, it is not difficult to understand why the chemical composition of a typical star is most frequently given with three quantities only: X (percentage of hydrogen), Y (percentage of helium) and Z (percentage of all other elements, in stellar astronomy traditionally referred to as metals); these quantities are usually mass fractions. As a quantitative example one may mention the case of the Sun. The corresponding amounts for our star are (Gehren, 1988): X is between 70% and 77%, depending on the value assumed for the helium fraction, which is between 21% and 28% and, consequently, Z is equal to 2%.

The example of the Sun shows that there is a serious helium problem, i.e. the problem is to estimate its mass fraction correctly. Fortunately, the same example also shows that the helium problem affects the estimate of the hydrogen mass fraction only, whereas that concerning the metals remains unaffected. However, to studies of the chemical composition in MW in most cases the quantity Z is of highest interest. In such a situation one determines the relative abundances of metals, i.e. the ratio of number of atoms for a given metal to hydrogen. However, there are 90 metals, therefore to obtain such an information for each of them and for a sufficiently large number of MW objects requires much time. Besides, the best solution is to compare the relative abundance for a given object of MW with that characterising a "standard" object, say the Sun.

So one introduces a new dimensionless quantity, known as *metallicity*. It is defined as the Briggs logarithm of the relative-abundance ratio taken for a chosen metal of a given object of MW and the Sun. The data of such kind have been obtained for many objects of MW (stars and star clusters). They indicate that individual deviations in metal abundances can appear, i.e. inside Z not all the metals have constant rates for all objects of MW. However, a general trend is noticed - that Z can be significantly different depending on what objects are considered. Therefore, in view of the difficulties mentioned above as a practical solution one accepts to choose one metal as "representative". Then the metallicity definition is applied to it. The chosen metal is iron. The reasons are the following. First, iron (see .s.) is among the most abundant metals. Second, its lines are dominant in the stellar spectra suitable to analysing for the purpose of obtaining the information concerning the metal abundances, say spectral types between B and K (e.g. Marochnik and Suchkov, 1984 - p. 33), which means that the data on the iron relative abundance can be obtained for a very high number of MW objects. Finally, in the case of iron the relative abundance can be obtained more accurately than in the case of other metals (Gehren, 1988). Therefore, in the further text the notion of metallicity will be related to iron and, consequently, the corresponding designation will be $[Fe/H]$. When the metallicity for an MW object is known, its metal fraction Z can be found

approximately as $Z = Z_{\odot} 10^{[Fe/H]}$.

The task of galactic astronomy, or more precisely of galactic statistics, concerning the chemical composition is to study the metallicity distribution of galactic objects.

4. THE BASIC FEATURES OF THE METALLICITY DISTRIBUTION IN THE MILKY WAY

Any statistical research in MW should, certainly, take into account the fact, of which we became aware with the pioneering works of Baade (e.g. 1944), that the structure of our Galaxy is composite. As well known, Baade introduced the concept of *populations*. The stellar populations have been very often mentioned in connexion with *subsystems*, even identified with them. The present author's opinion is that these two notions should, nevertheless, be distinguished. The subsystems (in galactic astronomy introduced by Lindblad as early as 1930-ies) concern, above all, the spatial distribution, whereas the populations involve the matter, whereby the concept originator (Baade) took into account first of all the physical properties. Therefore, the populations may be understood as the content of different subsystems. It should be also noticed that the populations are very often thought to have discrete character. As an example one can mention the idea of Suchkov and his co-workers generally presented in Marochnik and Suchkov (1984) and also in journal articles (e.g. Marsakov and Suchkov, 1977), according to which the objects of MW are closely grouped around the mean metallicities. The scatter within each of these groups is largely due to the errors rather than to be intrinsic. Later studies seem to be not in accordance with this concept. Therefore, the best choice is to accept as the starting point the well-known division of MW into classical subsystems, such as the the disc, the halo, etc. This division is based on the space distribution, or more precisely, on kinematical properties. On the other hand, there is no doubt that the kinematical properties are correlated with the physical ones. According to Sandage (e.g. 1986) among the physical properties the most important are metallicity and age.

Thus the statistics of MW, if the evolutional problems are not discussed, cannot avoid the correlation between metallicity and spatial distribution, i.e. kinematics. Among the classical subsystems of MW or, more precisely, those composed of the visible matter the three most important ones are the bulge, (thin) the disc and halo (e.g. Kulikovskij, 1978).

Therefore, any statistical research concerning the metallicities has to consider the objects of different subsystems separately. Here, it should be, certainly, emphasized that for an arbitrary galactic object under study, or a group of them, it is not easy to indicate the subsystem to which it belongs. Besides, for different subsystems different interpretations are possible. Therefore, it is not surprising that one finds different results for the metallicity distribution within a given subsystem only because not the same objects are treated. Clear and exact limits for the purpose of separating different subsystems cannot be established, among others because the metallicity distribution, itself, is also used as a separation criterion.

5. THE METALLICITY DISTRIBUTION IN THE BULGE OF THE MILKY WAY

The data concerning the bulge objects are in favour of its high metallicity . However, at this point one should be careful because the basic criterion for classifying the observed stars to belong to the bulge is their position, or very often their direction (the famous Baade's window). On the other hand the number density of the other subsystems is also expected to increase towards the galactic centre, hence many stars identified as bulge ones in reality may belong to other subsystems. This controversy should be, certainly, connected to the general bulge question, because, indeed, there are different concepts as to what, generally, a bulge of a galaxy (including the galactic one, also) could be (e.g. Freeman, 1987; Frogel, 1988). The present author will consider the bulge question in this text again, while now the state of matter concerning the disc and halo will be presented.

6. THE METALLICITY DISTRIBUTION IN THE DISC OF THE MILKY WAY

The disc has been often considered as the most important subsystem of MW not surprising at all observing that MW is a typical spiral galaxy, i.e., its light, is dominated by its disc. In addition, it seems doubtless that the Sun is a disc object. There is another class of objects for which there can be hardly any doubt that they belong to the disc. These are open clusters. Today more than 1000 open clusters are known, but for many of them the necessary data are missing, often even the heliocentric distance (e.g. Nagl, 2000). A brief inspection of the data is enough to indicate that the sample of open clusters is incomplete since among the known ones a strong paucity is noticed when, for instance, one goes towards the galactic centre. The reason is probably because they are very near the galactic plane and in the central parts the detection conditions are bad. In spite of all of this their metallicity distribution is characterised by a strong peak near the solar value ($[Fe/H] = 0$ - Fig. 2). Besides, as seen from the Fig. 1, it is not symmetric. In principle, the circumstance that in disc objects (or suspected as such) there are not of them with metallicities approaching $[Fe/H] = -1$ seems to be well known. This value has been even indicated as the bordering one for separating the disc from the halo.

7. THE METALLICITY DISTRIBUTION IN THE HALO OF THE MILKY WAY

The halo of MW has been always of special interest. Its objects are assumed as very old, perhaps with the highest age in MW. Among them a special attention has been traditionally paid to globular clusters. This is not surprising if borne in mind that their sample is, most likely, the most complete in MW. Also for almost all of them the heliocentric distances are known. The metallicity distribution (Fig. 2) is very interesting. It is, as established by Zinn (1985), bimodal. If, having regard to the comment from the previous subsection, only those with $[Fe/H] < -1$ are accepted as true halo objects, then their metallicity distribution is rather well described by a Gaussian curve centred on $[Fe/H] = -1.6$, where almost 70% of them are within $[Fe/H] = -1.9$ and $[Fe/H] = -1.3$. As for the "metal-rich globular clusters, those

with $[Fe/H] > -1$, they also show a strong peak, however considering that they are much less numerous than the "metal-poor" ones, one should be careful in the interpretation. Namely, it cannot be excluded that their enhanced concentration between $[Fe/H] = -0.7 - -0.5$ is accidental (Nagl, 2000).

What is sure now is that the halo is the most metal-poor subsystem in MW. The metallicity data mentioned above confirm this statement clearly. This is the reason why the halo is so interesting. The lowest metallicity established for an MW globular cluster is -2.24 (...), whereas the corresponding value for the case of halo field star is about -4. It is not clear what could be the reason for such a discrepancy, perhaps extremely metal-poor globular clusters dissolved very early in the history of MW (e.g. Gehren, 1988). In studying halo field stars the problem of relating a particular star to the halo is somewhat problematic.

There is much in common in the metallicity distributions of the globular clusters and halo field stars. It even seems that there are halo field stars of almost the solar metallicity (Mc William, 1997). If this statement is correct, then it becomes more probable that the metal-rich globular clusters really belong to the halo. It is curious to notice that, though the metallicity distributions of the field stars and globular clusters, of course, do not coincide (one is to bear in mind, for instance, the lowest metallicities found in both groups), the mean metallicity for the former ones is also about -1.6 (Mc William, 1997), just as in the case of globular clusters (metal-poor, but they are much more numerous in MW).

Thus regardless of all unsolved and unexplained questions, such as: are all individual objects correctly identified with the corresponding subsystem? do the exceptionally metal-rich globular clusters (above the solar abundance, found just a few) also belong to the halo, or perhaps they are bulge objects? etc. - It is certain that the halo of MW is significantly metal-poorer than the disc.

8. METALLICITY GRADIENT IN MW

In the above text one has considered the metallicity distribution of individual objects on the basis of their identification with particular subsystems, where their galactocentric positions have not been taken into account. It should be noted that in galactic astronomy, as generally in stellar astronomy, stellar systems are considered as fluids. In view of this it is possible to study the dependence of the average metallicity (and of other statistical parameters) on the galactocentric position. However, in oder to be able to solve this problem correctly one should have for many galactocentric positions a large body of data, i.e. a large number of galactic objects situated in the immediate surroundings of these points with known metallicities. It is clear that this condition is fulfilled for one point only - the galactocentric position of the Sun. Of course, in such studies galactic objects belonging to different subsystems require separate treatments.

What remains to be done is to compare the metallicity distribution within a well-defined sample of galactic objects to the spatial one for the same sample. In such a way it is possible to get an insight in the change of the mean metallicity with the galactocentric position. As very good tracers for such studies appear star clusters. Then one can easily form samples with very reliable distances and, besides, the star clusters (especially globular) are very bright and their samples cannot be strongly biased for lack of completeness. On the other hand, the two known types of star

clusters are representatives of two different subsystems: the open ones belong to the disc, whereas the globular ones belong to the halo. It is not clear whether a part of globular clusters, with a relatively flat spatial distribution, belongs to the disc or to the halo, or, perhaps, these clusters belong to the thick disc. In the literature they have been chiefly considered as disc objects following Zinn (1985). However, there are different points of view (e.g. Nagl, 2000) according to which they, nevertheless, belong to the halo.

Thus a group of objects of MW with known metallicities and distances is analysed by means of a plot, say metallicity versus galactocentric distance (or distance to the axis of galactic rotation, resp. distance to the galactic plane). A trend is thereby, determined, usually applying the least squares, and, finally, one obtains the dependence of the mean metallicity on the position (distance used). Of course, such a treatment results in a linear trend and the coefficient multiplying the distance is referred to as the *metallicity gradient*. Since the bulge is small (compared to disc and halo), its gradient is not established. As for the other two subsystems, the corresponding metallicity gradients have been found. As could be expected, they are negative. With regard to what was said in the preceeding paragraph the most suitable samples for this purpose are those containing star clusters. So the metallicity gradient for the disc is approximately equal to -0.1 dex kpc $^{-1}$ (Friel, 1995). However, a gradient determination based on open clusters has also limitations because the very inner disc parts are practically free of open clusters. For this reason any extrapolation of this result towards the galactic centre is uncertain. In the case of the halo, due to its large extension perpendicular to the galactic plane, one frequently determines two metallicity gradients: in the galactic plane (radial) and perpendicular to it (vertical); of course the alternative possibility is to assume spherical symmetry for the halo and then there is only one gradient value. As already said, the obtained amounts are negative (no matter which gradient is used), but in the studies based on globular clusters most frequently applied approaches are without linear trends (e.g. Alfaro et al., 1993). As a consequence, there is no general value as in the case of the disc. Therefore, the mean metallicity in the disc and halo of MW is, most likely, a decreasing function of the galactocentric distance (to the rotation axis, resp. to the galactic plane), but the rate is rather small. The present author has not been able to find in the literature estimates concerning the spatial variation of other elements of metallicity distribution (e.g. dispersion).

9. CHEMICAL EVOLUTION OF MW

To consider the chemical evolution of a stellar system, in the present case MW, means to study the metallicity dependence on time. As said above, the available data on the chemical composition of individual stars concern their upper layers. On the other hand, the stars are "factories of chemical elements" (see preceeding sections) and, as a consequence, their chemical compositions are subject to changes in time. However, this change or, more precisely, the enrichment in heavy elements, takes place in the stellar interior. Because of this the observable chemical composition remains almost unchanged with time. In this way the most important relationship established in the studies of chemical evolution becomes that between age and metallicity. In general one may expect the oldest stars to be the most metal-poor because the processes of ejecting their matter can enrich with metals (and helium) the interstellar

matter. It is understandable that stars born later on can then be more metal-rich.

In the preceeding sections it was said that extremely metal-poor stars (with no metals) have not been discovered. It is also said that the halo is substantially metal-poorer than the disc. The age determinations are in favour of the halo being also substantially older than the disc. When mentioning age determinations, it should be said that they are much more easy and, consequently, much more reliable for star clusters, where one uses the colour-magnitude diagram, than that of individual stars. In the latter case one applies very often indirect criteria, say, the kinematics, especially for the disc. However, even for a star cluster, an age determination has not been deprived of difficulties considering that it has not been independent of the metallicity value assumed for the cluster (e.g. Marochnik and Suchkov, 1984 - p. 58).

The general situation concerning the age-metallicity relationship is rather controversial. In the case of the halo the metallicity spread is large, but the corresponding age spread is not, it is even possible that, for instance, the metal-poor globular clusters are almost co-eval. On the other hand, in the case of the disc there is an almost general agreement that the age spread attains 10 Gyr (e.g. Friel, 1995), but it is not certain if there is any correlation between age and metallicity. Twarog's (1980) finding of an apparent gradual enrichment of the disc in the heavy elements has become questioned, especially after using the data on the old open clusters where their relative paucity in the heavy elements can be alternatively interpreted by taking into account their large distances to the galactic centre in view of the negative abundance gradient mentioned above (e.g. Friel, 1995). A curious thing to be mentioned is that even the same paper can have different interpretations in different review papers, for instance, according to Friel (1995) the results of Edvardsson et al. (1993) are in favour of no age-metallicity relationship for the disc concluded on the basis of studying the data concerning old open clusters, but according to McWilliam (1997) these results are not against Twarog's (1980) age-metallicity relation. Some new metallicity determinations for young open clusters (e.g. Sung et al., 2002) give results which might be expected from Friel's (1995) disc metallicity gradient obtained on the basis of the data for old open clusters, i.e. against a strong age-metallicity relation. To all of this one should also add that the bulge, thought to be significantly rich in the heavy elements (see preceeding sections), seems in general to have a significant age (e.g. Frogel, 1988).

Two best known concepts concerning the general evolution of MW are, certainly, those of Eggen et al. (1962) and of Searle and Zinn (1978). According to the former one the matter of the galactic disc was subject to a rapid and strong vertical collapse to form a very flattenned structure as known nowadays. In the scenario of the latter paper the galactic evolution becomes more chaotic. In it an important role belongs to transient high-density regions which are places of formation of stars and star clusters, whereas the gas lost from these protogalactic star-forming regions was eventually swept into the disc.

The chemical evolution has been studied in detail for the case of the disc. The reason is the large body of data for the solar neighbourhood allowing the study, for instance, of the change in the local (at the Sun) surface density of the disc contributed by all kinds of matter (stellar and interstellar). In Twarog's (1980) paper one finds a short discussion concerning various models describing variations in time of parameters characterising the solar neighbourhood (e.g. initial mass function, star formation

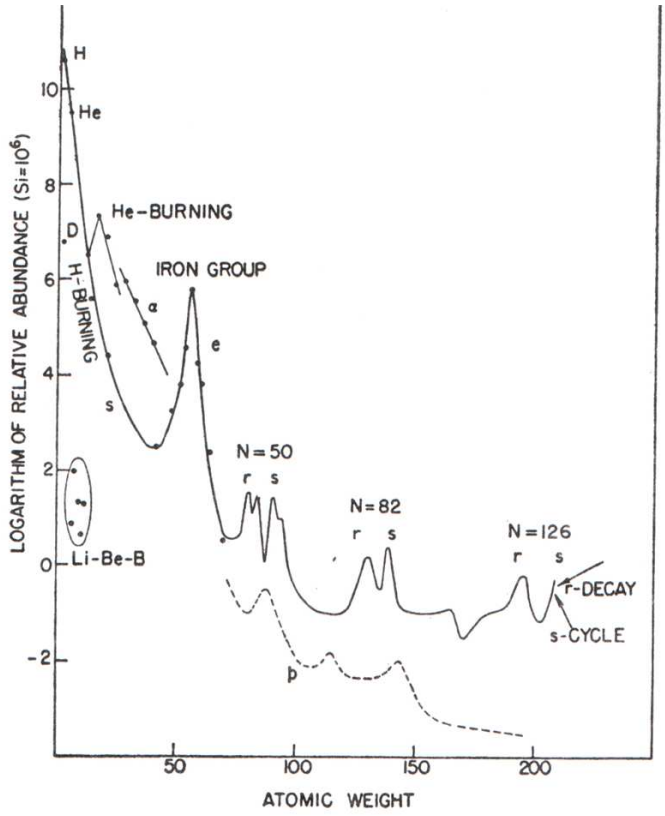

Fig. 1: The abundances of various nuclei according to Trimble (1996).

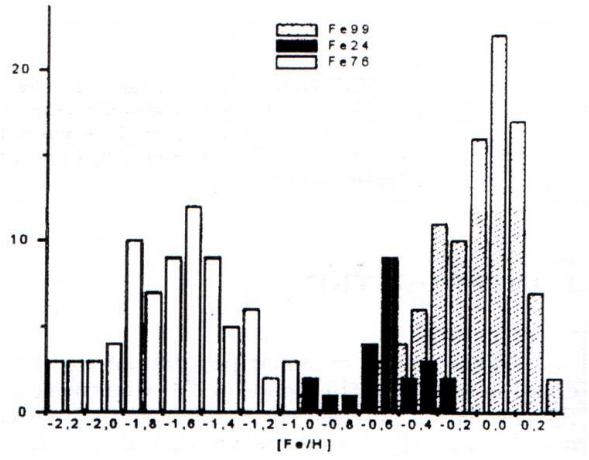

Fig. 2: The metallicity distribution for star clusters in MW - G76 "metal- -poor" globulars, G24 "metal-rich" globulars, G99 open clusters.

rate, etc.). These models can be compared to the results obtained by analysing the observational data, such as, for instance, Twarog's (1980) age-metallicity relation. Of course, a successful comparison requires the used data to be both sufficiently reliable and comprehensive. If this requirement is not fulfilled, then the consequence will be contradictory interpretations, as, for instance, that the disc has been gradually enriched in the heavy elements, i.e. it was subjected to a rapid enrichment which occurred long ago.

10. CONCLUSION

No doubt, in general, the chemical composition of MW is similar to the composition of other galaxies and the results are as could be expected on the basis of the Big-Bang theory. On the other hand, there are observational facts still waiting for a reasonable explanation, such as the large scatter in metallicity for objects supposed to belong to the halo, the bulge problem, etc. Therefore, a future work on the treatment of the metallicity data is necessary.

Acknowledgments. This work is a part of the project "Structure, Kinematics and Dynamics of the Milky Way" supported by the Ministry of Science and Technology of Serbia.

References

Alfaro, E.J., Cabrera-Cano, J., Delgado A.J.: 1993, *Astrophys. J.*, **402**, L53.
Baade, W.: 1944, *Astrophys. J.*, **100**, 137.
Edvardsson, B., Andersen, J., Gustafsson, B., Lambert, D.L., Nissen, P.E., Tomkin, J.: 1993, *Astron. Astrophys.* **275**, 101,
Eggen, O.J., Lynden-Bell, D., Sandage, A.: 1962, *Astrophys. J.*, **136**, 748.
Freeman, K.C.: 1987, *Annual Rev. Astron. Astrophys.*, **25**, 603.
Friel, E.D.: 1995, *Annual Rev. Astron. Astrophys.*, **33**, 381.
Frogel, J.A.: 1988, *Annual Rev. Astron. Astrophys.*, **26**, 51.
Gehren, T.: 1988, *Reviews in Modern Astron.*, **1**, 52.
Kulikovskij, P.G.: 1978, Zvezdnaya astronomiya, "Nauka", glav. red. fiz.-mat. lit. Moskva.
Marochnik, L.S., Suchkov, A.A.: 1984, Galaktika, "Nauka", glav. red. fiz.-mat. lit. Moskva.
Marsakov, V.A., Suchkov, A.A.: 1977, *Astron. zh.*, **54**, 1232.
McWilliam, A.: 1997, *Annual Rev. Astron. Astrophys.*, **35**, 503.
Nagl, M.: 2000, *Serbian Astron. J.*, **162**, 47.
Sandage, A.: 1986, *Annual Rev. Astron. Astrophys.*, **24**, 421.
Searle, L., Zinn, R.: 1978, *Astrophys. J.*, **225**, 357.
Sung, H., Bessel, M.S., Lee, B.-W., Lee, S.-G.: 2002, *Astron. J.*, **123**, 290.
Trimble, V.: 1996, *Astron. Soc. Pacific, Conference Series*, eds. S. S. Holt and G. Sonneborn, **99**, 3.
Twarog, B.A.: 1980, *Astrophys. J.*, **242**, 242.
Zinn, R.: 1985, *Astrophys.J.*, **293**, 424.

Publ. Astron. Obs. Belgrade No. 76 (2003), 75-84 *Invited lecture*

DETERMINATION OF PLASMA PARAMETERS FROM SHAPES OF ATOMIC SPECTRAL LINES

GORAN B. POPARIĆ

Faculty of Physics, University of Belgrade,
Studenski trg 14-16, P.O. Box 368, 11001 Belgrade, Serbia
E-mail: gopop@ff.bg.ac.yu

Abstract. This paper is concerned with the possibility of determination the basic plasma parameters such as temperature and electron density by using advanced numerical procedure for deconvolution of theoretical asymmetric convolution integral of a Gaussian and a plasma broadened spectral line profile $j_{A,R}(\lambda)$ for spectral lines. Special attention was dedicated to reliability of obtained parameters. The methods for verifying the validity of the theory predicted model function with real plasma conditions and for detecting the presence of other undesirable broadening mechanisms are given. The comparison with plasma parameters determined by using standard diagnostics methods is also presented.

1. INTRODUCTION

The investigation of broadening of the spectral lines through different plasma parameters, which represent physical conditions and state of plasmas, helps us to understand physical mechanisms leading to it. Theoretical knowledge of physical mechanisms of broadening based on plasma parameters, can be used for determining physical conditions and state of plasmas by analyzing the shapes of atomic spectral lines. That approach can be useful for determining parameters for laboratory plasmas as an independent method, but this is especially true in case of astrophysical plasmas. In fact, the only way of performing diagnostic of astrophysical plasmas is the investigation of their radiation (spectral lines and continuum). The investigation of the spectral line shapes and parameters is very important because most of the information about celestial objects is acquired in that way.

In principle three different agents may contribute to the final width and shape of a spectral line: natural broadening, Doppler broadening and interactions with neighboring particles (Griem, 1968, 1974, 1997). The natural broadening is usually very small compared to the other contributions and has the well-known Lorentzian or dispersion distribution. Doppler broadening originates from the statistical velocity distribution of the emitting atoms, being directly dependent upon the plasma temperature. In the case of Maxwell distribution of velocity the Doppler broadening has a Gaussian distribution. The third mechanism depends on the electric micro-fields of neighboring particles and includes Stark, Van der Waals and resonant broadenings. This mechanism becomes important with the increase of the pressure and represents the so-called pressure broadening. The profile

representing this broadening, in the cases when interactions between the emitter and ion is negligible in comparison with the interaction emitter electron, is a symmetric Lorentz function. For neutral and ionized emitters for which the interaction between emitter and ion is not negligible, more convenient distribution is asymmetric $j_{A,R}(\lambda)$ profile (Griem, 1974). In the case of neutral atoms, an important role may play the resonant and Van der Waals broadening and it should at least be estimated. This requires some independent measurements or estimation of neutral atom densities, in addition to the usual measurements of electron density and electron temperature.

One additional effect of the line broadening in plasma has to account for the radiative transfer. The lines may be broadened by self-absorption and this effect is especially important in the cases of strong lines and high pressures. Self-absorption will have the effect of destroying and especially broadening the lines and will therefore produce an apparently large width. In some cases, in conditions of inverse population, if induced (stimulated) emission exceeds the absorption, it may even cause line narrowing. This radiation additionally influences the shape of the line profile. There is also a contribution of instrumental broadening, which is characteristic of spectral device used for observation, and it must be known and taken into account appropriately.

Most measurements have been concerned with isolated lines of neutral atoms and of ions in low and intermediate charge states for a large number of elements. Besides, there is also a great need for reasonably accurate measurements under the well-defined plasma conditions. For most of these measured lines, the electron impact broadening should indeed be the dominant mechanism, except for very partially ionized gases. The state of the art in impact line broadening theory today is well represented by the convergence of fully quantum mechanical and semiclassical calculations. This situation is well described in a number of papers dealing with impact broadening, (Alexiou, 1995, 1997, 2000; Griem and Ralchenko, 2000).

All the mentioned processes exert influence on the shape of the spectral lines. Usually, it is resonable to presume Doppler and Stark broadening (or any other kind of pressure broadening), as being statistically independent processes. In this case the electron collision is irrelevant regarding the Doppler broadening, but it is so important for pressure broadening. Corresponding profile contributions can be separately convolved to obtain the total shape of the line. In order to analyze the experimental data the first step is the fit to Lorentzian profile. The fit to Voigt profile is more appropriate, because it includes Doppler broadening in the main Lorentzian profile. This profile can be used if the shape of the measured line is symmetric, which is the case of ionized emitters, where it is possibly to neglect the interactions between the emitter and perturbation partical - ion. In the case of neutral and ionized emitters for which the interaction between the emitter and ion is not negligible, the line profile is asymmetric. In principle there is no fundamental difference between the ionized emitters. However, the quasistatic approximation is better satisfied for singly than multiply ionized emitters within a given isoelectronic sequence because the relevant energy spacings are smaller and the times contributing to the relevant integrals are longer (Alexiou, 1994). The most convenient fit in these cases is the fit to the so-called "K" function i.e. the convolution integral (Griem, 1974) of a Gaussian and a plasma broadened spectral line profile $j_{A,R}(\lambda)$. Besides the $j_{A,R}(\lambda)$ and Doppler widths, the important role in "K" profile is played by the static ion broadening parameter A and Debye shielding and ion-ion correlation parameter R.

It should be mentioned that besides the quasistatic treatment of ions there is also the dynamic treatment of the ions (Griem, 1974; Barnard *et al.,* 1974) existing. If strong collisions do not overlap in time, the theory is valid for the whole range of ion broadenings,

from quasistatic to impact broadening. In this way, two situations are possible. First, quasistatic and dynamic ion treatment at the same time, in this case the resulting line pofil is asymmetric. Also, in this case it is possible the distinguish electron impact width and ion width. Second, if ions are not quasistatic (Alexiou, 1996, 1997; Oks, 1999), there is always a part of ion width which just adds to the electron impact width, and in this case the resulting line pofil is symmetric function. Experimentally, in this case, one cannot distinguish between the electronic and ionic impact contributions, and care must be taken at interpreting the line broadening parameters.

In the above text the asymmetry of the lines refers to a quasistatic broadening, consequently the approach ignores a number of important factors which too may contribute to the asymmetry of the lines, such as the gradients, quadrupoles, shifts or some other effects.

When the experimentalist gets a line without an apriori knowledge of the plasma parameters, he would like to be able to separate them from the experimental spectrum. Most measurements have been concerned with isolated lines of neutral atoms and of ions in low and intermediate charge states for a large number of elements. In the case of neutral and ionized emitters for which broadening by ions are not negligible, the line profile is often asymmetric. The most appropriate theoretical model function in these cases is the K profile (2), i.e., the convolution integral of a Gaussian and a plasma broadened spectral line profile $j_{A,R}(\lambda)$.

2. THEORETICAL BACKGROUND

In the general case of non-hydrogenic atomic lines the ion broadening in most cases is not negligible and the line profiles are described by an asymmetric function. In the quasistatic ion approximation (Griem, 1974) the profile of an isolated spectral line emitted by a non-hydrogenic emitter is given by

$$j_{A,R}(\lambda) = j_0 + j_{\max} \int_0^{\infty} \frac{H_R(\beta)}{1 + [2(\lambda - \lambda_0)/W_j - \alpha\beta^2]^2} d\beta \qquad (1)$$

where jo is the baseline, j_{max} maximum intensity, $H_R(\beta)$ an electric micro field strength distribution function of normalized field strength $\beta=F/Fo$. Fo is the Holtsmark field strength. $A(\alpha=A^{4/3})$ is the static ion broadening parameter as a measure of the relative importance of ion and electron broadenings. R is the ratio of the mean distance between ions to the Debye radius, i.e. the Debye shielding parameter and Wj is the width (FWHM) of the j profile. Electric micro field distributions in plasmas have been calculated by Hooper (1966, 1968).

Whenever the Gaussian contribution of plasma broadening is not negligible one has to use a deconvolution procedure to determine the Stark width of the line. The convolution integral of both Gaussian and Stark broadening $j_{A,R}(\lambda)$ profiles is given by

$$K(\lambda) = K_0 + K_{\max} \int_{-\infty}^{+\infty} \exp(-t^2) \otimes \left\{ \int_0^{\infty} \frac{H_R(\beta)}{1 + \left(2\frac{\lambda - \lambda_0 - \frac{W_G}{2\sqrt{\ln 2}} \cdot t}{W_e} - \alpha \cdot \beta^2 \right)^2} \cdot d\beta \right\} \cdot dt \tag{2}$$

where K_0 is the baseline, K_{max} the maximum intensity, and $H_R(\beta)$ an electric microfield strength distribution function (Hooper, 1966, 1968) of normalized field strength $\beta=F/F_0$. F_0 is the Holtsmark field strength. A ($\alpha=A^{4/3}$), the static ion broadening parameter is a measure of the relative importance of ion and electron broadenings and is given by Griem (1974). R is the ratio of the mean distance between ions to the Debye radius, i.e., the Debye shielding parameter and Wj is the width (FWHM) of the j profile. λ_0 is actual position of the center of a line.

3. NUMERICAL PROCEDURE

The proposed function for various line shapes (2), is of the integral form and includes several parameters. Some of these parameters can be determined in separate experiments, but not all of them. Furthermore, it is impossible to find an analytical solution for the integrals and methods of numerical integration to be applied. This procedure, combined with the simultaneous fitting of several free parameters, causes the deconvolution to be extremely difficult task and requires a number of computer supported mathematical techniques. Particular problems are the questions of convergence and reliability of deconvolution procedure, which are tightly connected with the quality of experimental data.

For the purpose of deconvolution iteration process we need to know the value of K function as a function of λ for every group of parameters (K_{max}, λo, Wj, W_G, R, A). The function $K(\lambda)$ is in integral form and we have to solve a triple integral in each step of iteration process of varying the above group of parameters. The first integral in the "K" function is the micro field strength distribution function $H_R(\beta)$, the second one is the $j_{A,R}(\lambda)$ function and the third is the convolution integral of a Gaussian and a plasma broadened spectral line profile $j_{A,R}(\lambda)$, denoted by $K(\lambda)$ - equation (2). All these integrals have no analytic solution and must be solved using the numerical integration.

The most difficult integral to deal with is the micro field strength distribution function, because this is a multidimensional integral. Straightforward manner would be the estimates of multidimensional integral by Monte Carlo method of integration. The numbers of random samples of points must be large in order to achieve satisfactory accuracy. That could be achieved at the cost in increased processor time. These reasons eliminate the Monte Carlo method of integration. The same reasons eliminate the Monte Carlo simulation method too. There are many theories developed for evaluating the micro field strength

distribution function. The best known are Holtsmark (1919), Baranger and Mozer (1959) and Hooper (1966, 1968) theories. Also developed was the phenomenological adjustable-parameter exponential method (APEX) (Iglesias, 1983, 1985), whose efficiency was demostrated by excellent agreement with computer simulations. The numerical evaluating of micro field strenght distribution function, as a function of β and R, in each step of iteration process, would impose a long processor time, and the method would be practically inapplicable. Instead, we have decided to solve the integral equation of micro field distribution in sufficient numbers of points (β, R), and after that we interpolated that two-dimensional surface by polynomial interpolation. In every iteration step, at varying parameters β, or R, we used previously hand determined interpolation polynomials for determining the value of micro field strength distribution in current points. For neutral and singly ionized atoms (emitters) there exists the tabular date-base in Hooper (1966, 1968). It should be noted, that this deconvolution procedure may involve any method of calculation of micro field strength distribution function depending on the kind and composition of analyzed plasmas.

The second integral in (2) is the $j_{A,R}(\lambda)$ and it is evaluated by summation method. The third integral is evaluted by the Gauss-Hermite method with $\exp(-t^2)$ as a weight function. In this manner the number of terms in the numerical sum is reduced in comparation with the summation methods. It must be noted, that in cases where ($W_G > 0.5W_j$) in (2) which are frequent physical situations in astrophysical plasmas (Popović *et al.,* 1999), this method of integration is not applicable. Then, the integration must be performed by clasical summation methods, which greatly slow down the iteration process, but these methods are the only correct, in these regions.

In general, the base line Ko in function (2) is a function of wavelength. In many cases it is nearly constant, or linear function, but in some cases it may have more complex dependence (Glenzer *et al.,* 1992). We have included in our procedure the fitting of background by cubic polinomial, as independent step, in order to prepare experimental data for the main deconvolution procedure.In this way, we have solved the equation (2) and now we can start with fitting procedure itself. For the equation (2), the fitting procedure will give the values for W_G, W_j, λo, R, A and K_{max}.

We are using the standard manner of defining the best fit: the sum of the squares of the deviations (Chi-Square) of the theoretical function from the experimental points is at its minimum. In other words, we are seeking the global minimum of the Chi-Square function which is hyper-surface of N dimensions in a hyperspace of N+1 dimensions, where N is equal to a number of parameters for appropriate theoretical function. N is equal to six for the "K" profile (Milosavljević and Poparić, 2001).

The necessary condition for the minimum of Chi-Square sum is that the partial derivatives of the function are equal to zero. Therefore, in the case of "K" profile we have a system of six nonlinear homogeneous equations with six parameters.. We are seeking the numerical solutions of these systems by using the well-known Newton method of successive approximations. Ostrowski and Kantorovich (Demidovich, 1987) have investigated the conditions of convergence of Newton method. In these cases we have two homogenous systems of algebraic and transcendental equations with real coefficients. The functions are defined and continuous, along with its partial derivatives of first and second orders. If the initial parameters lie in the domain sufficiently close to the expected solutions of the system, the conditions for convergence are fulfilled.

The seeking for the numerical solution of this problem by employing computer is accompanied by a number of numerical difficulties. The Newtons method requires

successive solving of the inverse Jacobi matrices of the system of equations for each step, which are error prone due to the errors of rounding. Moreover, the numerical partial derivatives in Jacobi matrix itself are sources of errors of rounding. These errors of rounding are destabilizing the convergence of solution of the system, although the all-mathematical conditions are fulfilled. The stabilization of iterative process may be achieved by weighting the non-diagonal elements of inverse Jacobi matrix by real numbers in the domain (0, 1] (Milosavljević and Poparić, 2001). We introduce the dynamic weighting of the off-diagonal Jacobian elements in the domain of (0,1]. During the iterative process, if the convergence of process becomes unstable, they are automatically adjusted by decreasing toward zero. The conditions of positive-definiteness of the weighted Jacobian matrix are always achieved by decreasing off-diagonal dynamic weighting parameters. For sufficiently small off-diagonal weighting parameters the weighted Jacobian matrix becomes diagonally dominant and positive-definite. The algorithm dynamically decreases weighting parameters until the condition for positive-definiteness is fulfilled. Also, when the convergence of process is stable, they can be increased in order to accelerate process. They are adjusted dynamically during the minimizing process. They are not fixed. In that manner, the stability of iterative process is achieved. So, our deconvolution method meets the condition of positive-definiteness and has no problems with stability and reproducibility (Milosavljević and Poparić, 2003). These modifications of Newton's method do not affect the conditions of convergence and uniqueness of mathematical solution, but do affect somewhat the speed of convergence. In this way we have contrived to give numerical solutions for fitting functions with more than three free parameters, which is difficult for non-polynomial fits.

This algorithm has shown a great stability in numerical sense, under variation of initial parameters. This has been demonstrated by fitting of about one hundred of experimental data sets, for "K" profile.

This sophisticated deconvolution method, which allows direct determining of all six parameters by fitting theoretical K-profile (2), on experimental data, requires sufficient number of experimental points per line, and small statistical errors. The upper limits of numerical conditionality of this method are a minimum twenty experimental points per line (the border of line is $(-3/2W_j+\lambda_o<\lambda<+3/2W_j+\lambda_o)$, where W_j (FWHM), and maximal statistical indeterminacy in intensity is 5% at every experimental point. Poor experimental measurements weaken the conditionality of the system of equations, and lead to non-applicability of this method. This has been concluded by testing the sensitivity of the algorithm by generating random statistical noise with Gaussian distribution in every point involved by theoretical profiles.

4. PROBLEMS OF RELIABILITY OF OBTAINED PARAMETERS

The theoretically proposed model function for various line shapes Eq. (2), is of the integral form and includes several parameters. Some of these parameters can be determined in separate experiments, but not all of them. If one has experimentally obtained spectra, in principle one cans determine parameters which included in model function by solving the inverse problem. Because of complexity of theoretical model function and its integral form various numerical methods have to be used. In order to solve the inverse problem we are looking for the best fit or for parameters when the sum of the squares of the deviations of the theoretical function from the experimental point is at its minimum. In this minimization we vary through six-dimensional parameter space (K_{max}, λ_0, W_j, W_G, R, A). Actually, we

are seeking for the global minimum of the chi-square function, which is the hyper surface of N dimensions in a hyperspace of N+1 dimensions, where N is equal to a number of parameters for the appropriate theoretical function. N is equal to six in the case of the K profile. The advanced numerical method which enables the determination of all of six parameters proposed by theory model function was developed and presented by Milosavljević and Poparić (2001).

A great number of parameters and the complex topology of the hyper surface of the chi-square function, as a function of parameters, through the numerical method finds the global minimum, naturally intrude the question of reliability of such obtained parameters. A special problem is statistical noise, which leads to forming local minimums in the hyper surface of the chi-square function and its more complex topology. This problem can be overcome by determination of a confidence region for every concrete case. There are well-known methods for this kind of estimations (Press *et al.,* 1995).

The next problem is the cases when there is possibility of presence of other broadening mechanisms, such as radiative transfer, reabsorbtion, turbulence, ion dynamics and other broadening mechanism which are not included in theoretical model function. The parameters obtained by solving inverse problem in those cases do not have physical sense. A special care had to be dedicated to detection of these undesirable effects. There are methods for quantitative checking if some theoretical proposed model function appropriately fits some experimental data. Testing can be performed by estimation of convergence of the chi-square sum during decreasing the statistical noise. Non-zero limes value would show that proposed theoretical model function does not well describe the physical process, e.g. there is a presence of some additional effects, which had not been included in modeling.

Also, another testing can be performed by comparing of estimated mean value of chi-square sum and actual chi-square sum obtained from experimental set of data, at the same statistical noise level. So, it always can retrieve the presence of additional undesirable effects. Moreover, its magnitude can be estimated. Deconvolution procedure (Milosavljević and Poparić, 2001) does not enable to eliminate undesirable effects such as reabsorption, radiative transfer, ion dynamic (e.g. falling of quasistatic approximation), and other broadening mechanisms, but it is very important that their presence can always be discovered. If these effects are not negligible, the estimated parameters would not have a sense. But it is important that these effects can always be quantitatively detected and their importance can be quantitatively estimated by comparing with statistical noise level. In the cases where they are not negligible, additional diagnostic and modeling are needed.

5. APLLICATION AND COMPARISONS WITH STANDARD DIAGNOSTICS METHODS

The plasma parameters were determined using standard diagnostics methods. Thus, the electron temperature was determined from the ratios of the relative line intensities of spectral lines helium, argon and krypton, respectively with an estimated error of ±10%, assuming the existence of the LTE. The electron density decay was measured using a well-known single wavelength He-Ne laser interferometer technique for the 632.8 nm transition with an estimated error of ±9%. Temporal evolution of electron temperatures and electron densities are presented in Figs. (1-3).

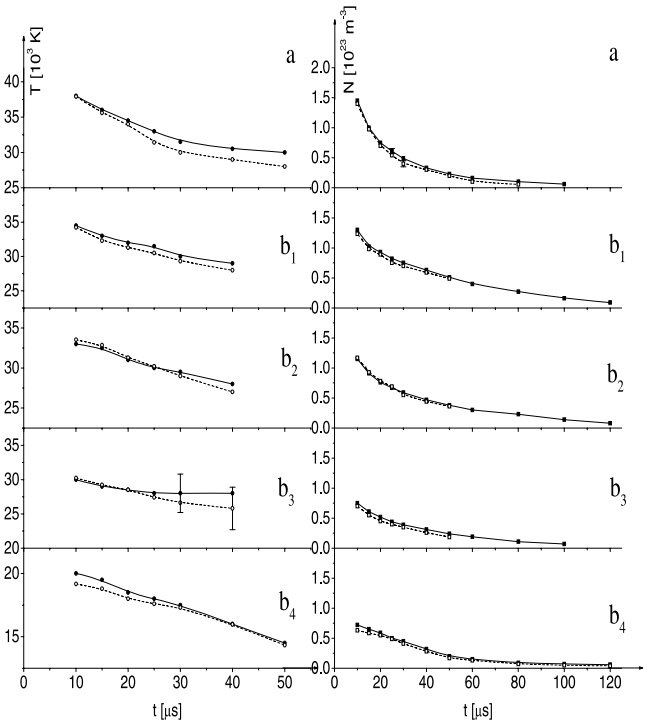

Fig. 1: Electron temperature (T) and density (N) decays for He I 706.52 nm. Full lines represent measured data using independent experimental techniques and dashed lines represent plasma parameters obtained using our line deconvolution procedure in various plasmas (Milosavljevic and Djeniže, 2003a). Error bars, indicated only in the case of the greatest disagreement (T in b_3), represent estimated accuracies of the measurements (±10%) and deconvolutions (±12%)

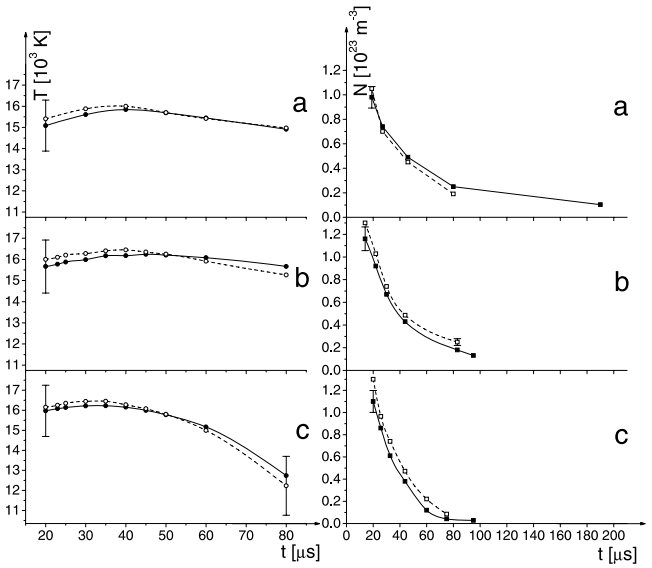

Fig. 2: Electron temperature (T) and density (N) decays for 5 lines of Ar I. Full lines represent measured data using independent experimental techniques and dashed lines represent plasma parameters obtained using our line deconvolution procedure in various plasmas (Milosavljevic and Djeniže, 2003b). Error bars, indicated only in the case of the greatest disagreement, represent estimated accuracies of the measurements (±10%) and deconvolutions (±12%)

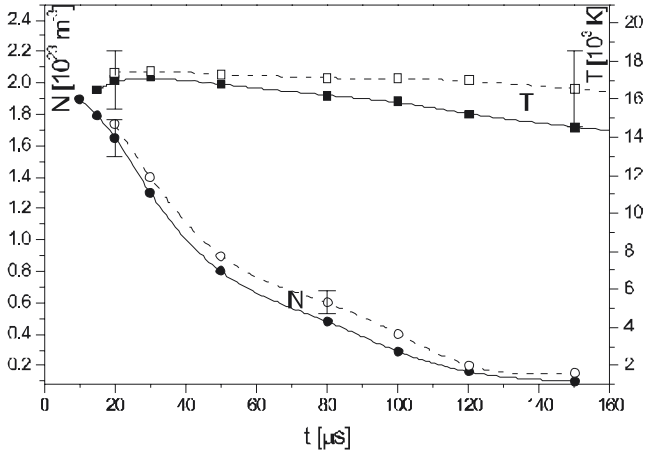

Fig. 3: Electron temperature (T) and density (N) decays for 20 lines of Kr I. Full lines represent measured data using independent experimental techniques and dashed lines represent plasma parameters obtained using our line deconvolution procedure in various plasmas (Milosavljevic *et al.,* 2003). Error bars, indicated only in the case of the greatest disagreement, represent estimated accuracies of the measurements (±10%) and deconvolutions (±12%).

As can be seen from Figs. (1-3) there is a good agreement between the plasma parameters which were determined using standard diagnostics methods and parameters obtained by deconvolution method over a wide range of temperature and electron density. It shows first that, the proposed model function well describes the broadening of spectral lines over this range of plasma parameters, and second, that the deconvolution procedure is numerically stable and gives reliable plasma parameters.

Acknowledgements. The author is grateful to Dr V. Milosavljević for permission to use some of his results of this forthcoming publication and also for helpful discussions. This work is a part of the projects "Determination of the atomic parameters on the basis of the spectral line profiles" and "Experimental investigation of laser and electron interactions with atoms, metal vapors and molecules" supported by the Ministry of Science, Technologies and Development of the Republic of Serbia.

References

Alexiou, S.: 1994, *Phys. Rev. Lett.,* **76,** 1836.
Alexiou, S.: 1995, *Phys. Rev. Lett.*, **75**, 3406.
Alexiou, S. *et al*.: 1997, *J. Quant. Spectrosc. Radiat. Transfer,* **58**, 399.
Alexiou, S. *et al.*: 2000, *J. Quant. Spectrosc. Radiat. Transfer,* **65** 15.
Baranger, M., Mozer, B.: 1959, *Phys. Rev.,* **115**, 521.
Barnard J., Cooper, J., Smith, E.W.: 1974, *J. Quant. Spectrosc. Radiat. Transfer,* **14**, 1025.
Demidovich, B.P., Maron, I.A.: 1987, *Computational Mathematics,* Mir Publishers, Moscow.
Glenzer, S., Uzelac, N.I., Kunze, H.J.: 1992, *Phys. Rev. A.,* **45**, 8795.
Griem, H.R.: 1968, *Phys. Rev.,* **165**, 258.
Griem, H.R.: 1974, *Spectral Line Broadening by Plasmas,* Academic press, New York.
Griem, H.R.: 1997, *Principles of Plasma Spectroscopy,* Univ.Press, Cambridge.
Griem, H.R., Ralchenko, Yu.V.: 2000, *J. Quant. Spectrosc. Radiat. Transfer*, **65**, 287.
Holtsmark, J.: 1919, *Ann. Physik,* **58**, 577.
Hooper, C.F.: 1966, *Jr., Phys. Rev.,* **149**, 77.
Hooper, C.F.: 1968, Jr., Phys. Rev. **165**, 215.
Iglesias, C. *et al.*: 1983, *Phys. Rev. A,* **28**, 1667.
Iglesias, C. *et al.*: 1985, *Phys. Rev. A,* **31**, 1698.
Milosavljević, V., Poparić, G.: 2001, *Phys. Rev. E.*,**63,** 036404.
Milosavljević, V., Poparić, G.: 2003, *Phys. Rev. E.*,**67,** 058402.
Milosavljević, V., Djeniže, S.: 2003a, *Eur. Phys. J. D.*, in press.
Milosavljević, V., Djeniže, S.: 2003b, *Astron. Astrophys.*, submitted.
Milosavljević, V., Djeniže, S., Dimitrijević, M.S.: 2003, *Phys. Rev. E,* submitted.
Popović, L.Č., Dimitrijević, M.S., Tankosić, D.: 1999, *Astron. Astrophys. Supp. Ser.,* **139,** 617.
Press, W.H., Teukolsky, S.A., Vetterling, W.T., Flannery, B.P.: 1995, *Numerical Recipes in C*, Cambrige University Press.
Oks, E.: 1999, *Phys. Rev. E,* **60**, 2480.

Publ. Astron. Obs. Belgrade No. 76 (2003), 85-104 *Invited lecture*

DIAGNOSTICS OF MAGNETOPLASMA COMPRESSOR OF COMPACT GEOMETRY

J. PURIĆ[1,2], I.P. DOJČINOVIĆ[1] , V.M. ASTASHYNSKI[3], M.M. KURAICA[1,2]

[1] *Faculty of Physics, University of Belgrade, P.O. Box 368, 11001 Belgrade, Serbia*

[2] *Center for Science and Technology Development, Obilicev Venac 26, Belgrade, Serbia*

[3] *Institute of Molecular and Atomic Physics, National Academy of Sciences of Belarus, F. Skaryna Avenue 70, 220072 Minsk, Belarus*

Abstract. Quasistationary plasma accelerator of magnetoplasma compressor type with semitransparent electrodes operating in an ion current transfer regime has been constructed and studied. Main discharge and compression plasma flow parameters have been measured. It has been found that the current cut off limiting the increase of the parameters in the case of classical plasma accelerators operating in the electron current transfer can be avoided by switching to the ion current transfer. It was made achievable by an especially designed electrode system shielded by the magnetic field, and therefore protected of the erosion as a main reason for energy losses leading to the current crisis. Due to the electrode transparency in two stage quasistationary plasma accelerator there is no limit in the maximal current value depending only on the condenser bank input energy used in the experiment. Consequently, the compression plasma flow velocity, electron density and temperature depend only on the energy transfer efficiency from supply source to plasma. It has been concluded that the efficiency is maximal when operating in the hydrogen in comparison with other working gases (argon, nitrogen etc.). It was found that, for an input energy of 6.4 kJ the maximal values of plasma flow velocity and electron density are of the order of ~100 km/s and ~10^{17} cm^{-3}, respectively. These accelerating systems are of special interest for development of new plasma technologies such as plasma solid surface modification and obtaining new materials including nano sized ones. Finally, these accelerators can be used for construction of plasma injectors to fusion devices.

1. INTRODUCTION

Traditional plasma accelerators have achieved a certain limit in their development and application (Morozov, 1990). The potential of farther increase of their plasma parameters practically has been exhausted in such accelerators (with inherent magnetic field and electron current transfer). Namely, in order to increase the plasma parameters, the discharge current of accelerator has to be increased. However, the increase in discharge current causes intense potential jump near the electrode (anode or cathode) and its heavy erosion (Morozov, 1969). There is no way to overcome this phenomenon within the concept of electron current transfer. That is why transition to systems with an ion current transfer is necessary (Morozov, 1990). Such systems are the quasistationary plasma accelerators of new generation. The plasma acceleration in a discharge device of these

accelerators is accompanied by compression flow formation at the outlet with plasma parameters much higher than those in inter-electrode gap. These accelerator systems are of special interest for development of new plasma technologies. High plasma parameters of compression flows, together with large discharge duration enable efficient usage of such flows for material surface modification. The duration of compression plasma flow in different material processing is very important, particularly for solid surface modifications and the investigation of plasma wall interaction, important for fusion research.

Magnetoplasma compressor (MPC) is the source of quasistationary compression plasma flows (Morozov, 1975). The importance of research connected with the MPC and the creation of compression plasma flows is not only in enabling the study of fundamental processes in plasma flows and their behavior in different configurations of electric and magnetic fields, but also, in application of such systems and their plasma flows in different plasma technologies. For example, they are very intensive radiation source from X-ray to microwave region. Also, they can be used for the hardening of different materials (such as steal and its alloys, for instance) surfaces, plasma deposition of the materials on the sample surfaces and its modifications including creation of submicrostructures of silicon and other semiconductors (Astashynski *et al*., 2002ab); acceleration of micro particles etc. On the other hand, the MPC can be used as the basic units for constructing the first stage of the two-stage quasistationary high current plasma accelerator (QHPA) (Morozov, 1990). Namely, a combination of several MPC can be used to produce fully ionized plasma at the entrance to the acceleration channel of QHPA. Among the different fields of QHPA applications we are mentioning here only its using as the plasma injector in some fusion devices (Ananin *et al*., 2002).

The aim of this work is to enlarge the knowledge about the MPC operation and to improve methods of controlling its plasma parameters. The emphasis is on the investigation of a quasistationary phase of compression plasma flows and development of the appropriate methods for measuring of their electrical and thermodynamic parameters.

2. BASIC THEORY OF QUASISTATIONARY PLASMA ACCELERATORS

Quasistationary plasma accelerators are sources of quasistationary compression plasma flows in which the life time of the compression stable state is much longer (~100-1000 μs) than the flight time of the plasma in the acceleration channel of the accelerator (~1 μs) (Morozov, 1975). During a quasistationary phase the plasma flow parameters are slowly changing in time within certain volume (space). It is a consequence of an ion-drift acceleration of magnetized plasma realised using especially shaped accelerating channel (Morozov, 1990).

Elementary analysis of plasma flow (Morozov, 1990) based on the thin-tube aproximation showed that the accelerating channel has to have Laval nozzle profile. On the bases of equation of continuity, Bernoulli equation and magnetic flux conservation laws in standard notation:

$$df\rho v = const \tag{1}$$

$$\frac{v^2}{2} + i(\rho) + \frac{B^2}{\mu_0 \rho} = const \tag{2}$$

$$\frac{B}{\rho d} = const \tag{3}$$

the basic plasma parameters can be determineded. Here $i(\rho) = \int dp / \rho$ is enthalpy, f is the width of the tube and d is its average radius. Two extreme approximations can be used as follows.

In the acceleration regime, neglecting the enthalpy, maximal plasma velocity at the exit of the acceleration channel is $v_m = \sqrt{2} v_{A0}$. Here $v_{A0} = B_0 / \sqrt{\mu_0 \rho_0}$ is Alfven velocity at the entrance to the channel. With discharge current 100 kA (magnetic field 0.4 T at 5 cm distance from the electrode) and plasma density 10^{16} cm^{-3} for a hydrogen plasma, calculated plasma velocity at the exit of the channel is approximately 100 km/s.

As a result of this analyses one can find the dependences of maximal plasma velocity and voltage (between the electrodes) on discharge current and mass flow rate: $v_m \sim I^2 / \dot{m}$ and $U \sim I^3 / \dot{m}$, respectively. The dependences prove that the acceleration processes are predominantly determined by discharge current and mass flow rate. A deviation of the experimentally obtained dependencies from the above mentioned ones is the measure of the acceleration efficiency of the accelerators system as a whole.

In the compression regime (enthalpy included) degree of plasma compression in acceleration channel is:

$$\frac{\rho_{\max}}{\rho_0} = \left[(\gamma - 1) \frac{v_{A0}^2}{v_{S0}^2} \right]^{\frac{1}{\gamma - 1}} \tag{4}$$

and maximal temperature:

$$T_{\max} = \frac{\gamma - 1}{\gamma} \cdot \frac{M}{k} \cdot v_{A0}^2 \tag{5}$$

Here ρ_0 is electron density and $v_{S0} = \sqrt{\gamma \cdot p_0 / \rho_0}$ sound velocity at the entrance to the acceleration channel. With Alfven velocity 100 km/s and sound velocity 10 km/s, for adiabatic compression of hydrogen plasma ($\gamma=5/3$), maximal degree of compression is 550 and temperature 50 eV for these conditions.

From the above given analyses it follows that the increase of main plasma flow parameters (electron density and temperature and plasma flow velocity) can be achieved by an increase of the discharge current. However, large increase of the discharge current causes intense potential jump near anode and its heavy erosion. This cannot be avoided by the system with continual solid anode due to current slippage on its surface. Similar effects are seen in pulsed systems (plasma focus devices). However, these problems can be solved enabling an ion current transport in the accelerating system. The ion current transport has to be through the transparent anode and therefore the anode is made of rods (Morozov, 1990). For the same reasons, the cathode has to be made of rods. However, in this work it is only specially shaped.

A distinctive characheristic of compression flow is the "freezing" of magnetic field into plasma. In this type of plasma flows the existence of current loops (vortices) is detected. Namely, the presence of "swept-away" current into the compression plasma flows has been earlier noticed. The existence of the "swept-away" current is due to magnetic flux conservation (the magnetic field is frozen in plasma). It has been showed recently, that during an action of compression plasma flow on a sample surface current loops (vortices) can arise (Ananin *et al*., 1998).

3. EXPERIMENTAL SET-UP

The Magnetoplasma compressor of compact geometry (MPC-CG) used in this experiment was described elsewhere (Astashinskii *et al*., 1989; Astashinskii *et al*., 1991; Doichinovich *et al*., 2001), therefore only a few details are given here for the sake of completeness.

The electrode system of MPC (Fig. 1) consists of the conically shaped copper central electrode (cathode) with radius 3 and 0.6 cm, 5 cm in length, with divertor on the top. Cylindrical outer electrode (anode) is made of 8 copper rods (0.8 cm in diameter and 14 cm in length), symmetrically positioned along the circle of 5 cm in diameter. Conically shaped cathode of MPC defines the profile of the acceleration channel.

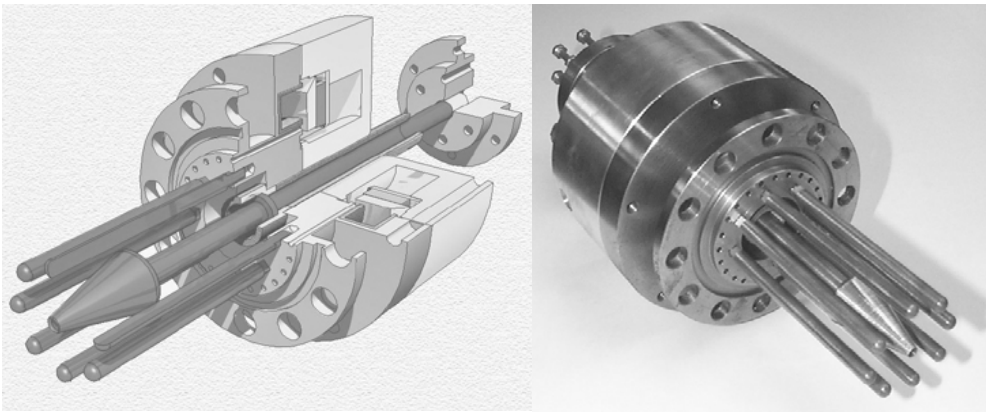

Fig. 1: Magnetoplasma compressor of compact geometry (MPC-CG).

The ions can be introduced into the acceleration channel through anode made of rods from the region between anodes rods and vacuum chamber being produced by "swept-away" currents. Namely, the gas around the anode is playing the role of virtual electrode. The self-magnetic field shielding of the anode rods (transparent anode) diminishes the level of the erosion. Anode rods are connected with the carrier, which enables MPC connection to the vacuum chamber.

A specially shaped insulator is positioned between anode rods carrier and the cathode to avoid the discharge breakdown on the surface of the insulator. It diminishes the level of impurities in plasma (Astashinskii *et al*., 1989). The insulator quality and its shape together with sufficient distance between carrier and the cathode enabled necessary

stability of the ionization zone, i.e., its shifting towards the insulator is avoided (Ananin *et al*., 1990).

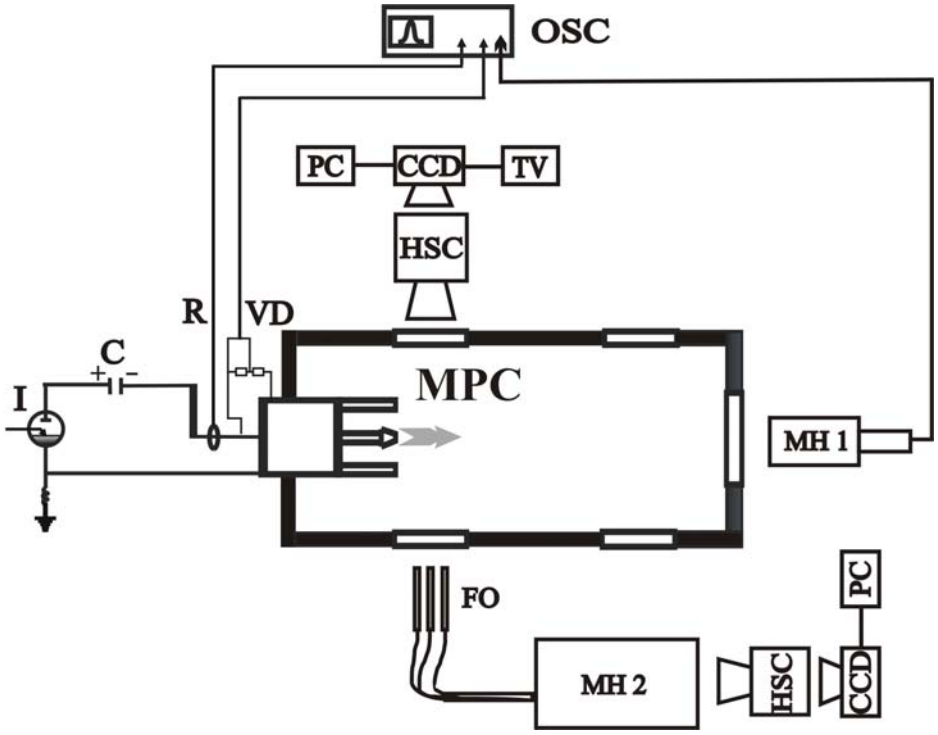

Fig. 2: Experimental set-up: C - capacitor, I - ignitron, OSC - oscilloscope for signals registration from Rogovski coil (R), voltage divider (VD) and McPherson spectrometer (MH1), HSC - high speed camera, FO - fiber optics, MH2 - Jobin Yvon spectrometer.

Stability of the compression plasma flow is achieved by the azimutal discharge simetry and homogeneous discharge current distribution through the electrodes surfaces. The discharge simetrisation is achieved by the special sectional formation of the condenser bank energy supply, appropriate connection design and continual working gas introduction through transparent anode.

In order to obtain as pure as possible plasma flow by MPC the ion separation per *M/q* (Morozov, 1969) the cathode top is shaped as a divertor. Due to Lorenz force heavier impurity ions stay close to electrode, e.g. go into divertor. If particular ion leaves the cathode, the high pressure zone ($\sim 10^4$ Pa) of the plasma flow pushes it back into divertor.

The discharge device of MPC is situated in a 30 x 30 x 150 cm vacuum chamber. Two-stage mechanical vacuum pump is used to evacuate the MPC vacuum chamber below 1 Pa; and then the chamber is filled with different working gas at given pressures. The MPC can operate with different working gasses and their mixtures as Ar, H_2, N_2, Ar + 3% H_2, at various pressures in two following modes: the working gas can be introduced using an electromagnetic pulse valve system witch allows mass rate in the range from 3-12 g/s; and in the regime of residual gas at different pressures from 10 to 10000 Pa. All measurements described here have been made with MPC operating in the residual gas

regime. The electrode system is connected through an ignitron (I) with 800 μF capacitor banks (C) (Fig. 2). Discharge current and the voltage between the MPC electrodes were measured using the Rogovski coil (R) and the voltage RC-divider (VD), respectively. The signals were simultaneously recorded by two-channel Tektronix TDS3032 oscilloscope (OSC).

Time and space developments of compression plasma flows and plasma velocity were determined using the photographs obtained by IMACON 790 high speed camera (HSC) operating in frame and streak modes (Fig. 2). For synchronization a sensitive photocell trigger unit was used.

Imaging technique performs digitalization during recording. CCD video camera, coupled to Imacon's output screen, gives composite video output to be fed into the PC. Video board performs capturing in real time and storing digital information in memory. When the recording ends, image processing software enables choosing the maximum illuminated frame from the video recording. For very low light level recording (for optical spectra) the image intensifier can be mounted on the Imacon's exit screen. Then CCD is optically coupled to intensifier's output screen. The exposure of CCD is not critical since the persistence of the Imacon's output phosphor is 80 μs.

Plasma velocity and shock front velocity were determined from streak records, using parallelly positioned slit with compression plasma flow axis in front of IMACON camera. The calibration of high-speed camera was effected using "Pulse generator" Hadland Photonics as a calibrator, within frequency range from 1 kHz to 100 MHz.

The electron density and temperature time dependences are obtained from end-on and side-on observations (Fig. 2). The profiles of spectral lines were obtained observing by shot by shot technique from the front side of MPC and averaging over several shots using McPherson 218 spectrometer (MH1, with Ar+3%H_2 as a working gas) and by side on observation using IMACON 790 high speed camera equipped with intensifier and CCD camera for line profile registration using Jobin Yvon HR 320S spectrometer (MH2, with H_2 as a working gas).

Time and spatially resolved spectroscopy measurements of hydrogen Balmer alpha line radiation from MPC plasma have been made using a HR320S spectrometer - IMACON 790 high speed camera system. Plasma was observed through a set of 10 fibers (FO) distributed along z axis starting from the outlet of the cathode with 7 mm separation up to 6.3 cm distance. All optical fibers were mounted in a certain order onto the entrance slit of the monochromator. It offers the possibility to obtain a set of line profiles in one shot at different positions from the cathode and at different times.

4. ELECTRICAL AND ENERGY DISCHARGE PARAMETERS

Analyzing the obtained current and voltage signals the electrical and energy discharge parameters were determined. Using such parameters it was possible to conclude whether or not the compression plasma flow was organized properly. Typical oscilloscope current and voltage traces for MPC operating in Ar + 3% H_2 are given in Fig. 3 (a).

The obtained current maximum was up to 100 kA, duration up to 150 μs (current half period ~70 μs), inductivity 0.5-0.7 μH and resistance 30-40 mΩ. The existence of phase shift between the current and voltage proved the absence of the discharge breakdown along the insulator surface (Astashinskii *et al*., 1989).

Using the current and voltage traces from Fig. 3 (a) the discharge volt-ampere characteristics (Fig. 3 (b)), as well as the change of the instantaneous input discharge power $P(t) = I(t) \cdot U(t)$ (Fig. 3 (c)) and energy $W(t) = \int I(t) \cdot U(t) dt$ (Fig. 3(d)) are obtained. Volt-ampere curves are nonlinear in the time interval from 20 to 50 μs when the plasma flow is quasistationary stable which can be regarded as the verification of the effectiveness of the MPC operation.

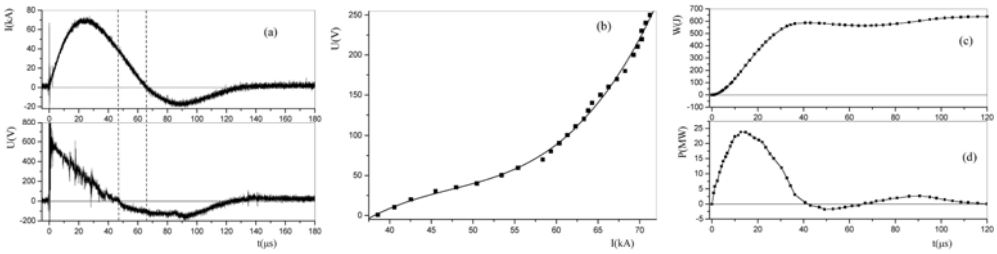

Fig. 3: Current and voltage oscilloscope traces (a), discharge volt-ampere characteristic (b), instantaneous power (c) and energy (d) time dependences.

Linear volt-ampere characteristics were obtained in the case of classical plasma accelerators with continual electrodes (Kovrov and Shubin, 1974), as well as in the case of atmospheric pressure discharges (Astashinskii *et al.*, 1991). There is no phase shift between current and voltage if the discharge breakdown is going on the isolator surface. Therefore volt-ampere characteristics are linear. From Fig. 3 (d) one can conclude that the energy transfer from capacitor bank to the discharge is terminated at the end of the first current half-period (~60 μs).

Analyzing volt-ampere characteristics of discharge in Ar, N_2 and H_2 (Fig. 4) one can conclude that most effective energy transfer from supply to plasma is in hydrogen as a working gas (largest volt-ampere characteristics slope).

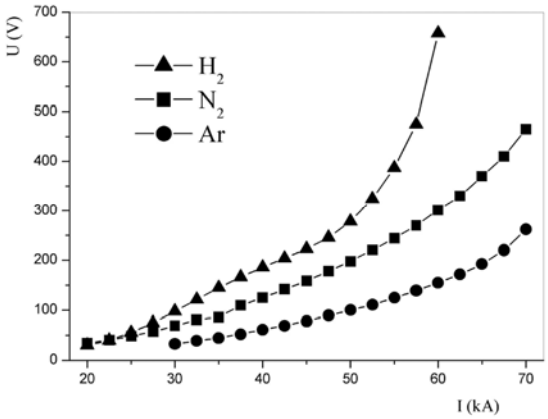

Fig. 4: Discharge volt-ampere characteristic in Ar, N_2 and H_2.

5. COMPRESSION PLASMA FLOW IN TIME EVOLUTION

Using IMACON 790 high speed camera operating in frame and streak mode, the evolution in time of breakdown, shock wave formation, compression plasma flow creation and after glow discharge were registered in Ar, N_2 and H_2 at 10-3000 Pa pressures, and 2.5-4.1 kV voltages.

Although MPC discharge development depends on the initial conditions, first of all working gas and its pressure, as well as on energy supply voltages, a general picture of the dynamics of the compression plasma flow formation can be obtained on the bases of high speed camera images (Fig. 5). Discharge development can be divided in four phases: (i) discharge breakdown and plasma accelerating along the cathode conical part; (ii) radial plasma compression and relaxation of accompanied plasma flow oscillations; (iii) quasistationary stable state of compression plasma flow; (iv) decay of compression plasma flow followed by after glow effects.

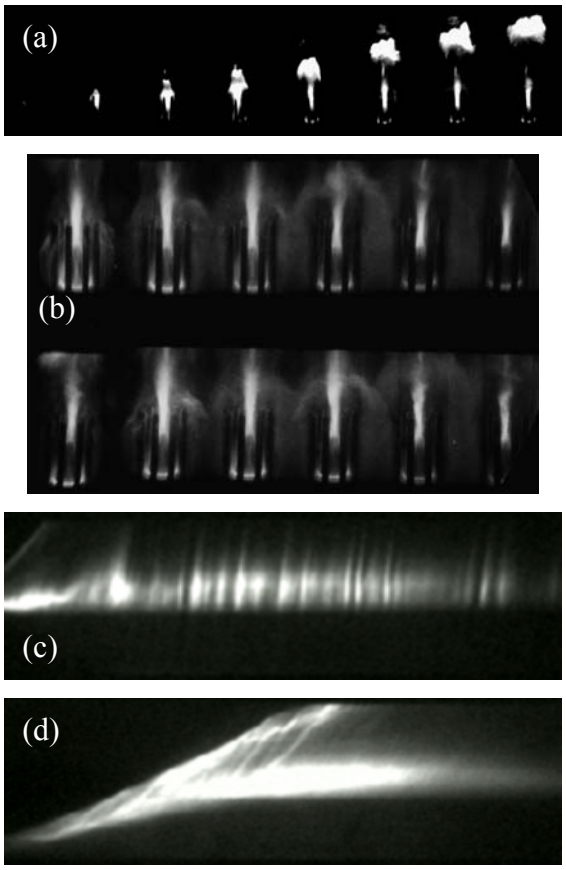

Fig. 5: MPC discharge development in argon obtained by IMACON 790 high speed camera operating in framing mode with time intervals of 4 μs (a) and 2 μs (b) and exposure time 400 ns; and streak mode with 1 μs/mm at 100 Pa (c) and 3000 Pa (d) pressures.

The first phase starts after the triggering pulse switching on ignitron, resulting with discharge breakdown in the inter electrodes region of MPC lasting till the plasma gets out from that region. The breakdown starts at the top of the cathode (maximal distance from the anode rods) or from the widest conical cathode part (narrowest cross section of the accelerating channel, i.e. minimal distance from anode rods) depending on the working gas pressure. During this phase discharge current increases and therefore the magnetic field increases, too. At the real beginning of the discharge, the electric field is established in the whole volume of the accelerating channel. However, the increasing magnetic field, carrying practically the whole energy, is established only at the entrance to the acceleration channel. In the MPC inter electrode region the plasma is accelerated due to the Ampere force F_{Az} as the result of the radial component of plasma current I_r interaction with azimuth magnetic field B_φ: $\vec{f} = \vec{j} \times \vec{B}$ (Fig. 6).

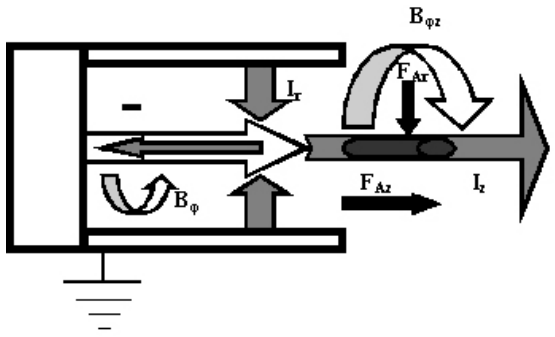

Fig. 6: Scheme of MPC principle.

It is found that plasma during this phase reaches the end of the electrodes after about 5-10 μs from the beginning of discharge.

The second phase usually starts with strong radial plasma compression at the top of the cathode lasting up to plasma oscillations relaxation within compression flow. This is the transition phase to a quasistationary (stable) phase. At the beginning of the phase the first plasma front is formed initiating a shock wave. At the same time axis-simetrically in the accelerating system, at the outlet of MPC, the compression plasma flow is created (Fig. 5). The compression plasma flows are formed about 15-20 μs after the beginning of the discharge current. The only exception is in hydrogen when this process is going on during ~10 μs. Plasma flow is compressed due to interaction between the longitudinal component of current swept-away I_z from discharge device, and intrinsic azimuth magnetic field $B_{\varphi z}$ (Fig. 6), as well as, due to the dynamic pressure of plasma flow converging to the system axis (the inertial compression). The presence of the "swept-away" current in the plasma flow is caused by the magnetic field frozen in plasma.

The energy from condenser bank supply is transferred to the plasma through magnetic field. The plasma is accelerating and therefore its kinetic energy is increasing. Due to plasma compression its enthalpy is increasing. After plasma leaving the compression zone, its total energy again is transferred in plasma kinetic energy.

During this second phase an ionization zone is formed in the region of accelerating channel having minimal cross section (Fig. 5). Ions produced by "swept-away" current in the external region behind the anode made of rods, come to the accelerating channel. Within 15-30 μs the radial oscillations of compression plasma flow occur.

The first plasma front after coming to the top of cathode, is leaving inter-electrodes part of the MPC being followed by the compression plasma flow formed at the cathode top. The front is occupying the deceleration zone of compression plasma flow due to its interaction with working gas.

The third quasistationary phase is starting after termination of the above described transitional processes when a stable compression plasma flow is created. Shape and duration of compression plasma flow depend on the working gas and its pressure, as well as on input energy. For instance, durations of compression plasma flow in Ar and N_2 are shorter at high pressures (~30 μs) than at low pressures (~40 μs). However, in hydrogen the stable compression plasma flow exists about 50 μs. During this phase plasma parameters are changing slowly and conditions for local thermodynamic equilibrium (LTR) are fulfilled.

It this experiment it has been found that the compression plasma flow length is the function of the working gas, the pressure and discharge current. Generally, the length is increasing with pressure lowering and maximum discharge current increasing. It is especially expressed in argon as a working gas and, also, in hydrogen but at lower pressure (Fig. 7). Diameters of compression plasma flows are 0.5-1.5 cm in the zone of maximal compression. It was found that they decrease with pressure decreasing and discharge current increasing.

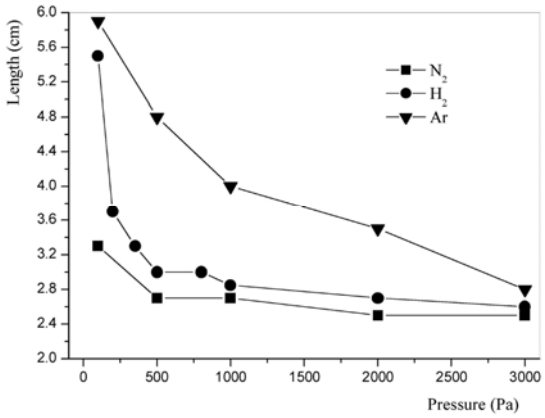

Fig. 7: Length of compression plasma flow for different working gases as the functions of pressure.

Compression plasma flow velocities are measured using photographs obtained by high speed camera operating in streak mode similar to one presented in Fig. 5. In this Figure a discrete microstructure of compression plasma flow (light and dark regions) is observed. These structures are occurring with 5-10 MHz frequencies. From the slopes of the structures compression plasma flow velocities are determined and given in Fig. 8 for

different working gases as the functions of pressures. From Fig. 8 one can conclude that plasma flow velocities in argon and nitrogen are decreasing with pressure increasing.

However, in hydrogen the maximum value of plasma flow velocity is observed at 1000 Pa pressure. For pressures lower than 1000 Pa the plasma flow velocity is decreasing with pressure decreasing. This can be explained by the enhanced erosion of the cathode at pressure lower than 1000 Pa. It is a consequence of the impurities present in the plasma flow (mass of working gas is increased). This effect is not found in the case of nitrogen and argon as working gas, although from Fig. 8 one can conclude that for 100 Pa pressure in all cases plasma flow velocities are almost the same.

It is of interest to note once again that maximal plasma flow velocity values are obtained for hydrogen. This, together with non-linear volt-ampere characheristics shape, proves that the hydrogen is the most favorable working gas in MPC, regarding the energy transfer effectiveness from the condenser bank supply to plasma.

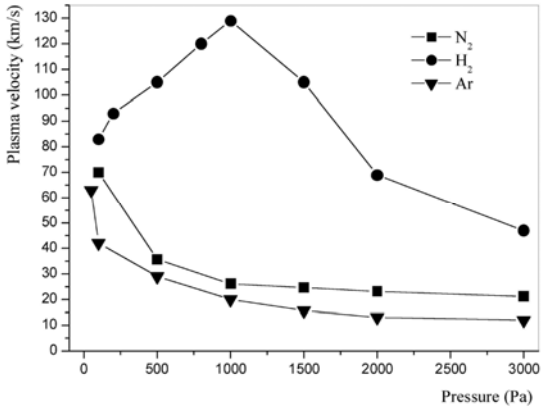

Fig. 8: Plasma flow velocity for different working gases as the functions of pressure (6.4 kJ supply energy).

MPC-CG is a quasistationary plasma source because life time of the created compression flow is much longer than characteristic flight time of plasma in the accelerating channel. For the average plasma velocity of 50 km/s (5 cm/μs) and accelerating channel ~5 cm long, flight time is ~ 1 μs. The stable compression plasma flow state is terminated 70-80 μs after the discharge beginning. It is in good accordance with current pulse duration.

The fourth phase of the MPC operation is the compression plasma flow decay. Its beginning and duration depend on the initial conditions determined by the characheristics of condenser bank energy supply. If the input energy can be continually supplied quasistationary phase can be unlimited in time and the decay phase can be unlimitedly postponed.

In that case MPC will operate as stationary plasma source. Namely, the continual ionization processes are taking part in working gas introduced in interelectrode region. The ionized gas (plasma) is steadily accelerated and permanently compressed.

In this experiment the duration of MPC discharge is approximately 140 μs for energy supply of 5-10 kJ. However, plasma current loops owing to the magnetic field

confined in plasma can exist longer in chamber disappearing slowly at the chamber walls. The so-called swept away currents have sufficient energy to excite the atoms and ions of working gas. Therefore, the radiation from the working gas lasts longer then the discharge in the accelerator (Doichinovich *et al*., 2001).

The presence of cathode erosion (Fig. 9 (a)) as well as anode protection from the erosion can be regarded as the proof of the ion current transport occurring. The cathode erosion is a consequence of cathode potential drop and current slippage along the cathode surface.

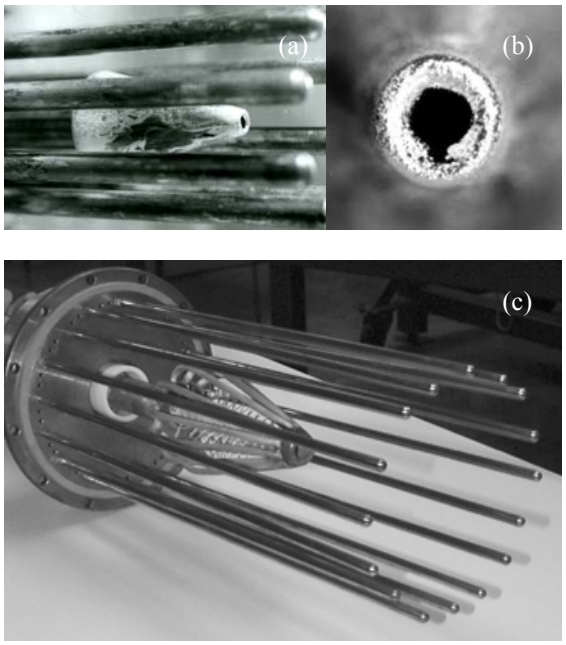

Fig. 9: Erosion of MPC cathode: (a) side on image; (b) the top of the cathode image; (c) MPC with transparent electrodes (self shielded by magnetic field).

The cathode erosion is especially intensive in MPC working in argon at low pressure (~100 Pa). Also, the material deposition originating from the cathode is present at the divertor top (Fig. 9 (b)).

In order to avoid cathode erosion it has been specially designed and constructed similarly to the one used in accelerating channel of two stage quasi-stationary plasma accelerator (Ananin *et al*., 1990; Morozov, 1990; Kuraica *et al.*, 2002) (Fig. 9 (c)).

6. PLASMA FLOW PARAMETERS

Plasma flow electron density and temperature are measured using spectroscopy methods. Plasma reproducibility was within ±10% as measured from intensity of continuum

radiation. The estimated experimental errors of plasma electron density and temperature measurements are within ±10% and ±15%, respectively. Electron density is determined using Stark profiles of H_α and H_β spectral lines analyses (Fig. 10). The profiles were obtained using shot-by shot technique, observing from the front side of MPC and averaged over several shots when operating in Ar + 3% H_2 working gas mixture (Fig. 2). The electron density time dependences are obtained from the comparison of the measured Stark widths with theoretical results of Gigosos and Cardenoso (1996). They are presented in Fig. 11 (a).

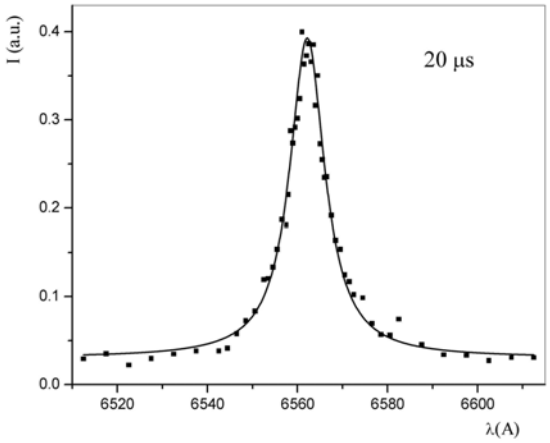

Fig. 10: Line profile of H_α as obtained by end-on observation in Ar + 3% H_2 mixture (n_e = $8 \cdot 10^{16}$ cm^{-3} and T_e = 13 200 K).

Compression plasma flow parameters predominantly depend on discharge current. Electron density time dependence correlation with discharge current time evolution is determined by a dynamical coefficient n_e/I (Ananin *et al*., 1998) (Fig. 11).

The dinamical coefficient n_e/I is a measure of plasma flow stationarity. It is constant when and where the compression plasma flow is quasi-stationary stable. Namely, electron density "follows" the discharge current time evolution. In the beginning of plasma flow creation n_e/I is decreasing, since discharge current increases faster than the electron density. However, during the compression plasma flow decay this parameter increases as a consequence of faster discharge current decreasing (in comparison with compression plasma flow vanishing).

Physical processes within compression plasma flows depend on the discharge current time dependence. These processes can be studied by the investigation of spectral lines and continuum radiation, as well as by the study of discharge current time dependence. Time dependences of several hydrogen spectral lines obtained in Ar + 3% H_2 gas mixture are given in Fig. 12.

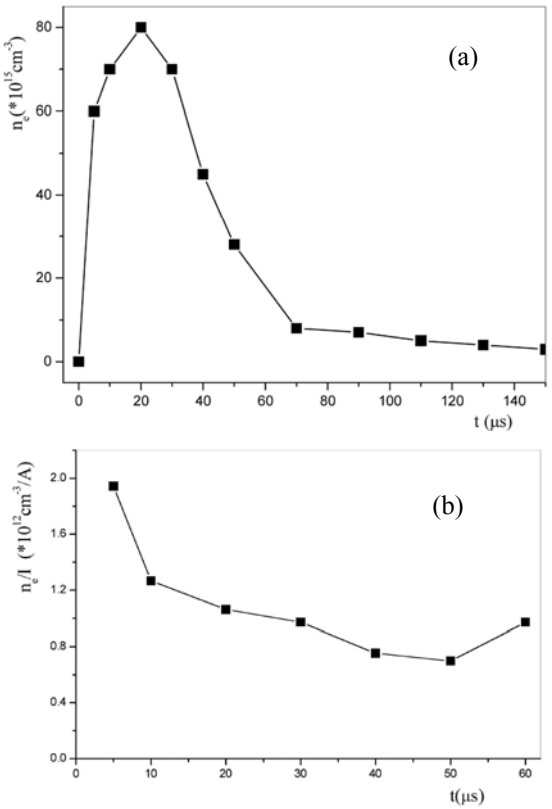

Fig. 11: The electron density (a) and dynamical coefficient n_e/I (b) time dependences.

From Fig. 12 one can conclude that the intensities of H_α, H_β and H_γ have reached their maximal values at different instants. It is found that H_α maximum is the latest in comparison with other two lines maxima (H_β and H_γ). The maxima of all investigated lines are very wide (with constant intensity for about 20 μs). The intensities of H_α and H_β spectral lines last 3 to 4 times longer than the current signal (signal from Rogovski coil). That effect of the afterglow radiation existence was observed, also, for the neutral argon line intensities (ArI 696.5 nm).

The continuum and ion argon line intensities time dependences on compression plasma flow of MPC operating in Ar + 3% H_2 gas mixture are also analyzed. Continuum radiation and the Ar II 480.6 nm spectral line intensities (Fig. 12) are following the discharge current time dependence, reaching maximal values at the same time (~25 μs), although intensities of singly charged argon ion lines last longer (up to the end of discharge current second half period ~130 μs) than the continuum radiation (up to the end of the first half period ~80 μs). It is obvious that the argon ions are emitted from the most compressed region of the plasma flow. When the discharge is terminated the compressed plasma flow is disappearing, and the argon singly charged ions are neutralized by recombination.

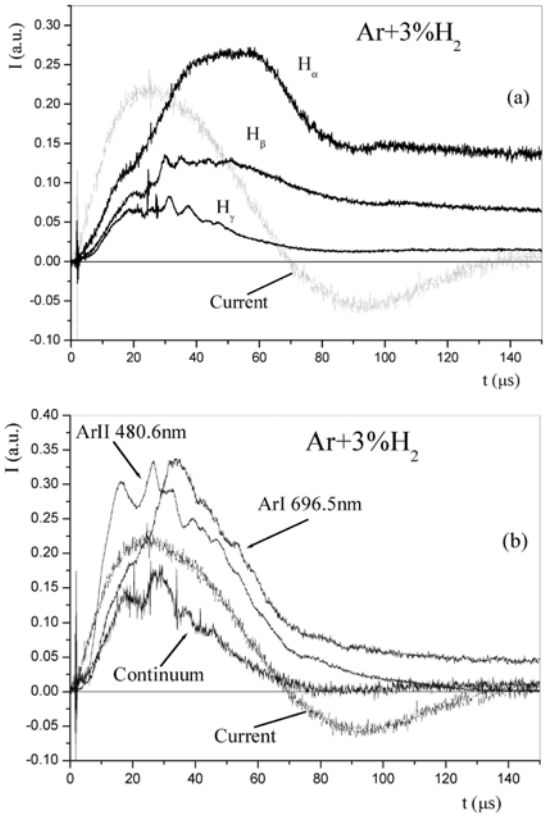

Fig. 12: Intensities of: a) H_α, H_β and H_γ; b) ArI 696.5 nm, Ar II 480.6 nm spectral lines versus time compared with continuum radiation intensity and discharge current time evolutions.

The intensity maxima of all spectral lines are appearing in the time interval (20-60) μs from the beginning of discharge, i.e. in the period of maximal compression of the plasma flow. In that period the plasma flow is in quasistationary stable state, which is verified by Fig. 6. The compression plasma flow starts disappearing 70 μs after beginning of the discharge. The swept away currents have enough energy to excite hydrogen and argon atoms and due to that, the radiation is observed several hundreds microseconds after the discharge termination (Doichinovich *et al*., 2001).

The axial and temporal electron density distributions of the compression plasma flow are obtained from the Stark halfwidth of Balmer alpha line profiles comparison with theoretically calculated ones (Gigosos and Cardenoso, 1996). Measurements have been made in pure hydrogen at 1000 Pa pressure from side on observation. The experimental setup used is given in Fig. 3. Spectral line intensities registration was performed using high speed camera operating in framing mode ($1 \cdot 10^5$ frame/s) and thereby from the analyses of these profiles the electron density axial distribution in time was enabled. One hundred of H_α profiles were obtained per one MPC shot using this method.

Temporal and spatial electron density distribution of MPC plasma determined using Stark profiles of H_α spectral lines are given in Fig. 13. Electron density has its maximum at 20 μs and is approximately constant ~$(3\text{-}4)\cdot10^{17}cm^{-3}$ within the 0.5-4 cm region along the z axis. For distances greater than 4 cm an appreciable electron density is noticed only at 10 μs record, which can be explained by the action of shock wave on the ionization of working gas. Contrary to this, after 10 μs electron density suddenly decreases for all positions larger than 4 cm, i.e. out of compression plasma flow region.

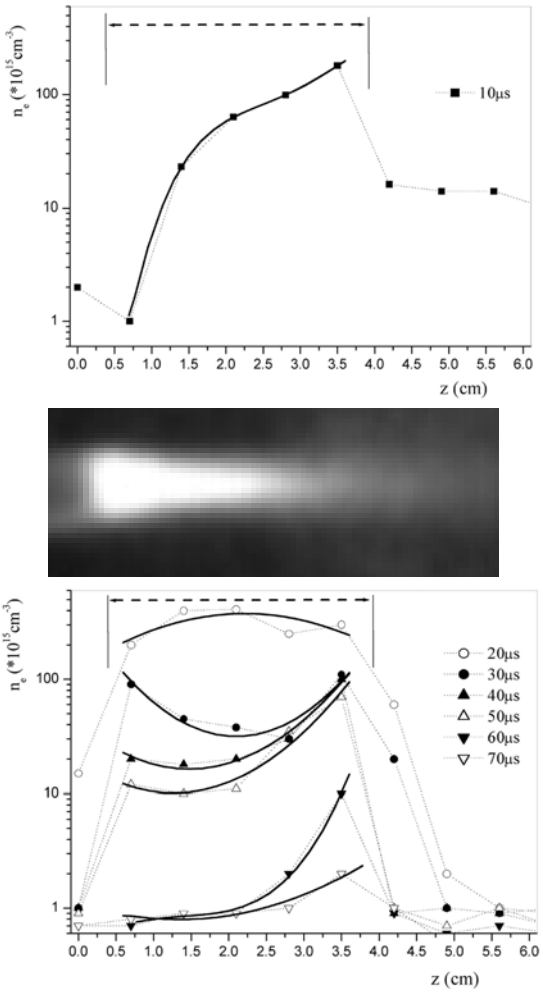

Fig. 13: The electron density time dependences from side-on observation in H_2 with one high speed camera frame.

The axial and temporal distributions of Balmer alpha line intensity are given in Fig. 14. An increase of line intensity during 20 μs rise time is found in every position along the MPC z axis. Maximum line intensity reached at 20 μs is constant from 0.5 to 4.5 cm from the top of the cathode, along the z axis. Balmer alpha line intensity then decreases versus

time in every position. The maximum of line intensity is observed within the 1.5-2 cm region in time interval of 30-70 μs. Further than 4.5 cm along z axis line intensity is very low for every time record.

By comparing the obtained Balmer alpha line intensity and the electron density axial distribution in time one can come the following conclusions: (i) both distributions have their maxima 20 μs after the discharge beginning, gradually decreasing later on; and (ii) a range of high values for both distributions is the same and is localized within 0.5-4 cm region along z axis.

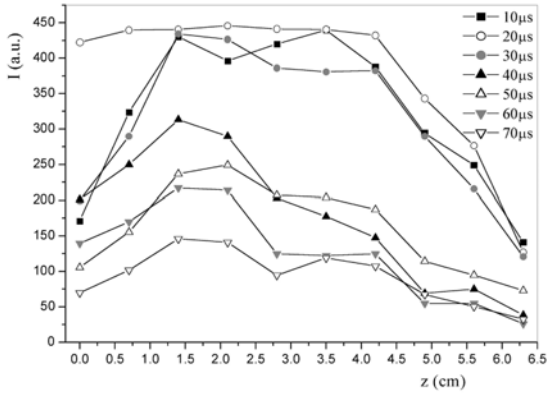

Fig. 14: The Balmer alpha line intensity time dependences from side-on observation in H_2.

All this can be regarded as the verification of stable quasistationary compression plasma flow existence, created by the MPC plasma accelerator.

In the paper of Astashinskii *et al.* (1992) it was reported that the electron density within accelerating channel is of the order of 10^{16} cm^{-3}. Here, we have found that electron density obtained by quasistationary plasma accelerator is a weak function of the working gas type and pressures and strongly dependent on the discharge current. Therefore, we have used this value in order to calculate the degree of compression and have obtained it to be approximately 20.

The electron temperature was measured in the MPC operating in Ar + 3% H_2 gas mixture using a method based on the relative intensity ratios of spectral lines originated from two successive ionization stages of argon, using Saha equation.

The experimental set-up used is given in Fig. 3. The measurement has been made using Ar I 696.5 nm and Ar II 480.6 nm argon line intensities by end on observation. The obtained electron temperature time dependence is given in Fig. 15. It was found that within quasi-stationary plasma flow region the average temperature is 13000 K, which is in good agreement with previous experiments (Ananin *et al*., 1990; Astashinskii *et al.*, 1992).

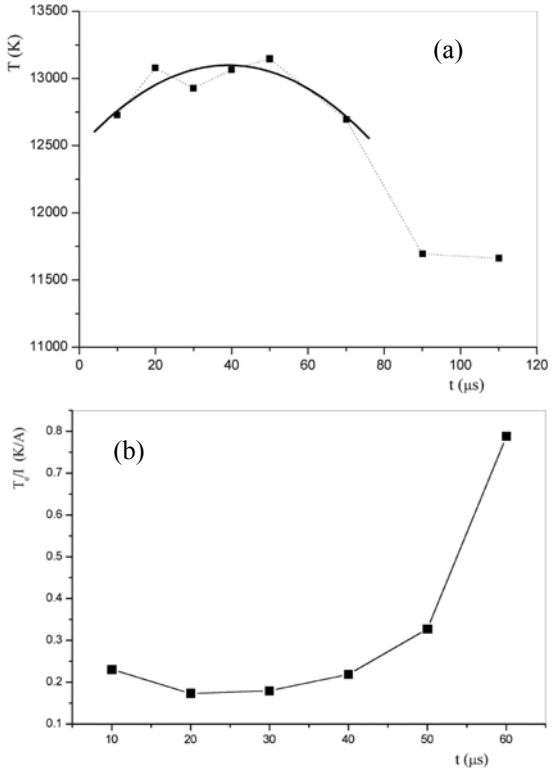

Fig. 15: The electron temperature (a) and dynamical coefficient T_e/I (b) time dependences.

Similarly to the definition of dinamical coefficient of electron density, it is of interest to do the same for electron temperature (T_e/I). It was calculated from the experimentally obtained values of temperature and discharge current and presented in Fig. 15. It was found that during the quasi-stationary phase this parameter is constant. However, during compression plasma flow decay this parameter increases which is in good accordance with conclusion drawn in the case of n_e/I dinamical coefficient behavior.

Using the equation for an ideal gas state it is possible to calculate gas kinetic pressure within compression plasma flow. For 1-2 eV temperature and 10^{17} cm^{-3} density, the pressure is of the order of 10^4 Pa.

Compression plasma flow current can be calculated from the balance between the gaskinetic plasma pressure and azimuth self-magnetic field pressure

$$\frac{B^2}{2\mu_0} = nk(T_e + T_i) \tag{6}$$

e.g. from Benet equation (with $T=T_e=T_i$)

$$\mu_0 I^2 = 16\pi^2 R^2 nkT \tag{7}$$

where R is the radius of compression flow.

In this experiment for $n_e \sim 2 \cdot 10^{23}$ m^{-3}, $T_e \sim 15000$ K, $R \sim 8 \cdot 10^{-3}$ m, and consequently plasma flow current is ~15 kA, which is 20% of the discharge current maximal value (~80 kA).

7. CONCLUSION

The advantages of magnetoplasma compressor of compact geometry, as compared to other types of accelerators, are high stability of the compression flows generated, controllability of their composition (different gases and their mixtures), size (up to 6 cm in length and 1 cm in diameter), and plasma parameters (up to $4 \cdot 10^{17}$ cm^{-3} and temperature up to 2-3 eV), as well as the discharge duration sufficient for practical applications (up to 70-80 μs). Besides, the operation in the ion current transfer mode with the minimization of the electrodes erosion represents the main advantage of the quasistationary plasma accelerators in comparison with the classical ones. Also, there is no limit in increasing their main parameters (plasma flow duration, flow velocity, temperature and plasma density) due to the discharge current cut off in the case of classical plasma accelerators. The "current crisis" can be avoided by the electrodes protection from the erosion as a result of the magnetic field self shielding. All limitations are connected with input energy of the accelerator. Therefore, MPC described here is a favorable one for constructing the first stage of two stage quasi-stationary plasma accelerator which can be used as possible plasma injector in fusion device and investigation of plasma wall interaction in fusion reactor.

References

Ananin, S.I., Astashinskii, V.M., Bakanovich, G.I., Kostyukevich, E.A., Kuzmitski, A.M., Man'kovskii, A.A., Min'ko, L.Ya., Morozov, A.I.: 1990, *Sov. J. Plasma Phys*., **16**, 102.

Ananin, S.I., Astashynski, V.M., Burakov, V.S., Kostyukevich, E.A., Kuzmitski, A.M., Tarasenko, N.V., Dojcinovic, I., Kuraica, M.M., Puric, J., Videnovic, I.R.: 2002, *29th EPS Conference on Plasma Phys. and Contr. Fusion*, Montreux 2002, Switzerland, **26B**, P-5.049.

Ananin, S.I., Astashinskii, V.M., Kostyukevich, E.A., Man'kovskii, A.A., Min'ko, L.Ya.: 1998, *Plasma Physics Reports*, **24**, 936.

Astashynski, V.M., Ananin, S.I., Askerko, V.V., Avramenko, V.B., Kostyukevich, E.A., Kuzmitski, A.M., Uglov, V.V., Anishchik, V.M., Astashynski, V.V., Kvasov, N.T., Danilyuk, A.L., Purić, J., Kuraica, M.M., Dojčinović, I., Videnović, I.R.: 2002, *16th ESCAMPIG*, Grenoble 2002a, France, **1**, 149.

Astashynski, V.M., Ananin, S.I., Askerko, V.V., Avramenko, V.B., Kostyukevich, E.A., Kuzmitski, A.M., Uglov, V.V., Anishchik, V.M., Astashynski, V.V., Kvasov, N.T., Danilyuk, A.L., Puric, J., Kuraica, M.M., Dojcinovic, I., Videnovic, I.R.: 2002b, *29th EPS Conference on Plasma Phys. and Contr. Fusion*, Montreux 2002, Switzerland, **26B**, P-2.027.

Astashinskii, V.M., Bakanovich, G.I., Kuzmitski, A.M., Min'ko, L.Ya.: 1992, *Journal of Engineering Physics and Termophysics*, **62,** 281.
Astashinskii, V.M., Bakanovich, G.I., Kostyukevich, E.A., Kuzmitski, A.M., Man'kovskii, A.A., Min'ko, L.Ya.: 1989, *J. Appl. Spectroscopy*, **50**, 887.
Astashinskii, V.M., Efremov, V.V., Kostyukevich, E.A.: 1991, *Sov. J. Plasma Phys.* (Engl. Transl.), **17**, 545.
Astashinskii, V.M., Min'ko, L.Ya., Man'kovskii, A.A.: 1991, *J. Appl. Spectroscopy*, **55,** 903.
Doichinovich, I.P., Gemishich, M.P., Obradovich, B.M., Kuraitsa, M.M., Astashinskii, V.M., Puric, Ya.: 2001, *J. Appl. Spectroscopy*, **68**, 629.
Gigosos, M.A., Cardenoso, V.: 1996, *Journal of Phys. B*, **29,** 4795.
Kovrov, P.E., Shubin, A.P.: 1974, *Physics and Application of Plasma Accelerators* (in Russian), Nauka i Tekhnika, Minsk, 1974, 78.
Kuraica, M.M., Astashynski, V.M., Dojčinović, I., Purić J.: 2002, *21st SPIG,* Soko Banja 2002, Serbia, 510.
Morozov, A.I.: 1969, *Nuclear Fusion Special Suppl.*, 111.
Morozov, A.I.: 1975, *Sov. J. Plasma Phys.* (Engl. Transl.), **1**, 95.
Morozov, A.I.: 1990, *Sov. J. Plasma Phys.* (Engl. Transl.), **16**, 69.

Publ. Astron. Obs. Belgrade No. 76 (2003), 105 - 116 *Invited lecture*

IMPORTANCE OF STARK DAMPING IN THE STUDY OF ABUNDANCE STRATIFICATION IN AP STARS

T. RYABCHIKOVA[1,2]

[1] *Institute of Astronomy, Russian Academy of Sciences, Pyatnitskaya 48, 119017 Moscow, Russia*
E–mail: ryabchik@inasan.rssi.ru

[2] *Institute for Astronomy, University of Vienna, Türkenschanzstrasse 17, 1180 Vienna, Austria*
E–mail: ryabchik@astro.univie.ac.at

Abstract. In this paper I point out the importance of the accurate Stark widths and shifts for abundance stratification study in the atmospheres of Ap stars. The cases of Ca, Ba and Si empirical distributions are discussed.

1. INTRODUCTION

Among the stars of the Upper Main Sequence (UMS) there is a large class of late A - early B stars which have anomalously strong or anomalously weak lines of different chemical elements in their spectra. This class has a common name – chemically peculiar or Ap stars. A variety of peculiarities are observed in the form of underabundances (He in He-weak stars; CNO in magnetic Ap stars; Ca and Sc in Am stars, metals in λ Boo stars) as well as overabundances (He in He-rich stars, Si in Si-stars; Mn, Hg and other heavy elements in HgMn stars; iron peak (Cr in particular), rare-earths elements in most of Ap and Am stars). A temperature range occupied by Ap stars is 6500 – 20000 K. Most of Ap stars have global magnetic field from hundreds of Gauss to a few dozens of kG. Ap stars are usually slow rotators compared with the normal stars of the same effective temperature. This is sufficient to stabilize stellar atmosphere and to allow chemical element separation while in the normal UMS star atmosphere, where rotational velocities are large enough, rotationally-induced mixing or turbulent stellar winds homogenize the atmosphere, and we do not observe any significant abundance anomalies.

To explain the observed abundance anomalies in Ap stars Michaud (1970) has proposed a radiative diffusion, which together with the gravitational settling may produce both underabundances and overabundances of the chemical elements. The net result of the element separation in stabilized stellar atmosphere is the abundance stratification.

Babel (1992, 1994) was the first to performe theoretical and empirical stratification analysis in the atmospheres of cooler part of Ap stars. He provided theoretical distributions versus optical depth (or *abundance profiles*) for Ca, Ti, Cr, Mn and Sr, which may be represented by simple step-like function. According to his model the Fe-peak elements are underabundant in the upper atmospheric layers and are accumulated at the optical depths below $\log \tau_{5000} = -1$. Recent self-consistent diffusion model calculations for Ap star β CrB by F. Leblanc (see Ryabchikova, Wade and LeBlanc, 2003) supported the results by Babel and provided similar abundance profiles for many other chemical elements. Still theoretical abundance profiles differ from the empirically derived element distributions. The latter mainly depend on our knowledge of the accurate atomic parameters of spectral lines and atmospheric models.

2. THE ROLE OF STARK EFFECT IN ABUNDANCE STRATIFICATION STUDY

There are a number of spectroscopic features in Ap stars which cannot be described with the best chemically homogeneous atmospheric models. They are discussed in details by Ryabchikova et al. (2003). The most significant spectroscopic evidence for stratification is the impossibility to fit the core and the wing of the strong spectral line with the same abundance. This phenomenon is observed in UMS peculiar stars through the entire temperature range of chemical peculiarity. In hot Ap stars He I lines usually have wider wings and less deep line cores compared to the normal stars (see, for example, Figs. 5, 6 of the paper by Bonifacio, Castelli and Hack, 1995). In HgMn stars the core and wing anomaly is observed in the resonance UV Ga II and Ga III lines (Smith, 1995 - Fig. 1 of his paper). The spectra of the cooler Ap stars will be considered below.

Theoretical abundance profiles in most of Ap stars predict element overabundances in rather deep atmospheric layers where the temperature and electron density are high even in the cooler Ap stars thus favouring the Stark effect. In the next subsections I shall give a few examples where Stark shifts and widths are very important in abundance stratification study.

2. 1. CALCIUM LINES

The pioneering stratification studies in the atmospheres of Ap stars by Babel (1992, 1994) were based on the resonance Ca II lines. Babel stressed that 'Ca II K and H lines in Ap stars give precious information about abundance stratification'. This is illustrated in Fig. 1 for the Ap star γ Equ ($T_{\rm eff}$=7700 K) taken from Ryabchikova et al. (2002). Ca II K line is fitted rather well with the Ca abundance distribution similar to theoretical abundance profile from Babel's calculations (Fig. 2).

One can easily see that it is enough to have a precise observed profile of this spectral line to reconstruct Ca abundance distribution in stellar atmosphere. Unfortunately Ca II K line is situated between two hydrogen lines, whose wings are overlapped with Ca II K wings. Also, the core of Ca II K line is certainly affected by NLTE effects. Therefore we need to investigate other spectral lines of both Ca I and Ca II to reconstruct the empirical Ca distribution. There are two Ca II lines in the red spectral region with less severe blending, which show anomalously wide wings in

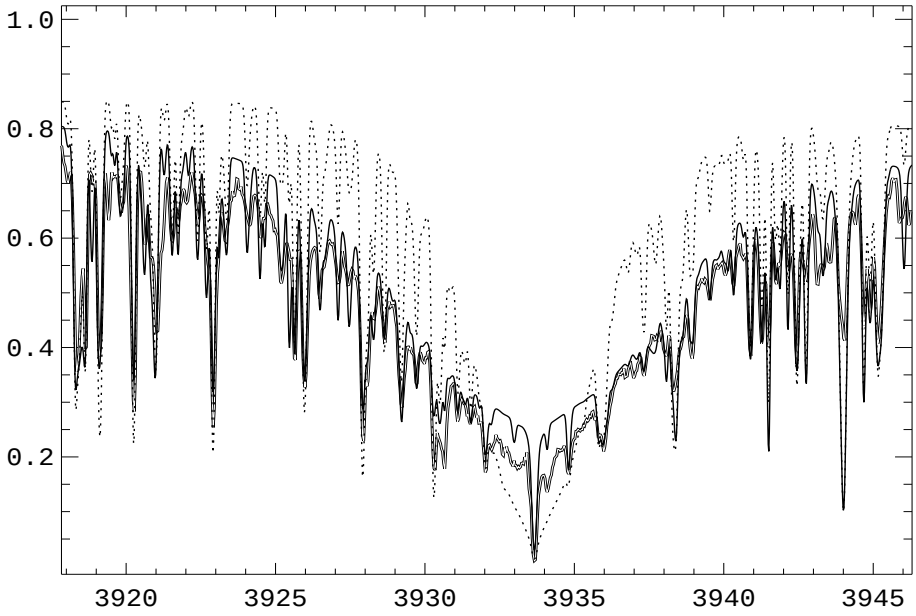

Fig. 1: Ca II K line in the spectrum of γ Equ (left panel). Observations are shown by the double line, the synthetic spectrum using the best homogeneous Ca abundance is shown by dotted line, while the synthetic spectrum calculated with an empirically-derived Ca abundance profile (Fig. 2) is shown by solid line.

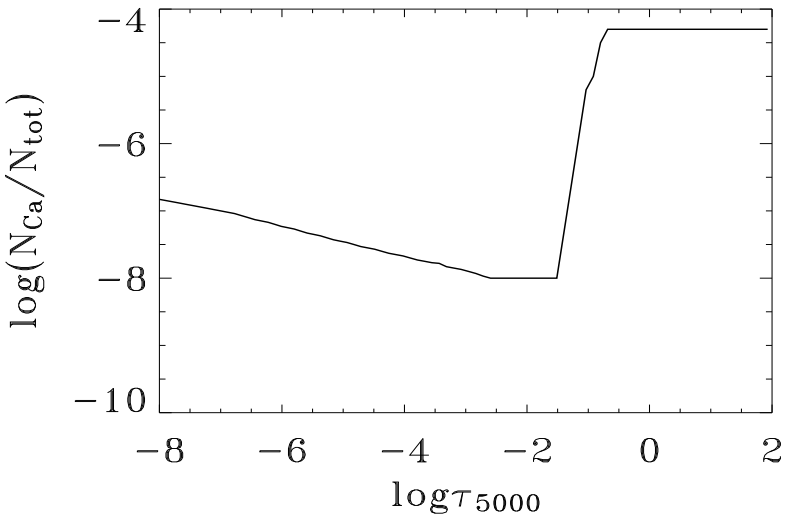

Fig. 2: Ca distribution in the atmosphere of Ap star γ Equ

practically all Ap stars with $T_{\rm eff}\leq$9000 K. These lines, λ 5339.19 Å and λ 6456.87 Å belong to the transitions between the common low level 4f ^2F and the upper levels 7g ^2G, 6g ^2G. In VALD database (Kupka et al., 1999) the corresponding Stark broadening constants for these lines are –3.35 and –4.31, respectively. Stark damping constants here are written in the form $\log(\gamma_S/N_{\rm e}$, where $N_{\rm e}$ – is electron density in cm^{-1}. I synthesized both lines for γ Equ atmospheric model using the uniform mean Ca abundance from Ryabchikova et al. (1997) and the stratified abundance shown in Fig. 2. Oscillator strengths for both lines are taken from TOPBASE (Seaton et al., 1992) as the best representing the same solar lines. Note that Stark damping constants in VALD were calculated by Kurucz (1993). A comparison between the observed spectrum and my calculations is shown in Fig. 3 by dotted line (homogeneous atmosphere) and by dashed line (stratified atmosphere, Kurucz γ_S data). Using the same $\log(\gamma_S/N_{\rm e}) = -3.7$ for both lines I get better agreement between the observed and synthetic spectra (solid line in Fig. 2). Stratified Ca abundance in γ Equ is necessary to fit simultaneously Ca I lines $\lambda\lambda$ 6449.81 and 6455.50, which have the lower levels with different excitation energies. New calculations of the Stark widths and shifts for more Ca II lines are needed to improve the empirical Ca distribition in the atmospheres of γ Equ and other cool Ap stars.

2. 2. BARIUM LINES

In most of Ap stars Ba is ionized, therefore we observe only Ba II lines and mainly the strongest ones. It is not possible to make a differential analysis of the strong and weak Ba II lines to search for the possible stratification effects. At the same time in the coolest Ap stars, like one of the craziest representative of the whole class, the famous Przybylski's star (HD 10165, $T_{\rm eff}$=6600 K), a few Ba I lines were identified and measured (see Cowley et al., 2000). It was not possible to fit both Ba I and Ba II line profiles and/or total line intensities (equivalent widths) with the same homogeneous Ba abundance. But a simple step-like Ba distribution, shown in Fig. 6 by dashed line, where the upper limit of Ba abundance was found by fitting Ba II λ 6141 line wings seems to produce a satisfactory fit of the strong Ba II and weak Ba I lines. In these calculations I used the approximation formulae for Stark damping constant as introduced by Cowley (1971) and used in SYNTH code (Piskunov, 1992). A small extra abundance step is required fot proper fit if the Ba II line wings are concerned. Comparison of the observed and synthetic spectra with the homogeneous and stratified Ba abundance is shown in Fig. 4.

If instead I use Stark widths calculated for Ba II lines by Dimitrijević and Sahal-Bréchot (1997) then I need to correct a little bit Ba distribution near the top of the abundance jump (solid line in Fig. 6) to obtain the same fit as before for Ba II λ 6141 line (top panel in Fig. 5 - solid line). It is evident that an improved Ba distribution provides better fit also for Ba I λ 6063 line (bottom panel in Fig. 5 - solid line). It illustrates the importance of accurate Stark damping constants for abundance stratification studies. With the accurate Stark parameters we hope to get as accurate empirical element distributions as possible with the current models of stellar atmospheres.

And finally, I would like to demonstrate that not only Stark widths, but also Stark shifts may play a significant role in abundance stratification analysis.

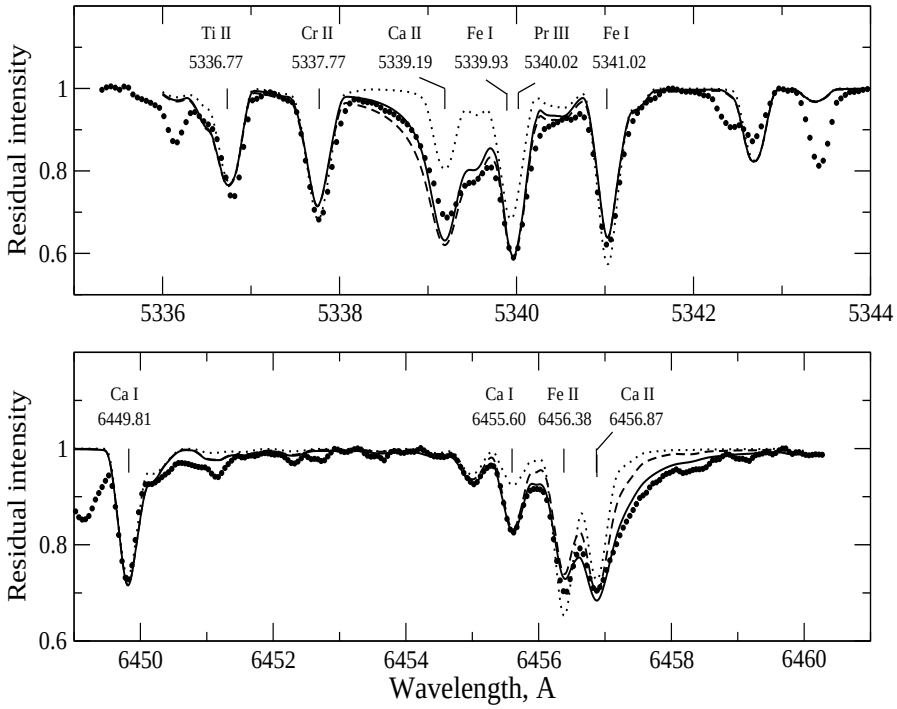

Fig. 3: A comparison between the observed and synthetic spectra in Ap star γ Equ in the region of Ca II $\lambda\lambda$ 5339.19 and 6456.87 lines. Dotted line – calculations with the uniform mean Ca abundance, dashed and solid lines – calculations with different Stark widths discussed in the text.

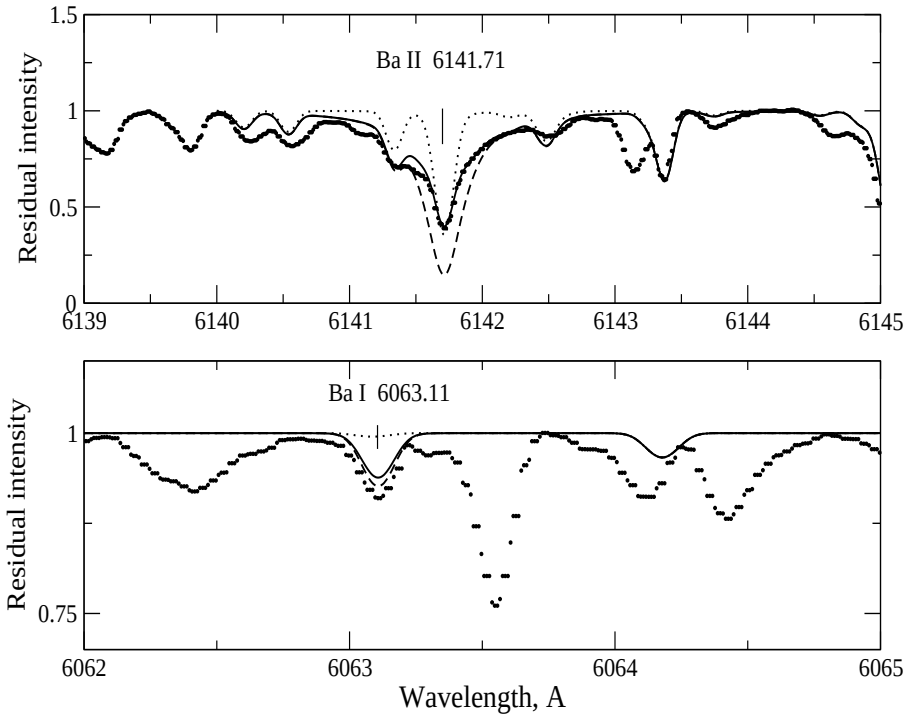

Fig. 4: Ba I and Ba II lines in the spectrum of Przybylski's star, HD 101065 (filled circles). Residual intensity means an observed flux relative to continuum. Dotted and dashed lines represent the synthetic spectra calculated with a homogeneous Ba abundance designed to fit the line core ($\log(Ba/N_{tot})$=-9.20) and the line wing ($\log(Ba/N_{tot})$ = -7.60) of the Ba II λ 6141 line. The solid line represents synthetic spectra calculated with the Ba distribution shown in Fig. 6 by dashed line. The position of the Ba features is marked by vertical lines.

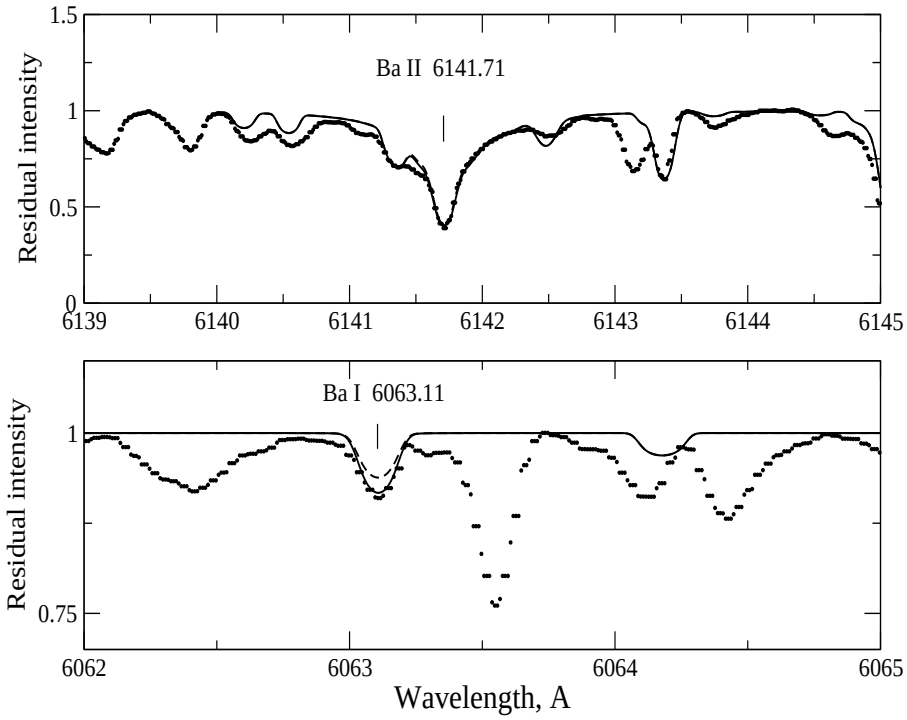

Fig. 5: A comparison between the observed (filled circles) and calculated Ba I and Ba II lines. Calculations with the Stark constants from an approximation formula and with the corresponding Si distribution from Fig. 5 are shown by dashed line, while calculations with the Stark widths from Dimitrijević and Sahal-Bréchot (1997) and with the improved Ba stratification profile are shown by solid line.

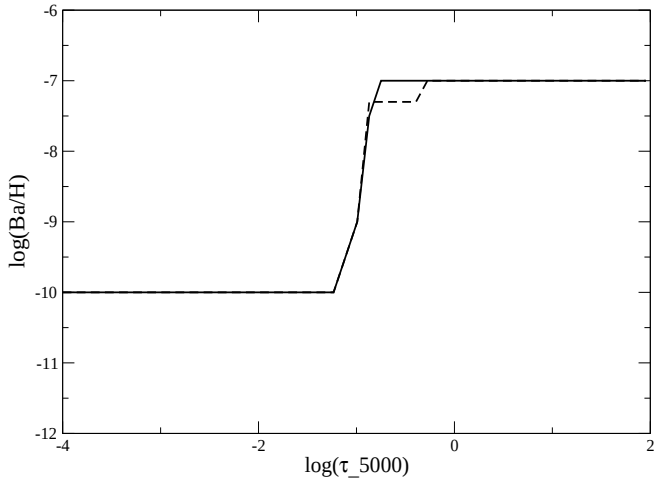

Fig. 6: Ba abundance distribution in the atmosphere of HD 101065 as derived using approximate formulae for Stark damping (dashed line) and with semiclassical Stark calculations by Dimitrijević and Sahal-Bréchot (1997) (solid line).

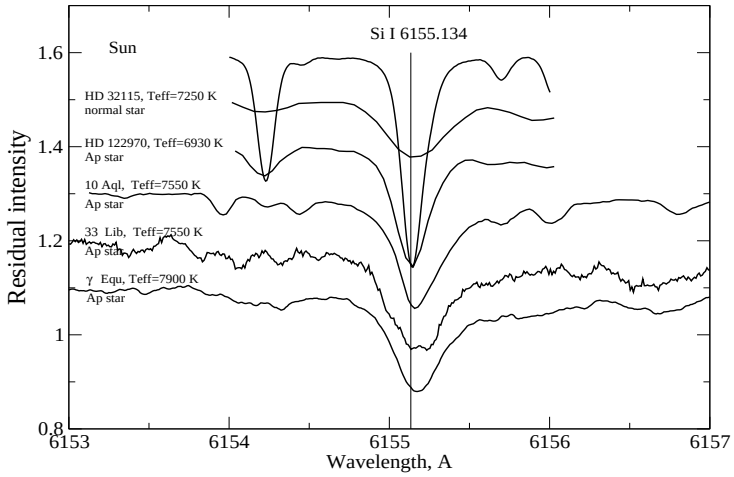

Fig. 7: Si I λ 6155 line in spectra of a few stars with different effective temperatures. The laboratory position of the line is marked by vertical line.

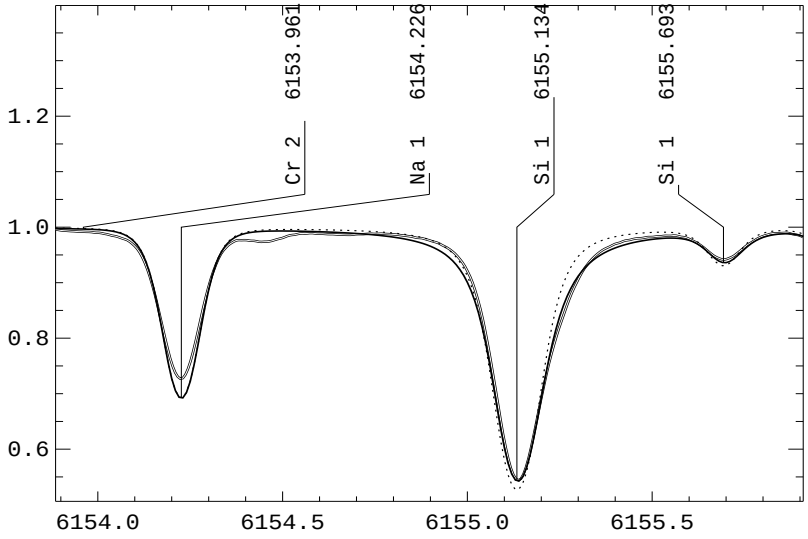

Fig. 8: A comparison between the observed Si I 6155 Å line profile in the solar spectrum and synthetic spectra calculated with Stark widths and shifts (solid line) and with Stark width calculated by approximate formulae and without Stark shift taken into account (dotted line). X- and Y-coordinates are wavelenghths and residual intensities.

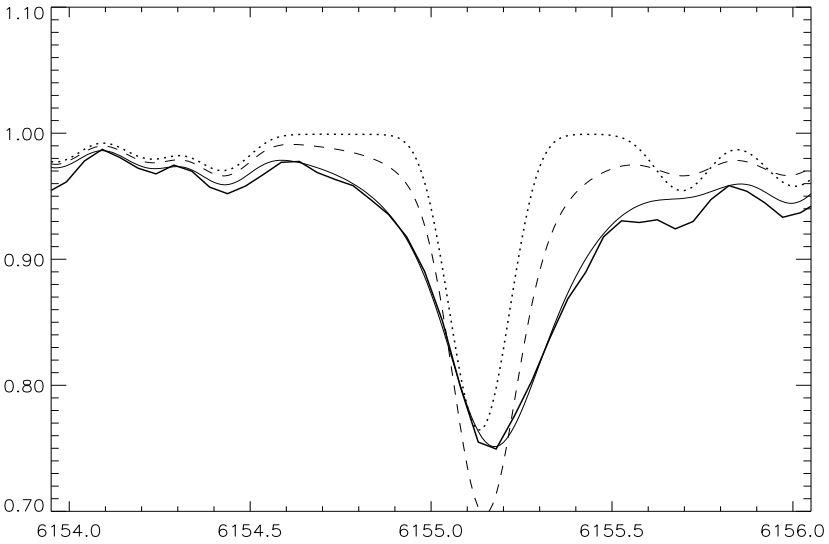

Fig. 9: A comparison between the observed Si I 6155 Å line profile in the spectrum of Ap star 10 Aql (heavy line) and synthetic spectra calculated with Stark widths and shifts and Si abundance stratification (light line), with the same Stark parameters but for homogeneous Si distribution (dashed line), and with Stark width calculated by approximate formulae for the same stratification (dotted line). X- and Y-coordinates are wavelenghths and residual intensities

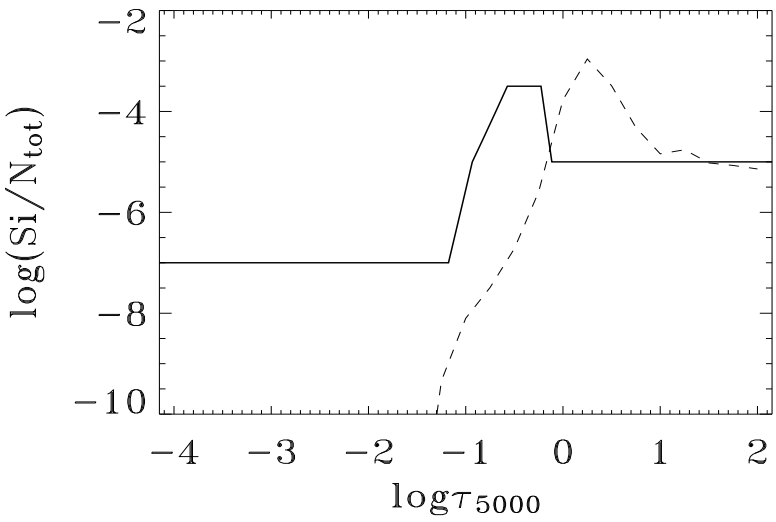

Fig. 10: Si distribution in the atmosphere of Ap star 10 Aql as obtained from analysis of Si I 6155 Å line profile (solid line). Theoretical Si distribution obtained from self-consitent model diffusion calculations is shown by dashed line.

2. 3. SILICON LINES

Silicon is one of the most peculiar elements in the atmospheres of hotter members of magnetic Ap stars which gives the name for a whole subgroup – Si-stars. Usually we observe the lines of the singly-ionised Si, and rather accurate Stark widths for Si II lines are available (Lanz et al., 1988). Working on the abundance analysis of the cooler Ap stars with $T_{\rm eff}\leq$8000 K I have noticed an anomaly in the line profile of Si I λ 6155. This line is shifted to the red and has rather strong asymmetry in the red wing. It is illustrated in Fig. 7. Even the solar line is slightly asymmetric.

Stark constants calculations performed by Dimitrijević et al. (2003) for a few neutral Si lines revealed rather large values for Stark widths and also shifts. First we have modelled Si I lines in the solar spectra. Next two Figs. are taken from Dimitrijević et al. (2003). A fit of the synthetic spectrum to the observed solar Si I λ 6155 line is shown in Fig. 8.

Then spectral synthesis was performed for the same line in Ap star 10 Aql, where Si I λ 6155 line has very pronounced asymmetry (Fig. 9). With the homogeneous Si abundance in stellar atmosphere it was not possible to fit the line profile properly (dashed line in Fig. 9). Again, a rather simple step-like Si distribution shown in Fig. 10 is enough to reproduce successfully an observed line profile (solid line in Fig. 9).

It is possible to compare an empirical Si stratification with the results of the self-consistent model diffusion calculations by F. Leblanc (Ryabchikova et al., 2003). Theoretical Si distribution for slightly hotter model ($T_{\rm eff}$=7700 K) is shown by dashed line in Fig. 10. While theoretical and empirical Si distributions are shifted by about

0.5 dex in optical depth scale, both provide the same abundance gradients in stellar atmosphere. It is encouraging that both empirical and theoretical distributions provide similar abundance profiles, although they are shifted from each other in the optical depths.

3. CONCLUSIONS

An empirical study of the abundance stratification in the atmospheres of Ap stars is difficult, even impossible without accurate data for Stark damping constants. Stark wings of the spectral lines allow to reconstruct vertical abundance gradients produced by element separation processes operating in stabilized stellar atmospheres. It imposes very important constraints for the theories of these separation processes.

References

Babel, J.: 1992, *Astron. Astrophys.*, **258**, 449.
Babel, J.: 1994, *Astron. Astrophys.*, **283**, 189.
Bonifacio, P., Castelli, F., Hack M.: 1995, *Astron. Astrophys. Suppl. Ser.*, **110**, 441.
Cowley, C.R., Ryabchikova, T.A., Kupka, F., Bord, D.J., Mathys, G., Bidelman, W.P.: 2000, *Mon. Notic. Roy. Astron. Soc.*, **317**, 299.
Cowley, C.R.: 1971, *Observatory*, **91**, 139.
Dimitrijević, M.S., Sahal-Bréchot, S.: 1997, *Astron. Astrophys. Suppl. Ser.*, **122**, 163.
Dimitrijević, M.S., Ryabchikova, T., Popović, L.Č., Shulyak, D., Tsymbal, V. 2003 : *Astron. Astrophys.*, (in press)
Kupka, F., Piskunov, N.E., Ryabchikova, T.A., Stempels, H.C., Weiss, W.W.: 1999, *Astron. Astrophys. Suppl. Ser.*, **138**, 119.
Kurucz, R.L.: 1993, *CDROM20-23*, SAO, Cambridge
Lanz, T., Dimitrijević, M.S., Artru, M.-C.: 1988, *Astron. Astrophys.*, **192**, 249.
Michaud, G.: 1970, *Astrophys. J.*, **160**, 641.
Piskunov, N.E.: 1992, in *Stellar Magnetism*, ed. Yu. V. Glagolevskij, I.I. Romanyuk, Nauka, St. Petersburg, p.92
Ryabchikova, T., Wade, G., LeBlanc, F.: 2003, in *Modelling of Stellar Atmospheres*, ed. N. E. Piskunov, W. W. Weiss, D. F. Gray, IAU Symp. 210, (in press).
Ryabchikova, T., Piskunov, N., Kochukhov, O., Tsymbal, V., Mittermayer, P., Weiss, W. W.: 2002, *Astron. Astrophys.*, **384**, 545.
Ryabchikova, T., Adelman, S.J., Weiss, W.W., Kuschnig, R.: 1997, *Astron. Astrophys.*, **322**, 234.
Seaton, M.J., Zeippen, C.J., Tully, J.A., et al.: 1992, *Rev. Mex. Astron. Astrophys.*, **23**, 19.
Smith, K.C. 1995: *Astron. Astrophys.*, **297**, 237.

Publ. Astron. Obs. Belgrade No. 76 (2003), 117 - 131 *Invited lecture*

EARLY-TYPE GALAXIES: FROM SPECTRA TO DYNAMICAL ANALYSIS

SRDJAN SAMUROVIĆ[1,2,3]

[1] *Astronomical Observatory, Volgina 7, 11000 Belgrade, Serbia and Montenegro*

[2] *Dipartimento di Astronomia, via Tiepolo 11, 34131 Trieste, Italy*

[3] *Osservatorio Astronomico di Trieste, via Tiepolo 11, 34131 Trieste, Italy*
E–mail: srdjan@ts.astro.it

Abstract. A brief summary is given of some important aspects of observations and modelling of early-type galaxies. Photometric and long-slit spectroscopic observations, as well as two- and three-integral modelling of the early-type galaxy IC3370 are given as an example.

1. INTRODUCTION

Early-type galaxies (elliptical and lenticular galaxies) belong to the left-hand end of the Hubble's tuning-fork diagram. Shape of elliptical galaxies varies in form from round to elongated. One can use the simple formula $n = 10[1 - (b/a)]$, where (b/a) denotes the apparent axial ratio, to write the type of these galaxies: En. Therefore, E0 are round galaxies, and E6 are highly elongated systems. Research over last 20 years brought new knowledge about ellipticals and we now know that these galaxies are much more complex systems that they seemed. The elliptical galaxies contain little or no gas or dust. The old stars that are prevalent are cold, and therefore belong to the last spectral types. In the middle of the Hubble's diagram there is a class of galaxies designated as type S0, known as lenticular galaxies. They have a smooth central brightness condensation similar to an elliptical galaxy that is surrounded by a large region of less steeply declining brighteness. They have disks that do not show any conspicuous structure. Because of their appearance, and also because of their stellar content (e.g., spectral type), they look more like ellipticals rather than spiral galaxies. In this paper I will present observations and modelling of the galaxy IC3370 classified as E2-E3 (RC3, de Vaucouleurs et al., 1991).

2. OBSERVATIONS

IC3370 is a bright galaxy, classified as E2-E3 elliptical galaxy, absolute blue magnitude -21.4, heliocentric radial velocity 2930$\pm$24 km/s (see Fig. 1). It covers 2.9$\times$2.3 arcmin

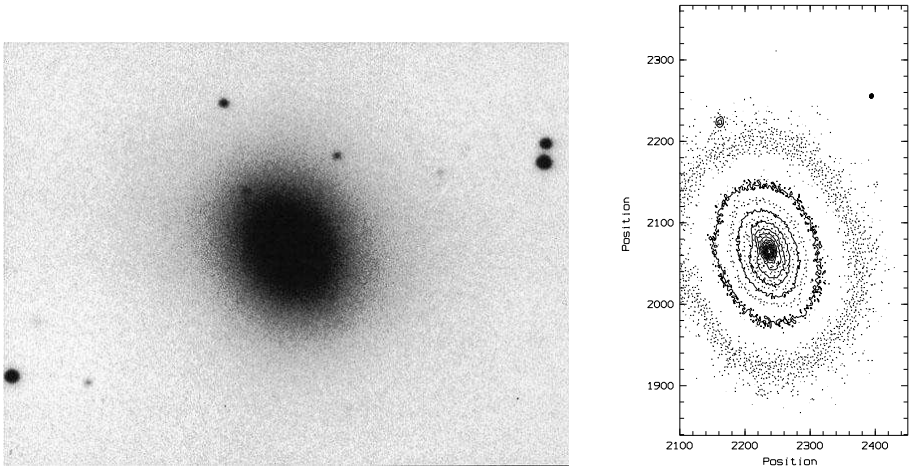

Fig. 1: Galaxy IC3370: image taken from NED (left) and contour plot (right)

on the sky (RC3). However, it is a rather unusual elliptical galaxy and according to Jarvis (1987, hereafter referred to as J87) it should be classified as S0pec (see below).

2. 1. PHOTOMETRIC OBSERVATIONS

I have used frames kindly provided by O. Hainaut using ESO NTT and EMMI in the RILD mode on July 3-4, 2002. The photometry of IC3370 is very interesting and it is given in detail in J87. I present here some additional elements that are complementary to that study and are of importance for the analysis that I am undertaking (more details will be available in Samurović and Danziger (2003)).

One should note that J87 took for the major axis the position angle (PA) of 40°, Carollo, Danziger and Buson (1993) took for the same axis PA of 51°, while the spectra in this study were taken using PA = 60°. The reason for these differences lies in a very particular photometry of this galaxy that has strong isophotal twisting as shown in J87 and in Fig. 2 (see position angle (P.A.) plot). This is the evidence of the fact that this galaxy is triaxial, because the isophotes of an axisymmetric system must always be aligned with one another (Binney and Merrifield, 1998, hereafter BM98). Fasano and Bonoli (1989) using sample of 43 isolated elliptical found that the twisting observed in these galaxies is intrinsic (triaxiality). Jarvis has taken the mean position angle of isophotes to be equal to $40 \pm 2°$ which is true for the data up to $80''$. However, at larger radii the PA tends to increase, so the usage of larger value of 60° (and 150° for the minor axis) is justified (see Fig. 2).

In Fig. 2 I present relevant photometrical data obtained using IRAF task `ellipse`: ellipticity, magnitude in B band for major axis (filled circles) and minor axis (open circles), a_4 parameter (fourth harmonic deviations from ellipse) and the position angles, as a function of distance. The value of a_4 is positive up to one effective radius[1] (for almost all values of radius), thus indicating that the isophotes are disky, while beyond one effective radius, isophotes become boxy since a_4 is negative. Since a_4 increases rapidly up to $\sim 5''$ this can lead to the conclusion of the embedded disk.

[1]Effective radius is the radius of the isophote containing half the total luminosity.

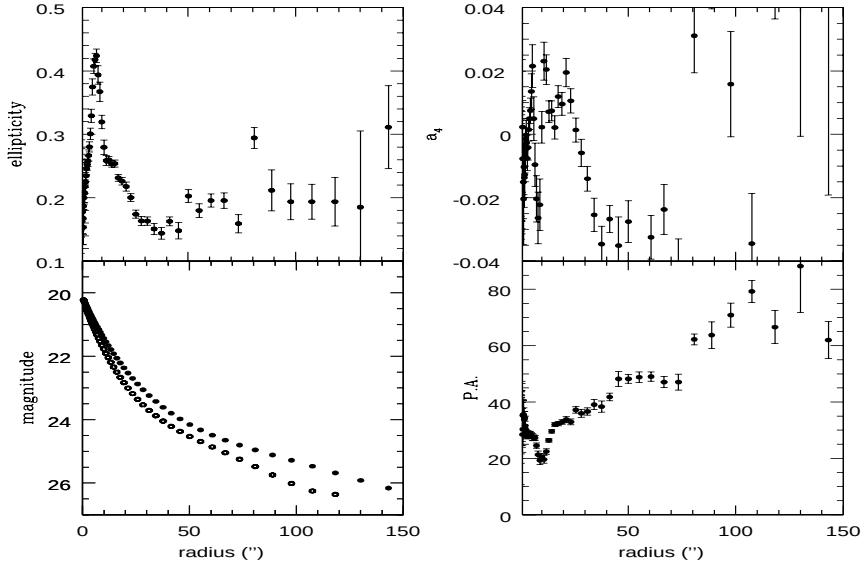

Fig. 2: Photometric profiles for IC3370. From top to bottom (left): ellipticity, surface brightness for the B filter (for major axis: full circles; for minor axis: open circles), (right): a_4 parameter and position angle.

The existence of the stellar disk was shown in J87. These photometric data will be necessary for the dynamical modelling that will be given below.

2. 2. LONG-SLIT SPECTRA

Long-slit spectra observations kindly provided by J. Danziger were taken during 1998 March 1-3, using ESO NTT and EMMI in the Red Medium Spectroscopy mode. The central wavelength was chosen to be near the Mg_2 feature: $\sim$ 5150 $\AA$. The range that was covered was $\sim$ 700 $\AA$. Several exposures were taken for different position angles: for the galactic major axis (P.A. = 60°) total exposure of 21,600 s, for the minor axis (P.A. = 150°) total exposure of 7,200 s. The spectra were rebinned at the telescope over 2 pixels giving a scale of 0.56 arcsec pixel $^{-1}$. I did standard data reduction procedures in ESO MIDAS: bias subtraction, division with the normalized dome flat field, filtering of the cosmic rays. Wavelength calibration was done using Helium-Argon comparison lamp spectra. Sky subtraction was done by taking average of 30 rows near the edges of the exposure frames. In the end the spectra were rebinned in the logarithmic scale. Also, spectra of several template stars were reduced as described above, continuum divided, and averaged over several rows in order to obtain one stellar template spectrum of high signal-to-noise ratio (S/N). In Fig. 3 I present a central galactic spectrum and a template star spectrum (K0 III star HR2701).

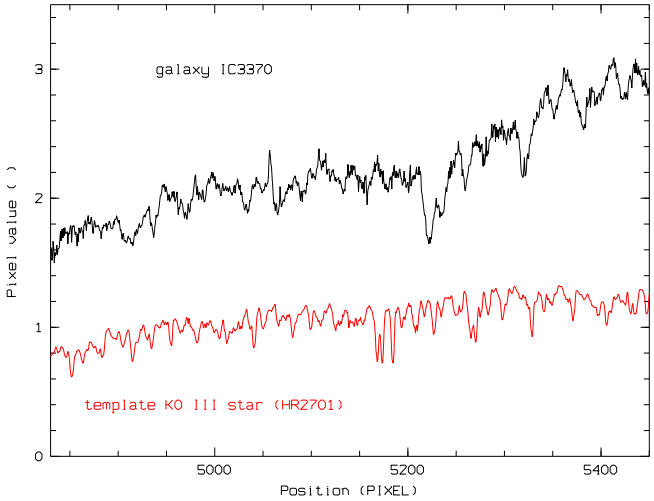

Fig. 3: Reduced central spectrum of the galaxy IC3370 (above) and template star (below). Spectra have been wavelength calibrated: x axis is in Angstroms. Note effects of velocity dispersion and redshift in the case of the galaxy; y axis is in arbitrary units.

3. STELLAR KINEMATICS: THEORETICAL APPROACH

In the case of IC3370, as in the case of all external galaxies, one cannot obtain data necessary for the reconstruction of the distribution function directly: one can observe line-of-sight velocities and angular coordinates. Since individual stars cannot be resolved, one has to deal with integrated stellar light that represents the average of the stellar properties of numerous unresolved stars that lie along each line of sight (LOS). Each star will have a slightly different LOS velocity, and therefore its spectral features will be shifted by a different amount: $\Delta u = c\Delta\lambda/\lambda = v_{\rm LOS}$. The final galaxy spectrum will be shifted and broadened, as shown in Fig. 3. First step in analysis of the shifts and broadenings is to define the line of sight velocity distribution (LOSVD, also called velocity profile, VP): this is a function $F(v_{\rm LOS})$ that defines the fraction of the stars that contribute to the spectrum that have LOS velocities between $v_{\rm LOS}$ and $v_{\rm LOS} + dv_{\rm LOS}$ and is given as $F(v_{\rm LOS})dv_{\rm LOS}$. Now, if one assumes that all stars have identical spectra $S(u)$ (where u is the spectral velocity in the galaxy's spectrum), then the intensity that is received from a star with LOS velocity $v_{\rm LOS}$ is $S(u - v_{\rm LOS})$. When one sums over all stars one gets:

$$G(u) \propto \int dv_{\rm LOS} F(v_{\rm LOS}) S(u - v_{\rm LOS}). \qquad (1)$$

This relation represents the starting point for a study of stellar kinematics in external galaxies (cf. BM98). The observer gets $G(u)$ for a LOS through a galaxy by obtaining its spectrum. If the galaxy is made of certain type of stars, one can estimate $S(u)$ using a spectrum of a star from the Milky Way galaxy (see Fig. 3,

lower part).

The solution of Eq. (1) seems rather simple. It would be enough to take its Fourier transform:

$$\tilde{F}(k) \propto \frac{\tilde{G}(k)}{\tilde{S}(k)} \tag{2}$$

where quantities with tilde sign are the Fourier transforms of the original functions. This is however very difficult task, since $\frac{\tilde{G}(k)}{\tilde{S}(k)}$ will be plagued by large errors that vary from point to point and the simple derivation of $F(v_{\rm LOS})$ will not be easy (for details, see BM98). Therefore, less direct methods have been invented to solve this problem.

First we can define the simplest properties of a LOSVD. Its mean value is given as:

$$\bar{v}_{\rm LOS} = \int dv_{\rm LOS} v_{\rm LOS} F(v_{\rm LOS}). \tag{3}$$

Its dispersion is given as:

$$\sigma^2_{\rm LOS} = \int dv_{\rm LOS} (v_{\rm LOS} - \bar{v}_{\rm LOS})^2 F(v_{\rm LOS}). \tag{4}$$

One possible solution is to assume that LOSVD has the Gaussian form. Sargent et al. (1977) invented the method known as Fourier Quotient Method, that has a problem of large errors for the ratio $\frac{\tilde{G}(k)}{\tilde{S}(k)}$ that vary from point to point. Cross-correlation method based on the calculation of the cross-correlation function between the galaxy and the stellar spectra was pioneered by Simkin (1974) and developed further by Tonry and Davis (1979).

LOSVD can be modeled as truncated Gauss-Hermite ($F_{\rm TGH}$) series that consists of Gaussian that is multiplied by a polinomial (van der Marel and Franx, 1993):

$$F_{\rm TGH}(v_{\rm LOS}) = \Gamma \frac{\alpha(w)}{\sigma} \exp(-\frac{1}{2}w^2) \left[1 + \sum_{k=3}^{n} h_k H_k(w)\right] \tag{5}$$

here Γ represents the line strength, $w \equiv (v_{\rm LOS} - \bar{v})/\sigma$, $\alpha \equiv \frac{1}{\sqrt{2\pi}} \exp(-w^2/2)$, where $\bar{v}$ and σ are free parameters. h_k are constant coefficients and $H_k(w)$ is a Gauss-Hermite function, that is a polynomial of order k. I will truncate the series at $k = 4$ (although higher values are also possible), for which the polynomials are:

$$H_3(w) = \frac{1}{\sqrt{6}}(2\sqrt{2}w^3 - 3\sqrt{2}w), \tag{6}$$

$$H_4(w) = \frac{1}{\sqrt{24}}(4w^4 - 12w^2 + 3). \tag{7}$$

Now LOSVD can be calculated by varying the values of $\bar{v}$, σ, h_3 and h_4 until the convolution of the function $F_{TGH}(v_{\rm LOS})$ with a template star spectrum best reproduces the observed galaxy spectrum. The optimal fit is then reached using a non-linear least-square fitting algorithm. If the form of the LOSVD is close to the Gaussian form, then $\bar{v}$ and σ will be approximately equal to $\overline{v_{\rm LOS}}$ and $\sigma_{\rm LOS}$. Parameters h_3 and h_4 are important because they measure asymmetric and symmetric departures from the

Gaussian. If one detects positive (negative) value of the h_3 parameter that would mean that the distribution is skewed towards higher (lower) velocities with respect to the systemic velocity. On the other hand, if one detects $h_4 > 0$ this means that the distribution is more peaked than the Gaussian at small velocities with more extended high-velocity tails; for $h_4 < 0$ the distribution is more flat-topped than the Gaussian. In the study of the dark matter in the early type galaxies the value of h_4 parameter plays a crucial role because it is constraining the level of tangential anisotropy which is extremely important since it is well known that the excess of tangential motions can mimic the existence of the dark matter haloes in these galaxies (Danziger 1997). The influence of changes in their values on the form of the LOSVD is given in Fig. 4.

4. STELLAR KINEMATICS: OBSERVATIONAL RESULTS

Internal part of the galaxy IC3370 can be considered 'disky' as it was shown before. Its rotation curve of the major axis is steeply rising to ~ 120 km s^{-1} within 20 arcsec and remains constant out to ~ 120 arcsec (> 3 effective radii). As it is usual in the case when a galaxy has a substantial rotational velocity, LOSVD is skewed, namely h_3 has the opposite sign to $\overline{v}_{\rm los}$. The values of h_4 parameter are consistent with zero value out to the ~ 3 R$_e$ thus indicating the lack of tangential anisotropies. Small deviations from the zero value are visible in the case of the minor axis. In Fig. 5 I present the extracted kinematical parameters of IC3370 for major (PA= 60°) and minor (PA= 150°) axes. Note that this galaxy shows signs of minor-axis stellar rotation: within $|r| \lesssim 10''$ velocity rapidly increases up to ~ 60 km s^{-1}. In Fig. 6 the reconstruction of LOSVD for IC3370 is given.

5. MODELLING

5. 1. TWO-INTEGRAL MODELLING

For the two-integral modelling procedures I used the modelling technique developed by Binney, Davies and Illingworth (1990, hereafter BDI), and subsequently used by van der Marel, Binney and Davies (1990), van der Marel (1990), and Cinzano and van der Marel (1994) (hereafter CvdM). Of all these papers only in CvdM the modelling includes also h_3 and h_4 parameters. Statler et al. (1999) used the modified version of this method to analyze mass distribution in NGC 1700. Here I briefly present the assumptions and the modelling steps.

Two-integral modelling is the first step in understanding of the dynamics of the elliptical galaxies, because in cases of small departures from triaxiality (which is far more probable, and true in case of IC3370 as it has been shown above), comparison of real systems with the models can provide useful insights. The assumptions of axisymmetry and the fact that the velocity dispersion tensor is everywhere isotropic are the starting points for the procedure that includes the following three steps (cf. BDI): (i) inversion of the luminosity profiles and obtaining three-dimensional luminosity density that provides the mass density (under assumption of constant mass-to-light ratio); (ii) evaluation of the potential and derivation of the velocity dispersion and azimuthal streaming (under assumptions that the form of the distribution function is $f(E, L_z)$, where E is the energy and L_z is the angular momentum of the individual star about the symmetry axis of the galaxy and that the velocity dispersion is isotropic) and (iii) comparison of the projected kinematical quantities from the model

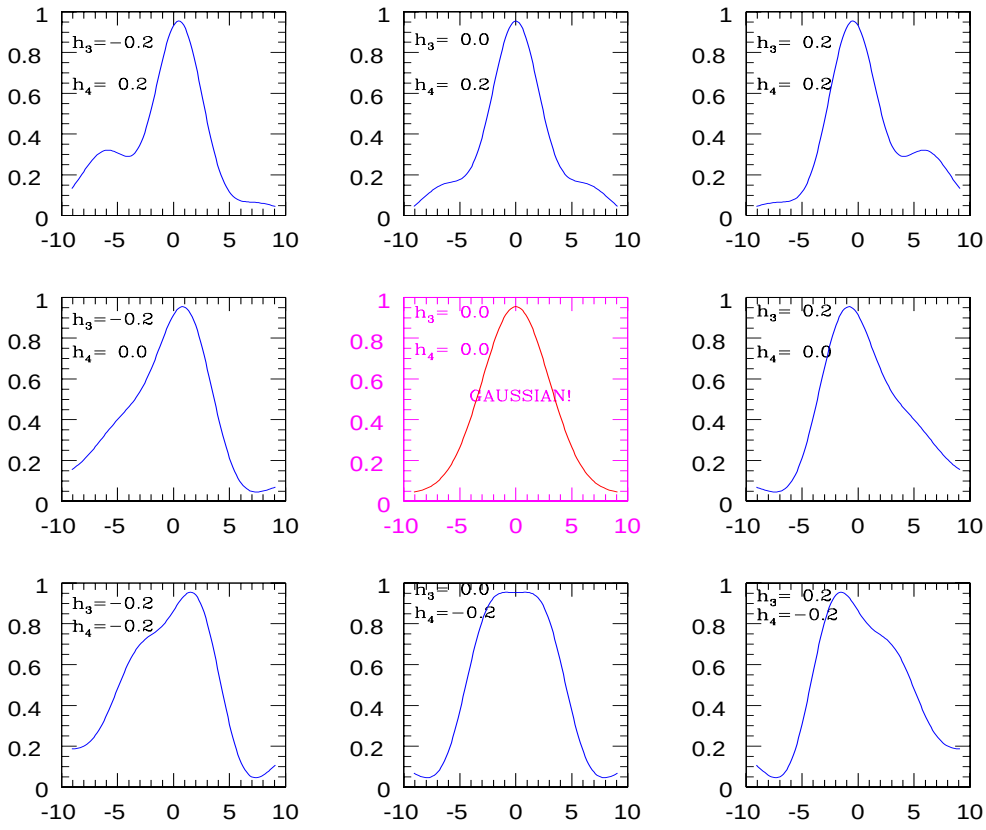

Fig. 4: Plots demonstrating various combinations of h_3 and h_4. Pure Gaussian is in the center (both h_3 and h_4 are equal to zero). h_3 parametrizes the skewness of the line profile, while h_4 measures whether the profile is more or less peaked than a Gaussian.

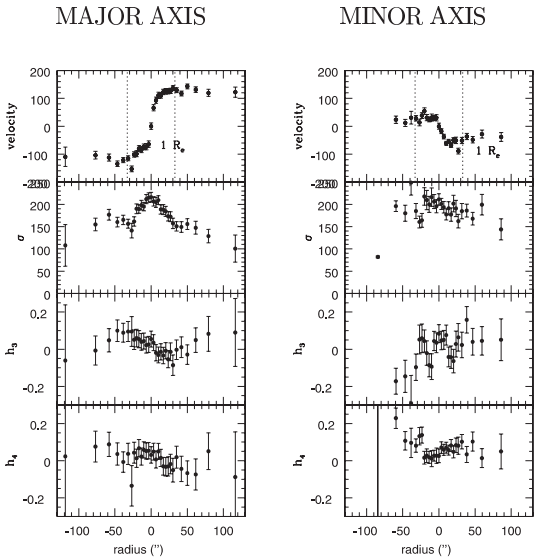

Fig. 5: Large scale kinematics for IC3370 for two different position angles. Left: major axis (PA = 60°) Right: minor axis (PA = 150°). From top to bottom: the mean line-of-sight velocity (in km/s), dispersion (in km/s), h_3 and h_4 parameters as a function of distance along different axes. The dotted lines indicate effective radius, $R_e \approx 31''$ in both cases.

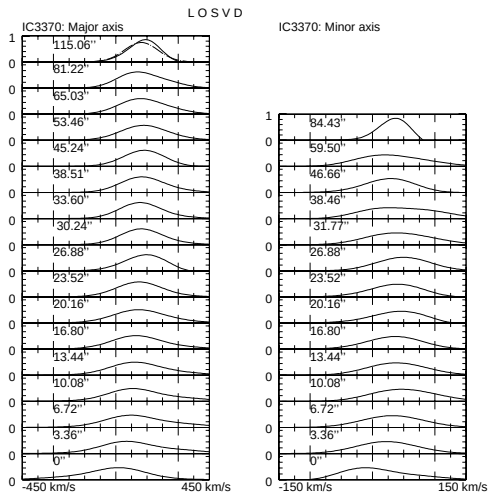

Fig. 6: LOSVD of IC3370 using data from Fig. 5. For a point at $115.06''$ the Gaussian is plotted as a dot-dashed line.

with the observed kinematic parameters; optionally, a disk, and/or a dark halo can be included in the modelling procedure.

The details of the modelling procedure are given in CvdM, and here I only briefly present some choices that I made and give the flowchart in Fig. 7. I assumed that the galaxy consists of a buldge and a disk; the dark matter halo is also included in the modelling procedure (see below). For the inclination I took $i = 50°$, because this value provided the best results in the modelling procedure. This value is in agreement with the value implied by the observed axial ratio of the isophotes, q_a: $i \geq \arccos q_a \gtrsim 46°$. I deprojected the photometry data using Lucy's algorithm to get the three-dimensional luminosity density. Then I obtained the mass density ρ using assumption of a constant mass-to-light ratio. The next step uses a three dimensional axisymmetric luminosity density, in order to evaluate the potential using a multipole expansion, and to solve the Jeans equations to find σ^2 and $\overline{v_\phi^2}$ for every point in the meridional plane. Since I assume that the distribution function is of the form $f(E, L_z)$ the second radial velocity moment, $\overline{v_R^2} \equiv \sigma_R^2$, and the second vertical velocity moment, $\overline{v_z^2} \equiv \sigma_z^2$ are everywhere equal and $\overline{v_R v_z} = 0$. The Jeans equations are:

$$\frac{\partial \rho \overline{v_z^2}}{\partial z} + \rho \frac{\partial \Phi}{\partial z} = 0 \tag{8}$$

$$\frac{\partial \rho \overline{v_R^2}}{\partial R} + \rho \frac{\partial \Phi}{\partial R} + \frac{\rho}{R}[\overline{v_R^2} - \overline{v_\phi^2}] = 0. \tag{9}$$

I solve them searching for unknowns $\overline{v_\phi^2}$ and $\sigma_R^2 = \sigma_z^2$. Using a free parameter, k, one can, as usual, assign a part of the second azimuthal velocity moment $\overline{v_\phi^2}$ to streaming:

$$\overline{v_\phi} = k\sqrt{\overline{v_\phi^2} - \sigma_R^2}.$$

Then I project the dynamical quantities on to the sky to get predictions.

My results of dynamical modelling are given in Fig. 8. It is obvious that this kind of modelling can provide rather good fit for the velocity in case one takes $k = 1$ (velocity dispersion is isotropic), adds disk potential and assumes that there is no dark matter. When one adds the potential of the dark matter (given as an isochrone Henon potential, as in Carollo and Danziger 1994) the fit for the major axis still remains good. The fit for $k = 0.6$ can be ruled out, while the fit for which disk potential is added and when there is no dark matter potential is good in the outer parts while in the inner parts it gives the velocity that is too large. The fits for dispersion, h_3 and h_4 are similar in four aforementioned cases. The dispersion along the major axis in the case in which one assumes the existence of the dark halo can be modeled using this approach, however a better fit is obtained without this assumption, since the dispersion continues to decrease. In the case of the minor axis, note that for the velocity all $k = 1$ models provide rather accurate values (again, $k = 0.6$ model can be ruled out). All four assumptions fail to produce observed dispersion values along the minor axis: observed values are always greater than the ones derived from the two-integral modelling. This two-integral model for given mass-to-light ratio underestimates minor axis dispersions. Model will be flattened by enhanced $\overline{v_\phi^2}$ which does not contribute to minor axis profile. Real galaxies are flattened by enhanced σ_R^2

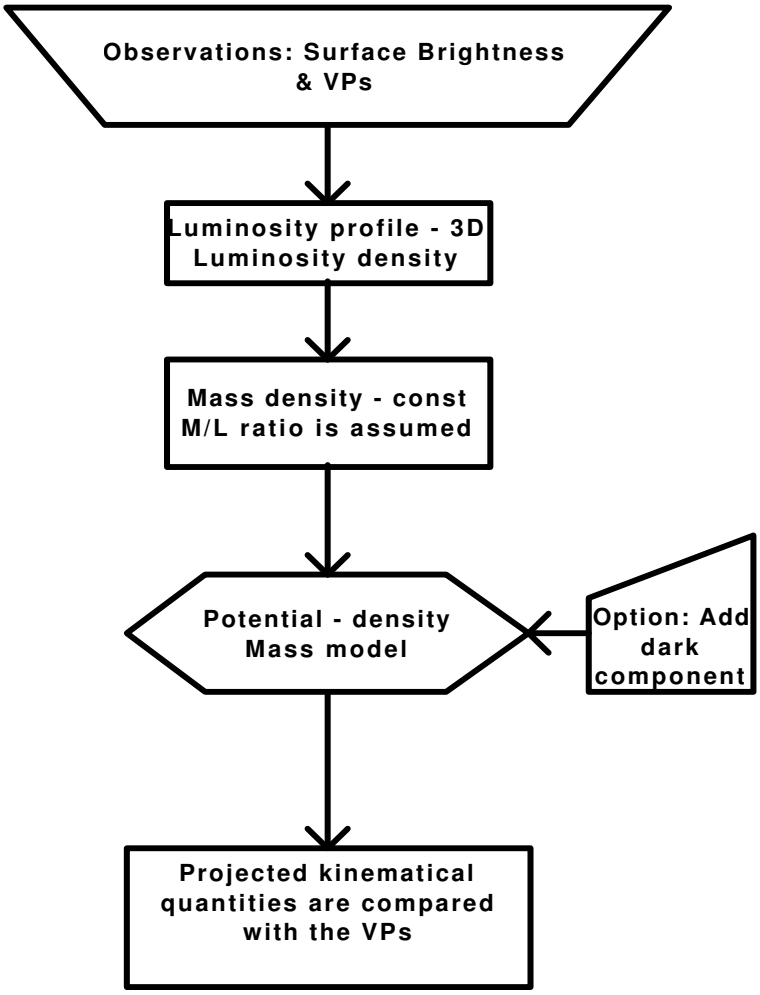

Fig. 7: Flowchart of two-integral modelling procedure. (VP stands for velocity profile).

which contributes on the minor axis. The radius of the disk that I have used to get a successful fit was 6 arcsec (0.9 kpc for $h = 0.71$).

The conclusion that can be drawn is that one can model IC3370 using two-integral modelling, but this approach is not completely satisfying because the observed dispersion on the minor axis deviates from the modeled one. Also, strictly speaking, this approach is not completely valid, since this galaxy is triaxial. The small values of h_4 parameter suggest that there are no big anisotropies in the outer part of the galaxy.

Judging from the results of this kind of modelling one cannot say firmly whether IC3370 is embedded in the dark halo, and one is faced with a situation similar to the one of NGC2663 from Carollo et al. (1995) paper. The inclusion of the dark matter in the modelling is not required, but as suggested in the analysis of S0 galaxy NGC 5866 for which the existence of the dark matter is not needed (Gerssen, 2000), the complete absence of dark halo is not likely. Another example found in the literature is the one of NGC 4472 (E2/S0 galaxy) for which the dispersion can be fitted both with and without the dark matter halo (Saglia et al., 1993).

5. 2. THREE-INTEGRAL MODELLING

For axisymmetric potentials one can have orbits that have three integrals of motion: E, L_z and I_3. There is no general expression for the third integral, I_3. The assumption that the distribution has the form $f = f(E, L_z, I_3)$ broadens the range of possible axisymmetric motions. Three-integral models are used for modelling triaxial systems. Schwarzschild (1979) invented a very powerful method that can be used for construction of axisymmetric and triaxial models of galaxies in equilibrium without explicit knowledge of the integrals of motion. The basic steps of this approach are the following: one specifies the mass model $\rho(r)$ and finds its potential and then constructs a grid of cells in a position space. Then initial conditions are chosen for a set of orbits and for every orbit one integrates the equations of motion for many orbital periods and measures how much time the orbit spends in each cell (that measures how much mass the orbit contributes to that cell). Finally, one needs to determine the non-negative weights for each orbit such that the summed mass in each cell is equal to the mass given by the original $\rho(r)$. For the last step one can use different methods; for example, Schwarzschild (1979) used linear programming. Non-negative least square (NNLS) method (Lawson and Hanson, 1974) was used in this work.

Schwarzschild original idea has recently been further developed: namely, models are now made that match the bulk kinematics and LOSVD of observed galaxies. Rix et al. (1997) used such approach to search for dark matter in elliptical galaxies. Cretton and van der Bosch (1999) used it to confirm the presence of nuclear black holes. Recently, Gebhardt et al. (2003) used orbit superposition method for detection of central black holes in 12 galaxies. These works deal with the axisymmetric modelling only. I have used Rix et al. (1997) algorithm to build a new Schwarzschild modelling code that uses the so-called self-organizing maps (SOMs) (Kohonen, 1997; Murtagh, 1995) to extract velocity profiles from the large orbits library. The flowchart is presented in Fig. 9.

The details of the modelling procedure are given in Rix et al. (1997). I give here only several important equations. Namely, one searches for non-negative superposition of orbital weights, γ_k, that best matches the observational constraints within the error bars:

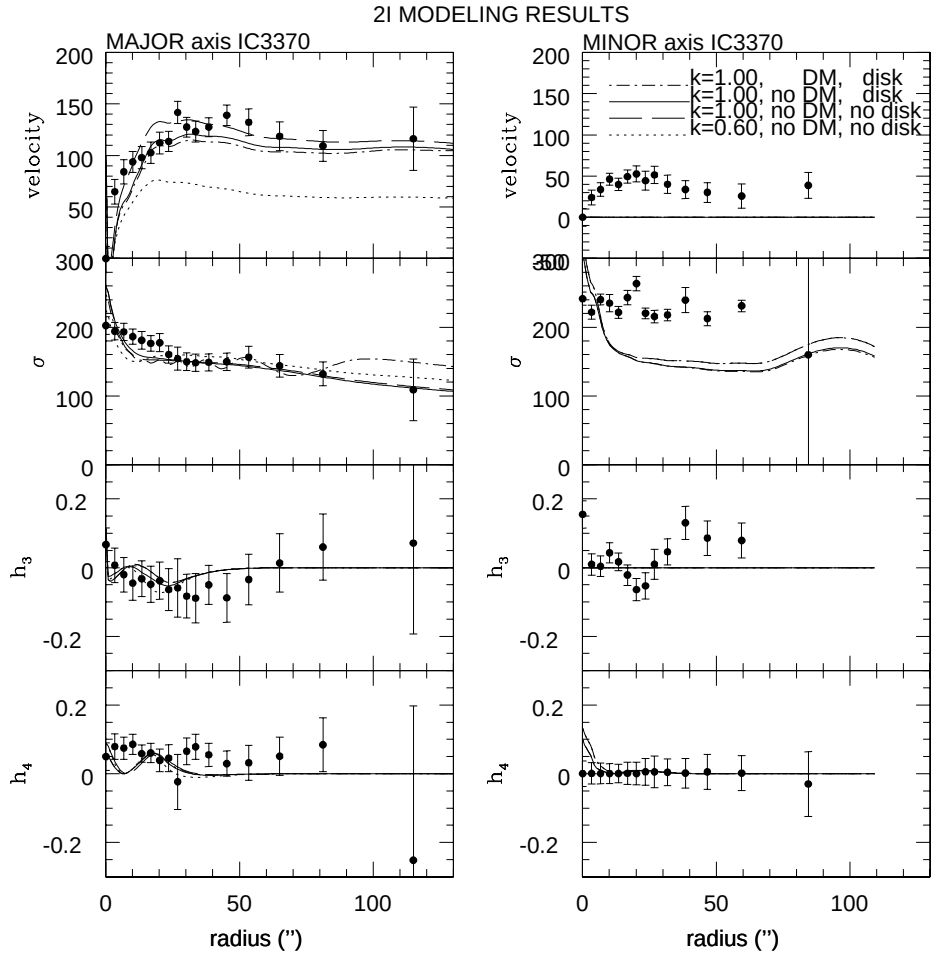

Fig. 8: Results of two-integral dynamical modelling of IC3370. Left: major axis modelling. Right: minor axis modelling. Solid lines represent cases with $k = 1$ with disk included and without dark matter. Dotted lines belong to $k = 0.6$ case, without the disk included and without the dark matter. Dot-dashed lines are for the case with $k = 1$ with the disk and dark matter included, and the dashed lines are for the case with $k = 1$ and no disk and no dark matter included (see text for details)

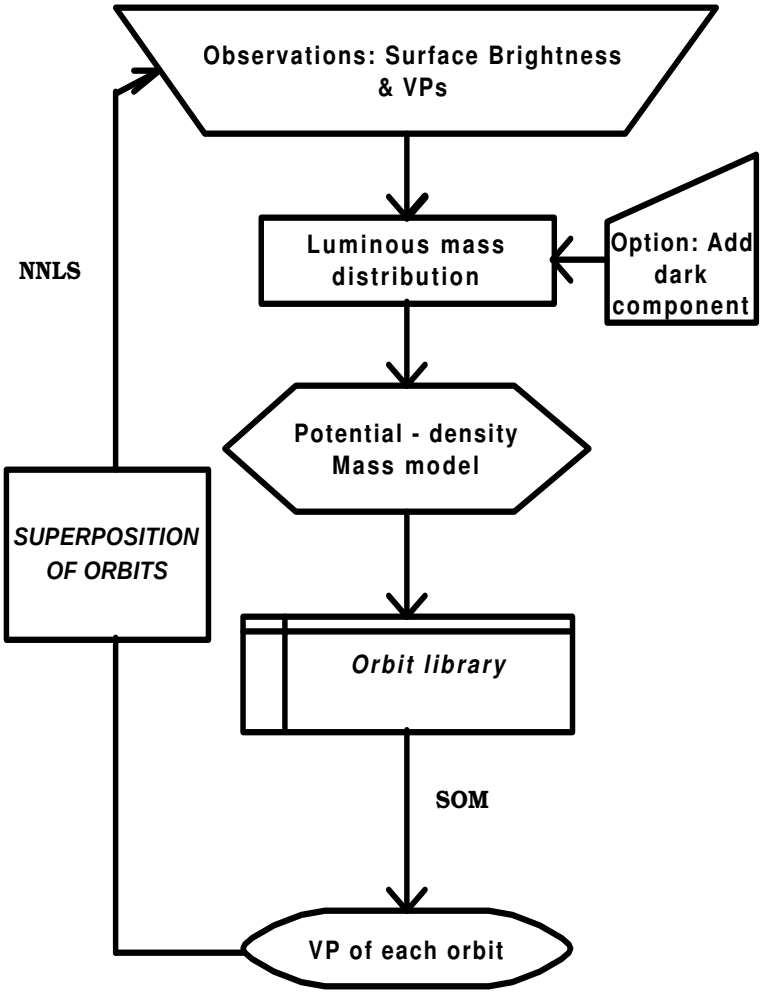

Fig. 9: Flowchart of three-integral modelling procedure. (SOM stands for self-organizing maps, NNLS for non-negative least squares).

$$\chi^2 \equiv \sum_{l=1}^{N_p}\left(\frac{M_l^{\rm obs}-\sum\gamma_k M_l^k}{\Delta M_l^{\rm obs}}\right)^2+\sum_{l=N_p+1}^{N_c}\sum_{m=1}^{4}\left(\frac{M_l^{\rm obs}h_{m,l}^{\rm obs}-\sum\gamma_k M_l^k h_{m,l}^k}{\Delta(M_l^{\rm obs}h_{m,l}^{\rm obs})}\right)^2, \quad (10)$$

Here, N_p are photometric constraints and $N_k = N_c - N_p$ are kinematic constraints (N_c is the number of constraint positions). Least squares problem that has to be solved for the occupation vector $(\gamma_1, \ldots, \gamma_{N_0})$, with the constraints $\gamma_k \geq 0$, for $k = 1, \ldots, N_0$ for $m = 1, 2, 3, 4$ is the following:

$$\begin{bmatrix} M_1^1 & \ldots & \ldots & M_1^{N_0} \\ M_2^1 & \ldots & \ldots & M_2^{N_0} \\ \vdots & \vdots & \vdots & \vdots \\ M_{N_p}^1 & \ldots & \ldots & M_{N_p}^{N_0} \\ M_{Np+1}^1 h_{1,N_p+1}^1 & \ldots & \ldots & M_{Np+1}^{N_0} h_{1,N_p+1}^{N_0} \\ \vdots & \vdots & \vdots & \vdots \\ M_{N_c}^1 h_{1,N_c}^1 & \ldots & \ldots & M_{N_c}^{N_0} h_{1,N_c}^{N_0} \\ \vdots & \vdots & \vdots & \vdots \\ \vdots & \vdots & \vdots & \vdots \\ M_{Np+1}^1 h_{M,N_p+1}^1 & \ldots & \ldots & M_{Np+1}^{N_0} h_{M,N_p+1}^{N_0} \\ \vdots & \vdots & \vdots & \vdots \\ M_{N_c}^1 h_{M,N_c}^1 & \ldots & \ldots & M_{N_c}^{N_0} h_{M,N_c}^{N_0} \end{bmatrix} \begin{bmatrix} \gamma_1 \\ \vdots \\ \vdots \\ \gamma_{N_o} \end{bmatrix} = \begin{bmatrix} M_1^{\rm obs} \\ M_2^{\rm obs} \\ \vdots \\ M_{N_p}^{\rm obs} \\ M_{Np+1}^{\rm obs} h_{1,N_p+1}^{\rm obs} \\ \vdots \\ M_{N_c}^{\rm obs} h_{1,N_c}^{\rm obs} \\ \vdots \\ \vdots \\ M_{Np+1}^{\rm obs} h_{M,N_p+1}^{\rm obs} \\ \vdots \\ M_{N_c}^{\rm obs} h_{M,N_c}^{\rm obs} \end{bmatrix} \quad (11)$$

Here, M denotes mass fractions, "obs" is related to the observed quantities. The total number of orbits is N_0.

I used this code for testing several astrophysically important potentials in a library of 729 orbits. Some very preliminary results are obtained for the logarithmic potential (Binney and Tremaine, 1987) that describes the flat rotation curves of galaxies. The model fits both velocity and velocity dispersion, because of the choice to fit them perfectly. For an axisymmetric potential that has the form

$$\Phi(R,z) = \frac{1}{2}v_0^2 \ln(R_c^2 + R^2 + z^2/q^2) \quad (12)$$

(R_c is the core radius, q describes the flattening of the potential and is taken to be $q = 0.7$ in this case) tube orbits cannot reproduce h_3 and h_4 parameters. For the triaxial potential:

$$\Phi(x,y,z) = \frac{1}{2}v_0^2 \ln(R_c^2 + x^2 + y^2/p^2 + z^2/q^2) \quad (13)$$

(here p and q are intrinsic axial ratios; they again describe flattening of the potential, and were taken to be $p = 0.8$ and $q = 0.7$ in this case) again h_4 cannot be fitted correctly. Fitting of h_3 with tube orbits can give some agreement, while fit for h_3 with box orbits is not satisfying. The conclusion is that widely used logarithmic potential

does not fit this galaxy, under aforementioned assumptions, although further checks are necessary (for example, using more orbits and using the regularization procedure). The results will be given in Samurović and Danziger (2003).

One possible way how the problem of triaxial modelling should be attacked would be to find the behavior of p and q parameters along the galaxy using observational constraints and to calculate potential for every point using these values (Eq. 13). This work is currently in progress.

Acknowledgements. I would like to thank my PhD thesis supervisors John Danziger and Francesca Matteucci for their encouragement and help. This work is a part of the project "Astrophysical Spectroscopy of Extragalactic Objects" supported by the Ministry of Science, Technologies and Development of Serbia. This research has made use of the NASA/IPAC Extragalactic Database (NED) which is operated by the Jet Propulsion Laboratory, California Institute of Technology, under contract with the National Aeronautics and Space Administration.

References

Binney, J.J., Davies, R.D., Illingworth, G.D.: 1990, *Astrophs. J.*, **361**, 78 (BDI).
Binney, J.J., Merrifield, M.R.: 1998 *Galactic Astronomy*, Princeton University Press (BM98).
Binney, J.J., Tremaine, S.D.: 1987, *Galactic Dynamics*, Princeton University Press.
Carollo, C.M., Danziger, I.J., Buson, L.: 1993, *Mon. Not. Roy. Astron. Soc.*, **265**, 553.
Carollo, C.M., Danziger, I.J.: 1994, *Mon. Not. Roy. Astron. Soc.*, **270**, 743.
Carollo, C.M., de Zeeuw, P.T., van der Marel, R.P., Danziger, I.J., Qian, E.E.: 1995, *Astrophys. J.*, **441**, L25.
Cinzano, P., van der Marel, R.P.: 1994, *Mon. Not. Roy. Astron. Soc.*, **270**, 325.
Cretton, N., van der Bosch: 1999, *Astrophys. J.*, **514**, 704.
Danziger, I.J.: 1997, *Dark and Visible Matter in Galaxies, ASP Conference Series, Vol. 117*, eds. Massimo Persic and Paolo Salucci.
De Vaucouleurs, G.: 1991, *Third Reference Catalogue of Bright Galaxies, version 3.9*
Fasano, G., Bonoli, C.: 1989, *Astron. Astrophys. Suppl. Ser.*, **79**, 291.
Gebhardt, K. et al.: 2003, *Astrophys. J.*, **583**, 92.
Gerssen, J.: 2000, *PhD Thesis*, University of Groningen.
Jarvis, B.: 1987, *Astron. J.*, **94**, 30 (J87).
Kohonen, T.: 1997, *Self-Organizing Maps*, Springer-Verlag.
Lawson, C.L., Hanson, R.J.: 1974, *Solving Least Squares Problems*, Englewood Cliffs, New Jersey: Prentice–Hall
Murtagh, F.: 1995, *Journal of Classifications*, **12**, 165.
Rix, H.-W., de Zeeuw, P.T., Cretton, N., van der Marel, R.P., Carollo, C.M.: 1997, *Astrophys. J.*, **488**, 702.
Saglia, R.P., Bertin, G., Bertola, F., Danziger, I.J., Dejonghe, H., Sadler, E.M., Stiavelli, M., de Zeeuw, P.T., Zeilinger, W.W.: 1993, *Astrophys. J.*, **403**, 567.
Samurović, S., Danziger, I.J.: 2003, in preparation.
Sargent, W.L.W., Schechter, P.L., Boksenberg, A., Shortridge, K.: 1977, *Astrophys. J.*, **212**, 326.
Schwarzschild, M.: 1979, *Astrophys. J.*, **232**, 236.
Simkin, S.M.: 1974, *Astron. Astrophys.*, **31**, 129.
Statler, T., Dejonghe, H., Smecker-Hane, T.: 1999, *Astron. Journal*, **117**, 126.
Tonry, J., Davis, M.: 1979, *Astron. Journal*, **84**, 1511.
van der Marel, R.P.: 1991, *Mon. Not. Roy. Astron. Soc.*, **253**, 710.
van der Marel, R.P., Binney, J.J., Davies, R.D.: 1990, *Mon. Not. Roy. Astron. Soc.*, **245**, 582.
van der Marel, R.P., Franx, M.: 1993, *Astrophys. J.*, **407**, 525.

Publ. Astron. Obs. Belgrade No. 76 (2003), 133 *Invited lecture*

GRAVITATION AND THERMODYNAMICS INTERPLAY, AND PERFECT-FLUID IMPLICATIONS

NICHOLAS K. SPYROU

Department of Physics, Aristoteleion University of Thessaloniki, 540 06 Thessaloniki, Greece

Abstract. This talk will have to do with dynamical description of bounded gravitating and thermodynamic perfect-fluid sources, as models of astrophysical and cosmological large-scale structures, with specific emphasis on the consequences of this binary nature of the structures on their physical parameters, theoretically proposed and observationally determined, like pressure, temperature, thermodynamic energy, mass density, gravitational field, etc, as important factors determining the conditions for the formation of the spectral lines.

Publ. Astron. Obs. Belgrade No. 76 (2003), 135-146 *Invited lecture*

STARK WIDTH AND SHIFT DEPENDENCE ON THE REST CORE CHARGE OF THE EMITTERS FOR MULTIPLY CHARGED IONS SPECTRAL LINES

M. ŠĆEPANOVIĆ[1], J. PURIĆ[2]

[1]*Faculty of Sciences and Mathematics, University of Montenegro,*
P. O. Box 211, 81000 Podgorica, Serbia and Montenegro
E-mail: maras@rc.pmf.cg.ac.yu

[2]*Faculty of Physics, University of Belgrade,*
P. O. Box 364, 11001Belgrade, Serbia and Montenegro

Abstract. Stark width and shift simultaneous dependence on the upper level ionization potential and rest core charge of the emitter has been evaluated and discussed. It has been verified that the found relations, connecting Stark broadening parameters with upper level ionization potential and rest core charge of the emitters for particular electron temperature and density, can be used for prediction of Stark line width and shift data in case of ions for which observed data, or more detailed calculations, are not yet available. Stark widths and shifts published data are used to demonstrate the existence of other kinds of regularities within similar spectra of different elements and their ionization stages. The emphasis is on the Stark parameter dependence on the upper level ionization potential and on the rest core charge for the lines from similar spectra of multiply charged ions. The found relations connecting Stark widths and shift parameters with upper level ionization potential, rest core charge and electron temperature were used for a prediction of new Stark broadening data, thus avoiding much more complicated procedures.

1. INTRODUCTION

Almost three decades have passed since the first monograph (Griem, 1974) on Stark broadening of spectral lines was published, and the first attempt was undertaken to find possible types of Stark width and shift regularities (Purić and Ćirković, 1973; Purić *et al.*, 1974). Along width the development of the theory of the Stark broadening, numerous experiments were performed to provide new Stark broadening data and to check the theoretical predictions. During last twenty years a large number of experimental and theoretical papers were published. Only a limited number of these, concerning Stark broadening and shift regularities, has been reviewed here. A substantial addition to the theoretical and experimental investigation of the Stark broadening and shift of numerous spectral lines from different atoms and ion represents the search for possible types of regularities of the Stark parameters. According to the approach to the problem of regularities all relevant published papers can be divided into two groups. The first group of papers (see Purić, 1996 and references therein) is concerned with evaluation of different types of regularities, such as dependence on the atomic charge number, ionization potential, atomic polarizability, principal quantum number and rest core charge of the emitter (as "seen" by an electron undergoing transition), based on the Stark width and shift theoretical formulas obtained in different approximations: semiclassical, semiempirical and adiabatic.

In the second group of papers (Wiese and Konjević, 1976, 1992) regularities were searched among the experimental results and conclusions were drawn on the bases of the analyses of the configuration of the atomic energy levels and transition probabilities, the expected regularities were discussed within a multiplet, supermultiplet, spectral series, transition arrays, homologous and isoelectronic sequences without an attempt to find a certain functional relation between Stark parameters and particular atomic structure parameter.

So far, the regularities have been found within: multiplet and spectral series (Wiese and Konjević, 1976, 1992), supermultiplet (Konjević and Dimitrijević, 1981; Wiese and Konjević, 1992), transition array (Wiese 1982, 1992; Purić, 1996 and references therein), isoelectronic sequence, isonuclear sequence, homologous sequence, particular transition along the Periodic system of the elements (Purić, 1996 and references therein) within one stage of the ionization or within several ionization stages (Purić *et al.*, 1991), as far the influence of the atomic structure is concerned. Stark parameters dependence on the plasma parameters-the electron density and temperature has been investigated in great number of published papers (Purić, 1996 and references therein) theoretically and experimentally. It was found that Stark widths and shifts of nonhydrogenic atoms and ions lines linearly depend on the electron density, and they are just the weak functions of the electron temperature. However, Stark parameters temperature dependence for particular spectral line can be far from being weak function.

Some recent reviews (Lanz and Artru, 1987; Smith, 1989) indicate that the experimentally determined Stark widths, as well as the existing theoretical data, cannot satisfy the need for all observed stellar lines, although it is an active field of research. Therefore, it is of interest to exploit any possible theoretical approach that might provide simple relations, for example, from the systematic trends found in the Stark broadening data. Several simple empirical formulas have been used in stellar studies, which take into account the dependence of the Stark width on the electron density, and on the excitation energy of the transition. For example, using the semiempirical approach (Griem, 1968) it was found that the width is proportional to n^{*4} (n^* is the effective quantum number of the upper level). Similarly, after using the modified semiempirical approach the Stark broadening parameters dependence on n^* (leading term proportional to n^{*4}) and the angular quantum number l, was obtained (Dimitrijević, 1987). Another approach (Kurucz, 1979) gave width proportional to n^{*5}. A different approach, based on the systematic trends found in Stark broadening parameters has been developed in series of articles (Purić, 1996 and references therein), in the case of neutral atoms and singly charged ion resonances and off-resonances (ns-np transitions: $\Delta n=0$ or 1 for resonances and $n=n_o+1$ for off-resonances; n_o is the main quantum number of the ground energy level of a corresponding emitter). Similar regularities were found for the isoelectronic sequences (see e.g. Purić *et al.*, 1988a; Djeniže *et al.*, 1992), for the isonuclear sequences (the same type of transition within several stages of ionization of a particular emitter (see e.g. Purić *et al.*, 1988b; Djeniže *et al.*, 1988)); and for the same type of transition within homologous groups of atoms or ions (see e.g. Purić *et al.,* 1988ab; Djeniže *et al.,* 1991ab). In recently published paper (Purić *et al.,* 1991) the same method was applied to doubly and triply charged ion resonances and off-resonances. The proposed method is based on the fact, that the Stark widths and shifts in wavelength or angular frequency units exhibit a systematic dependence on the ionization potential, upper or lower energy level of the corresponding transition when measured from the ionization limit and not from the ground level. In order to avoid misunderstanding the positive value of such quantity (χ) is called the upper or lower level ionization potential, respectively. Moreover, a systematic dependence has been found also on the rest core

charge (Z_c) of the emitter as seen by the electron undergoing transition. Since the simple relations based on such trends may be useful in astrophysics, when Stark broadening data for many lines are needed, it was tried to obtain and analyse such relations. Therefore, the Stark parameter dependencies on χ and Z_c were deduced form the large-scale semi-classical (Griem, 1974) or semiempirical (Griem, 1968) and modified semiempirical (Dimitrijević and Konjević, 1987) calculations. The obtained relations were checked using the existing experimental and theoretical data (Purić, 1996).

Despite continuous acquisition of Stark broadening data (Purić, 1996 and references therein) little is known about lines of heavy and multiply ionised emitters. This paucity of data particularly hampers opacity modelling of stellar atmospheres. Line widths, assumed when analysing or synthesizing the majority of stellar spectra involve either unreliable approximations or outright ignoring of Stark broadening (even though it may exceed natural broadening several times). In Purić *et al.* (1991) it was shown that physically based interpretation of the broadening regularities could provide Stark parameters with a useful combination of reliability and computational simplicity. The approach focused on the strong connection between Stark width and shift and the energy required to ionise the emitter from the transition's upper state. Theoretically derived functional relations for line width and shift, successfully fitted to a number of spectral lines as shown in a series of articles (Purić *et al.,* 1991), are of the form:

$$\omega = N_e f(T) a_1 Z_c^{c_1} \chi^{-b_1} \tag{1}$$

$$d = N_e f(T) a_2 Z_c^{c_2} \chi^{-b_2} \tag{2}$$

where ω and d are the line width and shift, χ is the corresponding upper state ionization potential, and $a_{1,2}$ and $b_{1,2}$ are coefficients independent of temperature, electron density and ionization potential for particular transition, and Z_c is the rest core charge of the emitter, as "seen" by the electron undergoing transition.

Equations (1) and (2) can be used (i) in the case of the lines originating from the same type of transitions (e.g., resonances or off-resonances) within one stage of ionization (Dimitrijević, 1982), or within several stages of ionization (Purić, 1991); (ii) within particular isoelectronic sequences (see e.g. Purić *et al.*, 1988ab; Djeniže *et al.,* 1991a), and (iii) within a given isonuclear sequence (see e.g. Purić *et al.,* 1988ab; Labat *et al.*, 1991; Djeniže *et al.,* 1991a).

In the case of a particular transition within a given homologous group of atom or ions, it is more convenient to use the slightly different relations in the function of the nuclear charge number of the emitter Z ($Z=Z_c+1$, Z_c+2, etc. for neutral, singly charged ions... respectively) (Purić *et al.,* 1988ab):

$$\omega = N_e f(T) a_1 Z^{c_1} \chi^{-b_1} \tag{3}$$

$$d = N_e f(T) a_2 Z^{c_2} \chi^{-b_2} \tag{4}$$

For the same plasma conditions and for the exactly analogous transitions within the different atomic spectra, corresponding a and b constants are similar. Consequently, one can determine empirically, from experiment or more sophisticated calculations, averaged empirical values for $A=aN_ef(T)$ and b.

For lower temperatures of astrophysical interest, $f(T)$ tends to be $f(T)=T^{-1/2}$ in the case of ionised emitters, and one can scale different theoretical and experimental Stark parameters values to other temperatures by using $T^{-1/2}$ dependence (for validity conditions see e.g. Griem, 1974) when using in the regularity studies. In the case of higher temperatures the dependence on the temperature is weaker. In some cases, when only an

estimated value is needed and temperature does not vary too much, one can use an averaged empirical value for a temperature range taking into account that the accuracy gets lower.

In the semiclassical (Griem, 1974) or the semiempirical (Griem, 1968) and modified semiempirical (Dimitrijević and Konjević, 1987) formulas, ionization potentials are included through the expression for effective quantum number, Stark broadening functions (see Griem, 1974), and the wavelength; therefore one can always find an appropriate, more or less approximate, expression for ω and d satisfying mathematical conditions for a series expansion:

$$f(x) = \sum k_n x^n \tag{5}$$

where $f(x)$ stands for ω and d and x for the ionization potential. Moreover, one can always try to fit ω and d with an $f(x)=\alpha x^{\beta}$ expression. In astrophysics ω is sometimes successfully represented as $\omega = \alpha T^{\beta}$ in order to make easier the use of data for the whole temperature range within a model of the stellar atmosphere. The expressions given by Eqs. (1)-(4), all of the same type,

$$\omega, d = A\chi^{-b} \tag{6}$$

are suitable for the calculations of new data by an interpolation or extrapolation, if the necessary coefficients from the known Stark parameter values for particular case mentioned above are determined.

One can try to obtain the coefficients A and b (see Eq.(6)) or k_n, n (see Eq.(5)) analytically and investigate the series expansion convergence and the quality of $f(x)=\alpha x^{\beta}$ fit. For instance, in the case of $np^{k-1}(n+1)s$-np^k resonance transitions of singly ionised emitters the analytical expressions for the corresponding coefficients of the series expansion were obtained (Dimitrijević, 1982) starting from the semiempirical formula (Griem, 1968). Such procedure may provide usable analytical expressions only with additional approximations and for special cases. Another way, used in a large number of papers is to try to obtain the proposed simple relations from a lot of the existing experimental data or more sophisticated calculations, in order to prove that Stark broadening parameters may be fitted with proposed relations and to obtain the corresponding α and β coefficients.

Accuracy of the obtained data using the described procedure is expected to be comparable with accuracy of the data used in verification of Stark width and shift dependencies on the upper level ionization potential. Therefore, it is very important for this method to have a set of data, calculated or measured, for the same plasma conditions, in particular the electron temperature and density. This makes it possible to avoid the influence of density and temperature scaling, Debye screening effect and different ion broadening contributions to the Stark widths and shifts used in the trends analyses.

The approach based on the Stark parameters dependence on the upper level ionization potential differs from earlier Stark broadening trend analyses primarily in the choice of the variable conveying atomic structure information. Prior work of several authors was based on the hydrogenic model. Consequently, it used integer principle quantum numbers instead of the upper state ionization potential χ chosen here. Both variables take into account the density of states perturbing the emitting state. Advantages of the present method are: (i) χ-based trend analyses achieve better fits; (ii) in χ values the lowering of the ionization potential (Inglis and Teller, 1939) is taken into account, predicting merging with continuum when the plasma environment causes a line's upper

state ionization potential to approach zero; and (iii) the χ dependence on ω, d is theoretically expected as shown in the following part of this review.

2. THEORY

Stark broadening and shift result from perturbations of the states of optically active electrons. Accordingly, Stark parameters are expressed in terms of atomic matrix elements as follows (Griem, 1974):

$$\begin{aligned}\omega + id = 2\pi N \cdot \int_{\rho_{\min}}^{\infty} \rho d\rho \Bigg[\frac{2}{3} iB\left(\frac{\hbar}{m\rho v}\right)^2 \sum_{l_{i',f'}} \left(\left\langle l_{i',f'} \left| \frac{r}{a_0} \right| l_{i',f'} \right\rangle \right)^2 \frac{\max(l_{i',f'}, l_{i,f})}{2l_{if}+1} \cdot \\ \cdot \left[A(z_{i'f'}) + iB(z_{if}) \right] + \frac{2}{15}\left(\frac{\hbar a_0}{m v \rho^2}\right) \sum_{l_{i',f'}} \left(\left\langle l_{i',f'} \left| \frac{r}{a_0} \right| l_{i,f} \right\rangle \right)^2 \cdot (2l_{i'f'}+1) \begin{pmatrix} l_{i',f'} & 2l_{i,f} \\ 0 & 0\ 0 \end{pmatrix} \cdot \\ \cdot \left[A_q(z_{i',f'}) + iB_q(z_{i',f'}) \right] + \frac{4}{15}\left(\frac{\hbar a_0}{m v \rho^2}\right)^2 \left(\left\langle l_i \left| \frac{r}{a_0} \right| l_i \right\rangle \right)^2 \left(\left\langle l_f \left| \frac{r}{a_0} \right| l_f \right\rangle \right)^2 \cdot (2l_i+1) \cdot \\ \cdot (2l_f+1) \begin{pmatrix} l_i & 2l_i \\ 0 & 0\ 0 \end{pmatrix} \begin{pmatrix} l_f & 2l_f \\ 0 & 0\ 0 \end{pmatrix} \begin{pmatrix} l_i & 2l_i \\ l_f & 1\ l_f \end{pmatrix} \Bigg]\end{aligned} \tag{7}$$

for atoms, and

$$\omega + id = \frac{4\pi}{3v}\left(\frac{\hbar}{m}\right)^2 N \sum_r \left(\left\langle l_r \left| \frac{r}{a_0} \right| l_i \right\rangle \right)^2 \frac{\max(l_{i'}, l_i)}{2l_i+1} (a_c + ib_c) \tag{8}$$

for singly charged ions, with

$$\begin{aligned} a_c + ib_c = \frac{3}{2}(0.60 \pm i \cdot 0.44) \left[2\pi \sum_{l_{i'}} \left(\left\langle l_{i'} \left| \frac{r_i}{a_0} \right| l_i \right\rangle \right)^2 \frac{\max(l_{i'}, l_i)}{2l_i+1} \right]^{2/5} \cdot \\ \cdot \left[\sum_{l_{i'}} \left(\left\langle l_{i'} \left| \frac{r_i}{a_0} \right| l_i \right\rangle \right)^2 \frac{\max(l_{i'}, l_i)}{2l_i+1} \right]^{=1} \end{aligned} \tag{9}$$

These, in turn, can be related to quantum numbers as through Eq. (7) from Griem (1974):

$$\sum \left| \left\langle J' \left| r_i \right| J' \right\rangle \right|^2 = \frac{a_0^2}{2J+1} S \tag{10}$$

where a_0 is the Bohr radius, J is the total orbital quantum number and S is the line strength.

When LS coupling is assumed, S can be factored:

$$S = \sigma(M)\sigma(L)\sigma^2 \tag{11}$$

where $\sigma(M)$ and $\sigma(L)$ are tabulated (Allen, 1963) multiuplet and intra multiplet relative line strengths, and σ is the integral of the radial wave function for the transition. Often it is

acceptable to model the jumping electron as being under the influence of a screened central charge. In the Coulomb approximation (Bates and Damgaard, 1949):

$$\sigma(n_{l-1}^*, l-1, n_l^*, l) = \frac{1}{Z_c}\left[\frac{3n_l^*}{2}\left(\frac{\left|n_l^{*2} - l^2\right|}{4l^2 - 1}\right)\right]^{1/2} \varphi(n_{l-1}^*, n_l^*, l) \tag{12}$$

where l is the larger of azimuthal quantum numbers, l_i , l_f, $\varphi(n_{l-1}^*, n_l^*, l)$ is a tabulated correction factor (Oertel and Shomo, 1968), and n^* is the effective principle quantum number:

$$n^* = Z_c\left(\frac{E_H}{E_\infty - E}\right)^{1/2} = Z_c\left(\frac{E_H}{\chi}\right)^{1/2} \tag{13}$$

where E_H, and E_∞ are the ionization potentials of hydrogen and the emitter and E is the state energy. In Moore (1949) extensive energy tabulations are given. Two cases can be considered:

$$n_l^{*2} = \frac{Z_c^2 E_H}{E_\infty - E_l} = \begin{cases} \dfrac{Z_c^2 E_H}{\chi_i}; l = l_i \\ Z_c^2 E_H \displaystyle\sum_{v=0}^{\infty} (-1)^v \frac{(E_i - E_f)^v}{\chi_i^{v+1}}; l = l_f \end{cases} \tag{14}$$

where the second version of Eq. (14) is Taylor expansion of 1 / $(E_\infty - E_l)$ for $\chi_i > E_i - E_f$; knowing that $E_\infty = \chi_i + E_i$ and $E_l = E_f$.

Eqs. (12) and (14) can be combined to give the explicit dependence of the transition integral on the potential χ and rest core charge Z_c of the emitter. Stark broadening functions *A(z), b(z),* and *B(z), b(z)* (Griem, 1974) can be expressed as serial Bessel functions. Substitutions in Eqs. (7) and (9) and their rearranging then yield explicit functional dependence on χ and Z_c:

$$\omega, d = \left(\frac{Z_c E_H}{\chi}\right)^2 \sum_{v=0}^{\infty} A_v \left(\frac{Z_c}{\chi}\right)^v \tag{15}$$

For highly stripped ions, $\chi >> Z_c E_H$, and Eq. (15) reduces to

$$\omega, d \approx \left(\frac{Z_c}{\chi}\right)^2 \tag{16}$$

Occasionally a single term will dominate the series in Eq. (15). This occurs for: (a) particular spectral series, multiplet, supermultiplet and transition arrays; (b) analogous transitions of homologous atoms and ions; (c) a fixed transition of ions within an isoelectronic sequence, and (d) the same transition within a particular isonuclear group of ions as it will be demonstrated in the next section of this review.

A new approach to the problem of the Stark broadening regularities was proposed (Salakhov *et al.,* 1991). Instead of looking for regularities within Stark broadening parameters of the spectral lines, the regularities were found for Stark parameters of the corresponding energy levels connected with the dipole transitions. It was found that Stark width (ΔE_q) and shift (Δd_q) of a given energy level can be expressed as:

$$\Delta E_q = A(n_q^*)^b \tag{17}$$

$$\Delta d_q = B(n_q^*)^b \tag{18}$$

where coefficients *A, B, a,* and *b* are independent of the effective quantum number. Stark width and shift of a line from transition between initial (i) and final (f) energy level, neglecting interference term, are given as

$$\omega = \Delta E_i + \Delta E_f \tag{19}$$

$$d = \Delta q_i + \Delta q_f \tag{20}$$

where Δq_i and Δq_f have to be taken with their appropriate signs. Stark parameters E_q and Δd_q can be determined using the existing data bases for particular type of transition.

In addition, it was found that one particular term in the series given by Eq. (5) is predominant, so the general form of the above mentioned dependencies is

$$\omega = A_k \chi^{-k} \tag{21}$$

where the coefficient A_k is independent of the upper level ionization potential χ, and simultaneously it is a function of rest core charge, electron density and temperature. In order to investigate Stark parameter regularities, an accurate set of theoretical and experimental data is needed for multiplet, supermultiplet, transition array, homologous, isoelectronic, and isonuclear sequences; or the same type of transition (for instance resonance) along the periodical system of elements for different stages of ionization, under the same plasma conditions characterized by particular electron density and temperature. Therefore, the Stark parameter dependencies on the electron density and temperature have to be well determined to make possible the normalization of the data given for different temperatures and densities to particular ones at which the types of regularities have to be investigated. Of special interest are dependencies on the rest core charge of the emitter within isoelectronic or isonuclear sequences or on the nuclear charge number within particular transitions of homologous group of atoms or ions, and on the upper level ionization potential in all the above mentioned cases. The Stark parameter dependence on the electron density is well established, and in the case of nonhydrogenic emitters it is linear. However, Stark width dependence on the electron temperature is different from line to line for all spectra. Therefore, the correction to the temperature dependence has to be done with great care for all data used, in particular case of the verification of certain type of mentioned dependencies and regularities. For instance, instead of the commonly adopted temperature dependence of $T^{-1/2}$ for ion lines, one has to use, from line to line (Purić and Šćepanović, 1999), the whole spectrum of functions of the form:

$$f(T) = A + BT^{-C} \tag{22}$$

Different kinds of regularities within Stark parameters of given spectra can be explained on the bases of their dependencies on the upper level ionization potential. A general form of that dependence in the case of the particular transition array is

$$\omega, d = N_e f(T) / z^c = a\chi^{-b} \tag{23}$$

where ω/d is the line width/shift in angular frequency units; χ is the corresponding upper level ionization potential expressed in *eV*; *z* is the rest core charge of the emitter as seen by the electron undergoing the transition. The coefficients *a, b* and *c* are independent of the ionization potential (for particular electron temperature and density) for a given transition.

Moreover, it has been found that the coefficient c is a universal constant approximately equal to 5.20. The procedure for Stark broadening data predictions was

described elsewhere. A comprehensive set of Stark broadening data of the investigated ions has been used here to demonstrate the existence of Stark width data regularities within this group of spectral lines.

3. RESULTS AND DISCUSSION

It has been verified that Eq. (23) is appropriate for all investigated transitions in all groups of the ions above mentioned, at different temperatures and electron densities. Namely, for Stark width, it was found that the best fit can be obtained if $f(T)$ is taken as given by Eq. (22) instead of $T^{1/2}$ (for some of 450 calculations of lines see Fig. 1).

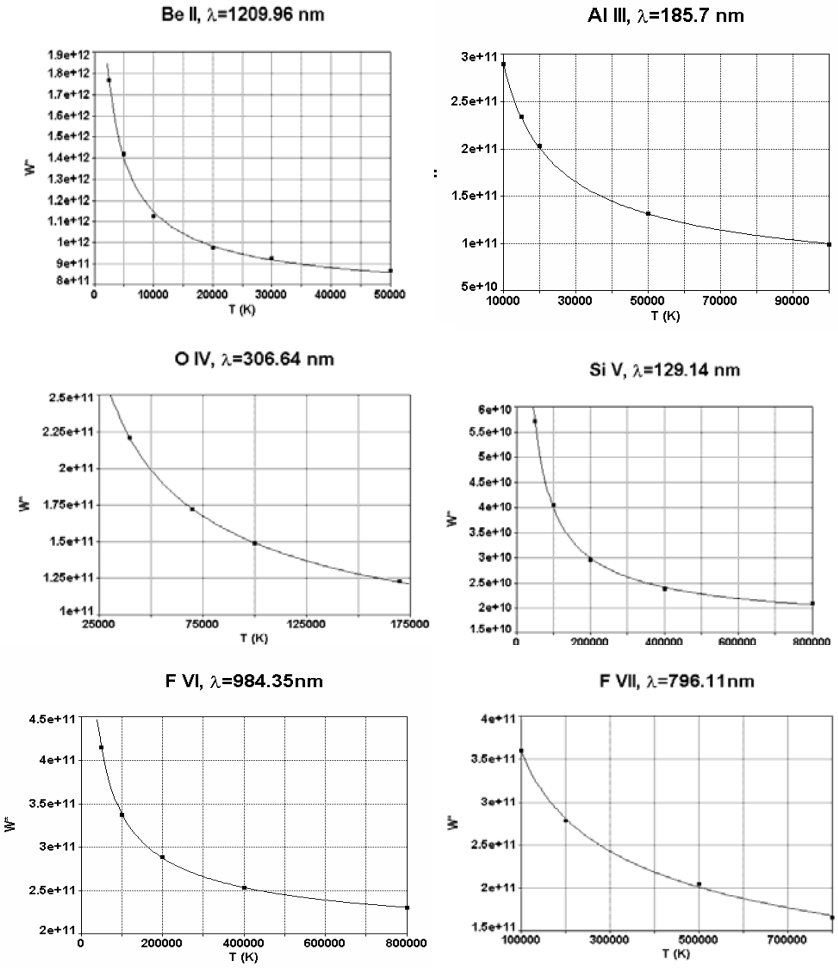

Fig. 1: Reduced Stark width dependencies on the rest core charge, within spectral lines originating from 2*p*-*nd* (n = 3, 4, 5), 2*s*-*np* (n = 2, 3), 2*p*-3*s*, 3*d*-*np* (n = 4, 5), 3d-4*f*, 3*p*-*nd* (n = 3, 4, 5), 3*p*-*ns* (n = 4, 5), 3*s*-*np* (n = 3, 4, 5), 4*s*-*np* (n = 4, 5), 4*p*-*nd* (n = 4, 5), 4*p*-5*s*, 5*p*-5*d* and 5*s*-5*p* were found (Purić and Šćepanović, 1999 and references therein) and shown in Fig. 2. It was found that the appropriate coefficients are a = 1.95 x 10^{12} and b = 3.1.

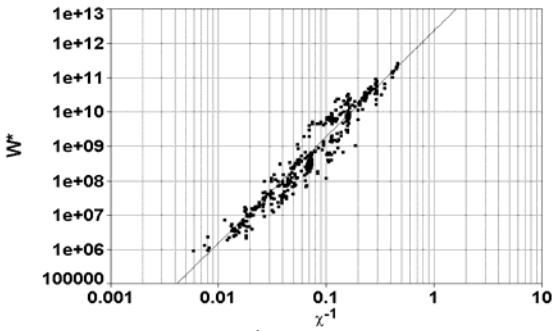

Fig. 2: Reduced Stark width W* (rad s^{-1}) vs. inverse value of upper level ionization potential χ (eV) of the multiply charged ion of different elements along the periodic system.

Experimental reduced Stark width dependencies on the upper level ionisation potential and the rest core charge within spectral lines originating from 3*s*-3*p* and 3*p*-3*d* similar transition under the different plasma condition we used and calculated (Šćepanović and Purić, 2003 and references therein). After being well established and checked using existing theoretical data these dependencies can be used to predict additional Stark broadening data for the lines for which neither theoretical nor experimental data are yet available. The function of the inverse of the upper level ionisation potential χ of the corresponding transition is given in Fig.3 (Šćepanović and Purić, 2003) for 3*s*-3*p* and in Fig. 4 (Šćepanović and Purić, 2003) for 3*p*-3*d*.

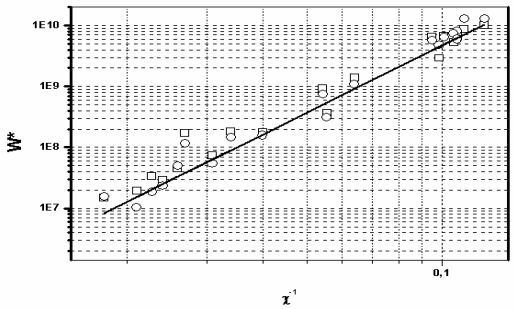

Fig. 3: Reduced Stark width W* (rad s^{-1}) vs. inverse value of upper level ionization potential χ (eV) of the multiply charged ion of different elements for 3s-3p transition array, squares for experimental width, circles for calculated width and line for the trend.

Making use of the theoretical results to find the systematic trends (Šćepanović and Purić, 2003 and references therein), it was found that the coefficients are as follows: a = 2.21 x 10^{13} and b = 3.67 for 3*s*-3*p* transitions, a = 4.22 x 10^{12} and b = 3.4 for 3*p*-3*d* transitions. In Fig. 5 (Šćepanović and Purić, 2003) we used the established coefficients from Fig. 2.

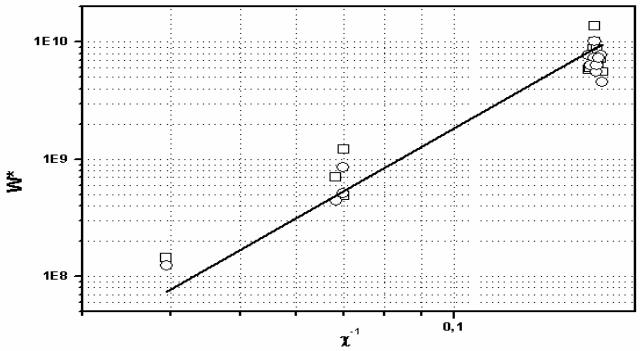

Fig. 4: Reduced Stark width W* (rad s^{-1}) vs. inverse value of upper level ionization potential χ (eV) of the multiply charged ion of different elements for 3p-3d transition array, squares for experimental width, circles for calculated width and line for the trend.

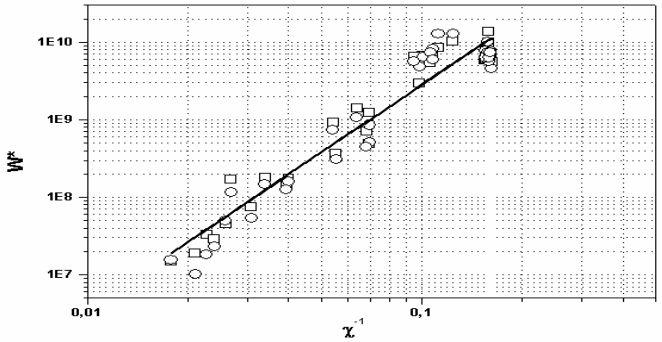

Fig. 5: Reduced Stark width W* (rad s^{-1}) vs. inverse value of upper level ionization potential χ (eV) of the multiply charged ion of different elements for 3p-3d and 3p-3d transition array, squares for experimental width, circles for calculated width and line for the trend.

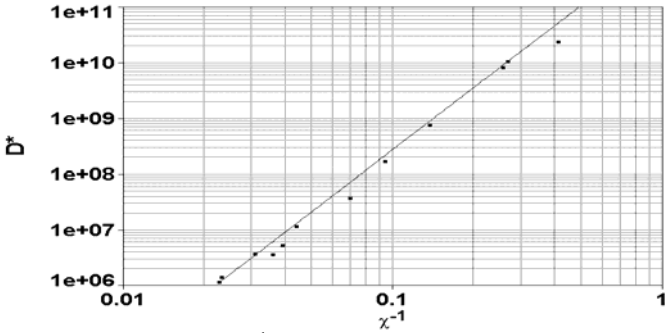

Fig. 6: Reduced Stark shift D* (rad s^{-1}) vs. inverse value of upper level ionization potential χ (eV) of the multiply charged ion of different elements from *3p-ns* (*n*=2,3) transition arrays.

Reduced Stark width dependencies on the rest core charge, within spectral lines originating from *3p-ns* (*n*=2,3) transition arrays were found (Šćepanović and Purić, 2002 and references therein) and shown in Fig. 6. It was found that the appropriate coefficients are $a = 1.57 \times 10^{12}$ and $b = 3.7$. The corresponding correlation factor for all the figures was almost equal to unity.

All data correspond to an electron density $N_e = 10^{23}$ m^{-3} and for different temperatures being normalized using Eq. (22) at $T = 10^5$ K.

5. CONCLUSION

Searching for different types of regularities and systematic trends, which can simplify complicate theoretical calculations especially used in astrophysics, is of great interest. Therefore the aim of this paper was to establish as precisely as possible the Stark parameters dependence on the rest core charge ot the emitters. The dependence was verified through introduction of the Stark widths and shifts reduced values $\omega^* = \omega \cdot z^{-5.20}$, and $d^* = d \cdot z^{-5.20}$, where z is the rest core charge of the emitter seeing by the electron undergoing transition (z = 1, 2, 3, ….for neutral atom, singly, doubly charged ion…respectively) and demonstrating their dependence on the upper level ionization potential. This work successfully proves the existence of the regularities. They are graphically presented for different transition arrays for various ion stages of many elements. Temperature dependence is very important for studying Stark parameters regularities and therefore we have used theoretical values obtained by different authors for 450 spectral lines originating from different stages of ionisations of investigated elements in order to determine Stark parameters temperature dependence through introduced coefficients *A, B* and *C* for these lines used in systematic trends analysis for temperature data normalization. Normalization at an electron density was used as being linear function for non-hydrogenic emitters.

In studying regularities of Stark widths we have treated 23 transition arrays. First, we have successfully found *a* and *b* coefficients values for the introduced reduced Stark broadening parameters $\omega^* = \omega \cdot z^{-5.20}$ for the investigated transition arrays separately to determine their dependences on the upper level ionisation potential. Second, we have treated Stark widths reduced values all together (for all investigated spectral lines originating from different transition arrays and ionisation stages) and have found that they satisfy a universal dependence on the upper level ionization potential similar to those obtained treating transition arrays separately. The obtained theoretical dependence has been compared with experimentally determined Stark widths for 46 spectral lines published so far and an agreement within ± 17 % was found.

Similar procedure was used to obtain Stark shift reduced values dependence on the upper level ionization potential. In this case we had for analysis a smaller sample of published data especially for temperature correction. Therefore, temperature normalization has been done using Stark shift dependence as inverse value of square root of electron temperature. We have studied 9 transition arrays and for each of them we found values of *a* and *b* coefficients. .Finally, Stark parameters reduction using their dependence on the rest core charge of the emitter and the found dependences on the upper level ionization potential can be regarded as being well established using the published theoretical and experimental data so far. Therefore they can be used to estimate the needed Stark widths and shift data for the lines not investigated so far.

References

Allen, C.W.: 1963, *Astrophysical Quantities*, London Univ. Press.

Bates, D.R, Damgaard A.: 1949, *Trans. Roy. Soc. London, Ser. A,* **242**, 101.

Dimitrijević, M.S.: 1982, *Astron. Astrophys.*, **112**, 251.

Dimitrijević, M.S., Konjević., N.: 1987, *Astron. Astrophys.*, **172**, 345.

Djeniže, S., Labat, J., Srećković, A., Labat, O., Platiša, M., Purić, J.: 1991b, *Physica Scripta,* **44**, 148.

Djeniže, S., Srećković, A., Labat, J., Purić, J., Platiša, M.: 1992, *J. Phys. B,* **25**, 785.

Djeniže, S., Srećković, A., Labat, J.: 1991a, *J. Quant. Spectrosc. Radiat. Transfer*., **46**, 433.

Djeniže, S., Srećković, A., Milosavljević, M., Labat, O., Platiša M., Purić, J.,: 1988, *Z. Phys. D,* **9**, 129.

Griem, H.R.: 1968, *Phys. Rev.* 165, 258.

Griem, H.R.: 1974, *Spectral Line Broadening by Plasmas* (New York Academic).

Inglis, D.R., Teller, E.: 1939, *Astrophys. J.*, **90**, 439.

Konjević, N., Dimitrijević, M.S.: 1981, *Spectral Line Shapes*, 241.

Kurucz, R.L.: 1979, *Astrophys. J. Suppl. Series*, **40**, 1.

Labat, J., Djeniže, S., Purić, J., Labat, J.M., Srećković, A.: 1991, *J. Phys. B,* **24**, 1251.

Lanz, T., Artru, M.C.:1987, *Phys. Scripta,* **32**, 115.

Moore, C.E.: 1949, *Atomic E*nergy *Levels*, Nat. Bur. Stand. (U. S.) Circ. 467, Vols. I, II and III.

Oertel, G.K., Shomo, L.P.: 1968, *Astrophys. J. Suppl. Series*, **16**, 175.

Purić, J.: 1996, *J. Appl. Spectrosc.*, **63**, 816.

Purić, J., Ćirković, Lj.: 1973, *IX ICPIG, Prague, Contributed Papers*, 398.

Purić, J., Ćirković, Lj., Labat, J.: 1974, *Fizika*, **6**, 211.

Purić, J., Ćuk, M., Dimitrijević, M.S., Lesage, A.: 1991, *Astrophys. J.*, **382**, 353.

Purić, J., Djeniže, S., Srećković, A., Ćuk, M.: 1988, *Fizika,* **20**, 485.

Purić, J., Djeniže, S., Srećković, A., Ćuk, M., Labat, J., Platiša, M.: 1988, *Z. Phys. D,* **10**, 431.

Purić, J., Šćepanović, M.: 1999, *Astrophys. J.*, **521**, 490.

Salakhov, M.H., Sarandaev, E.V., Fishman, I.S.: 1991, *Optika i Spektroskopia,* **71**, 882.

Šćepanović, M., Purić, J.: 2002, *21st SPIG, Contributed papers*, 330.

Šćepanović, M., Purić, J.: 2003, *J. Quant. Spectrosc. Radiat. Transfer*., **78**, 197.

Smith, P.L.: 1989, in *Atomic and Molecular Data required for Ultraviolet and Optical Astrophysics,* Harvard College Observatory: Report of the Atomic and Molecular Astrophysics Laboratory.

Wiese, W.L., Konjević, N.: 1976, *Physics of Ionized Gases, Contributed papers*, 416.

Wiese, W.L., Konjević, N.: 1982, *J. Quant. Spectrosc. Radiat. Transfer*., **28**, 185.

Wiese, W.L., Konjević, N.: 1992, *J. Quant. Spectrosc. Radiat. Transfer*., **47**, 185.

Publ. Astron. Obs. Belgrade No. 76 (2003), 147 - 162 *Contributed paper*

THE IRON K_α-LINE AS A TOOL FOR ANALYSIS OF BLACK HOLE CHARACTERISTICS

A.F. ZAKHAROV[1,2,3]

[1] *National Astronomical Observatories, Chinese Academy of Sciences, 100012, Beijing, China*

[2] *Institute of Theoretical and Experimental Physics, Moscow, Russia*

[3] *Astro Space Centre of Lebedev Physics Institute, Moscow, Russia*
E–mail: zakharov@vitep1.itep.ru

Abstract. Recent X-ray observations of microquasars and Seyfert galaxies reveal broad emission lines in their spectra, which can arise in the innermost parts of accretion disks. Simulations indicate that at low inclination angle the line is measured by a distant observer as characteristic two-peak profile. However, at high inclination angles ($> 85^0$) two additional peaks arise. This phenomenon was discovered by Matt et al. (1993) using the Schwarzschild black hole metric to analyze such effect. They assumed that the effect is applicable to a Kerr metric far beyond the range of parameters that they exploited. We check and confirm their hypothesis about such a structure of the spectral line shape for the Kerr metric case. We use no astrophysical assumptions about the physical structure of the emission region except the assumption that the region should be narrow enough. Positions and heights of these extra peaks drastically depend on both the radial coordinate of the emitting region (annuli) and the inclination angle. It was found that these extra peaks arise due to gravitational lens effect in the strong gravitational field, namely they are formed by photons with some number of revolutions around black hole. This conclusion is based only on relativistic calculations without any assumption about physical parameters of the accretion disc like X-ray surface emissivity etc. We discuss how analysis of the iron spectral line shapes could give an information about an upper limit of magnetic field near black hole horizon.

1. SIGNATURES OF HIGHLY INCLINATED ACCRETION DISKS NEAR GBHCs AND AGNs

More than ten years ago it was predicted that profiles of lines emitted by AGNs and X-ray binary systems[1] could have an asymmetric double-peaked shape (e.g. Chen et al., 1989; Fabian et al., 1989; Matt et al., 1993). Generation of the broad K_α fluorescence lines as a result of irradiation of a cold accretion disk was discussed by many authors (see, for example, Matt et al., 1991; Matt et al., 1992ab; Matt and Perola, 1992; Matt et al., 1993; Bao, 1993; Martocchia et al., 2002b and references

[1]Some of them are microquasars (for details see, for example, Greiner, 1999; Mirabel, 2000; Mirabel and Rodriguez, 2002).

therein). Popović et al. (2001, 2003) discussed influence of microlensing on the distortion of spectral lines including Fe K_α line, that can be significant in some cases. Zakharov et al. (2003c) showed that the optical depth for microlensing could be significant for cosmological distributions of microlenses. Recent X-ray observations of Seyfert galaxies, microquasars and binary systems (Fabian et al., 1995; Tanaka et al., 1995; Nandra et al., 1997ab; Malizia et al., 1997; Sambruna et al., 1998; Yaqoob et al., 2001; Ogle et al., 2000; Miller et al., 2002 and references therein) confirm these considerations in general and reveal broad emission lines in their spectra with characteristic two-peak profiles. A comprehensive review by Fabian et al. (2000) summarizes the detailed discussion of theoretical aspects of possible scenarios for generation of broad iron lines in AGNs. These lines are assumed to arise in the innermost parts of the accretion disk, where the effects of General Relativity (GR) must be taken into account, otherwise it appears very difficult to find a natural explanation for observed line profile.

Numerical simulations of the line structure are be found in a number of papers: (Kojima, 1991; Laor, 1991; Bao and Stuchlik, 1992; Bao, 1993; Bao et al., 1994; Bromley et al., 1997; Fanton et al., 1997; Pariev and Bromley, 1997, 1998; Pariev et al., 2001; Ruszkowski, 2000; Ma, 2002). They indicate that the accretion disks in Seyfert galaxies are usually observed at the inclination angle θ close to 30^0 or less. This occurs because according to the Seyfert galaxy models, an opaque dusty torque surrounds the accretion disk which does not allow us to observe the disk at larger inclination angles.

However, at inclination angles $\theta > 80^0$, new observational manifestations of GR could arise. Matt et al. (1993) discovered such phenomenon for a Schwarzschild black hole, moreover the authors predicted that their results could be applicable to a Kerr black hole over the range of parameters exploited). The authors mentioned that this problem was not analyzed in detail for a Kerr metric case and it would be necessary to investigate this case. Below we do not use a specific model on surface emissivity of accretion (we only assume that the emitting region is narrow enough). But general statements (which will be described below) can be generalized to a wide disk case without any problem. Therefore, in this paper we check and confirm their hypothesis for the Kerr metric case and for a Schwarzschild black hole using other assumptions about surface emissivity of accretion disks. In principle, such a phenomenon could be observed in microquasars and X-ray binary systems where there are neutron stars and black holes with stellar masses.

In section 3 we discuss disk models used for simulations. In section 4 we present the results of simulations with two extra peaks in the line profile. These extra peaks exist because of the gravitational lens effect in the strong field approximation of GR. In section 5 we discuss results of calculations and present some conclusions.

1. 1. NUMERICAL METHODS

We used an approach discussed in detail in papers by Zakharov (1991, 1994), Zakharov and Repin (1999, 2002abc, 2003a). The approach was used in particular to simulate spectral line shapes. For example, Zakharov et al. (2003a) used this approach to simulate the influence of a magnetic field on spectral line profiles. This approach is based on results of a qualitative analysis (done by Zakharov, 1986, 1989 for different types of geodesics near a Kerr black hole). The equations of photon motion in the

Kerr metric are reduced to the following system of ordinary differential equations in dimensionless Boyer – Lindquist coordinates (Zakharov, 1991, 1994):

$$\frac{dt}{d\sigma} = -a\left(a\sin^2\theta - \xi\right) + \frac{r^2+a^2}{\Delta}\left(r^2+a^2-\xi a\right), \quad (1)$$

$$\frac{dr}{d\sigma} = r_1, \quad (2)$$

$$\frac{dr_1}{d\sigma} = 2r^3 + \left(a^2-\xi^2-\eta\right)r + (a-\xi)^2 + \eta, \quad (3)$$

$$\frac{d\theta}{d\sigma} = \theta_1, \quad (4)$$

$$\frac{d\theta_1}{d\sigma} = \cos\theta\left(\frac{\xi^2}{\sin^3\theta} - a^2\sin\theta\right), \quad (5)$$

$$\frac{d\phi}{d\sigma} = -\left(a - \frac{\xi}{\sin^2\theta}\right) + \frac{a}{\Delta}\left(r^2+a^2-\xi a\right), \quad (6)$$

where $\Delta = r^2 - 2r + a^2$; $\eta = Q/M^2E^2$ and $\xi = L_z/ME$ are the Chandrasekhar constants (Chandrasekhar, 1983) which are derived from the initial conditions of the emitted quantum in the disk plane. The system (1)-(6) has two first integrals

$$\epsilon_1 \equiv r_1^2 - r^4 - \left(a^2-\xi^2-\eta\right)r^2 - 2\left[(a-\xi)^2+\eta\right]r + a^2\eta = 0, \quad (7)$$

$$\epsilon_2 \equiv \theta_1^2 - \eta - \cos^2\theta\left(a^2 - \frac{\xi^2}{\sin^2\theta}\right) = 0, \quad (8)$$

which can be used for the accuracy control of computation.

Solving Eqs. (1)–(6) for monochromatic quanta emitted by a ring we can calculate a spectral line shape $I_\nu(r,\theta)$ which is registered by a distant observer at inclination angle θ.

1. 2. DISK MODEL

To simulate the structure of the emitted line it is necessary first to choose a model for the emissivity of an accretion disk. We exploit two different models, namely we consider a narrow and thin disk moving in the equatorial plane near a Kerr black hole as the first model and as we analyze the inner wide part of an accretion disk with a temperature distribution which is chosen according to the Shakura and Sunyaev (1973) with fixed inner and outer radii r_i and r_o as the second model. Usually a power law is used for wide disk emissivity (see, for example, Laor, 1991; Matt et al., 1991; Martocchia and Matt, 1996; Martocchia et al., 2000; Martocchia et al., 2002a). However, other models for emissivity can not be excluded for such a wide class of accreting black holes, therefore, to demonstrate how another emissivity law could change line profiles we investigate such an emissivity law.

First, we assume that the source of the emitting quanta is a narrow thin disk rotating in the equatorial plane of a Kerr black hole. We also assume that the disk is opaque to radiation, so that a distant observer situated on one disk side cannot measure the quanta emitted from its other side.

For the second case of the Shakura – Sunyaev disk model, we assume that the local emissivity is proportional to the surface element and and T^4, where T is the

local temperature. The emission intensity of the ring is proportional to its area. The area of the emitting ring (width dr) differs in the Kerr metric from its classical expression $dS = 2\pi r dr$ and should be replaced with

$$dS = \frac{2\pi\left(r^2 + a^2\right)}{\sqrt{r^2 - r r_g + a^2}}\, dr. \tag{9}$$

For simulation purposes we assume that the emitting region lies entirely in the innermost region of the α-disk (zone a) from $r_{out} = 10\, r_g$ to $r_{in} = 3\, r_g$ and the emission is monochromatic in the co-moving frame.[2] The frequency of this emission is set as unity by convention.

1. 3. SIMULATION RESULTS

Spectral line profiles of a narrow ring observed at large inclination angles $\theta > 85^0$ and different radii r are shown in Fig. 1 (a Kerr metric generalization of Fig. 1 from Matt et al., 1993 which was drawn using calculations for the Schwarzschild case). The ring is assumed to move in the equatorial plane of a Kerr black hole with an almost extreme rotation parameter $a = 0.9981$. The inclination angle increases from left to right and the radial coordinate from bottom to top. Figure 1 indicates that there are practically no new specific features of profiles, thus, the line profile remains one-peaked with a maximum close to $1.6\, E_{lab}$ and a very long red wing without any significant details.

For the lowest radii there are no signatures of multiple peaks of spectral line shapes even for high inclination angles (the bottom row in Fig. 1 which corresponds to $r = 0.8\, r_g$).

Increasing the radius to $r = 1.2\, r_g$, an additional blue peak arises in the vicinity of the blue maximum at the highest inclination angle $\theta = 89^0$. The red maximum is so small that no details can be distinguished in its structure. At lower inclination angles $\theta \leq 88^0$ the blue maximum also has no details and the entire line profile remains essentially one-peaked.

For $r = 3\, r_g$ additional details in the blue peak appear for $\theta \geq 85^0$. Thus, for $\theta = 85^0$ we have a fairly clear bump, at $\theta = 88^0$ it changes into a small complementary maximum and for $\theta = 89^0$ this maximum becomes well-distinguished. Its position in the last case differs significantly from the main maximum: $E_3 = 1.12\, E_{lab}$, $E_4 = 1.34\, E_{lab}$.

When further increasing the radius the red maximum also bifurcates. This effect becomes visible for $r = 5\, r_g$ and $\theta \geq 88^0$. Thus, for $\theta = 85^0$ we have only a faintly discernible (feebly marked) bump, but for $\theta = 88^0$ both complementary maxima (red and blue) arise. For $\theta = 89^0$ we have already four maxima in the line profile: $E_1 = 0.63\, E_{lab}$, $E_2 = 0.66\, E_{lab}$, $E_3 = 1.07\, E_{lab}$, $E_4 = 1.28\, E_{lab}$. Note that the splitting for the blue and red maxima is not equal, moreover, $E_4 - E_3 \approx 7\ (E_2 - E_1)$.

For $r = 10\, r_g$ the profile becomes more narrow, but the complementary peaks appear very distinctive. We have a four-peak structure for $\theta \geq 88^0$. It is interesting to note that for $\theta = 89^0$ the energy of the blue complementary peak is close to its laboratory value.

[2] We use as usual the notation $r_g = 2GM/c^2$.

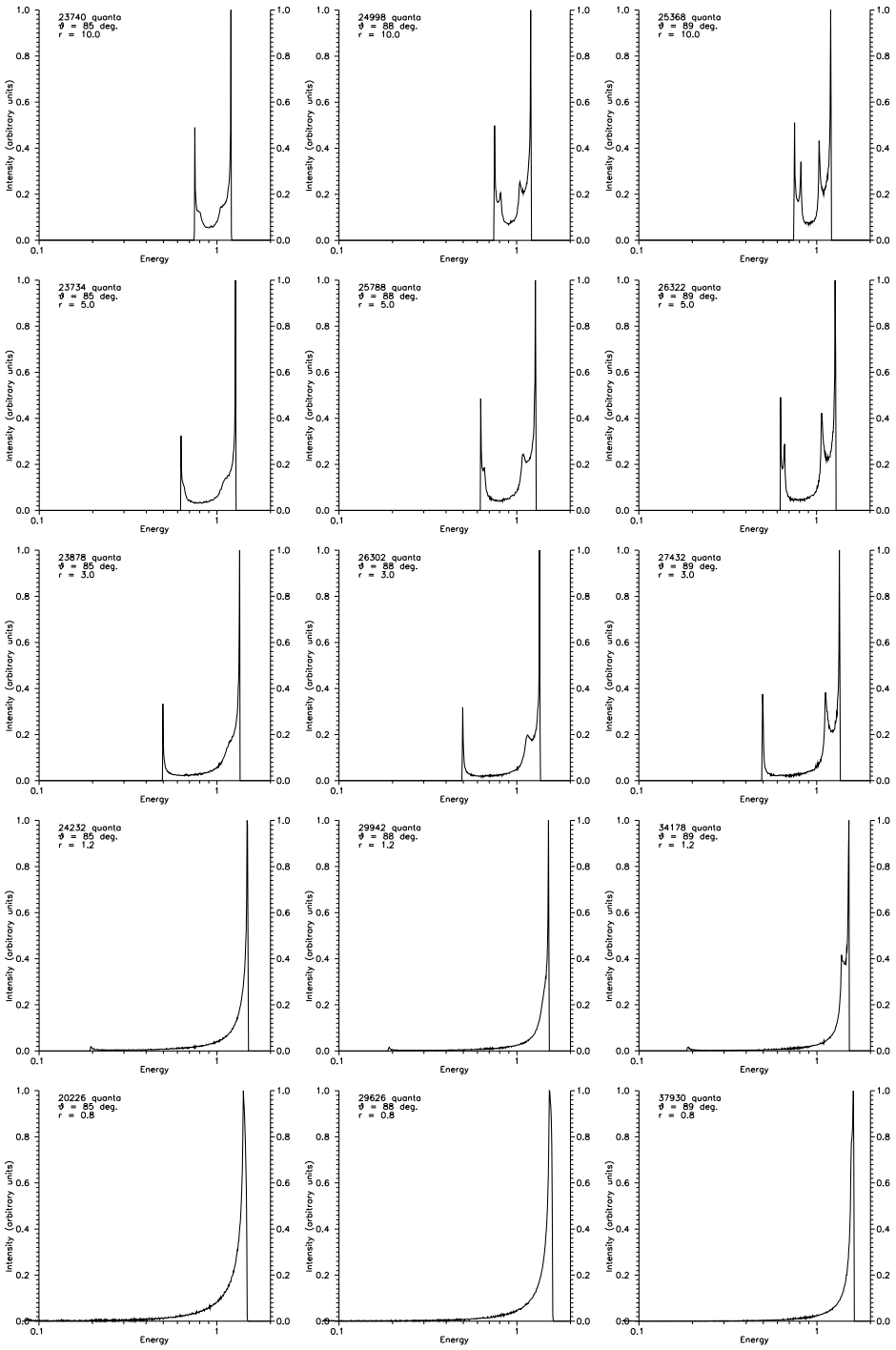

Fig. 1: Line profiles for high inclination angles, $\theta > 85^0$, due to gravitational lens effects in the strong gravitational field approach. The Kerr (rotation) parameter was chosen as $a = 0.9981$. The radii decrease from top to bottom, the inclination angles increase from left to right; their values are shown in each panel along with the number of quanta included in the spectrum.

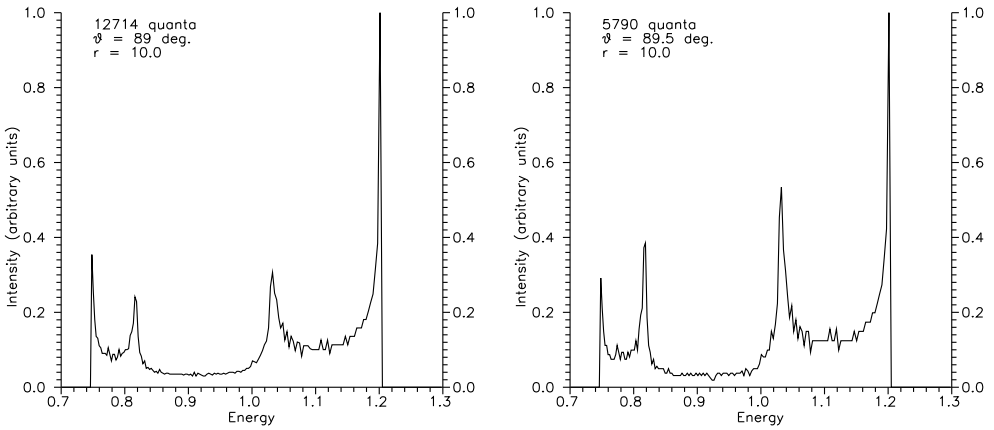

Fig. 2: Details of a hot spot line profile for the most distinctive case with $r = 10\,r_g$ and $a = 0.9981$ (see the top row of Fig. 1). The images of all orders are counted. The left panel includes all the quanta, registered at infinity with $\theta > 89^0$. The right panel includes the quanta with $\theta > 89.5^0$.

Note that the effect almost disappears when the radial coordinate becomes less than r_g, i.e. for the orbits which could exist only near a Kerr black hole.

Figure 2 demonstrates the details of the spectrum presented in the top row in Fig. 1. Thus, the left panel includes all the quanta emitted by a hot spot at $r = 10\,r_g$ with $\theta > 89^0$ at infinity (the mean value could be counted as 85.5^0 if the quanta distribution were uniform there) but with much higher resolution than in Fig. 1. The spectrum has four narrow distinctive maximum separated by lower emission intervals. In the right panel, which includes all the quanta with $\theta > 85.5^0$, the right complementary maximum is even higher than the main one. The blue complementary maxima still remains lower than its main counterpart, but it increases rapidly its intensity with increasing inclination angle. It follows immediately from the comparison of the left and right panels. The "oscillation behavior" of the line profile between the maxima has a pure statistical origin and is not caused by the physics involved.

As an illustration, a spectrum of an entire accretion disk at high inclination angles in the Schwarzschild metric is shown in Fig. 3. (In reality we have calculated geodesics for the quanta trajectories in the Schwarzschild metric using the same Eqs. (1)–(6) as for a Kerr metric, but assuming there $a = 0.01$.) The emitting region (from 3 to $10\,r_g$) lies as a whole in the innermost region of the α-disk (the detailed description of this model was given by Shakura and Sunyaev, 1973; Lipunova and Shakura 2002).

As follows from Fig. 3, the blue peak may consist of two components, whereas the red one remains unresolved.

1. 4. DISCUSSION AND CONCLUSIONS

The complicated structure of the line profile at large inclination angles is explained by the multiple images of some pieces of the hot ring. We point out that the result was obtained in the framework of GR without any extra physical and astrophysical assumptions about the character of the radiation etc. For a Kerr black hole we assume

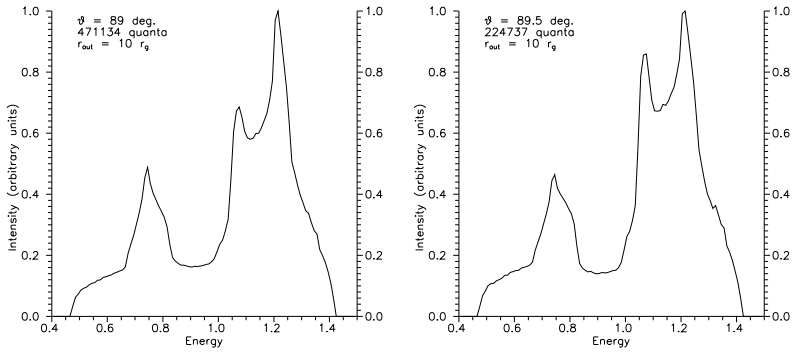

Fig. 3: Details of the line structure for an α-disk in the Schwarzschild metric with outer and inner edges of emitting region equal to $r_{out} = 10\, r_g$ and $r_{in} = 3\, r_g$, respectively. The left panel includes all the quanta, registered at infinity with $\theta > 89^0$. The right panel includes the quanta with $\theta > 89.5^0$.

only that the radiating ring is circular and narrow.

The problem of multiple images in the accretion disks and extra peaks was first considered by Matt et al. (1993) (see also Bao and Stuchlik, 1992; Bao, 1993; Bao et al., 1994; Bao et al., 1996). Using numerical simulations Matt et al. (1993) proved the statement for the Schwarzschild metric and suggested that the phenomenon is applicable to a Kerr metric over the range of parameters that the authors have analyzed. They noted also that it is necessary to perform detailed calculations to confirm their hypothesis. We verified and confirmed their conjecture without any assumptions about a specific distribution of surface emissivity or accretion disk model (see Figs. 1, 2).

We confirmed also their conclusion that extra peaks are generated by photons which are emitted by the far side of the disk, therefore we have a manifestation of gravitational lensing in the strong gravitational field approach for GR.

Some possibilities to observe considered features of spectral line profiles were considered by Matt et al. (1993) and Bao (1993). The authors argued that there are non-negligible chances to observe such phenomenon in some AGNs and X-ray binary systems. For example, Bao (1993) suggested that NGC 6814 could be a candidate to demonstrate such a phenomenon (but Madejski et al., 1993 found that the peculiar properties of NGC6814 are caused by a cataclysmic variable like an AM Herculis System).

However, it is clear that in general the probability to observe objects where one could find such features of spectral lines is small. Moreover, even if the inclination angle is very close to 90^0, the thickness of the disk (shield or a torus around an accretion disk) may not allow us to look at the inner part of accretion disk. Here, we discuss astrophysical situations when the the inclination angle of the accretion disk is high enough.

About 1% of all AGN or microquasar systems could have an inclination angle of the accretion disk $> 89^0$. For example, Kormendy et al. (1996) found that NGC3115 has a very high inclination angle about 81^0 (Kormendy and Richstone, 1992 discovered

a massive dark object $M \sim 10^9 M_\odot$(probably a massive black hole) in NGC3115). Perhaps we have a much higher probability to observe such a phenomenon in X-ray binary systems where black holes with stellar masses could exist. Taking into account the precession which is actually observed for some X-ray binary systems (for example, there is a significant precession of the accretion disk for the SS433 binary system (Cherepashchuk, 2003)[3] moreover since the inclination of the orbital plane is high ($i \sim 79^0$ for this object) we may sometimes observe almost edge-on accretion disks of such objects. Observations indicated that there is a strong evidence that the optically bright accretion disk in SS433 is in a supercritical regime of accretion. The first description of a supercritical accretion disk was given by Shakura and Sunyaev (1973). Even now such a model is discussed to explain observational data for SS433 (Cherepashchuk, 2002). We used the temperature distribution from the Shakura – Sunyaev model (Shakura and Sunyaev, 1973; Lipunova and Shakura, 2002) for the inner part of accretion disk to simulate shapes of lines which could be emitted from this region (Fig. 3). Therefore, we should conclude that the properties of spectral line shapes discovered by Matt et al. (1993) are confirmed also for such emissivity (temperature) distributions which correspond to the Shakura – Sunyaev model.

Thus, such properties of spectral line shapes are robust enough with respect to wide variations of rotational parameters of black holes and the surface emissivity of accretion disks as it was predicted by Matt et al. (1993). So, their conjecture was confirmed not only for the Kerr black hole case but also for other dependences of surface emissivity of the accretion disk. A detailed description of the analysis was given by Zakharov and Repin (2003a).

2. MAGNETIC FIELDS IN AGNs AND MICROQUASARS

Magnetic fields play a key role in dynamics of accretion discs and jet formation. Bisnovatyi-Kogan and Ruzmaikin (1974, 1976) considered a scenario to generate superstrong magnetic fields near black holes. According to their results magnetic fields near the marginally stable orbit could be about $H \sim 10^{10} - 10^{11}$ G. Kardashev (1995, 2001) has shown that the strength of the magnetic fields near supermassive black holes can reach the values $H_{max} \approx 2.3 \cdot 10^{10} M_9^{-1}$ G due to the virial theorem[4], and considered a generation of synchrotron radiation, acceleration of $e^{+/-}$ pairs and cosmic rays in magnetospheres of supermassive black holes at such high fields. It is magnetic field, which plays a key role in these models. Below, based on the analysis of iron K_α line profile in the presence of a strong magnetic field, we describe how to detect the field itself or at least obtain an upper limit of the magnetic field.

General status of black holes is described in a number of papers (see, e.g. Zakharov, 2000 and references therein). Since the matter motions indicate very high rotational velocities, one can assume the K_α line emission arises in the inner regions of accretion discs at distances $\sim (1 \div 3)\, r_g$ from the black holes. Let us recall that the innermost stable circular for non-rotational black hole (which has the Schwarzschild metric) is located at the distance $3\, r_g$ from the black hole singularity. Therefore, a rotation of black hole could be the most essential factor.

[3]Shakura (1972) predicted that if the plane of an accretion disk is tilted relative to the orbital plane of a binary system, the disk can precess.

[4]Recall that equipartition value of magnetic field is $\sim 10^4$ G only.

Wide spectral lines are considered to be formed by radiation emitted in the vicinity of black holes. If there are strong magnetic fields near black holes these lines are split by the field into several components. This phenomenon is discussed below. Such lines have been found in microquasars, GRBs and other similar objects (Mirabel and Rodriguez, 2002; Miller et al., 2002).

To obtain an estimation of the magnetic field we simulate the formation of the line profile for different values of magnetic field. As a result we find the minimal B value at which the distortion of the line profile becomes significant. Here we use an approach, which is based on numerical simulations of trajectories of the photons emitted by a hot ring moving along a circular geodesics near black hole, described earlier by Zakharov (1993, 1994, 1995) and Zakharov and Repin (1999).

2. 1. INFLUENCE OF A MAGNETIC FIELD ON THE DISTORTION OF THE IRON K_α LINE PROFILE

Here we consider the influence of a magnetic field on the iron K_α line profile [5] and show how one can determine the value of the magnetic field strength or at least an upper limit.

The profile of a monochromatic line (Zakharov and Repin, 1999; Zakharov and Repin, 2002a) depends on the angular momentum of a black hole, the position angle between the black hole axis and the distant observer position, the value of the radial coordinate if the emitting region represents an infinitesimal ring (or two radial coordinates for outer and inner bounds of a wide disc). The influence of accretion disc model on the profile of spectral line was discussed by Zakharov and Repin (2003b).

We assume that the emitting region is located in the area of a strong quasi-static magnetic field. This field causes line splitting due to the standard Zeeman effect. There are three characteristic frequencies of the split line that arise in the emission. The energy of central component E_0 remains unchanged, whereas two extra components are shifted by $\pm\mu_B H$, where $\mu_B = \dfrac{e\hbar}{2m_e c} = 9.273 \cdot 10^{-21}$ erg/G is the Bohr magneton. Therefore, in the presence of a magnetic field we have three energy levels: $E_0 - \mu_B H$, E_0 and $E_0 + \mu_B H$. For the iron K_α line they are as follows: $E_0 = 6.4 - 0.58\dfrac{H}{10^{11}\,\mathrm{G}}$ keV, $E_0 = 6.4$ keV and $E_0 = 6.4 + 0.58\dfrac{H}{10^{11}\,\mathrm{G}}$ keV.

Let us discuss how the line profile changes when photons are emitted in the comoving frame with energy $E_0(1+\epsilon)$, but not with E_0. In that case the line profile can be obtained from the original one by $1+\epsilon$ times stretching along the x-axis which counts the energy. The component with $E_0(1-\epsilon)$ energy should be $(1-\epsilon)$ times stretched, correspondingly. The intensities of different Zeeman components are approximately equal (Fock, 1978). A composite line profile can be found by summation the initial line with energy E_0 and two other profiles, obtained by stretching this line along the x-axis in $(1+\epsilon)$ and $(1-\epsilon)$ times correspondingly. The line intensity depends on the direction of the quantum escape with respect to the direction of the magnetic field (Berestetskii et al, 1982). However, we neglect this weak dependence (undoubtedly, the dependence can be counted and, as a result, some details in the spectrum profile can be slightly changed, but the qualitative picture, which we discuss, remains unchanged).

[5] We can also consider X-ray lines of other elements emitted by the area of accretion disc close to

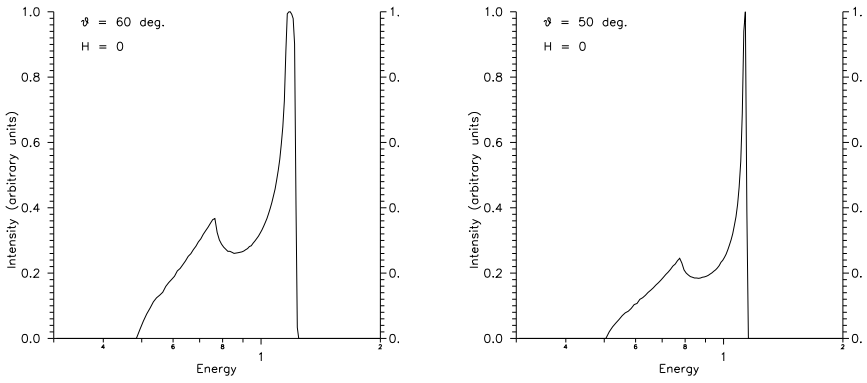

Fig. 4: Profile of monochromatic spectral line, emitted by α-disc in Schwarzschild metric for $r_{out} = 10\, r_g$, $r_{in} = 3\, r_g$ and inclination angles $\theta = 60^\circ$ (left panel) and $\theta = 50^\circ$ (right panel) with zero value of magnetic field. The line profile is represented as registered by a distant observer.

Another indicator of the Zeeman effect is a significant induction of the polarization of X-ray emission: the extra lines possess a circular polarization (right and left, respectively, when they are observed along the field direction) whereas a linear polarization arises if the magnetic field is perpendicular to the line of sight.Despite of the fact that the measurements of polarization of X-ray emission have not been carried out yet, such experiments can be realized in the nearest future (Costa et al., 2001).

The line profile without any magnetic field is presented in Fig. 4 for different values of disc inclination angles: $\theta = 60^0$ and $\theta = 50^0$ respectively. Note, that at $\theta = 50^0$ the blue peak appears to be taller and more narrow. Figs. 5,6 present the line profiles for the same inclination angles and different values of magnetic field: $H = 4{\cdot}10^{10}$, $8{\cdot}10^{10}$, $1.2 \cdot 10^{11}$, $2 \cdot 10^{11}$ G. At $H = 4 \cdot 10^{10}$ G the shape of spectral line does not practically differ from the one with zero magnetic field. Three components of the blue peak are so thin and narrow that they could scarcely be discerned experimentally today. For $H < 4 \cdot 10^{10}$ G and $\theta = 60^0$ the splitting of the line does not arise at all. At $\theta = 50^0$ the splitting can still be revealed for $H = 3 \cdot 10^{10}$ G, but below this value ($H < 3 \cdot 10^{10}$ G) it also disappears. With increasing the field the splitting becomes more explicit, and at $H = 8 \cdot 10^{10}$ G a faint hope appears to register experimentally the complex internal structure of the blue maximum.

While further increasing the magnetic field the peak profile structure becomes apparent and can be distinctly revealed, however, the field $H = 2 \cdot 10^{11}$ G is rather strong, so that the classical linear expression for the Zeeman splitting

$$\Delta E = \pm \mu_B H \tag{10}$$

should be modified. Nevertheless, we use Eq.(10) for any value of the magnetic field, assuming that the qualitative picture of peak splitting remains correct, whereas for $H = 2 \cdot 10^{11}$ G the exact maximum positions may appear slightly different. If the Zeeman energy splitting ΔE is of the order of E, the line splitting due to magnetic fields is described in a more complicated way. The discussion of this phenomenon is

the marginally stable orbit; further we talk only about iron K_α line for brevity.

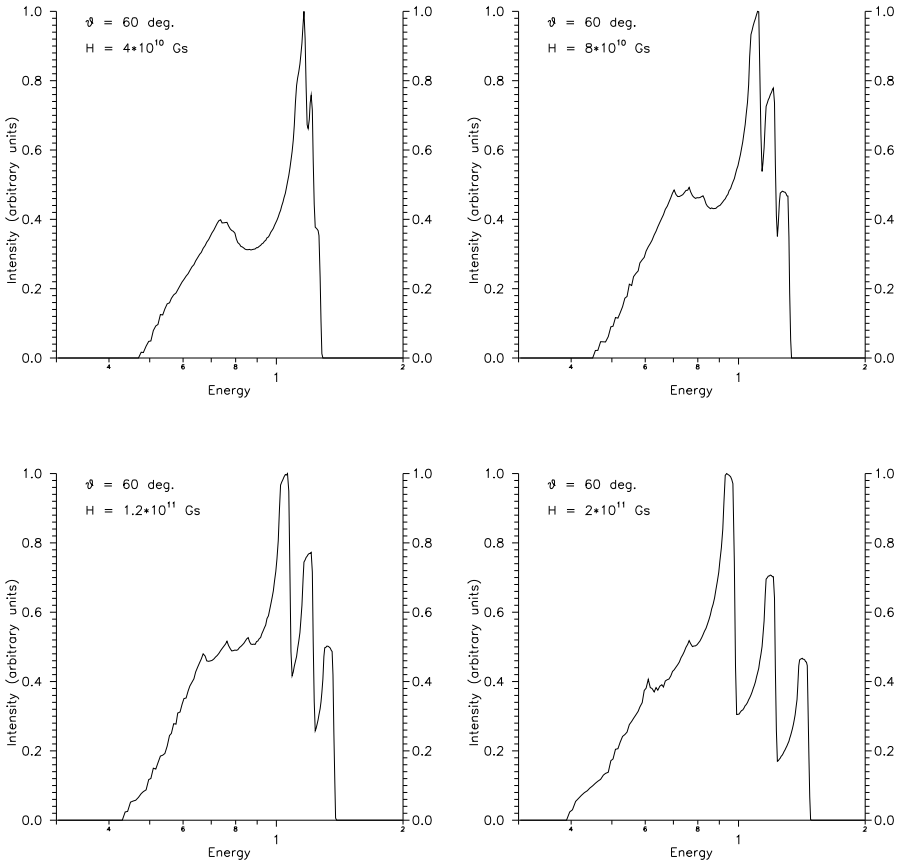

Fig. 5: Distortions of the line profile from the left panel in Fig. 4, arising due to a quasi-static magnetic field existing in the disc. The Zeeman effect leads to the appearance of two extra components with the energies higher and lower than the basic one. The values of the magnetic field are shown at each panel.

not a point of this paper, our aim is to pay attention to the qualitative features of this effect.

Let us discuss possible influence of high magnetic fields on real observational data. We will try to estimate magnetic fields when one could find the typical features of line splitting from the analysis of the spectral line shape. Further we will choose some values of magnetic field and simulate the spectral line shapes from observational data for these values, assuming that these observational data correspond to an object with no significant magnetic fields. We will try to find signatures of the triple blue peak analyzing the simulated data when magnetic fields are rather high. Assuming that there are no essential magnetic fields (compared to 10^{10} G) for some chosen object (for example, for MCG 6-30-15) we could simulate the spectral line shapes for the same objects but with essential magnetic fields. Figure 7 demonstrates a possible influence of the Zeeman effect on observational data. As an illustration we

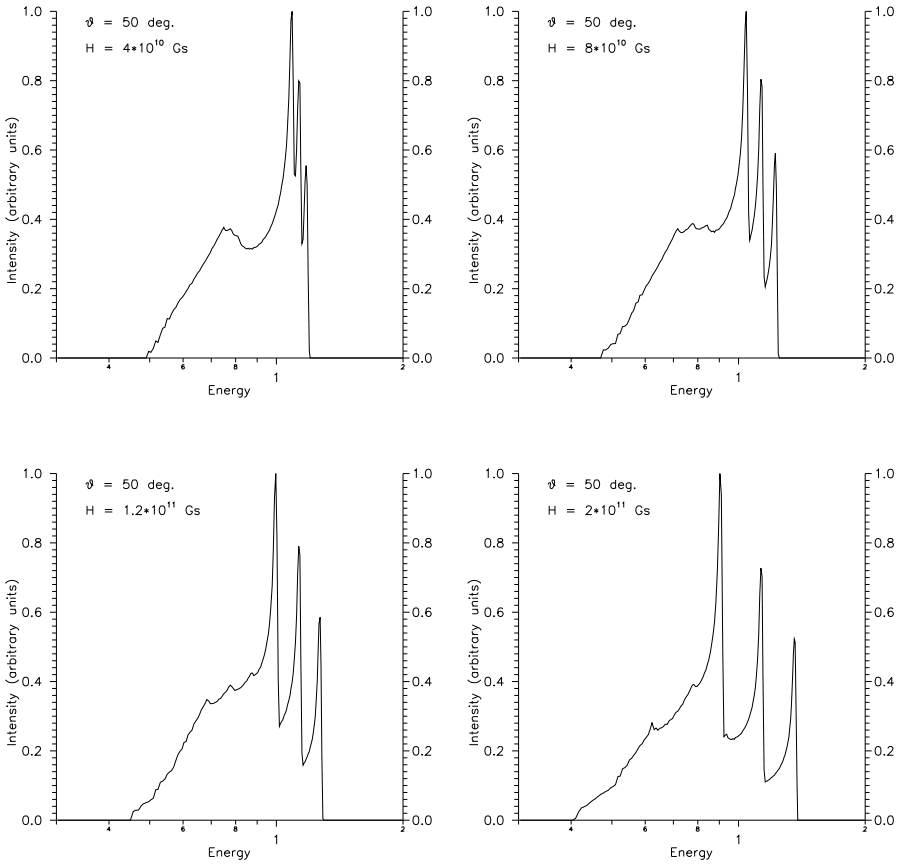

Fig. 6: The same as in Fig. 5, but for $\theta = 50^0$. The right panel in Fig. 4 demonstrates the same spectrum without magnetic field.

consider the observations of iron K_α line which have been carried out by ASCA for the galaxy MCG-6-30-15. They are presented in Fig. 7 by the dashed curve. Let us assume that the actual magnetic field in these data is negligible. Then we can simulate the influence of the Zeeman effect on the structure of observations and see if the simulated data (with a magnetic field) can be distinguishable within the current accuracy of the observations. The results of the simulated observation for the different values of magnetic field are shown in Fig. 7 by solid line. From these figures one can see that classical Zeeman splitting in three components, which can be revealed experimentally today, changes qualitatively the line profiles only for rather high magnetic field. Something like this structure can be detected, e.g. for $H = 1.2 \cdot 10^{11}$ G, but the reliable recognition of three peaks here is hardly possible.

Apparently, it would be more correct to solve the inverse problem: try to determine the magnetic field in the disc, assuming that the blue maximum is already split due to the Zeeman effect. However, this problem includes too many additional factors, which can affect on the interpretation. Thus, besides magnetic field the line width

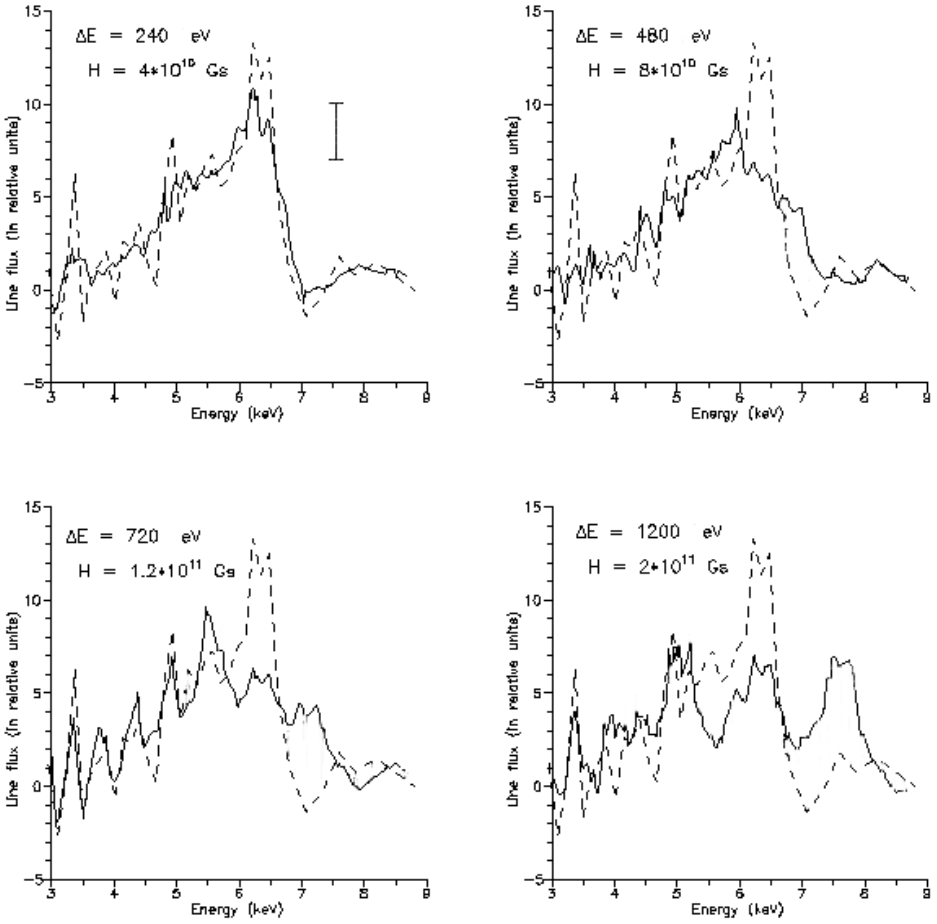

Fig. 7: Influence of a magnetic field on the observational data. The dashed line represents the ASCA observations of MCG-6-30-15 (Tanaka et al., 1995). The vertical bar in the top left panel corresponds to a typical error in observation data. Solid lines show possible profiles of K_α line in the presence of a magnetic field. The field value and the appropriate Zeeman splitting are indicated in each panel.

depends on the accretion disc model as well as on the structure of emitting regions. Problems of such kind may become actual with much better accuracy of observational data in comparison with their current state.

2. 2. DISCUSSION

It is evident that duplication (triplication) of a blue peak could be caused not only by the influence of a magnetic field (the Zeeman effect), but by a number of other factors. For example, the line profile can have two peaks when the emitting region represents two narrow rings with different radial coordinates (it is easy to conclude that two emitting rings with finite widths separated by a gap, would yield a similar effect). Despite the fact that a multiple blue peak can be generated by many causes (including the Zeeman effect as one of possible explanation), the absence of the multiple peak

can lead to a conclusion about the upper limit of the magnetic field.

It is known that neutron stars (pulsars) could have huge magnetic fields. So, it means that the effect discussed above could appear in binary neutron star systems. The quantitative description of such systems, however, needs more detailed computations.

With further increasing of observational facilities it may become possible to improve the above estimation. Thus, the Constellation-X launch suggested in the coming decade seems to increase the precision of X-ray spectroscopy as many as approximately 100 times with respect to the present day measurements (Weawer, 2001). Therefore, there is a possibility in principle that the upper limit of the magnetic field can also be 100 times improved in the case when the emission of the X-ray line arises in a sufficiently narrow region.

A detailed discussion of the magnetic field influence on spectral line shapes for flat accretion flows was given by Zakharov et al. (2003a) and for non-flat accretion flows by Zakharov et al. (2003b).

Acknowledgments. I am grateful to E.F. Zakharova for the kindness and support necessary to complete this work. I would like to thank Belgrade Observatory, Dipartimento di Fisica Universita di Lecce, INFN, Sezione di Lecce and the National Astronomical Observatories of the Chinese Academy of Sciences for the hospitality and profs. L. Č. Popović, M. S. Dimitrijević, F. DePaolis, G. Ingrosso, J. Wang and Dr. Z. Ma for very useful discussions.

This work was supported partly by the National Natural Science Foundation of China, No.:10233050 and the Russian Foundation for Basic Research, grant 00–02–16108.

References

Bao, G.: 1993, *Astrophys. J.,* **409**, L41.
Bao, G., Hadrava, P., Ostgaard, E.: 1994, *Astrophys. J.,* **435**, 55.
Bao, G., Stuchlik Z.: 1992, *Astrophys. J.,* **400**, 163.
Bao, G., Hadrava, P., Ostgaard, E.: 1996, *Astrophys. J.,* **464**, 684.
Berestetskii, V.B., Lifshits, E.M., Pitaevskii, L.P.: 1982, *Quantum electrodynamics,* Pergamon Press, Oxford.
Bisnovatyi-Kogan, G.S., Ruzmaikin, A.A.: 1974, *Astrophys. Space Sci.*, **28**, 45.
Bisnovatyi-Kogan, G.S., Ruzmaikin, A.A.: 1976, *Astrophys. Space Sci.,* **42**, 401.
Bromley, B.C., Chen, K., Miller, W.A.: 1997, *Astrophys. J.,* **475**, 57.
Chandrasekhar, S.: 1983, *Mathematical Theory of Black Holes*, Clarendon Press, Oxford.
Chen K., Halpern, J.P., Filippenko A.V.: 1998, *Astrophys. J.,* **344**, 115.
Cherepashchuk, A.M.: 2002, *Space Sci. Rev.,* **102**, 23.
Costa E., Soffitta P., Belazzini R. et al., 2001, *Nature,* **411**, 662.
Cui, W., Zhang, S.N., Chen W.: 1998, *Astrophys. J.,* **492**, L53.
Cunningham, C.T., Bardeen, J.M.: 1973, *Astrophys. J.*, **183**, 237.
Cunningham, C.T.: 1975, *Astrophys. J.,* **202**, 788.
Fabian, A.C., Rees, M., Stella, L., White, N.E.: 1989, *Mon. Not. Roy. Astron. Soc.,* **238**, 729.
Fabian, A.C., Nandra, K., Reynolds, C.S. et al.: 1995, *Mon. Not. Roy. Astron. Soc.,* **277**, L11.
Fabian, A.C., Iwazawa, K., Reynolds, C.S., Young, A.J.: 2000, *Publ. Astron. Soc. Pac.*, **112**, 1145.
Fanton, C., Calvani, M., de Felice, F., Čadež, A: 1997, *Publ. Astron. Soc. Japan,* **49**, 159.

Fock, V.A.: 1978, *Fundamentals of quantum mechanics,* Mir, Moscow.
Greiner, J.: 2000, *Cosmic Explosions, Proc. of 10th Annual Astrophysical Conference in Maryland,* eds. S.Holt and W.W.Zang, AIP Conference proceedings, **522**, 307.
Karas, V., Vokrouhlický, D., Polnarev, A.G.: 1992, *Mon. Not. Roy. Astron. Soc.,* **259**, 569.
Kardashev, N.S.: 1995, *Mon. Not. Roy. Astron. Soc.*, **276**, 515.
Kardashev, N.S.: 2001, *Mon. Not. Roy. Astron. Soc.*, **326**, 1122.
Kojima, Y.: 1991, *Mon. Not. Roy. Astron. Soc.*, **250**, 629.
Kormendy, J., Richstone, D.: 1992, *Astrophys. J.,* **393**, 559.
Kormendy, J., Bender, R., Richstone, D. et al.: 1996, *Astrophys. J.,* **459**, L57.
Laor, A.: 1991, *Astrophys. J.,* **376**, 90.
Lipunova, G.V., Shakura, N.I.: 2002, *Astronomy Reports,* **46**, 366.
Ma, Z.: 2002, *Chin Phys. Lett.,* **19**, 1537.
Madejski, G.M., Done, C., Turner, T.J. et al., 1993, *Nature,* **365**, 626.
Malizia, A., Bassani, L., Stephen, J.B. et al. 1997, *Astrophys. J.,* **113**, 311.
Martocchia, A., Matt, G.: 1996, *Mon. Not. Roy. Astron. Soc.,* **282**, L53.
Martocchia, A., Karas, V., Matt, G.: 2000, *Mon. Not. Roy. Astron. Soc.,* **312**, 817.
Martocchia, A., Matt, G., Karas, V.: 2002a, *Astron. Astrophys.*, **383**, L23.
Martocchia, A., Matt, G., Karas, V. et al.: 2002b, *Astron. Astrophys.,* **387**, 215.
Matt, G., Fabian, A.C., Ross, R.R.: 1993, *Mon. Not. Roy. Astron. Soc.,* **262**, 179.
Matt, G., Perola, G.C., Piro, L., 1991, *Astron. Astrophys.,* **267**, 643.
Matt, G., Perola, G.C.: 1992, *Mon. Not. Roy. Astron. Soc.,* **259**, 63.
Matt, G., Perola, G.C., Piro, L., Stella, L.: 1992a, *Astron. Astrophys.,* **257**, 63.
Matt, G., Perola, G.C., Piro, L., Stella, L.: 1992b, *Astron. Astrophys.,* **263**, 453.
Matt, G., Perola, G.C., Stella, L.: 1993, *Astron. Astrophys.,* **267**, 643.
Miller, J.M., Fabian, A.C., Wijnands, R. et al.: 2002, *Astrophys. J.*, **570**, L69.
Mirabel, I.F.: 2001, *Astrophys. Space Sci.* **276**, 319.
Mirabel, I.F, Rodriguez, L.F.: 2002, *Sky and Telescope,* May, 33.
Nandra, K., George, I.M., Mushotzky, R.F. et al.: 1997a, *Astrophys. J.,* **476**, 70.
Nandra, K., George, I.M., Mushotzky, R.F. et al.: 1997b, *Astrophys. J.,* **477**, 602.
Ogle, P.M., Marshall, H.L., Lee, J.C. et al.: 2000, *Astrophys. J.,* **545**, L81.
Pariev, V.I., Bromley, B.C.: 1997, *Proc. of the 8-th Annual October Astrophysics Conference in Maryland "Accretion Processes in Astrophysical Systems: Some Like it Hot!" College Park, MD, October 1997* Eds. Stephen S. Holt and Timothy R. Kallman, AIP Conference Proceedings **431**, 273.
Pariev, V.I., Bromley, B.C.: 1998, *Astrophys. J.,* **508**, 590.
Pariev, V.I., Bromley, B.C., Miller, W.A.: 2001, *Astrophys. J.,* **547**, 649.
Paul, B., Agrawal, P.C., Rao, A.R. et al.: 1998, *Astrophys. J.,* **492**, L63.
Popović L.Č., Mediavilla, E.G., Munoz, J.A.: 2001, *Astron. Astrophys.,* **378**, 295.
Popović, L.Č., Mediavilla, E.G., Jovanović, P. et al.: 2003, *Astron. Astrophys.,* **398**, 975.
Ruszkowski, M.: 2000, *Mon. Not. Roy. Astron. Soc.,* **315**, 1.
Sambruna, R.M., George, I.M., Mushotsky, R.F. et al.: 1998, *Astrophys. J.,* **495**, 749.
Shakura, N.I.: 1972, *Astron. Zhurn.,* **49**, 921.
Shakura, N.I., Sunyaev R.A.: 1973, *Astron. Astrophys.,* **24**, 337.
Sulentic, J.W., Marziani, P., Zwitter, T. et al.: 1998a, *Astrophys. J.,* **501**, 54.
Sulentic, J.W., Marziani, P., Calvani, M.: 1998b, *Astrophys. J.,* **497**, L65.
Tanaka, Y., Nandra, K., Fabian, A.C. et al.: 1995, *Nature,* **375**, 659.
Weaver, K.A., Krolik, J.H., Pier, E.A.: 1998, *Astrophys. J.,* **498**, 213.
Weaver, K.A., 2001, *Relativistic Astrophysics*, Eds. J.C. Wheeler, H. Martel, Texas Symposium, American Institute of Physics, AIP Conference Proceedings, **586**, 702.
Yaqoob, T., Serlemitsos, P.J., Turner, T.J. et al.: 1996, *Astrophys. J.,* **470**, L27.
Yaqoob, T., McKernan, B., Ptak, A. et al.: 1997, *Astrophys. J.,* **490**, L25.
Yaqoob, T., George, I.M., Nandra, K. et al.: 2001, *Astrophys. J.,* **546**, 759.
Zakharov, A.F.: 1986, *Sov. Phys. - Journ. Experim. and Theor. Phys.,* **64**, 1.
Zakharov, A.F.: 1989, *Sov. Phys. – Journ. Experimental and Theoretical Phys.,* **68**, 217.
Zakharov, A.F.: 1991, *Soviet Astron.*, **35**, 147.
Zakharov, A.F.: 1993, *Preprint MPA* **755**.

Zakharov, A.F.: 1994, *Mon. Not. Roy. Astron. Soc.*, **269**, 283.
Zakharov, A.F.: 1995, *17th Texas Symposium on Relativistic Astrophysics, Ann. NY Academy of Sciences,* **759**, 550.
Zakharov, A.F.: 2000, *Proc. of the XXIII Workshop on High Energy Physics and Field Theory*, IHEP, Protvino, 169.
Zakharov, A.F., Kardashev N.S., Lukash V.N., Repin, S.V.: 2003a, *Mon. Not. Roy. Astron. Soc.,* **342**, 1325.
Zakharov, A.F., Ma, Z., Bao, Y.: 2003b, to *Astron. Astrophys.,* (submitted).
Zakharov A.F., Popović L.Č., Jovanović P. et al. 2003c, to *Astron. Astrophys.,* (submitted).
Zakharov, A.F., Repin, S.V.: 1999, *Astronomy Reports*, **43**, 705.
Zakharov, A.F., Repin, S.V.: 2002a, *Astronomy Reports*, **46**, 360.
Zakharov, A.F., Repin, S.V.: 2002b, *Proc. of the Eleventh Workshop on General Relativity and Gravitation in Japan,* Eds. J. Koga, T. Nakamura, K. Maeda, K. Tomita, Waseda University, Tokyo, 68.
Zakharov, A.F., Repin, S.V.: 2003a, *Astron. Astrophys.,* **406**, 7.
Zakharov, A.F., Repin, S.V.: 2003b, *Astronomy Reports*, **47**, 410.
Zakharov, A.F., Repin, S.V.: 2003c, *Advances in Space Res.* (accepted).

Publ. Astron. Obs. Belgrade No. 76 (2003), 163-166 *Contributed paper*

THE COMPLETE CALCULATION OF STARK BROADENING PARAMETERS FOR THE NEUTRAL COPPER ATOMS SPECTRAL LINES OF 4s ^{2}S-4p ^{2}P^0 AND 4s^2 ^{2}D-4p ^{2}P^0 MULTIPLETS IN THE DIPOLE APPROXIMATION

E.M. BABINA, G.G. IL'IN, O.A. KONOVALOVA, M.KH. SALAKHOV, E.V. SARANDAEV

Physics Department, Kazan State University, Kremlevskaya str., Kazan, Russia, 420008
E-mail: sarev@ksu.ru

Abstract. The complete calculation of Stark broadening parameters for the neutral copper atoms spectral lines of 4s ^{2}S-4p ^{2}P^0 and 4s^2 ^{2}D-4p ^{2}P^0 multiplets in the dipole approximation according to Cooper and Oertel (1969) is carried out in which the necessary coordinate operator matrix elements have been found through the known experimental absorption oscillator strengths. The importance of taking into account such aspects as the ''back reaction'' of copper atom on perturbers (electrons) in inelastic collisions and corrections to the broadening function in the classical-path approximation ($\hat{\lambda}$ cutoff) is discussed.

The knowledge of the Stark broadening parameters of the copper atoms spectral lines is of great interest for the diagnostics of the laboratory and astrophysical plasmas. However for the row of the important spectral lines to which the spectral lines of 4s ^{2}S-4p ^{2}P^0 multiplet (Cu I 324.754 nm and Cu I 327.396 nm resonance spectral lines) and 4s^2 ^{2}D-4p ^{2}P^0 multiplet (Cu I 510.554 nm, Cu I 570.024 nm and Cu I 578.213 nm spectral lines) we do not have yet enough reliable experimental data and the theoretical data obtained on the basis of the quantum-mechanical calculations. In this paper the new theoretical values of the parameters for the mentioned lines are presented.

The theoretical values of the Stark broadening parameters of the copper atoms spectral lines of 4s ^{2}S-4p ^{2}P^0 and 4p ^{2}P^0 multiplets have been presented by Konjević and Konjević (1986), Dimitrijević *et al.* (1996), Grishina *et al.* (1998a, 1988b, 1999) and Sibgatullin *et al.* (2000). In Konjević and Konjević (1986) the quantum-mechanical calculations have been carried out for the first time in the dipole approximation for the lines of 4s^2 ^{2}D-4p ^{2}P^0 multiplet by using simplified semiclassical formulae given by Dimitrijević and Konjević (1986) in which the necessary coordinate operator matrix elements taking account of the interaction of the different energetic levels have been found in the Coulomb approximation. In Dimitrijević *et al.* (1996), Grishina *et al.* (1998a, 1998b, 1999) and Sibgatullin *et al.* (2000) the quantum-mechanical calculations in the dipole approximation have been carried out with more rigorous representation of the coordinate operator matrix elements through the known experimental absorption oscillator strength that has allowed for the first time to carry out the calculations also for the resonance spectral lines of 4s ^{2}S-4p ^{2}P^0 multiplet for which the Coulomb approximation is customary unacceptable in the case of heavy atoms. Thereby favourable circumstances have contributed that for the spectral lines of 4s ^{2}S-4p ^{2}P^0 and 4s^2 ^{2}D-4p ^{2}P^0 multiplets of the neutral copper atoms the perturbing levels are

sufficiently widely spaced from the disturbed levels and between the levels the convenient transitions for the experimental investigations are possible which fall in UV- and visible region of the spectrum.

Table 1. The Stark widths of the Cu I spectral lines for $n_e=10^{17}$ см$^{-3}$.

λ, nm	T, K	$2\omega_e$, nm (2)/(1)	$2\omega_e$, nm (3)	A (2)/(1)	A (3)	ω_{tot}, nm (2)/(1)	ω_{tot}, nm (3)
	5000	0.0117 (0.0103)	0.00846	0.0450 (0.0498)	0.0575	0.0120 (0.0105)	0.0088
	10000	0.0122 (0.0126)	0.0099	0.0436 (0.0427)	0.0512	0.0127 (0.0131)	0.0139
510.554	20000	0.0139 (0.0156)	0.0123	0.0396 (0.0362)	0.0435	0.0146 (0.0163)	0.0129
	30000	0.0161 (0.0177)	0.0142	0.0364 (0.0311)	0.0390	0.0163 (0.0184)	0.0149
324.754	17000	0.00473 (0.00567)	0.00401	0.0350 (0.0301)	0.0396	0.00520 (0.00627)	0.00419*
	5000	0.00403 (0.00332)	0.00267	0.0357 (0.0413)	0.0485	0.00412 (0.00339)	0.00276
	10000	0.00400 (0.00433)	0.00304	0.0359 (0.0338)	0.0440	0.00414 (0.00447)	0.00317
327.396	20000	0.00475 (0.00581)	0.00408	0.0315 (0.0271)	0.0354	0.00493 (0.00600)	0.00425
	30000	0.00563 (0.00687)	0.00508	0.0278 (0.0239)	0.0300	0.00583 (0.00708)	0.00527

(1) - in the brackets (...) the calculation results of the works (Grishina, Il'in *et al.* 1998a, 1998b) are presented without the accounting for the ''back reaction'' and $\hat{\lambda}$ cutoff;
(2 - the calculation results of the work (Grishina, Il'in *et al.* 1999) with the accounting for the ''back reaction'';
(3) - the new calculation results with the accounting for the ''back reaction'' and $\hat{\lambda}$ cutoff.
* - in (Sculjan, Bucovic *et al.* 1995) for the Cu I 324.754 nm spectral line the experimental width ω_{tot}=0.0097 nm has been obtained at T=17000 K and $n_e=0.66\cdot10^{17}$ см$^{-3}$ that gives the width $\omega_{tot}\approx$0.015 nm at $n_e=10^{17}$ см$^{-3}$ in the proportion to an increase of n_e. This value of ω_{tot} is greater by 3.6 fold than the theoretical value of ω_{tot} in Table 1.

In Dimitrijević *et al.* (1996) the calculations have been carried out according to the scheme in Dimitrijević and Konjević (1986) and Konjević and Konjević (1986) by using the known values of the absorption oscillator strengths presented in Radzig and Smirnov

(1986). In Grishina *et al.* (1998a, 1998b) the calculations have been carried out by using more rigorous the quantum-mechanical formulae in Griem (1974), Griem *et al.* (1962) according to the scheme described in Griem (1962) and the results have been obtained which differ noticeably from the results of the work Dimitrijevic *et al.* (1996).

Table 2. The Stark shifts of the Cu I spectral lines for $n_e=10^{17}$ см$^{-3}$

(in the wave-length scale all the shifts and η are positive).

λ, nm	T, K	d_e, nm (2)/(1)	d_{tot}, nm (2)/(1)	d_{tot}, nm (3)	$\eta=d_e/\omega_e$. (2)/(1)	$\eta=d_e/\omega_e$ (3)
	5000	0.00783	0.00802	0.00800	1.33	1.85
		(0.00799)	(0.00816)		(1.56)	
	10000	0.00889	0.00917	0.00916	1.45	1.79
		(0.00883)	(0.00912)		(1.40)	
510 554	20000	0.00947	0.00984	0.00983	1.36	1.54
		(0.00929)	(0.00967)		(1.19)	
	30000	0.00945	0.00986	0.00985	1.21	1.33
		(0.00925)	(0.00968)		(1.05)	
	5000	0.00230	0.00234	0.00234	1.14	1.71
		(0.00237)	(0.00242)		(1.43)	
	10000	0.00254	0.00262	0.00262	1.27	1.67
		(0.00251)	(0.00259)		(1.16)	
327.396	20000	0.00250	0.00260	0.00260	1.05	1.23
		(0.00243)	(0.0254)		(0.84)	
	30000	0.00234	0.00245	0.00245	0.83	0.92
		(0.00227)	(0.00239)		(0.66)	

(1), (2), (3) - see the comments to Table 1.

In Grishina *et al.* (1999) the calculations have been carried out according to the scheme of the work Cooper and Oertel (1969) in which in contrast to the scheme of the work Griem (1962) the inelastic collisions of electrons with the atoms are taken into account more strictly by way of accounting for an effect of the atoms (''back reaction'') on the perturbing electrons flying by the atoms. In Sibgatullin *et al.* (2000) the calculations have been carried out also according to the scheme of the work Cooper and Oertel (1969) however apart from the accounting for ''back reaction'' the estimation of the role of the $\lambda\!\!\!^{-}$ cutoff, as it is called, has been carried out at the specifying the cross section of the impact broadening by the electrons with the strong collisions in the limits of the Weisskopf radius. The $\lambda\!\!\!^{-}$ cutoff in point of fact consists in the cutting out in the broadening cross-section of the central part with the radius equaling the value of the de Broglie wave-length (divided by 2π) and in the elimination from the consideration of the broadening of the close electron transits because of the uncertainty in the trajectory of electrons according to the

Heisenberg's uncertainty relation for the coordinate and impulse of the electron and correspondingly of the small probability of very close transits.

This paper continues the work of Sibgatullin *et al.* (2000) in which only estimation results have been presented for the Cu I 327.396 nm resonance spectral line. The calculation program used by us in Grishina *et al.* (1998a, 1998b, 1999) and Sibgatullin *et al.* (2000) has been extended by the accounting of the $\hat{\lambda}$ cutoff whereby some errors of the program have been eliminated that results in the small correction of the calculation data of works Grishina *et al.* (1998a, 1998b, 1999). Some new results with the accounting for the $\hat{\lambda}$ cutoff obtained by us are presented in Tables 1 and 2 for some copper atoms spectral lines of 4s ^{2}S-4p ^{2}P^0 and 4s^2 ^{2}D-4p ^{2}P^0 multiplets. In Tables 1 and 2 ω_e and d_e are correspondingly the electron impact half-width and shift in the wave-length scale, A is the ionic broadening parameter, $\omega_{tot}=2\omega_e[1+1.75A(1-0.75R]$ and $d_{tot}=d_e+2A(1-0.75R)\omega_e$ are correspondingly the full width and shift when the ionic broadening is taken into account also (R is the Debay schielding parameter) (Griem 1974). Table 1 and 2 allow to present on the example of the copper atoms spectral lines the full picture of the effect of the accounting for the ''back reaction'' and $\hat{\lambda}$ cutoff on the results of calculations carried out in the dipole approximation. As it is seen from Table 1 and 2 the accounting for the ''back reaction'' and $\hat{\lambda}$ cutoff effect on the results of calculations and these circumstances must be taken into consideration at the comparison of the experimental and theoretical profiles of the spectral lines. However as a whole the effect for the accounting of the ''back reaction'' and $\hat{\lambda}$ cutoff is comparatively moderate and substantially does not change the results of calculations obtained by using the scheme described Griem (1962) in which the ''back reaction'' and $\hat{\lambda}$ cutoff are not taken into account.

References

Cooper, J., Oertel, G.K.: 1969, *Phys. Rev.*, **180**, 286.

Dimitrijević, M.S., Il'in, G.G., Salakhov, M.Kh., Sarandaev, E.V.: 1996, *18th SPIG Contributed papers*, 283.

Dimitrijević, M.S., Konjević, N.: 1986, *Astron. Astrophys.* **163**, 297.

Grishina, N.A., Il'in, G.G., Salakhov, M.Kh., Sarandaev, E.V.: 1998a, *19th SPIG Contributed papers*, 361.

Grishina, N.A., Il'in, G.G., Salakhov, M.Kh., Sarandaev, E.V.: 1998b, *Coherent Optics and Optical Spectroscopy*, Kazan, Russia, 43.

Grishina, N.A., Il'in, G.G., Salakhov, M.Kh., Sarandaev, E.V.: 1999, *Coherent Optics and Optical Spectroscopy*, Kazan, Russia, 23.

Konjević, R., Konjević, N.: 1986, *Fizika*, **18,** 327.

Radzig, A.A, Smirnov, B.M.: 1986, *Atomic and Ionic Parameters*, Energoizdat, Moscow.

Griem, H.R.: 1962, *Phys. Rev.*, **128**, 515.

Griem, H.R., Baranger, M., Kolb, A.C., Oertel, G.: 1962, *Phys. Rev.*, **125**, 177.

Griem, H.R.: 1974, *Spectral Line Broadeninig by Plasmas*, Academic Press, New York.

Skuljan, Lj., Bucović, S., Djeniže, S.: 1995, *Publ. Obs. Belgrade*, **50**, 127.

Sibgatullin, M.E., Il'in, G.G., Salakhov, M.Kh., Sarandaev, E.V.: 2000, *Coherent Optics and Optical Spectroscopy*, Kazan, Russia, 123.

Publ. Astron. Obs. Belgrade No. 74 (2002), 167 - 170 *Poster*

ON THE STARK BROADENING OF THE FOUR TIMES IONIZED SILICON SPECTRAL LINES

NEBIL BEN NESSIB[1], MILAN S. DIMITRIJEVIĆ[2], SYLVIE SAHAL-BRÉCHOT[3]

[1] *Groupe de Recherche en Physique Atomique et Astrophysique, Faculté des Sciences de Bizerte 7021 Zarzouna, Tunisia.*

[2] *Astronomical Observatory, Volgina 7, 11160 Belgrade, Serbia, Yugoslavia*

[3] *Laboratoire d'étude du Rayonnement et de la Matière en Astrophysique, FRE CNRS 2460,Observatoire de Paris-Meudon, 92195 Meudon, France.*

E–mail: nebil.bennessib@planet.tn

E–mail: mdimitrijevic@aob.aob.bg.ac.yu

E–mail: Sylvie.Sahal-Brechot@obspm.fr

Abstract. Using a semiclassical perturbation approach, we have compared Stark broadening parameters for 16 Si V multiplets calculated with oscillator strengths obtained with the SUPERSTRUCTURE code and within the Coulomb approximation. In order to complete Stark broadening data for most important charged perturbers in stellar atmospheres, Stark broadening parameters for proton−, He II−, and Si II−impact line widths and shifts are presented also.

1. Introduction

The semiclassical - perturbation formalism (Sahal-Bréchot, 1969ab) has been used in a series of papers for large scale calculations of Stark broadening parameters for a number of spectral lines of various emitters from neutrals up to twelve time charged ions (see e.g. Dimitrijević, 1997 and references therein). The results of such calculations are of interest for a number of different problems in physics, astrophysics and plasma technology. Results for four-times charged ions, are of interest for the consideration of radiative transfer through subphotospheric layers (Seaton, 1988), for modelling of some hot stars atmospheres as e.g. PG 1159 pre-white dwarfs with effective temperature 100 000 - 140 000 K (Werner and Heber, 1991), as well as for the fusion plasmas and laser-produced plasmas research. The development of soft X-ray lasers, where Stark broadening data are needed to calculate gain values, model radiation trapping and to consider photoresonant pumping schemes (see e.g. Fill and Schöning, 1994 and, Griem and Moreno, 1980), excited an additional interest for such results.

With the development of space-borne spectroscopy, with the possibility to obtain high resolution spectra in a wide weavelength range including X-rays, not detectable

from the Earth's surface, the interest for such results is increasing. For example an analysis of X-ray spectrum of some stars obtained with the high resolution space observatory CHANDRA show spectra which can be rich in emission lines in the soft X-ray region, including Si V lines.

The aim of this contribution is twofold. First of all we want to perform parallel determination of Si V Stark broadening parameters, by using oscillator strengths obtained by using SUPERSTRUCTURE code and the method of Bates and Damgaard (1949, see also Oertel and Shomo, 1968), in order to ascertain what error is introduced in the Stark broadening parameters due to uncerntainties of oscillator strength values and due to the use of Coulomb approximation. Secondly, our aim is to provide new semiclassical Stark broadening data for Si V, whose spectrum is poorly known and it is not possible to obtain a sufficiently complete set of experimental atomic energy levels needed for adequate semiclassical perturbation calculations.

2. RESULTS AND DISCUSSION

The energy levels of SiV are calculated using the general purpose atomic structure code SUPERSTRUCTURE developed at the University College in London and described in Eissner et al. (1974). All details of the calculation procedure of atomic energy levels will be given in Ben Nessib et al. (2003). By using atomic energy levels obtained by SUPERSTRUCTURE code, we have calculated also oscillator strengths with the help of the Coulomb approximation of Bates and Damgaard (1949, see also Oertel and Shomo, 1968).

Stark broadening parameter calculations have been performed within the semiclassical perturbation method (Sahal-Bréchot, 1969ab). A detailed description of this formalism with all inovations and optimizations is given in Sahal-Bréchot (1969ab), Fleurier et al (1974), Dimitrijević and Sahal-Bréchot (1996) and Dimitrijević (1996), and all details of calculation of Stark broadening parameters will be given in Ben Nessib et al. (2003).

The results for 16 Si V multiplets, for electron-impact broadening widths (FWHM - full width at half maximum) and shifts calculated with atomic energy levels obtained using the SUPERSTRUCTURE Code (using the Thomas Fermi potential model) and with oscillator strengths obtained using for the same code and with the Bates and Damgaard method (using the Coulomb approximation) will be published in Ben Nessib et al. (2003). As an example of obtained results, data for 5 multiplets are shown here in Table 1 for a perturber density of $10^{17}\mathrm{cm}^{-3}$ and temperatures from 50,000 up to 500,000 K. Such temperature interval is of interest for modelling and analysis of X wavelength range spectra as spectra obtained by CHANDRA, modelling of some hot stars (e.g. PG 1195 type) atmospheres, subphotospheric layers, soft X ray lasers and laser produced plasma research. Higher temperatures are of interest for fusion plasma research as well as for stellar interiors considerations. We also specify a parameter C (Dimitrijević and Sahal-Bréchot, 1984), which gives an estimate for the maximum perturber density for which the line may be treated as isolated, when it is divided by the corresponding full width at half maximum. For each value given in Table 1 the collision volume (V) multiplied by the perturber density (N) is much less than one and the impact approximation is valid (Sahal-Bréchot, 1969ab).

If we compare results for Stark widths obtained with oscillator strengths calculated with SUPERSTRUCTURE (W_S) and by using Bates and Damgaard Coulomb

Table 1: Electron-impact broadening line widths (FWHM - full width at half maximum) and shifts for Si V calculated with atomic energy levels obtained with SUPERSTRUCTURE code and with oscillator strengths obtained with SUPERSTRUCTURE code (W_S and S_S) and with the Coulomb approximation of Bates and Damgaard (1949)(W_{BD} and S_{BD}). The results bear on perturber densities of 10^{17}cm^{-3} and temperatures from 50,000 up to 500,000 K. Transitions and averaged wavelengths for the multiplet (in $\AA$) are also given. By dividing C by the corresponding full width at half maximum (Dimitrijević and Sahal-Bréchot 1984), we obtain an estimate for the maximum perturber density for which the line may be treated as isolated and tabulated data may be used.

TRANSITION	T(K)	$W_S(A)$	$S_S(A)$	$W_{BD}(A)$	$S_{BD}(A)$
Si V 2P-3S	50000.	0.257E-04	0.543E-06	0.309E-04	0.228E-06
120.4 A	100000.	0.181E-04	0.137E-05	0.211E-04	0.164E-05
C= 0.11E+19	150000.	0.149E-04	0.144E-05	0.172E-04	0.181E-05
	200000.	0.132E-04	0.153E-05	0.153E-04	0.191E-05
	300000.	0.112E-04	0.168E-05	0.130E-04	0.210E-05
	500000.	0.930E-05	0.166E-05	0.108E-04	0.206E-05
Si V 2P-3D	50000.	0.384E-04	-0.244E-06	0.425E-04	-0.709E-06
98.3 A	100000.	0.275E-04	0.253E-06	0.302E-04	0.184E-06
C= 0.54E+18	150000.	0.228E-04	0.367E-06	0.251E-04	0.394E-06
	200000.	0.201E-04	0.268E-06	0.222E-04	0.252E-06
	300000.	0.170E-04	0.323E-06	0.188E-04	0.312E-06
	500000.	0.141E-04	0.425E-06	0.157E-04	0.446E-06
Si V 3S-3P	50000.	0.847E-02	-0.779E-04	0.926E-02	-0.945E-04
1308.0 A	100000.	0.605E-02	-0.107E-03	0.662E-02	-0.132E-03
C= 0.13E+21	150000.	0.503E-02	-0.961E-04	0.551E-02	-0.117E-03
	200000.	0.444E-02	-0.111E-03	0.487E-02	-0.135E-03
	300000.	0.377E-02	-0.120E-03	0.416E-02	-0.146E-03
	500000.	0.313E-02	-0.109E-03	0.347E-02	-0.132E-03
Si V 3S-3P	50000.	0.855E-02	-0.366E-04	0.962E-02	-0.976E-04
1333.2 A	100000.	0.611E-02	-0.546E-04	0.688E-02	-0.137E-03
C= 0.13E+21	150000.	0.507E-02	-0.480E-04	0.572E-02	-0.124E-03
	200000.	0.447E-02	-0.582E-04	0.507E-02	-0.142E-03
	300000.	0.379E-02	-0.593E-04	0.432E-02	-0.152E-03
	500000.	0.314E-02	-0.509E-04	0.361E-02	-0.139E-03
Si V 3S-3P	50000.	0.409E-02	-0.608E-04	0.368E-02	0.116E-04
759.7 A	100000.	0.294E-02	-0.841E-04	0.266E-02	-0.439E-05
C= 0.32E+20	150000.	0.246E-02	-0.763E-04	0.223E-02	0.319E-05
	200000.	0.218E-02	-0.782E-04	0.198E-02	0.936E-05
	300000.	0.186E-02	-0.889E-04	0.170E-02	0.486E-05
	500000.	0.155E-02	-0.888E-04	0.143E-02	0.359E-06

approximation (W_{BD}), the average ratio of W_{BD} and W_S is 1.09 for T = 50 000 K and 1.10 for 500 000 K, confirming the adequacy of Coulomb approximation for Stark broadening calculations in the case of ions as Si V. For shifts disagreements are larger but one should have in view that shifts obtained here are typically 2-3 orders of magnitude smaller than widths. Namely, unlike widths where all important contributions are with a positive sign, for shifts we have in the present case cancellations of important contributions with different signs so that the final accuracy, usually estimated at 20-30 per cent of the width value, is in present case bad.

In conclusion, we see that using the SUPERSTRUCTURE code, one obtains simultaneously a set of energy levels and oscillators strengths, enabling an *ab initio* calculation of Stark broadening parameters. It is suitable particularly for multicharged ions when other theoretical and experimental atomic data are scarse. This work also verifies the use of the Coulomb approximation for oscillator strengths calculations in the Stark broadening calculations for multicharged ions like Si V.

Acknowledgements: This work is a part of the project GA-1195 "Influence of collisional processes on astrophysical plasma lineshapes", supported by Ministry of Science, Technologies and Development of Serbia.

References

Bates, D.R., Damgaard, A.: 1949, *Phil. Trans. Roy. Soc. London A*, **242**, 101.
Ben Nessib, N., Dimitrijević, M.S., Sahal-Bréchot, S.: 2003, *Physica Scripta*, submitted.
Dimitrijević, M.S.: 1996, *Zh. Prikl. Spektrosk.*, **63**, 810.
Dimitrijević, M.S., Sahal−Bréchot, S.: 1984, *J. Quant. Spectrosc. Radiative Transfer*, **31**, 301.
Dimitrijević, M.S., Sahal-Bréchot, S.: 1996, *Physica Scripta*, **54**, 50.
Eissner, W., Jones, M., Nussbaumer, H.: 1974, *Computer Phys. Commun.*, **8**, 270.
Fill, E.E., Schöning, T.: 1994, *J. Appl. Phys.*, **76**, 1423.
Fleurier, C., Sahal-Bréchot, S., Chapelle, J.: 1977, *J. Quant. Spectrosc. Radiative Transfer*, **17**, 595.
Griem, H.R., Moreno, J.C.: 1980, in: *X-Ray Lasers*, ed. G. Tallents, Institute of Physics, Bristol, 301.
Oertel, G.K., Shomo, L.P.: 1968, *Astrophys. J. Suppl. Ser.*, **16**, 175.
Sahal−Bréchot, S.: 1969a, *Astron. Astrophys.*, **1**, 91.
Sahal−Bréchot, S.: 1969b, *Astron. Astrophys.*, **2**, 322.
Seaton, M.J.: 1988, *J. Phys. B*, **21**, 3033.
Werner, K., Heber, U.: 1991, *Astron. Astrophys.*, **247**, 476.

Publ. Astron. Obs. Belgrade No. 76 (2003), 171 - 174 *Contributed paper*

TWO-COMPONENT MODEL FOR III ZW 2 BROAD LINE REGION

E. BON[1], N. STANIĆ[1], D. ILIĆ[2], A. KUBICELA[1],
E.G. MEDIAVILLA[3], L.Č. POPOVIĆ[4]

[1] *Astronomical Observatory, Volgina 7, 11160 Belgrade, Serbia*
E–mail: ebon@aob.aob.bg.ac.yu

[2] *University of Belgrade, Department of Astronomy, Serbia*
E–mail: dilic@matf.bg.ac.yu

[3] *Instituto De Astrofisica De Canarias, La Palma, Tenerife, Spain*
E–mail: egm@iac.es

Abstract. We have modelled the central emitting broad line region (BLR) of the III Zw2 using the H_α H_β Ly_α and Mg II (2798) broad lines. We proposed that two-component model, consisting of inner Keplerian relativistic disk and an outer emitting structure that surrounds the disk, can explain the shape of III Zw 2 Broad Lines

1. INTRODUCTION

According to Arp (1968) and Zwicky (1971) the active galaxy III Zw 2 (Mrk 1501) appears to be essentially stellar-like, with faint wisps extending towards the northwest. The broad emission lines of this object, suggest that this is a type 1 Seyfert galaxy or a quasar (Arp, 1968; Sargent, 1970; Osterbrock, 1977). Studies of III Zw 2 have been also done by other authors (Osterbrock, 1977; Kaastra and Korte, 1988; Corbin and Borson, 1996; and Crenshaw et al., 1999).

There have been some suggestions of the presence of a disk in III Zw 2 (Kaastra and Korte, 1988; Corbin and Borson, 1996; Shimura and Takahara, 1995; Rokaki and Boison, 1999.)

Here we studied the spectral line shapes of H_α, H_β, Ly_α and Mg II (2798) of III Zw 2 in order to identify features in emission lines that might be associated with the emission from a rotating disk.

2. SELECTION OF DATA AND METHOD OF ANALYSIS

We used spectra taken from three sources: (i) 35 spectra of Hβ line (wavelength interval 4750-5900 Å) observed at the Crimean Astrophysical Observatory (CrAO) by K. K.Chuvaev with the 2.6 m Shain telescope, during the period of 1972-1990 (HJD 2441361 till 2448153); (ii) spectra taken with HST (Faint Object Spectrograph - FOS) in 1992 which include the Lyα and MgIIλ2798 lines, and (iii) 3 spectra taken in 1998 with the Isaac Newton Telescope (INT) at La Palma Observatory including the Hα and Hβ lines.

Standard reduction procedures including flat-fielding, wavelength calibration, spectral response, and sky subtraction were performed with the help of the IRAF software package (see Popovic et al., 2003).

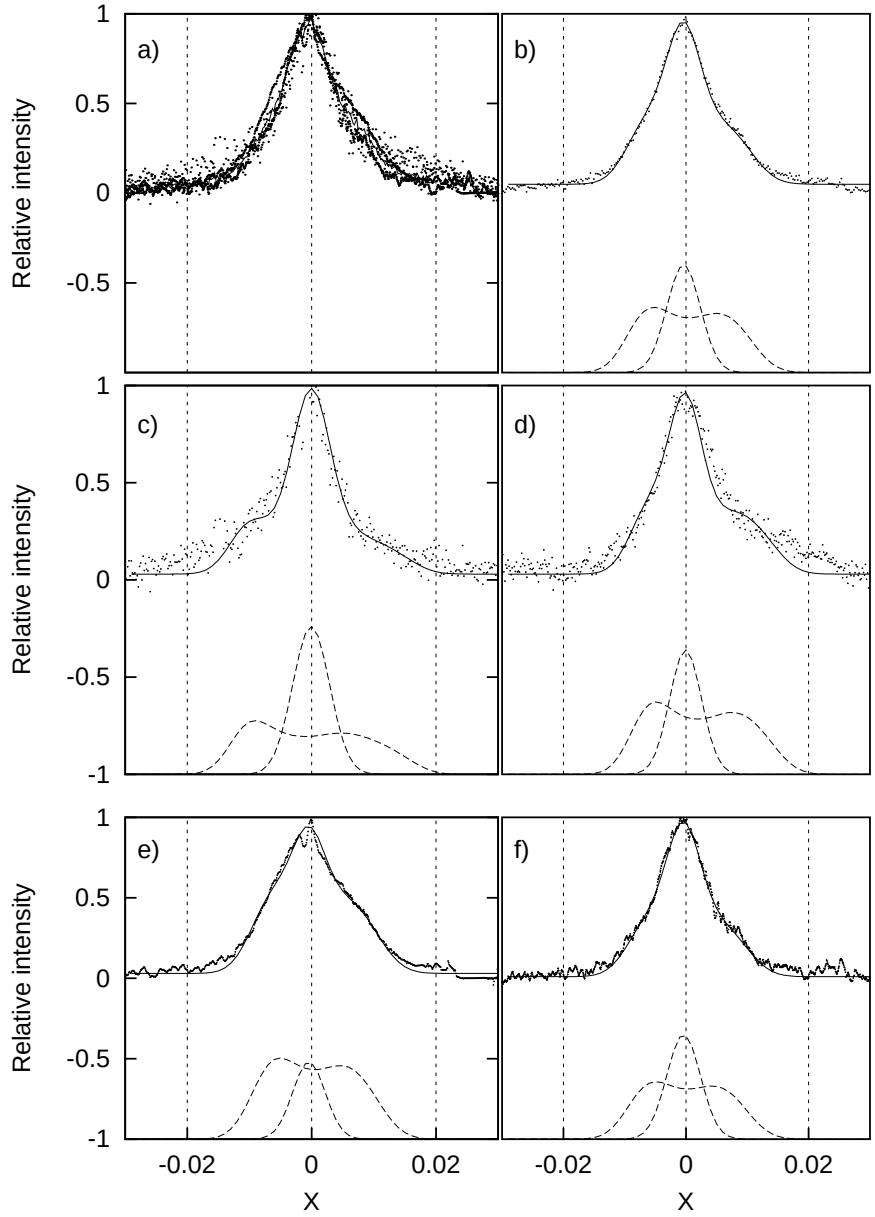

Fig. 1: Observed lines of III Zw 2 (dots), fitted with the disk model (double-peaked) and one Gaussian (dashed lines at the bottom); a) the comparison of all line profiles (dashed lines) with an averaged one (solid line); b) fits of the averaged line profile. Panels c,d,e,f represent fit of Lyα, Mg II, Hβ and Hα lines, respectively. The value of X is $(\lambda - \lambda_0)/\lambda_0$.

The red-shift of III Zw 2 was taken to be z=0.0898 (Véron-Cetty and Véron, 2000).

3. RESULTS

We fitted these line profiles with a disk model (Chen and Halpern, 1989, Chen et al., 1989) plus one Gaussian component which represents the region which surrounds the disk. For the disk we use the Keplerian relativistic model of Chen and Halpern (1989). The emissivity of the disk as a function of radius, R, is given as $\epsilon = \epsilon_0 R^{-p}$, where we suppose that the power index is $p = 3$, considering that the illumination is due to an extended source from the center of the disk and that the radiation is isotropic, Also, we express the disk dimension in gravitational radii ($R_g = GM/c^2$, where G is the gravitational constant, M is the mass of the central black hole, and c is the velocity of light). The local broadening (σ) and shift ($z_{\rm Disk}$) within the disk have been taken into account (Chen and Halpern, 1989).

All spectra were first 'cleaned' before this analysis by subtracting the components obtained from the Gaussian analysis that were found to originate from the other regions (narrow lines) or other elements (Fe II, OIII, N V). Also, the absorption lines were subtracted. After this, the features associated with the disk were visible not only in the asymmetrical wings of Mg II but also in the red and blue shoulders of the Lyα and Hα as well as in the triangular shape and the red shoulder of Hβ (see Fig. 1). To compare the line profiles we present in Fig. 1a the intensities normalized to the peak ones *vs.* $X = (\lambda - \lambda_0)/\lambda_0$. The considered lines have similar line shapes after this operation.

The results of the fit presented in Fig. 1b-f and Table 1 are the following:

(i)There is a very good consistency among the z and W parameters of the broad components representing the region surrounding the disk.

(ii) Red-shifts for the disk corresponding to Lyα, Hα, Hβ, and MgII are consistent. The average z for these four disk lines appears to be slightly blue-shifted (by about 600 km/s) with respect to the systemic one.

(iii) The inner radius of the Lyα emitting disk is clearly smaller than the others. Hα and Hβ exhibit a very good coincidence of the inner radii but the inner edge of the MgII emission ring seems to be closer to the disk center although this point should be viewed with caution.

4. CONCLUSIONS

The main conclusion which can be drawn from the present analysis of the Hα, Hβ, Lyα and MgIIλ2798 is that these lines mainly exhibit two Gaussian components that were red-shifted and blue-shifted to the central one. It has led us to the conclusion that this emission could be explained with a two-component model of emitting disk plus a surrounding region (see Popović et al., 2003). The disk emission (see van Groningen, 1983; Kaastra and Korte, 1988; Chen and Halpern, 1989; Rokaki and Boisson, 1999) can describe the line wings, and the core of the lines can be represented by emission of a region which surrounds the disk.

After fitting the III Zw2 Lyα, MgII, Hβ, and H$_\alpha$ lines we found that the two-component model can describe the shape of the broad lines, and that emission of a disc is present in these lines. The same two-component model (Keplerian relativistic

Table 1: The parameters of disk: z_{disk} is the shift and σ is the broadening term of Gaussian from disk indicating the random velocity in the disk, R_{inn} are the inner radii, R_{out} are the outer radii. The z_G and W_G represent the parameters of the Gaussian component. $< AV >$ is an averaged profile (see Fig. 1b). F_D/F_G represents the ratio of the relative disk and Gaussian fluxes.

Line	z_{disk}	σ (km/s)	R_{inn} (R_g)	R_{out} (R_g)	z_G	W_G (km/s)	F_D/F_G
Lyα	-800	850	200	900	-20	1280	1.11
Mg IIλ2789	-350	920	300	1000	-30	1100	1.86
Hβ	-600	920	400	1300	-130	1100	3.14
Hα	-600	850	450	1300	-120	1170	1.52
$< AV >$	-600	890	400	1200	-120	1170	1.72

disk + a surrounding emission region) can consistently fit the 4 BELs considered here (Lyα, MgII, Hβ, and Hα).

From the fitted disk parameters and the mass of the central object (Vestergaard, 2002) we can estimate that the Lyα disk has inner and outer radii of around 0.0018 and 0.01 pc, respectively. However, the inner radius is greater for the Mg II ($\sim$ 0.0027 pc) and for the Hα and Hβ lines ($\sim$ 0.0038 pc). This indicates a radial stratification in the disk. The relatively broad component present in the blue wings of the narrow [OIII] lines is another indication of stratification (see Popović et al., 2003) and perhaps could indicate a connection between the outer BLR and the NLR.

References

Arp, H.: 1968, *Astrophys. J.*, **152**, 1101.

Chen, K., Halpern, J.P., Filippenko, A.V.: 1989, *Astrophys. J.*, **339**, 742.

Chen, K., Halpern, J.P.: 1989, *Astrophys. J.*, **344**, 115.

Corbin, M.C., Boroson, T.A.: 1996, *Astrophys. J.*, **107**, 69.

Crenshaw, D.M., Kraemer, B.S., Boggess, A., Maran, S.P., Mushotzky, R.F., Wu, C.-C.: 1999, *Astrophys. J.*, **516**, 750.

Kaastra, J.S., de Korte, P.A.J.: 1988, *Astron. Astrophys.*, **198**, 16.

Osterbrock, D.E.: 1977, *Astrophys. J.*, **215**, 733.

Popović, L.Č., Mediavlilla, E.G., Kubičela, A., Jovanović, P.: 2002, *Astron. Astrophys.*, **390**, 473.

Popović, L.Č., Mediavilla, E.G., Bon, E., Stanić, N., Kubičela, A.: 2003, *Astrophys. J.*, submited.

Rokaki, E., Boisson, C.: 1999, *Mon. Not. Roy. Astronom. Soc.*, **307**, 41.

Sargent, W.L.W.: 1970, *Astrophys. J.*, **160**, 405.

Shimura, T., Takahara, F.: 1995,*Astrophys. J.* , **440**, 610.

van Groningen, E.: 1983,*Astron. Astrophys.*, **126**, 363.

Véron-Cetty, M.-P., Véron, P.: 2000, *A Catalogue of Quasars and Active Galactic Nuclei*, Sci. Report 19.

Vestergaard, M.: 2002, *Astrophys. J.*, **571**, 733.

Zwicky, F.: 1971, Lists of Compact Galaxies and Compact Parts of Galaxies (Pasadena: California Institute of Tehnology).

Publ. Astron. Obs. Belgrade No. 76 (2003), 175-178 *Contributed paper*

THE COMPLEX CORONAL STRUCTURE OF THE Oe STAR HD 175754

E. DANEZIS, A. ANTONIOU, E. LYRATZI, E. THEODOSSIOU,
M. STATHOPOULOU, D. NIKOLAIDIS, C. DRAKOPOULOS,
A. SOULIKIAS, M. KOUTROUMANOU

University of Athens, School of Physics, Department of Astrophysics, Astronomy and Mechanics, Panepistimiopolis, Zografos 157 84, Athens – Greece
E-mail: edanezis@cc.uoa.gr

Abstract. We present the study of the HD 175754 coronal regions, based on the model proposed by Danezis et al. (2003). By this model, we can calculate, for all the independent density regions, the apparent expansion/contraction velocities (V_{exp}), the apparent rotation velocities (V_{rot}), as well as the values of ξ, which is an expression of the optical depth.

HD 175754 is a luminous supergiant star of spectral type OeIIf with effective temperature 31800 ±1100 K (Morossi and Crivellari, 1980). Costero and Stalio (1981) and Costero et al (1981) studied the NV, SiIV and CIV profiles of this star and compared them with the profiles of similar type stars. They found individuality, which implies different structures and dynamics of the atmospheric layers above the photosphere. Carrasco et al. (1981) reported only small changes in the UV resonance line profiles. They interpreted them in terms of variations in dynamics and density/ionization structure of the stellar wind. Lamers et al (1982) noted the possibility of the presence of satellite components superimposed on the wide P Cygni profiles of the UV resonance lines. Finally, Franco et al (1983) studied the P Cygni profiles of the above resonance lines of HD 175754 observed at different epochs and they reported variability in the secondary satellite component. They proposed two different mechanisms for the explanation of the variability, namely, a thermal mechanism in a hot region at $Tc=2\times10^5$ K which produces the principal stationary component and a mechanism which gives rise to the secondary component by ionization of cooler high velocity stellar material from X-rays coming from inner coronal region.

In this paper we present the study of the HD 175754 coronal regions, based on the model proposed by Danezis et al. (2003), also presented at the 4th Serbian Conference on Spectral Lines Shapes (IV SCSLS) 2003, Arandjelovac, Serbia, under the title "On modelling SACs regions in early type atmospheres". This model presupposes that the regions, where these spectral lines are formed, are not continuous but consist of a number of independent absorbing density layers of matter, followed by an emission region and an external general absorption region. By this model, we can calculate, for all the independent density regions, the apparent expansion/contraction velocities (V_{exp}), the apparent rotation velocities (V_{rot}), as well as the values of ξ, which is an expression of the optical depth.

2. SPECTRAL ANALYSIS AND CONCLUSIONS

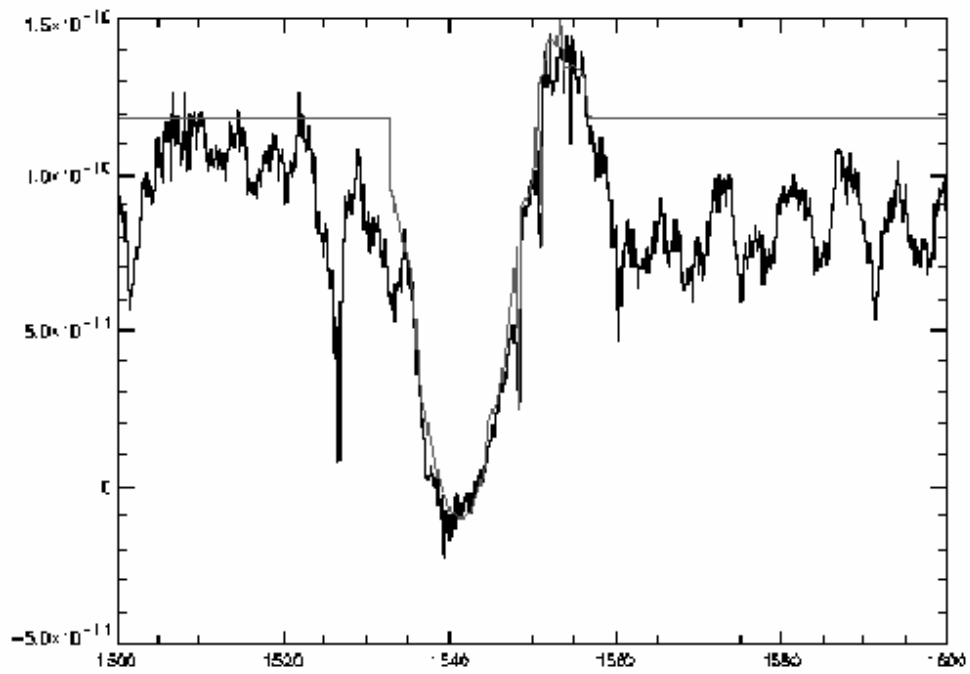

Fig. 1: The CIV resonance lines fittings of HD175754 (SWP 06269). The heavy line presents the observed spectral line profile and the light one the model's fit. The differences between the observed spectrum and its fit are sometimes hard to see, as we have accomplished the best fit.

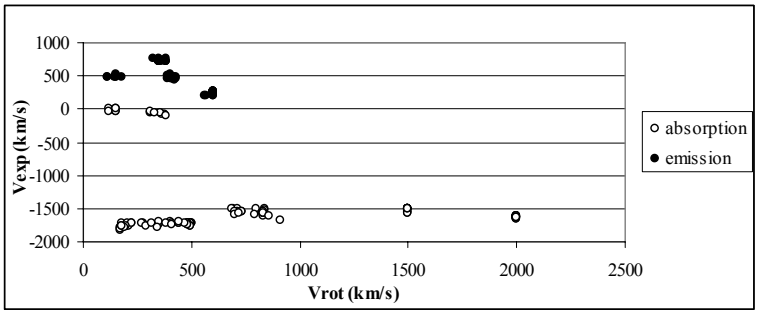

Diagram 1: Expansion/contraction velocities of the absorption and the emission components as a function of the rotation velocities. We can notice that the emission regions present only positive values of the apparent expansion/contraction velocities, while the respective apparent rotation velocities present values up to 600 km/s. For the absorption regions, we can discern two levels of negative expansion velocities. The first, about 0 km/s, present rotation velocities up to 400 km/s and the second, about -1500 km/s, presents rotation velocities between 100 and 2000 km/s.

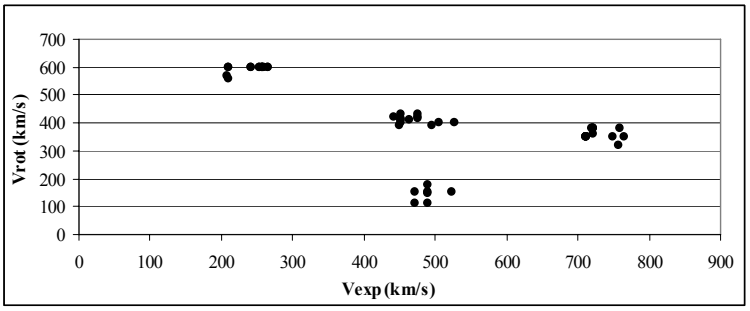

Diagram 2: Rotation velocities for the emission component as a function of the expansion/contraction velocities. We can notice that for small values of V_{exp} (about 250 km/s), the V_{rot} presents great values (about 600 km/s). For greater values of V_{exp} (about 500 km/s), we can discern two levels of V_{rot}, about 150 and 400 km/s, respectively. Finally, for V_{exp} about 750 km/s, the V_{rot} lies at 350 km/s.

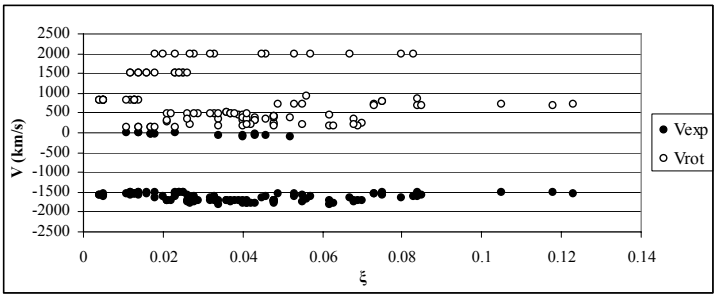

Diagram 3: Expansion/contraction and rotation velocities of all the SACs as a function of the ξ values. We can notice two levels of V_{exp} and V_{rot}. The first level of V_{exp} (about -1500 km/s) is observed for all values of ξ between 0 and 0.13. The second one is observed only for ξ values between 0 and 0.05. The V_{rot} values present a similar behavior. The first level (about 500 km/s) is presented for all ξ values, while the second one (about 2000 km/s) is presented only for ξ values between 0 and 0.08.

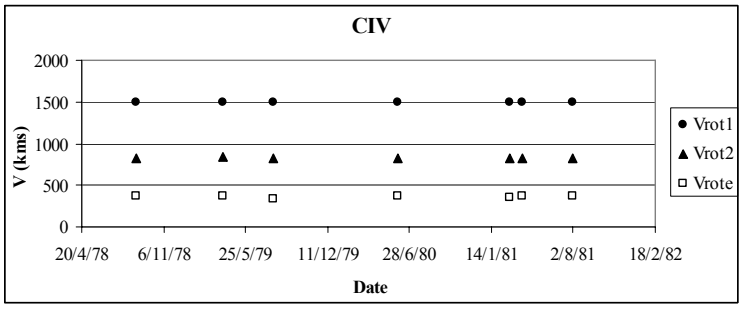

Diagram 4: Evolution with time of the apparent rotation velocities of the CIV absorption (Vrot1, Vrot2) and emission (Vrote) components. The V_{rot} for the three detected density regions remains constant with time.

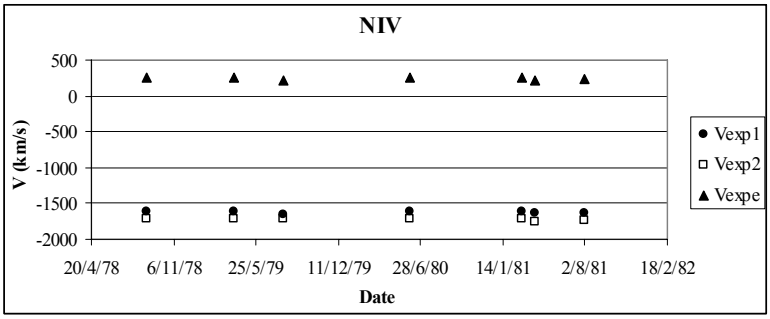

Diagram 5: Evolution with time of the expansion/contraction velocities of the NIV absorption (Vexp1, Vexp2) and emission (Vexpe) components. The V_{exp} for the three detected density regions remains constant with time.

Acknowledgements. This research project is being effected at the University of Athens, Department of Astrophysics - Astronomy and Mechanics, under the financial support of the Special Account for Research Grants, for which we thank very much.

References

Carrasco, I., Costero, R., Stalio, R.: 1981, *Astron. Astrophys.*, **100**, 183.

Costero, R., Stalio, R.: 1981, *Rev. Mexicana Astron. Astrophys.*, **6**, 237.

Costero, R., Doazan, V., Stalio, R., Thomas, R. N.: 1981, in C. Chiosi and R. Stalio (eds), "*Effects of Mass Loss an Stellar Evolution*", IAU Coll. 59. p. 31.

Danezis, E., Nikolaidis, D., Lyratzi, V., Stathopoulou, M., Theodossiou, E., Kosionidis, A., Drakopoulos, C., Christou G., Koutsouris, P.: 2003, *Astrophys. J. Suppl. Series*, **284**, Issue 4 (in press).

Franco, M.L., Kontizas, E., Kontizas, M., Stalio, R.: 1983, *Astron. Astrophys.*, **122**, 9.

Lamers, H.J.G.L.M., Gathier, R., Snow, T.P.: 1982, *Astrophys. J.*, **258**, 186.

Morossi, C., Crivellari, L.: 1980, *Astron. Astrophys. Suppl. Series*, **41**, 299.

Publ. Astron. Obs. Belgrade No. 76 (2003), 179-183 *Contributed paper*

ON MODELLING SACs REGIONS IN EARLY TYPE ATMOSPHERES

E. DANEZIS, E. LYRATZI, D. NIKOLAIDIS, M. STATHOPOULOU,
E. THEODOSSIOU, C. DRAKOPOULOS, A. SOULIKIAS, A. ANTONIOU

University of Athens, School of Physics, Department of Astrophysics, Astronomy and Mechanics, Panepistimiopolis, Zografos 157 84 Athens – Greece
E-mail: edanezis@cc.uoa.gr

Abstract. We test the ideas that probably DACs are not unknown absorption spectral lines, but spectral lines (satellite absorption components) of the same ion and the same wavelength as a main spectral line, shifted at different $\Delta\lambda$. In addition, DACs are not always discrete absorption spectral lines, but in most cases lines that are blended among themselves as well as with the main spectral line. This means that when we deal with a significant spectral line, which is accompanied by satellite absorption components, we should not regard them as independent spectral lines, but as a unified formation which must be dealt with as one spectral line splited into a series of components. For these reasons we prefer to name them Satellite Absorption Components (SACs) and not Discrete Absorption Components (DACs).

1. INTRODUCTION

Peton (1974) was the first to point out that, in the visual spectrum of the double system AX Mon (HD 45910), there existed a secondary component of the absorption line FeII λ 4233A, which, depending on the phase, appeared in the violet or in the red side of the main spectral line. For this reason the secondary component was named "satellite component".

Mullan (1984a,b, 1986) suggested that the satellite components may result from "corotating interaction regions" (CIRs), which may form in stars' winds depending on asymmetries in the wind velocity or density.

Danezis (1984, 1986) and Danezis *et al.* (1991) studied the UV spectra of AX Mon and noted that the absorption lines of many ionization potential ions, not only of those presenting P Cygni profile, are accompanied by two strong absorption components. This means that the regions where these spectral lines are created are not continuous, but they are formed by a number of independent density layers of matter.

The existence of satellite components in the UV spectrum of AX Mon has been detected by Sahade *et al.* (1984) and Sahade and Brandi (1985). Also, Hutsemekers (1985) noticed the same phenomenon in the UV spectrum of another Be star, HD 50138.

Bates and Halliwell (1986), naming the satellite components as "discrete absorption components" (DACs), constructed a model of ejection of gas parcels from above the star's photosphere, accelerated by radiation pressure. In order to describe the DACs, many

suggestions about the properties of the winds have been made, which propose that the DACs are due to disturbances in the wind such as material that forms spiral streams as a result of the star's rotation (Mullan 1984a, Prinja and Howarth 1988) or to mass ejections constructing "shells", "puffs" or gas "parcels" (Henrichs 1984, Underhill and Fahey 1984, Bates and Halliwell 1986, Grady *et al.* 1987, Lamers *et al.* 1988).

Laskarides *et al.* (1992a) observed one more satellite component in the spectral lines of ions with low ionization potential in the UV spectrum of AX Mon, this in the red side of the main lines. This fact indicates contraction of the outer layers of the gaseous envelope.

Waldron *et al.* (1992) tried to give an explanation to the large-scale ejection phenomena by modelling the full time-dependent hydrodynamic response of a stellar wind to a spherically symmetric propagating density shell, which suggests that a substantial amount of material must be present in front of the stellar disk to reproduce the observations. They concluded that DACs' behaviour in UV P Cygni line profiles was the result of the density shells (Lamers *et al.* 1978, Henrichs *et al.* 1980, 1983).

Cranmer and Owocki (1996) suggested that the DACs originate from "moderate size wind structures such as spatially localized clouds, streams or blobs".

Rivinius *et al.* (1997) proposed that when the "blobs" are in front of the stellar disk they give rise to the DACs appearance, otherwise they only contribute to some extra radiation emitted in all directions (Lamers 1994).

Markova (2000) concluded that the recurrence of DACs is hardly related to the stellar rotation and that the DACs are not due to single mass-conserving features, such as outward moving blobs, but that they may originate from outward moving, large-scale, high-density perturbations, which possibly originate from the photosphere, but develop in the outer wind through which wind material flows. These perturbations may be spherically symmetric density shells or curved structures like kinks.

Danezis *et al.* (1991, 1995, 1998, 2000a,b,c, 2001, 2002,a,b), Laskarides *et al.* (1992a, 1992b), Lyratzi *et al.* (2001) apart from their study of the UV spectrum of Be stars, where they found satellite components, have also studied the UV spectrum of several Oe stars and detected satellite components, not only for the spectral lines of low ionization potential, but also for the resonance lines of NV, CIV, SiIV and the spectral line NIV.

2. THE MAIN IDEA OF OUR RESEARCH

In this paper we test the ideas proposed by Danezis (1984, 1986) and Danezis *et al.* (1991). In these papers they proposed that probably DACs are not unknown absorption spectral lines, but spectral lines (satellite absorption components) of the same ion and the same wavelength as a main spectral line, shifted at different $\Delta\lambda$. In addition, DACs are not always discrete absorption spectral lines, but in most cases lines that are blended among themselves as well as with the main spectral line. In such a case they are not observable, but we can detect them through the analysis of our model (Danezis *et al.* 2002a, 2003). This means that when we deal with a significant spectral line, which is accompanied by satellite absorption components, we should not regard them as independent spectral lines, but as a unified formation which must be dealt with as one spectral line splited into a series of components. For these reasons we prefer to name them Satellite Absorption Components (SACs) and not Discrete Absorption Components (DACs). In the case of absorption spectral lines presenting SACs, as well as a P Cygni profile, the emission spectral line is created in an independent emitting density region.

3. THE MODEL: MATHEMATICAL EXPRESSION

Considering an area of gas consisting of i independent absorbing shells followed by a shell that both absorbs and emits and an outer shell of general absorption, we resort to the function:

$$I_\lambda = \left[I_{\lambda 0} \prod_i \exp\{-L_i \xi_i\} + S_{\lambda e}\left(1 - \exp\{-L_e \xi_e\}\right) \right] \exp\{-L_g \xi_g\} \quad (1)$$

where: $\mathbf{I_{\lambda 0}}$**:** the initial radiation intensity,

$\mathbf{L_i}$, $\mathbf{L_e}$, $\mathbf{L_g}$: are the distribution functions of $k_{\lambda i}$, $k_{\lambda e}$, $k_{\lambda g}$ respectively. Each L depends on the values of the apparent rotational velocity as well as of the radial expansion or contraction velocity of the density shell, which forms the spectral line

$\xi = \int_0^s \Omega \rho ds$ is an expression of the optical depth τ, where Ω: an expression of k_λ and has the same units as k_λ,

$\mathbf{S_{\lambda e}}$: the source function, which, at the moment when the spectrum is taken, is constant and

$L = \sqrt{1 - \cos^2 \theta_0}$ if $\cos\theta_0 < 1$ and $L = 0$ if $\cos\theta_0 \geq 1$,

where $\cos\theta_0 = \dfrac{-\lambda_0 + \sqrt{\lambda_0^2 + 4\Delta\lambda^2}}{2\Delta\lambda z_0}$, where $2\theta_0$ is the angular width of the equatorial disk of matter, λ_0 is the wavelength of the center of the spectral line and $\lambda_0 = \lambda_{lab} + \Delta\lambda_{\exp}$, with λ_{lab} being the laboratory wavelength of the spectral line produced by a particular ion and $\Delta\lambda_{\exp}$ the radial Doppler shift and $\dfrac{\Delta\lambda_{\exp}}{\lambda_{lab}} = \dfrac{V_{\exp}}{c}$.

$z_0 = \dfrac{V_{rot}}{c}$, where V_{rot} is the apparent rotation velocity of the i density shell of matter and $\Delta\lambda = |\lambda_i - \lambda_0|$, where the values of λ_i are taken in the wavelength range we want to reproduce.

As we can understand from the above, the spectral line's profile, which is formed by the i density shell of matter, must be accurately reproduced by the function $e^{-L_i \xi_i}$ by applying the appropriate values of V_{roti}, V_{expi} and ξ_i.

Acknowledgements. Dr. Danezis E., Dr. Theodossiou E. and Lyratzi E. would like to thank Dr. M.S. Dimitrijević, former Director of the Astronomical Observatory of Belgrade for his help and comments. This research project is being effected at the University of Athens, Department of Astrophysics - Astronomy and Mechanics, under the financial support of the Special Account for Research Grants, which we thank very much.

References

Bates, B., Halliwell, D.R.: 1986, *Mon. Not. Roy. Astron. Soc.*, **223**, 673.
Cranmer, S.R., Owocki, S.P.: 1996, *Astrophys. J.*, **462**, 469.
Danezis, E.: 1984, *The nature of Be stars, PhD Thesis*, University of Athens.

Danezis, E.: 1986, *IAU, Colloq. No 92, Physics of Be Stars*, Cambridge University Press.
Danezis, E., Theodossiou, E., Laskarides, P.G.: 1991, *Astrophys. J. Suppl. Series*, **179**, 111.
Danezis, E., Theodossiou, E., Laskarides, P.G.: 1995, A first approach to the shell structure of Be Binary stars, *2nd Hellenic Astronomical Conference*, 29 July, Thessaloniki, Greece.
Danezis, E., Nikolaidis, D., Theodossiou, E., Stathopoulou, M., Kosionidis, A.: 1998, Satellite spectral components and moving shells in the atmospheres of Early Type Stars - The example of HD 175754. *Proceedings of the 65th Czech and the 7th European Joint Conference, JENAM '98*, Prague, Czech Republic, September.
Danezis, E., Nikolaides, D., Theodossiou, E., Kosionidis, A., Stathopoulou, M., Lyratzi, E., Drakopoulos, C., Bourma, P.: 2000a, A simple model for the complex structure of moving atmospheric shells in Oe and Be stars. The example of HD 36861, some first conclusions. *JENAM 2000*, May 29-June 3, Moscow, Russia.
Danezis, E., Nikolaides, D., Theodossiou, E., Kosionidis, A., Stathopoulou, M., Lyratzi, E., Drakopoulos, C., Bourma, P.: 2000b, A simple model for the complex structure of moving atmospheric shells in Oe and Be stars. The example of HD 66811, some first conclusions. *JENAM 2000*, May 29-June 3, Moscow, Russia.
Danezis, E., Nikolaides, D., Theodossiou, E., Kosionidis, A., Stathopoulou, M., Lyratzi, E., Drakopoulos, C., Bourma, P.: 2000c, A simple model for the complex structure of moving atmospheric shells in Oe and Be stars. The example of HD 152408, some first conclusions. *JENAM 2000*, May 29-June 3, Moscow, Russia.
Danezis, E., Lyratzi, E., Theodossiou, E., Nikolaides, D., Stathopoulou, M., Kyriakopoulou, A., Christou, G., Drakopoulos, C.: 2001, Application of a new model of density layers of matter to the expanding gaseous envelope of the star HD 175754. *Proceedings of the 5th Hellenic Astronomical Society Conference* September 2001, Crete, Greece.
Danezis, E., Nikolaidis, D., Lyratzi, E., Stathopoulou, M., Theodossiou, E., Kosionidis, A., Drakopoulos, C., Christou, G., Koutsouris, P.: 2002a, A new model of density layers of matter in the expanding gaseous envelope of Oe and Be stars. *Proceedings of the IAU Symposium 210: Modeling of stellar atmospheres*, June 17 21, 2002, Uppsala, Sweden.
Danezis, E., Lyratzi, E., Nikolaidis, D., Theodossiou, E., Stathopoulou, M., Christou, G., Drakopoulos, C., Kosionidis, A., Soulikias, A.: 2002b, Applications of a new model of density layers of matter in the expanding gaseous envelope of Oe and Be stars. *Proceedings of the IAU Symposium 210: Modeling of stellar atmospheres*, June 17 21, 2002, Uppsala, Sweden.
Danezis, E., Nikolaidis, D., Lyratzi, V., Stathopoulou, M., Theodossiou, E., Kosionidis, A., Drakopoulos, C., Christou G., Koutsouris, P.: 2003, *Astrophys. J. Suppl. Series*, **284**, Issue 4 (in press).
Grady, C.A., Sonneborn, G., Chi-chao Wu, Henrichs, H.F.: 1987, *Astrophys. J. Suppl. Series*, **65**, 673.
Henrichs, H.F., Hammerschlag - Hensberge, G., Lamers, H.J.G.L.M.: 1980, in *Proc. 2nd European IUE Conf*. Tübingen, ed. B. Battrick and J. Mort (*ESA SP* – **157**) (Noordwijk: ESO), **4**, 147.
Henrichs, H.F., Hammerschlag - Hensberge, G., Howarth, I.D., Barr, P.: 1983, *Astrophys. J.*, **268**, 807.
Henrichs, H.F.: 1984, *Proc. 4th European IUE Conf.*, *ESA SSSP*-**218**, p.43, eds Rolfe, E., Battrick, B., Rome.
Hutsemekers, D.: 1985, *Astron. Astrophys. Suppl. Series*, **60**, 373.
Lamers, H.J.G.L.M., Snow, T.P.: 1978, *Astrophys. J.*, **219**, 504L.
Lamers, H.J.G.L.M., Snow, T.P., de Jager, C., Langerwerf, A.: 1988, *Astrophys. J.*, **325**, 342.
Lamers, H.J.G.L.M.: 1994, *Observational aspects of wind variability, Instability and Variability of Hot-Star Winds*, ed. Moffat A.F.J., Owocki S.P., Fullerton A.W., St.-Louis N., Kluwer, 41.
Laskarides, P.G., Danezis, E., Theodossiou, E.: 1992a, *Astrophys. J. Suppl. Series*, **179**, 13.
Laskarides, P.G., Danezis, E., Theodossiou, E.: 1992b, *Astrophys. J. Suppl. Series*, **183**, 67.
Lyratzi, E., Danezis, E., Nikolaides, D., Theodossiou, E., Stathopoulou, M. and Drakopoulos, C.: 2001, Application of a new model of density shells of matter to the expanding gaseous envelope of the star HD 45910 (AX Mon). *Proceedings of the 5th Hellenic Astronomical Society Conference* September 2001, Crete, Greece.

Markova, N.: 2000, *Astron. Astrophys. Suppl. Series*, **144**, 391.
Mulan, D.J.: 1984a, *Astrophys. J.*, **283**, 303.
Mulan, D.J.: 1984b, *Astrophys. J.*, **284**, 769.
Mulan, D.J.: 1986, *Astron. Astrophys.*, **165**, 157.
Peton, A.: 1974, *Astrophys. J. Suppl. Series*, **30**, 481.
Prinja, R.K., Howarth, I.D.: 1988, *Mon. Not. Roy. Astron. Soc.*, **233**, 123.
Rivinius, Th., Stahl, O., Wolf, B., Kaufer, A., Gäng, Th., Gummersbach, C.A., Jankovics, I., Kovács, J., Mandel, H., Peitz.J., Szeifert, Th., Lamers, H.J.G.L.M.: 1997, *Astron. Astrophys.*, **318**, 819.
Sahade, J., Brandi, E., Fontela, J.M.: 1984, *Astron. Astrophys. Suppl. Series*, **56**, 17.
Sahade, J., Brandi, E.: 1985, *Rev. Mexicana Astron. Astrophys.*, **10**, 229.
Underhill, A.B., Fahey, R.P.: 1984, *Astrophys. J.*, **280**, 712.
Waldron, W.L., Klein, L., Altner, B.: 1992, *ASP Conf. Series*, **22**, 181.

Publ. Astron. Obs. Belgrade No. 76 (2003), 185 - 189 *Contributed paper*

ON THE STARK BROADENING OF NEUTRAL GERMANIUM SPECTRAL LINES

MILAN S. DIMITRIJEVIĆ, PREDRAG JOVANOVIĆ, ZORAN SIMIĆ

Astronomical Observatory, Volgina 7, 11160 Belgrade, Serbia
E–mail: mdimitrijevic@aob.aob.bg.ac.yu
E–mail: pjovanovic@aob.aob.bg.ac.yu

Abstract. Stark broadening of the eleven transitions of neutral germanium within the $4p^2$ - 4p5s transition array has been analyzed within the frame of the semiclassical perturbation method. Obtained results have been compared with available experimental and theoretical data. The importance of the electron-impact broadening in the case of the 4226.562 Å line for A star atmospheres has been tested

1. INTRODUCTION

Stark broadening of germanium lines, has been discussed firstly in Minnhagen (1964), who considered correlation between observed wavelength shifts produced in electrodeless discharge tube and predicted Stark shifts in the spectrum of neutral germanium. Shifts in the wavelength of spectral lines in spark discharges have been investigated as well in the first experimental work on Ge I Stark broadening (Kondrat'eva, 1970). After these pioneer works, reliable data on Ge I spectral lines Stark broadening parameters have been obtained experimentally by Jones and Miller (1974) and Musiol et al. (1988). For Ge I $4p^2\ ^1S-5s^1S^o$ multiplet, Dimitrijević and Konjević (1983) performed semiclassical calculation within the frame of the theory developed by Griem et al. (1962) (see also Griem, 1974). Moreove, Lakićević (1983) estimated on the basis of regularities and systematic trends Stark broadening parameters for Ge I $4p^2\ ^3P-5s^3P^o$ multiplet. The estimates based on regularities and systematic trends, performed also Sarandaev et al. (2000) for Ge I $4p^2\ ^1S-5s^1P^o$ and $4p^2\ ^1S-5s^3P^o$ multiplets. Here, we will calculate within the semiclassical perturbation approach, Stark broadening parameters of 11 Ge I transitions within the $4s^24p^2$ - $4s^24p5s$ transition array, for conditions typical for astrophysical and laboratory plasmas. The obtained results will be compared with available experimental and theoretical values. Also, the importance of the electron-impact broadening for A type star atmospheres will be tested.

2. RESULTS AND DISCUSSION

Stark broadening parameters (the full line width at half maximum - W and the line shift -d) of neutral germanium, have been determined by using the semiclassical perturbation formalism (Sahal−Bréchot, 1969ab). The discussion of updatings and validity criteria, has been briefly reviewed e.g. in Dimitrijević (1996). All details of the determination of Stark broadening parameters will be published elsewhere (Dimitrijević et al. 2003) so that we note here only that the atomic energy levels needed for calculations have been taken from Sugar and Musgrove (1993).

Results for electron-, proton-, and Ar II-impact broadening parameters for 11 Ge I transitions for perturber density of 10^{16}cm^{-3} and temperatures from 2,500 K up to 50,000 K will be published in Dimitrijević et al. (2003), together with the complete comparison of available experimental and theoretical data and discussion.

In Table 1, our results are compared with experimental results of Jones and Miller (1974) and Musiol et al. (1988). With W_m, are denoted experimental full widths at half maximum in [Å], and with W_e and W_{GeII} our theoretical values for Stark widths due to electron- and Ge II-impacts, respectively. Namely, since ionization potentials of H, Ar and Ge are 13.595 eV, 15.755 eV and 7.88 eV respectively, the most appropriate way to estimate the influence of ion-impact broadening for considered experiments

Table 1: Comparison of our theoretical results for Stark broadening of Ge I lines with experimental results. With W_m, are denoted experimental full widths at half maximum in [Å], and with W_e and W_{GeII} our theoretical values for Stark widths due to electron- and Ge II-impacts, respectively. Accuracy is denoted as in Konjević et al. (1984) and Konjević and Wiese (1990), C means that error bars are within ±50% and D^+ that they are larger than ±50%. Under Ref., 1 is for Musiol et al. (1988) and 2. for Jones & Miller (1974).

Transition λ(Å)	T(K)	Ne 10^{17}cm^{-3}	W_m (Å)	W_e (Å)	W_{GeII} (Å)	Acc.	Ref.
$4p^2\ ^3P - 5s^3P^0$							
2754.59	12450	0.57	0.0509	0.0502	0.00644	C	1
2709.62	12450	0.57	0.0434	0.0490	0.00628	C	1
2651.57	12450	0.57	0.0358	0.0466	0.00596	C	1
2651.17	12450	0.57	0.0427	0.0517	0.00662	C	1
2592.53	12450	0.57	0.0452	0.0494	0.00633	C	1
$4p^2\ ^1S - 5s^3P^0$							
4685.83	11000	1	0.35	0.248	0.0339	C	2
$4p^2\ ^1D - 5s^3P^0$							
3124.82	12450	0.57	0.0628	0.0715	0.00928	C	1
$4p^2\ ^1D - 5s^1P^0$							
3039.07	12450	0.57	0.0622	0.0721	0.00924	C	1
$4p^2\ ^1S - 5s^1P^0$							
4226.56	11000	1	3.18	0.239	0.0318	C	2
	12450	0.57	0.0815	0.139	0.0185	D^+	1

is to compare electron-impact widths with widths due to impacts with ions of heavy electron donors like germanium. One can see that the ion contribution is around 13-14 per cent which is well within the estimated error bars of the semiclassical perturbation approach of ±30 per cent (Griem, 1974).

Jones and Miller (1974) determined experimentally Stark widths of Ge I $4p^2\ ^1S - 5s^1P^o$ 4685.83 Å and $4p^2\ ^1S - 5s^3P^o$ 4226.56 Å spectral lines by using gas-driven spectroscopic shock tube with hydrogen as a driver gas, and runs were with various filling pressure and different compositions of GeH_4, Ar and Ne. They used photographic technique and Konjević and Wiese (1990) in his critical analysis of experimental Stark broadening data stated that "self-absorption may have been an important factor for the 4226.56 Å line" in his experiment. In Konjević et al. (1984), the error bars of their results are critically estimated to be within ± 50% (accuracy denoted as C in their notation).

Musiol et al. (1988) determined experimentally Stark widths of 9 lines from Ge I $4p^2$-4p5s and $4p^2$-4p4d transition arrays by using wall-stabilized arc operated at atmospheric pressure with various mixtures of GeH_4 and Ar. In Konjević and Wiese (1990), the error bars of their results are critically estimated to be within ± 50% (accuracy denoted as C in their notation), except for 4226.56 Å line where accuracy is denoted as D^+ (error bars larger than ±50%).

Our results are in disagreement with experimental results of Jones and Miller (1974) for 4226.56 Å line. This result is in disagreement with other theoretical (Dimitrijević and Konjević, 1983; Sarandaev et al., 2000) and experimental (Musiol et al., 1988) results, and selfabsorption is indicated as a possible reason in Konjević and Wiese (1990). Ratio of experimental Stark width of Jones and Miller (1974) for 4685.83 Åline and our result is $W_m/W_e = 1.41$, what is within the estimated (Konjević et al., 1984) error bars of the experiment. Agreement of our values with experimental results of Musiol et al. (1988) is reasonable. The largest disagreement is for 4226.56 Å line, where $W_m/W_e = 0.59$, what is however within the estimated (Konjević et al., 1984) error bars of ±50 per cent. The agreement for other lines is considerably better. However, if we analyse experimental and theoretical widths within $4p^2\ ^3P$ - $5s^3P^o$ multiplet, one can notice that the largest difference of experimental values is for 2754.59 Å $4p^2\ ^3P_2$ - $5s^3P_1^o$ (W_m = 0.0509 Å) and 2651.57 Å $4p^2\ ^3P_0$ - $5s^3P_1^o$ (W_m = 0.0358 Å) line. The corresponding theoretical values are W_e = 0.0502 Å and 0.0466 Å respectively. Since both lines have the same upper energy level and the lower level contribution is small, this is in contradiction with findings that if the perturbing energy level positions are regular, line widths within a multiplet should be approximately the same (Wiese and Konjević, 1982). If we eliminate the influence of the wavelength differences multiplying values for 2651.57 Å line with $(2754.59/2651.57)^2$, we will obtain for theoretical width the value of 0.0503 Å which is practically equal to the calculated value for 2754.59 Å line (0.0502 Å). Contrary, for experimental width the scaled value is 0.0386 Å what is different from the experimental value of 0.0509 Å for 2754.59 Å line. It is interesting to obtain new experimental results for these lines in order to see if the reason is maybee the configuration mixing.

For Ge I $4p^2\ ^1S - 5s^1P^o$ multiplet, Dimitrijević and Konjević (1983) performed semiclassical calculation within the frame of the theory developed by Griem et al. (1962) (see also Griem, 1974). It should be noted that atomic data needed for calculations have not been taken in Sugar and Musgrove (1993), not available at that time,

but in Moore (1971) and, Kaufman and Edlén (1974). The comparison of semiclassical method of Griem et al. (1962) (see also Griem, 1974), used in Dimitrijević and Konjević (1983) and the semiclassical perturbation method (Sahal-Bréchot, 1969ab) used here, as well as explanation of differences, is given in Dimitrijević and Sahal-Bréchot (1996). The present results are considerably smaller. For example at $T = 10$ 000 K and $N_e = 10^{17}\mathrm{cm}^{-3}$, Dimitrijević and Konjević obtain a Stark width of 0.408Å and present results are 0.235Å.

Lakićević (1983) estimated on the basis of regularities and systematic trends Stark broadening parameters for Ge I $4\mathrm{p}^2\ {}^3P - 5s^3P^o$ multiplet, and he obtained that W is 0.1 Å and the absolute value of the shift 0.055 Å for an electron density of $10^{17}\mathrm{cm}^{-3}$ and T = 20 000 K. The distance between energy levels within the $5\mathrm{s}^3P^o$ term is not negligible in comparison with the distance to the nearest perturbing levels. Consequently, the particular line widths within the corresponding multiplet differ. Our width values vary between 0.087 and 0.097 Å and shift values between 0.072 and 0.080Å. If one takes into account the simplicity of this method, the agreement is good.

On the basis of examination of systematic trends (Purić, 1996), dependencies enabling the estimation of the Stark widths of spectral lines for s-p and p-s transitions of neutral atoms have been found by Sarandaev et al. (2000). These simple relations, based on the known ionization potential of the lower/upper level of the corresponding transitions and on the regularities and systematic trends, have been used to determine Stark widths for Ge I $4\mathrm{p}^2\ {}^1\mathrm{S}$ - $5\mathrm{s}^1\mathrm{P}^o$ and $4\mathrm{p}^2\ {}^1\mathrm{S}$ - $5\mathrm{s}^3\mathrm{P}^o$ transitions. For example at $T = 20\,000$ K and $N_e = 10^{17}\mathrm{cm}^{-3}$ they obtain for Ge I $4\mathrm{p}^2\ {}^1\mathrm{S}$ - $5\mathrm{s}^1\mathrm{P}^o$ a Stark width of 0.33 Å while the present value is 0.261 Å.

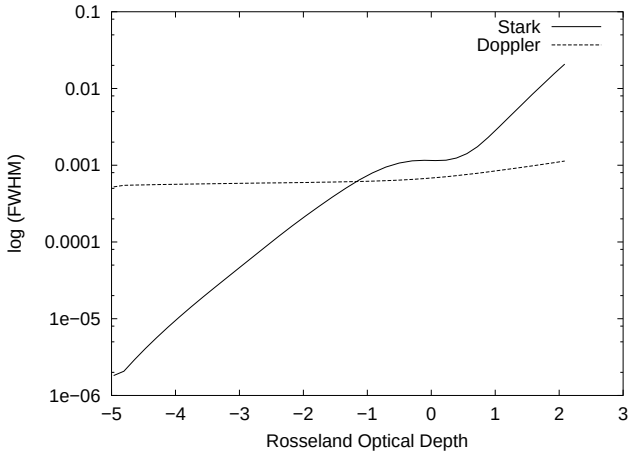

Fig. 1: Thermal Doppler (dotted line) and Stark widths (full line) for Ge I (λ = 4226.562 Å) spectral line as functions of Rosseland optical depth.

In order to see the influence of Stark broadening mechanism for Ge I spectral lines in stellar plasma conditions, we have calculated the Stark widths for Ge I 4226.562 Å spectral line for a Kurucz's (1979) A type star atmosphere model with $T_{eff} = 10$ 000 K and log g =4. From Fig. 1 one can see the existence of atmospheric layers where Doppler and Stark widths are comparable and where Stark width is dominant,

and that the Stark broadening effect should be taken into account in abundance determination, spectra synthesis and modeling of stellar plasmas.

New experimental determination of Stark broadening of neutral germanium spectral lines will be obviously useful for comparison with experimental and theoretical data as well as for astrophysical plasma investigation and modeling.

Acknowledgements. This work is a part of the project GA-1195 "Influence of collisional processes on astrophysical plasma lineshapes", supported by Ministry of Science, Technologies and Development of Serbia.

References

Dimitrijević, M.S.: 1996, *Zh. Prikl. Spektrosk.*, **63**, 810.
Dimitrijević, M.S., Jovanović, P, Simić, Z.: 2003, *Astron. Astrophys.*, in press.
Dimitrijević, M.S., Konjević, N.: 1983, *J. Quant. Spectrosc. Radiat. Transfer*, **30**, 45.
Dimitrijević M.S. and Sahal-Bréchot, S.: 1996, *Physica Scripta*, **54**, 50.
Grevesse, N.: 1984, *Phys. Scripta*, **T8**, 49.
Griem, H.R.: 1974, *Spectral Line Broadening by Plasmas, Academic Press*, New York.
Griem, H.R., Baranger, M., Kolb, A.C., Oertel, G.K.: 1962, *Phys. Rev.*, **125**, 177.
Jones, W.W., Miller, M.H.: 1974, *Phys. Rev.*, **A 10**, 1803.
Kaufman, V., Edlén, B.: 1974, *J. Phys. Chem. Ref. Data*, **3**, 825.
Kondrat'eva, E.V.: 1970, *Opt. Spectrosc.* (USSR), **29**, 434.
Konjević, N., Dimitrijević, M.S., Wiese, W.L.: 1984, *J. Phys. Chem. Ref. Data*, **13**, 619.
Konjević, N., Wiese, W.L.: 1990, *J. Phys. Chem. Ref. Data*, **19**, 1307.
Kurucz, R.L.: 1979, *Astrophys. J. Suppl. Series*, **40**, 1.
Lakićević, I.S.: 1983, *Astron. Astrophys.*, **127**, 37.
Minhagen, L.: 1964, *J. Opt. Soc. Am.*, **54**, 320.
Moore, C.E.: 1971, *Atomic Energy Levels*, Circular 467, Vol. II, U. S. Department of Commerce, NBS, Government Printing Office, Washington D.C.
Musiol, K., Labusz, S., Pokrzywka, B.: 1988, *J. Quant. Spectrosc. Radiat. Transfer*, **40**, 143
Purić, J.: 1996, *Zh. Prikl. Spektrosk.*, **63**, 816.
Sahal−Bréchot, S.: 1969a, *Astron. Astrophys.*, **1**, 91.
Sahal−Bréchot, S.: 1969b, *Astron. Astrophys.*, **2**, 322.
Sarandaev, E.V., Konovalova, O.A., Salakhov, M.Kh.: 2000, *J. Quant. Spectrosc. Radiat. Transfer*, **67**, 105
Sugar, J., Musgrove, A.: 1993, *J. Phys. Chem. Ref. Data*, **22**, 1213.
Wiese, W.L., Konjević, N.: 1982, *J. Quant. Spectrosc. Radiat. Transfer*, **28**, 185.

Publ. Astron. Obs. Belgrade No. 76 (2003), 191 - 195 *Contributed paper*

STARK BROADENING OF NEUTRAL GALLIUM SPECTRAL LINES IN ASTROPHYSICAL PLASMA

MILAN S. DIMITRIJEVIĆ, MIODRAG DAČIĆ, ZORICA CVETKOVIĆ, ZORAN SIMIĆ

Astronomical Observatory, Volgina 7, 11160 Belgrade, Serbia and Montenegro
E–mail: mdimitrijevic@aob.bg.ac.yu
E–mail: mdacic@aob.bg.ac.yu
E–mail: zcvetkovic@aob.bg.ac.yu
E–mail: zsimic@aob.bg.ac.yu

Abstract. Stark broadening of the eighteen transitions of neutral gallium has been analyzed within the frame of the semiclassical perturbation method. Results for electron-, and proton-impact widths and shifts are presented for temperatures from 2500 K up to 50000 K.

1. INTRODUCTION

The interest for atomic and spectroscopic data, increased considerably in astrophysics with space born spectroscopy development, since the number of stellar spectra obtained with resolution enabling the indentification and analysis in detail of a large number of spectral lines, increases as well. Consequently, Stark broadening of neutral gallium spectral lines is of interest not only for laboratory but also for astrophysical plasma research as e.g. for gallium abundance determination and opacity calculations (Seaton 1988).

Stark broadening parameters of gallium lines are also of interest for the consideration of regularities and systematic trends, and the corresponding results may be of interest in astrophysics for interpolation of new data and critical evaluation of existing ones.

The first investigations of the influence of the Stark broadening mechanism on gallium lines have been performed by Kondrat'eva and Fomichenko (1970) in a spark discharge and by Venkatesan et al. (1981). Lakićević (1983) estimated on the basis of regularities and systematic trends Stark width and shift of the Ga I $4p^2\mathrm{P}^o - 5s^2\mathrm{S}$ transition and N'Dollo and Fabry (1987) calculated within the semiclassical method and experimentally determined Ga I Stark widths. Here, we will calculate within the semiclassical perturbation approach, Stark broadening parameters of 18 Ga I transitions, for conditions typical of astrophysical and laboratory plasmas.

Table 1: Electron− and proton−impact broadening parameters for Ga I spectral lines, for perturber density of 10^{14}cm^{-3} and temperatures from 2500 up to 50,000 K. Transitions and averaged wavelengths for the multiplet (in Å) are also given. By dividing C by the corresponding full width at half maximum (Dimitrijević et al. 1991), we obtain an estimate of the maximum perturber density for which the line may be treated as isolated and tabulated data may be used.

PERTURBER DENSITY = 1.E+14cm-3					
PERTURBERS ARE:		ELECTRONS		PROTONS	
TRANSITION	T(K)	WIDTH(A)	SHIFT(A)	WIDTH(A)	SHIFT(A)
$4p^2\mathrm{P}^o - 5s^2\mathrm{S}$	2500.	0.173E-03	0.142E-03	0.438E-04	0.400E-04
	5000.	0.204E-03	0.166E-03	0.488E-04	0.450E-04
4125.8 A	10000.	0.236E-03	0.196E-03	0.546E-04	0.506E-04
C = 0.14E+18	20000.	0.257E-03	0.223E-03	0.610E-04	0.569E-04
	30000.	0.268E-03	0.209E-03	0.652E-04	0.608E-04
	50000.	0.287E-03	0.204E-03	0.708E-04	0.662E-04
$4p^2\mathrm{P}^o - 4d^2\mathrm{D}$	2500.	0.311E-03	-0.181E-03	0.757E-04	-0.452E-04
	5000.	0.311E-03	-0.176E-03	0.793E-04	-0.509E-04
2921.0 A	10000.	0.315E-03	-0.163E-03	0.838E-04	-0.572E-04
C = 0.14E+17	20000.	0.330E-03	-0.129E-03	0.894E-04	-0.644E-04
	30000.	0.339E-03	-0.117E-03	0.933E-04	-0.689E-04
	50000.	0.341E-03	-0.988E-04	0.990E-04	-0.751E-04
$4p^2\mathrm{P}^o - 5d^2\mathrm{D}$	2500.	0.124E-02	-0.762E-03	0.297E-03	-0.221E-03
	5000.	0.128E-02	-0.678E-03	0.322E-03	-0.251E-03
2484.0 A	10000.	0.135E-02	-0.496E-03	0.351E-03	-0.285E-03
C = 0.25E+16	20000.	0.140E-02	-0.375E-03	0.386E-03	-0.321E-03
	30000.	0.138E-02	-0.303E-03	0.410E-03	-0.343E-03
	50000.	0.135E-02	-0.219E-03	0.445E-03	-0.375E-03
$5s^2\mathrm{S}-5p^2\mathrm{P}^o$	2500.	0.504E-02	0.368E-02	0.170E-02	0.954E-03
	5000.	0.581E-02	0.339E-02	0.177E-02	0.107E-02
12005.6 A	10000.	0.696E-02	0.268E-02	0.186E-02	0.121E-02
C = 0.24E+18	20000.	0.889E-02	0.155E-02	0.197E-02	0.136E-02
	30000.	0.100E-01	0.105E-02	0.205E-02	0.146E-02
	50000.	0.112E-01	0.508E-03	0.216E-02	0.159E-02
$5s^2\mathrm{S}_{1/2} - 6p^2\mathrm{P}^o_{1/2}$	2500.	0.110E-01	0.808E-02	0.273E-02	0.210E-02
	5000.	0.119E-01	0.818E-02	0.297E-02	0.239E-02
6415.2 A	10000.	0.126E-01	0.732E-02	0.326E-02	0.271E-02
C = 0.18E+17	20000.	0.136E-01	0.555E-02	0.359E-02	0.305E-02
	30000.	0.141E-01	0.464E-02	0.382E-02	0.327E-02
	50000.	0.144E-01	0.363E-02	0.414E-02	0.357E-02
$5s^2\mathrm{S}_{1/2} - 6p^2\mathrm{P}^o_{3/2}$	2500.	0.117E-01	0.855E-02	0.286E-02	0.223E-02
	5000.	0.125E-01	0.854E-02	0.313E-02	0.254E-02
6398.3 A	10000.	0.133E-01	0.754E-02	0.344E-02	0.289E-02
C = 0.16E+17	20000.	0.142E-01	0.573E-02	0.380E-02	0.326E-02
	30000.	0.146E-01	0.476E-02	0.404E-02	0.349E-02
	50000.	0.148E-01	0.369E-02	0.439E-02	0.381E-02

Table 1: (continued)

PERTURBER DENSITY = 1.E+14cm-3					
PERTURBERS ARE:		ELECTRONS		PROTONS	
TRANSITION	T(K)	WIDTH(A)	SHIFT(A)	WIDTH(A)	SHIFT(A)
$5s^2\mathrm{S}_{1/2} - 7p^2\mathrm{P}^o_{1/2}$	2500.	0.311E-01	0.216E-01	0.732E-02	0.591E-02
	5000.	0.324E-01	0.198E-01	0.811E-02	0.684E-02
5361.3 A	10000.	0.338E-01	0.163E-01	0.903E-02	0.783E-02
C = 0.40E+16	20000.	0.344E-01	0.124E-01	0.101E-01	0.890E-02
	30000.	0.341E-01	0.994E-02	0.109E-01	0.957E-02
	50000.	0.333E-01	0.694E-02	0.119E-01	0.105E-01
$5s^2\mathrm{S}_{1/2} - 7p^2\mathrm{P}^o_{3/2}$	2500.	0.375E-01	0.248E-01	0.898E-02	0.735E-02
	5000.	0.390E-01	0.216E-01	0.100E-01	0.855E-02
5349.6 A	10000.	0.399E-01	0.175E-01	0.112E-01	0.981E-02
C = 0.28E+16	20000.	0.391E-01	0.129E-01	0.126E-01	0.112E-01
	30000.	0.382E-01	0.102E-01	0.136E-01	0.120E-01
	50000.	0.368E-01	0.693E-02	0.151E-01	0.132E-01
$5p^2\mathrm{P}^o - 5d^2\mathrm{D}$	2500.	0.419E-01	-0.259E-01	0.914E-02	-0.688E-02
	5000.	0.450E-01	-0.263E-01	0.992E-02	-0.782E-02
13004.3 A	10000.	0.479E-01	-0.241E-01	0.108E-01	-0.886E-02
C = 0.68E+17	20000.	0.500E-01	-0.202E-01	0.119E-01	-0.999E-02
	30000.	0.507E-01	-0.175E-01	0.127E-01	-0.107E-01
	50000.	0.509E-01	-0.143E-01	0.138E-01	-0.117E-01
$4d^2\mathrm{D}-5p^2\mathrm{P}^o$	2500.	0.253	0.147	0.608E-01	0.389E-01
	5000.	0.284	0.168	0.642E-01	0.440E-01
59974.3 A	10000.	0.308	0.175	0.685E-01	0.496E-01
C = 0.60E+19	20000.	0.327	0.161	0.736E-01	0.558E-01
	30000.	0.338	0.144	0.772E-01	0.597E-01
	50000.	0.351	0.122	0.823E-01	0.651E-01
$4d^2\mathrm{D}-6p^2\mathrm{P}^o_{1/2}$	2500.	0.946E-01	0.649E-01	0.220E-01	0.168E-01
	5000.	0.103	0.681E-01	0.239E-01	0.192E-01
17885.8 A	10000.	0.110	0.639E-01	0.262E-01	0.217E-01
C = 0.14E+18	20000.	0.115	0.542E-01	0.289E-01	0.245E-01
	30000.	0.117	0.467E-01	0.307E-01	0.263E-01
	50000.	0.118	0.365E-01	0.333E-01	0.287E-01
$4d^2\mathrm{D}-6p^2\mathrm{P}^o_{3/2}$	2500.	0.990E-01	0.678E-01	0.228E-01	0.177E-01
	5000.	0.107	0.701E-01	0.249E-01	0.202E-01
17754.4 A	10000.	0.114	0.647E-01	0.273E-01	0.229E-01
C = 0.12E+18	20000.	0.119	0.544E-01	0.302E-01	0.258E-01
	30000.	0.120	0.465E-01	0.321E-01	0.277E-01
	50000.	0.121	0.360E-01	0.349E-01	0.302E-01
$4d^2\mathrm{D}-7p^2\mathrm{P}^o_{1/2}$	2500.	0.148	0.100	0.342E-01	0.275E-01
	5000.	0.154	0.908E-01	0.378E-01	0.319E-01
11553.5 A	10000.	0.161	0.733E-01	0.421E-01	0.365E-01
C = 0.18E+17	20000.	0.163	0.506E-01	0.472E-01	0.415E-01
	30000.	0.162	0.364E-01	0.507E-01	0.446E-01
	50000.	0.157	0.268E-01	0.557E-01	0.488E-01

Table 1: (continued)

PERTURBER DENSITY = 1.E+14cm-3					
PERTURBERS ARE:		ELECTRONS		PROTONS	
TRANSITION	T(K)	WIDTH(A)	SHIFT(A)	WIDTH(A)	SHIFT(A)
$4d^2\mathrm{D}-7p^2\mathrm{P}^o_{3/2}$	2500.	0.177	0.114	0.416E-01	0.341E-01
	5000.	0.184	0.970E-01	0.464E-01	0.396E-01
11499.2 A	10000.	0.188	0.766E-01	0.519E-01	0.454E-01
C = 0.13E+17	20000.	0.184	0.511E-01	0.586E-01	0.517E-01
	30000.	0.180	0.344E-01	0.632E-01	0.556E-01
	50000.	0.173	0.257E-01	0.701E-01	0.610E-01
$5d^2\mathrm{D}-6p^2\mathrm{P}^o_{1/2}$	2500.	24.0	14.7	4.83	3.68
	5000.	26.0	14.6	5.26	4.20
231830.3 A	10000.	27.3	13.2	5.77	4.77
C = 0.22E+20	20000.	28.7	10.0	6.38	5.39
	30000.	29.3	8.31	6.79	5.78
	50000.	29.3	6.75	7.38	6.31
$5d^2\mathrm{D}-6p^2\mathrm{P}^o_{3/2}$	2500.	30.6	18.8	6.12	4.70
	5000.	33.0	18.5	6.68	5.37
256416.8 A	10000.	34.6	16.5	7.33	6.10
C = 0.26E+20	20000.	36.2	12.5	8.11	6.90
	30000.	36.8	10.3	8.64	7.40
	50000.	36.7	8.25	9.42	8.07
$5d^2\mathrm{D}-7p^2\mathrm{P}^o_{1/2}$	2500.	1.81	1.15	0.385	0.309
	5000.	1.91	1.08	0.427	0.358
37979.6 A	10000.	1.99	0.890	0.475	0.410
C = 0.20E+18	20000.	2.02	0.624	0.532	0.466
	30000.	2.00	0.491	0.571	0.501
	50000.	1.95	0.336	0.628	0.548
$5d^2\mathrm{D}-7p^2\mathrm{P}^o_{3/2}$	2500.	2.08	1.30	0.454	0.370
0.0	5000.	2.18	1.14	0.506	0.430
37398.7 A	10000.	2.23	0.917	0.566	0.494
C = 0.14E+18	20000.	2.19	0.620	0.639	0.562
	30000.	2.15	0.486	0.689	0.605
	50000.	2.07	0.310	0.764	0.663

2. RESULTS AND DISCUSSION

For the determination of Stark broadening parameters (the full line width at half maximum - W and the line shift -d) of neutral gallium, the semiclassical perturbation formalism has been used (Sahal−Bréchot, 1969ab). The theory and computer code have been updated and optimized several times and the discussion of updatings and validity criteria, has been briefly reviewed e.g. in Dimitrijević (1996). All details of the determination of Stark broadening parameters will be published elsewhere (Dimitrijević et al, 2003) so that we note here only that the atomic energy levels needed for calculations have been taken from Moore (1971).

Results for electron-, and proton-impact broadening parameters for 18 Ga I transitions for perturber density of $10^{14}\mathrm{cm}^{-3}$ and temperatures from 2,500 K up to 50,000 K are shown in Table 1. The comparison of our results with existing experimental and theoretical data will be presented and discussed in Dimitrijević et al. (2003).

The new experimental determinations of Stark broadening parameters will be of interest for the comparison with our and other existing experimental and theoretical data and will be equally useful for research and modelling of astrophysical plasmas.

Acknowledgements: This work is a part of the project GA 1195 "Influence of collisional processes on astrophysical plasma lineshapes", supported by Ministry of Science, Technologies and Development of Serbia.

References

Dimitrijević, M.S.: 1996, *Zh. Prikl. Spektrosk.*, **63**, 810.
Dimitrijević, M.S., Dačić, M., Cvetković, Z., Simić, Z.: 2003, *Astron. Astrophys.*, submitted.
Dimitrijević, M.S., Sahal-Bréchot, S., Bommier, V.: 1991, *Astron. Astrophys. Suppl. Series*, **89**, 581.
Kondrat'eva, E.V., Fomichenko, L.I.: 1970, *Opt. Spectrosc. (USSR)*, **29**, 434.
Lakićević, I.S.: 1983, *Astron. Astrophys.*, **127**, 37.
Moore, C.E.: 1971, *Atomic Energy Levels*, Circular 467, Vol. II, U. S. Department of Commerce, NBS, Government Printing Office, Washington D.C.
N'Dollo, M., Fabry, M.: 1987, *J. Physique*, **48**, 703.
Sahal−Bréchot, S.: 1969a, *Astron. Astrophys.*, **1**, 91.
Sahal−Bréchot, S.: 1969b, *Astron. Astrophys.*, **2**, 322.
Seaton, M.J.: 1988, *J. Phys. B*, **21**, 3033.
Venkatesan, T., Wagner, A., Nach, D.L., Mungo, A.J., Barr, D.: 1981, *Appl. Phys. Lett.*, **39**, 9.

Publ. Astron. Obs. Belgrade No. 76 (2003), 197 - 200 *Contributed paper*

THE EMISSION LINE SHAPES OF THE SEYFERT 1 GALAXY MRK817

D. ILIĆ [1], E. BON [2] , E.G. MEDIAVILLA[3], L.Č. POPOVIĆ [2]

[1] *Department of Astronomy, Faculty of Mathematics, University of Belgrade, Studentski trg 16, 11000 Belgrade, Serbia and Montenegro*
E–mail: dilic@matf.bg.ac.yu

[2] *Astronomical Observatory, Volgina 7, 11160 Belgrade 74, Serbia and Montenegro*
E–mail: ebon@aob.aob.bg.ac.yu
E–mail: lpopovic@aob.aob.bg.ac.yu

[3] *Instituto de Astrofísica de Canarias C/ Vía Làctea, s/n E38200 - La Laguna (Tenerife), Spain*
E–mail: emg@ll.iac.es

Abstract. The analysis of emission line region of Seyfert 1 galaxy Mrk817 is presented. We found that emission line region in Mrk 817 is very complex. Moreover, the Narrow Line Region shows complex structure. The spectral line shapes of Mrk 817 indicates at least three kinematically separated regions, one (or more) which emits the broad line component ($V \sim$ 5000 km/s), one which emits narrow components ($V \sim$ 450 km/s) and one extensive which emits also narrow component ($V \sim$ 150 km/s).

1. INTRODUCTION

Seyfert galaxies have very complex emission-line shapes (see e.g. Sulentic et al., 2000 and references therein). These lines are coming from two different emission regions; Narrow Line Region (NLR) and Broad Line Region (BLR) that are spatially and kinematically separated, as well as physically different (see e.g. Osterbrock, 1989). Active galaxy Mrk 817 is a Seyfert 1.5 galaxy with red-shift 0.03145 (Strauss and Huchra, 1988). The recent investigation by Kaspi (2000) shows that Broad Line Radius of Mrk 817 is very compact (around 15 light days). The spectral lines shapes indicate that the emission line region of Mrk 817 is very complex (Popović and Mediavilla, 1997). In order to find the composition of the emitting line region we have used spectral line observations with different telescopes performed with different spectral resolution.

The aim of this work is to find the kinematical parameters of BLR and NLR of Mrk 817 by analyzing the Balmer and [OIII] spectral line shapes as well as the variability of Hβ line flux. Here we will present the Gaussian analysis of the H$_\beta$, H$_\alpha$ and [OIII] lines.

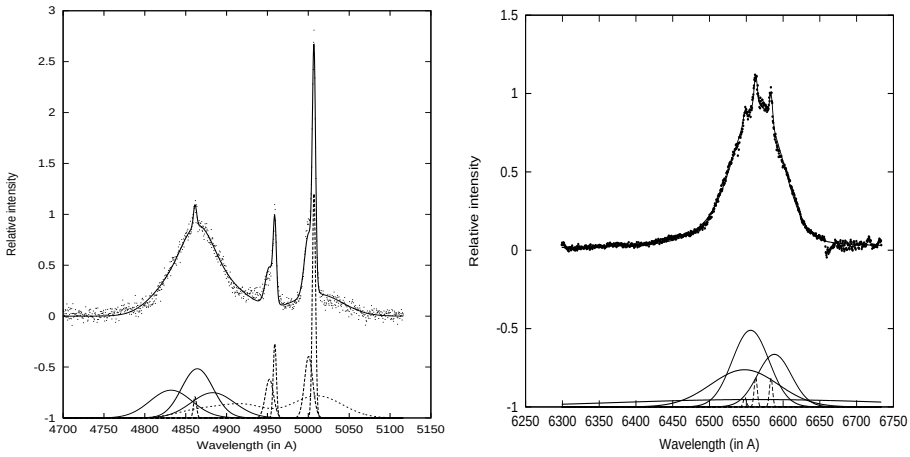

Fig. 1: **Left**: Decomposition of Hβ line of Mrk 817. The dots represent the observation and solid line is the best fit. The Gaussian components are shown at the bottom. The dashed lines at bottom represent the Fe II template, [OIII] and Hβ narrow lines. **Right**: The same as in Left, but for H_α. The Gaussian components are shown at the bottom. The dashed line at the bottom represent satellite N II lines and a narrow Hα component.

2. OBSERVATION AND DATA REDUCTION

We have used here three different sets of spectral observations of Mrk 817 wavelength line regions:

i) Observations with 2.5m Isaac Newton Telescope in La Palma Islands. The observations were performed in the period from 21th to 25th of January 2002. We used the Intermediate Dispersion Spectrograph (IDS) and the 235 camera in combination with the R1200Y grating. Two exposures of 550 and 500 s, included three Hβ and three Hα spectrum. The seeing was $1''.1$ and the slit width $1''$. The spectral resolution was around 1.0 Å . Standard reduction procedures including flat-fielding, wavelength calibration, spectral response, and sky subtraction were performed with the help of the IRAF software package.

ii) Observations with 4.2m William Herschel Telescope, at La Palma islands. The observation ware performed on 12/13 March 2001. The long-slit spectrograph (ISIS) was used, in combination with CCD cameras TEK4 (grating R158R). The spectral resolution was 2.9 Å . Also, the standard reduction procedures including flat-fielding, wavelength calibration, spectral response, and sky subtraction were performed with the help of the IRAF software package.

ii) Third set was observed at the Crimean Astrophysical Observatory by K.K.Chuvaev on 2.6m Shain telescope during the period of 1977-1991, and only Hβ line was observed. The spectral resolution was $\sim$ 8 Å. The spectrograph slit and the seeing were in the $1.8'' - 2.0''$, and $2'' - 3''$ ranges, respectively. The spectra of Hβ, were scanned with a two-coordinate CrAO microphotometer (as in the case of Akn 120, see e.g. Stanić et al. 2000, Popović et al., 2001). The reduction procedure includes

Table 1: The parameters of the Gaussian components (width, shift and intensity) of the Hα, Hβ and [OIII] λ4959,5007 lines.

Gaussian	H_α	H_β	Gaussian	*OIII*
W_B	2950	2250	W_{4959n}	165
z_B	-700	-1810	z_{4959n}	0
I_B	0.24	0.27	I_{4959n}	0.73
W_C	1610	1680	W_{4952b}	430
z_C	-320	180	z_{4959b}	-390
I_C	0.49	0.48	I_{4959b}	0.38
W_R	1500	2310	W_{5007n}	0.00055179
z_R	+1160	1350	z_{5007n}	0
I_R	0.34	0.25	I_{5007n}	2.20
W_{NLR}	140	160	W_{5007b}	430
z_{NLR}	0	0	z_{5007b}	-390
I_{NLR}	0.19	0.21	I_{5007b}	0.60

corrections for the film sensitivity, sky background, and instrumental spectral sensitivity. The wavelength and flux calibration were made using the SPE data reduction package, developed by S.G. Sergeev. The wavelength calibration was based on the night sky lines and narrow emission lines of the galaxy.

The spectra have been normalized to the [OIII]λ 5007 emission line.

The software package DIPSO was used for reducing the level of local continuum, by subtracting the N order polynomial, fitted through the dots taken to be on the local continuum in spectral range 4700 – 5100 Å for the Hβ . The same was done for the Hα local continuum in 6350- 6750 Å .

The red-shift of Mrk 817 was taken to be z=0.03145 (Straus and Huchra 1988, Véron-Cetty and Véron, 2000).

3. RESULTS

We fitted each line with a sum of Gaussian components using a χ^2 minimalization routine to obtain the best fit parameters. The fitting procedure has been described several times (see e.g. Popović et al., 2001, 2002; Popović 2003), but in this case we have assumed that the narrow emission lines can be composed by more Gaussian components. In the fitting procedure, we look for the minimal number of Gaussian components needed to fit the lines, taking into account the intensity ratio of [OIII] lines (the atomic value 1:3.03) and the fit of Fe II template (Korista, 1992) for the Hβ. For the two [NII] lines we assume their intensity ratio is 1:2.96 (Popović, 2003). It was found that three broad Gaussian and one narrow components could fit well the profiles of the Hα and Hβ lines.

The results of our analyses are presented in Figs. 1 and 2, and in Table 1. In Figs. 1 and 2 we can recognize clear evidence of substructure in these emission lines, not only in the broad component of the line, but also in the narrow emission lines. As one can see from the Figures, the line profiles of Hα and Hβ Mrk 817 lines are

very complex. The emission line region of Mrk 817 is composed at least from three kinematically separated emission line regions:

1) The BLR which also can be more complex (two or three kinematically different emission region);

2) The NLR1, which has internal random velocity around 450 km/s, and a systemic velocity toward the blue of 390 km/s. That indicates presence outflow of emitting gas in NLR1.

3) The NLR2 has the internal random velocity around 150 km/s.

The detailed discussion will be given elsewhere (Ilić et al. 2003).

Acknowledgments. This work was supported by the Ministry of Science, Technologies and Development of Serbia through the project P1196 "Astrophysical Spectroscopy of Extragalactic Objects" and the project P6/88 "Relativistic and Theoretical Astrophysics" supported by the IAC. L. Č. P. and E. B. thank the Institute for Astrophysics Canarias for the hospitality during his stay at the Institute.

References

Ilić D., Bon E., Mediavilla E., Popović, L.Č.: 2003, in preparation.

Korista, K.T.: 1992, *Astroph. J. Suppl. Series*, **79**, 285.

Osterbrock, D.E.: 1989, *Astrophysics of Gaseous Nebulae and Active Galactic Nuclei*, Mill Valle: University Science Press.

Popović, L.Č.: 2003, *Astrophys. J.*, accepted (astro-ph/0304390).

Popović, L.Č., Mediavlilla, E.G.: 1997, *Publ. Astron. Obs. Belgrade*, **57**.

Popović, L.Č., Stanić, N., Kubičela, A., Bon, E.: 2001, *Astron. Astrophys.*, **367**, 780.

Popović, L.Č., Mediavlilla, E.G., Kubičela, A., Jovanović, P.: 2002, *Astron. Astrophys.*, **390**, 473.

Stanić, N., Popović, L.Č., Kubičela, A., Bon, E.: 2000, *Serb. Astron. J.*, **162**, 7.

Strauss, M.A., Huchra, J.: 1988, *Astrophys. J.*, **95**, 1602.

Kaspi, S. et al.: 2000, *Astrophys. J.*, **533**, 631.

Sulentic, J.W., Marziani, P., Dultzin-Hacyan, D.: 2000, *Ann. Rev. of Astron. Astrophys.*, **38**, 521

Véron-Cetty, M.-P., Véron, P.: 2000, *A Catalogue of Quasars and Active Galactic Nuclei*, Sci. Report 19.

Publ. Astron. Obs. Belgrade No. 76 (2003), 201-204 *Contributed paper*

THE EXPERIMENTAL AND THEORETICAL INVESTIGATIONS OF THE ASYMMETRIC SELF-REVERSAL OF THE NEUTRAL COPPER ATOMS RESONANCE SPECTRAL LINE Cu I 327.936 nm UNDER CONDITIONS OF AN IMPULSE DISCHARGE

G.G. IL'IN, O.A. KONOVAlOVA, M.Kh. SALAKHOV,
E.V. SARANDAEV

Physics Department, Kazan State University, Kremlevskaya str., Kazan, Russia, 420008
E-mail: sarev@ksu.ru

Abstract. The asymmetric self-reversal of the neutral copper atoms resonance spectral line Cu I 327.936 nm under the conditions of an impulse capillary discharge in the air is investigated experimentally and theoretically for the purposeof the development of the asymmetric self-reversal theory, the estimation of Stark broadening parameters of the spectral line Cu I 327.936 nm and the check of the quantum-mechanical calculations results.

The direct recording of the Stark broadening of the copper atoms resonance spectral lines Cu I 324.7 nm and Cu I 327.4 nm under the conditions of optically transparent plasma presents a difficulty because of their narrowness and strong tendency to the self-absorption and even the self-reversal. For the experimental check of the quantum-mechanical calculations results obtained for the first time by us (Grishina *et al.* 1998, 1999; see also Dimitrijević *et al.* 1996) we have decided to use the asymmetric self-reversal of the Cu I 324.7 nm and Cu I 327.4 nm lines which we have observed under the conditions of an impulse capillary discharge in the air (Fishman *et al.* 1994). Grishina *et al.* (1998, 1999) presented only final experimental and theoretical results for the self-reversal Cu I 327.4 nm line which is the most convenient for investigations because of the small distortion of line wings by weak foreign spectral lines. In this paper some results of our investigations are presented in more detail.

The experimental photographic recording of the self-reversal Cu I 327.4 nm line profiles (simultaneously the hydrogen H_α line profiles have been recorded for the determination of the electron concentration n_e) has been carried out on the setup described in Fishman *et al.* (1994). The impulse capillary discharge between the horizontally placed electrodes was used as a source of plasma. The copper atoms have arrived in the plasma from the copper anode through a textolite capillary. The recording of spectra for the plasma cross-section located 0.5 mm from the capillary outlet has been carried out in the current maximum reached in 1.5 ms from the discharge begining with a time resolution of 0.15 ms.

The spectra photographing has allowed to obtain the Cu I 327.4 nm and H_α spectral lines profiles as the plots of the dependence of the intensity I on the wave-length λ for the different lines-of-sight with the transversal coordinate z in the investigated plasma cross-

section. Figures 1 and 2 show the results for one of spectra for the Cu I 327.4 nm line (the axial values of temperature T_0=22000 K and electron concentration n_{eo}=1.2·10^{18} см$^{-3}$).

The Cu I 327.4 nm line has appeared a strong self-reversal for all of the lines-of-sight in the plasma cross-section for which the photographic recording of the intensity has been possible. Figure 1 shows the normalized self-reversal profiles on the wave length scale for two lines-of-sight. All the profiles recorded are asymmetric: the long-wave peak of the intensity has the maximum I_{max1} which appreciably exceeds the maximal intensity I_{max2} of short-wave peak of the intensity. The asymmetry of the profiles becomes apparent also in the different values of the extent on the wave-length scale of the peaks of the intensity relative to the wave-length λ_0 which gives the position of the minimum of the intensity in the line centre as shown on Fig. 1: the extent χ_1 of the long-wave peak is appreciably larger than the extent χ_2 of the short-wave peak. Grishina *et al.* (1998, 1999) used the parameter of the wings asymmetry $\chi=\chi_1-\chi_2$ for the estimation of the electron half-width δ_{eo} for the self-reversal Cu I 327.4 nm line which corresponds to the plasma parameters T_o=22000 K and n_{eo}=1.2·10^{18} см$^{-3}$.

For the estimation of the plasma structure which is needed for the determination of δ_{eo} by χ the plots of the dependences of the intensity I_{max1}, the parameter of the peaks asymmetry I_{max1}/I_{max2} and the parameter of the wings asymmetry χ of the profiles at I/I_{max1}=0.1 on the transversal coordinate z have been constructed (see the dots in Fig.2). The plots show that the plasma in the investigated cross-section is close to the axially symmetric plasma. The diameter $2R_0$ of the emission zone where the exited copper atoms on the lower level of the Cu I 327.4 nm line are primarily located approximately equals 2.6 mm. The smooth variation of the dependence $\chi(z)$ in the limits of the emission zone reveals the smooth radial decrease of the electron half-width δ_e and electron concentration n_e in the limits of the emission zone.

The variation of the dependence $I_{max1}/I_{max2}(z)$ for the Cu I 327.4 nm line is very interesting for the purpose of obtaining the information about the Stark parameters of the line broadening (about the sign of electron shift and about the value of the parameter of the relative shift $\eta=\Delta_e/\delta_e$) and the character of the radial variation of the absorbing atoms concentration n_a on the lower level of the Cu I 327.4 nm line. Figures 1 and 2 show that for the central lines-of-sight the asymmetry of the peaks of the intensity of the self-reversal profiles is comparatively small. However for the peripheral lines-of-sight the parameter of the peaks asymmetry I_{max1}/I_{max2} increases sharply and on the boundary of the emission zone the maximal intensity I_{max1} of the big peak is 4-5 times greater than the maximal intensity I_{max2} of the small peak. Such large values of the parameter of the peaks asymmetry I_{max1}/I_{max2} are possible in the case when $|\eta|\geq 1$ - such calculation values of η have been obtained by us (Grishina *et al.* 1998, 1999).

The theoretical analysis of the complex variation of the dependence $I_{max1}/I_{max2}(z)$ for the Cu I 327.4 nm line calls for the construction of the multiparameters model of the inhomogeneous plasma and the carrying out of the calculations of the self-reversal profiles on the basis of computer calculations of an emission transfer equation for the different lines-of-sight in the plasma cross-section. The calculations have shown that in the given case the most suitable model is the one in which the half-width δ_e decreases smoothly approximately by a factor of 2 in the limits of the emission zone ($r\leq R_0$) with the increase of the plasma radius r (r=0 is the centre in the plasma cross-section) and sharply decreases in

the absorbing peripheral zone at $r>R_0$. The absorbing atoms are located primarily in the emission zone and the concentration of the absorbing atoms decreases sharply on the boundary of the emission zone. In Fig. 2 the solid curve C shows the theoretical dependence $I_{max1}/I_{max2}(z)$ with the following model structure: $|\eta|=1$; $\delta_e(r)/\delta_{eo}=\exp[-0.7(r/R_0)^2]$ at $r\le R_0$ and $\delta_e(r)/\delta_{eo}=\exp(-3)$ at $r>R_0$; $n_a(r)/n_a(0)=\exp[-4(r/R_0)^2]$ at $r\le R_0$; the absorption parameter $p_o=4$ obtained at the distance between the self-reversal maxima Δ_s (see Fig.1) in accordance with Il'in *et al.* (1997). The theoretical curve C rather well describes the experimental dependence $I_{max1}/I_{max2}(z)$.

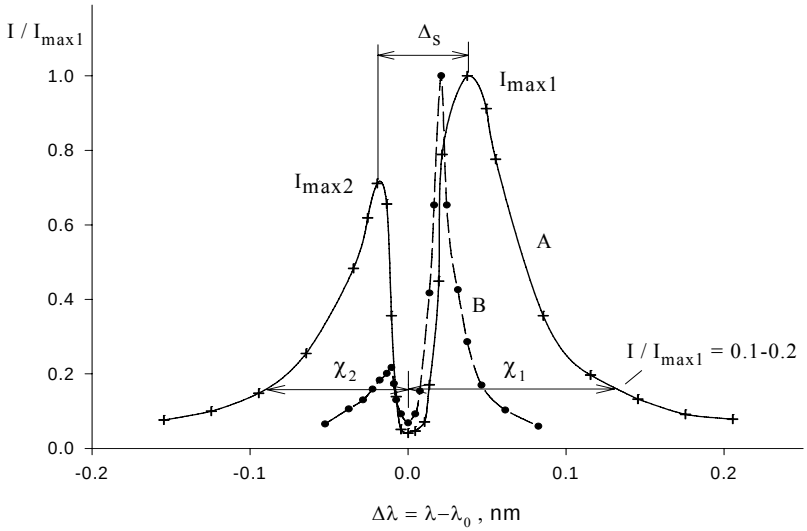

Fig. 1: The normalized self-reversal profiles of the Cu I 327.4 nm spectral line for the different lines-of-sight in the plasma cross-section of the impulse capillary discharge in the air: the profile A corresponds to one of the central lines-of-sight; the profile B corresponds to one of the peripheral lines-of-sight - the positions of the lines-of-sight are indicated in Fig. 2 depending on $I_{max1}/I_{max2}(z)$ (the dots A and B).

The results presented show that there are strong possibilities for a rather good simulation of the asymmetric self-reversal of the Cu I 327.4 nm line under the conditions of the impulse capillary discharge in the air used by us and for obtaining the reliable information from the self-reversal line. The simulation has shown that for the central line-of-sight ($z=0$) $\delta_{eo}\approx\chi(0)/3$ which gives in the present case at $\chi(0)=0.05$ nm the electron half-width $\delta_{eo}=0.017$ nm with the plasma parameters $T_o=22000$ K and $n_{eo}=1.2\cdot10^{18}$ см$^{-3}$. With such plasma parameters the quantum-mechanical calculation (Grishina *et al.* 1999) has given $\delta_{eo}=0.030$ nm. The experimental value of the electron half-width $\delta_{eo}=0.017$ nm

obtained from the asymmetric self-reversal of the Cu I 327.4 nm line is approximately by 1.7 times lower than the theoretical value.

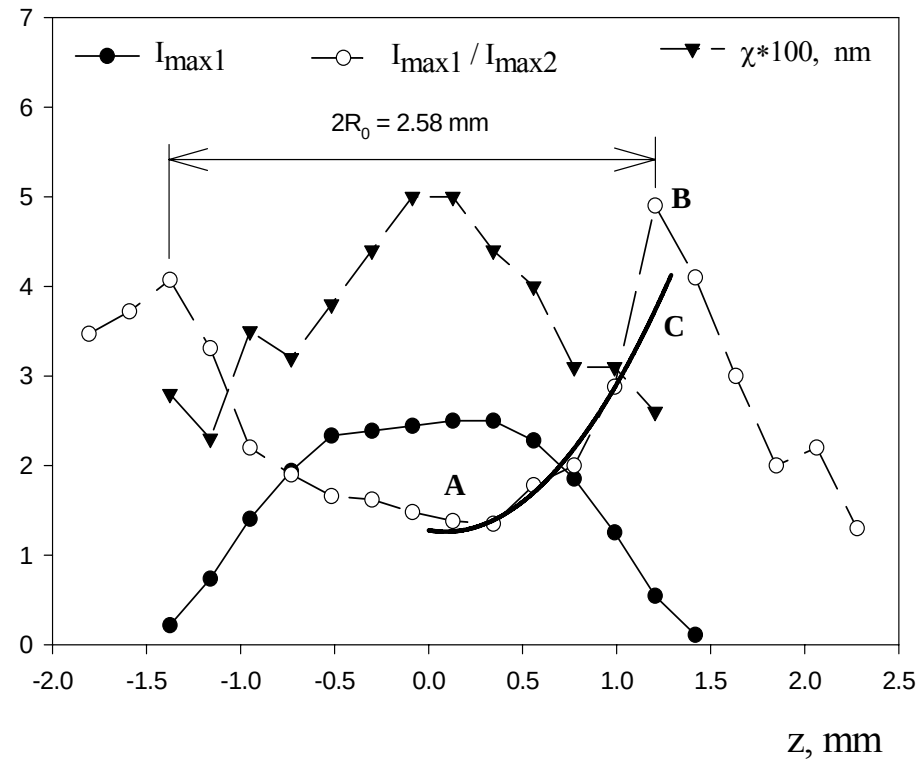

Fig. 2: The plots of the dependences $I_{max1}(z)$ (the intensity I_{max1} is given on the relative scale), $I_{max1}/I_{max2}(z)$ and $\chi(z)$ (the dots) for the Cu I 327.4 nm spectral line. The self-reversal profiles in Fig.1 correspond to the lines-of-sight pointed at the dependence $I_{max1}/I_{max2}(z)$ as the dots A and B. The solid curve C is the theoretical dependence $I_{max1}/I_{max2}(z)$.

References

Dimitrijević, M.S., Il'in, G.G., Salakhov, M.Kh., Sarandaev, E.V.: 1996, *18th SPIG Contributed papers*, 283.

Fishman, I.S., Sarandaev, E.V., Salakhov,: M.Kh.: 1994, *J. Quant. Spectrosc. Radiat. Transfer*, **52,** 887.

Grishina, N.A., Il'in, G.G., Salakhov, M.Kh., Sarandaev, E.V.: 1998, *19th SPIG Contributed papers*, 361.

Grishina, N.A., Il'in, G.G., Salakhov, M.Kh., Sarandaev, E.V.: 1999, *Coherent Optics and Optical Spectroscopy*, Kazan, Russia, 23.

Il'in, G.G., Konovalova, O.A., Sarandaev, E.V., Salakhov, M.Kh.: 1997, *Publ. Obs. Belgrade*, **57**, 127.

Publ. Astron. Obs. Belgrade No. 76 (2003), 205 - 210 *Contributed paper*

CORRELATION BETWEEN X-RAY CONTINUUM AND Fe Kα LINE VARIATION DUE TO MICROLENSING

P. JOVANOVIĆ, L. Č. POPOVIĆ, M. S. DIMITRIJEVIĆ

Astronomical Observatory, Volgina 7, 11160 Belgrade, Serbia
E–mail: pjovanovic@aob.bg.ac.yu

Abstract. The correlation between X-ray continuum and Fe Kα line variation due to microlensing event (MLE) is investigated. Concerning the shape of observed X-ray variations in three lensed quasars (MG J0414+0534, QSO 2237+0305, BAL QSO H1413+117 AT), we conclude that the Fe Kα forming region should be different in dimension than X-ray continuum emission region.

1. INTRODUCTION

The X-ray variability in continuum as well as in spectral lines (e.g. Fe Kα) is often present in the spectra of Active Galactic Nuclei - AGN (see e.g. Marshall et al. 1981, Turner et al. 1999, Manners et al. 2002).

Zakharov et al. (2003) found the significant probability that the high-redshifted QSOs are microlensed. Moreover, the microlensing effect in three macrolensed QSOs has been recently observed (Chartas et al., 2002; Dai et al., 2003; Oshima et al., 2001).

The influence of microlensing on Fe Kα spectral line shape was discussed in Popović et al. (2003), where it was noted that microlensing effect can be used for investigation of Fe Kα and continuum emission region structure.

The aim of this paper is to investigate the correlation between X-ray continuum and Fe Kα line variations due to microlensing, and to use the obtained results for discussion about the structure of Fe Kα and continuum emission region in AGN.

2. THEORY

The effects of microlensing on a compact accretion disk are analyzed using the ray tracing method (Bao et al, 1994; Bromley et al, 1997; Fanton et al, 1997; Čadež et al, 1998) considering only those photon trajectories that reach the sky plane at a given observer's angle $\theta_{\rm obs}$. If X and Y are the impact parameters that describe the

apparent position of each point of the accretion disk image on the celestial sphere as seen by an observer at infinity, the amplified brightness is given by

$$I_p = I\left(T(X,Y)\right)\delta(x - g(X,Y))A(X,Y) \tag{1}$$

where $x = \nu_{\rm obs}/\nu_0$ (ν_0 and $\nu_{\rm obs}$ are the transition and observed frequencies, respectively); $g = \nu_{\rm em}/\nu_{\rm obs}$ ($\nu_{\rm em}$ is the emitted frequency from the disk). $A(X,Y)$ is the amplification caused by microlensing.

In the case of microlensing by an isolated compact object (point-like microlens), the amplification is given by the relation (see e.g. Narayan and Bartelmann, 1999):

$$A(X,Y) = \frac{u^2(X,Y)+2}{u(X,Y)\sqrt{u^2(X,Y)+4}}, \tag{2}$$

where $u(X,Y)$ corresponds to the angular separation between lens and source in Einstein Ring Radius (ERR) units and is obtained from

$$u(X,Y) = \frac{\sqrt{(X-X_0)^2+(Y-Y_0)^2}}{\eta_0}, \tag{3}$$

X_0, Y_0 are the coordinates of the microlens with respect to the disk center (given in gravitational radii), and η_0 is the Einstein Ring Radius (ERR) expressed in gravitational radii.

To express I(T(X,Y)) we started from the standard Newtonian model of an accretion disk around a supermassive black hole. This model is based on the supposition that the locally released gravitational energy is emitted as a blackbody radiation of the temperature (Shalyapin et al, 2002):

$$T\left(r\right) = \left[\frac{3}{8\pi}\frac{GM}{\sigma r^3}\dot{M}\left(1-\sqrt{\frac{r_{in}}{r}}\right)\right]^{\frac{1}{4}}, \tag{4}$$

where σ is the Stefan constant, G is the gravitational constant, M is the central black hole mass, $\dot{M}$ is the accretion rate, and r_{in} is the inner radius of the accretion disk. The above formula can be approximated by the following expression (Takahashi et al, 2001):

$$T\left(r\right) \approx 2.2\times 10^5 \dot{M}_{26}^{1/4} M_8^{1/4} r_{14}^{-3/4}\left(1-\sqrt{\frac{r_{in}}{r}}\right)^{\frac{1}{4}} K, \tag{5}$$

where $\dot{M}_{26} = \dot{M}/10^{26}{\rm gs}^{-1}, M_8 = M/10^8 M_\odot, r_{14} = r/10^{14}{\rm cm}$. The emitted intensity in Eq. (1) is a Planck function of the temperature:

$$I\left(T(X,Y)\right) = \frac{2h\nu^3}{c^2}\frac{1}{e^{h\nu/kT(X,Y)}-1}, \tag{6}$$

where c is the speed of light, h - Planck constant, k - Boltzmann constant and T is temperature.

The total observed flux is then given by

$$F(x) = \int_{\rm image} I_p(x)d\Omega, \tag{7}$$

where $d\Omega$ is the solid angle subtended by the disk in the observer's sky and the integral extends over the whole emitting region.

3. RESULTS

Recent observations of gravitationally lensed quasars QSO 2237+0305 (Dai et al, 2003), MG J0414+0534, (Chartas et al, 2002) and BAL QSO H1413+117 AT (Oshima et al, 2001) suggest that sudden enhancements of Fe Kα line, characteristical only for some of the source images, are possibly caused by microlensing.

In order to study the influence of microlensing on the variations of X-ray continuum and Fe Kα spectral line shape, we adopted the standard black body radiation model of a relativistic accretion disk with inclination $i = 35^o$. In our analysis we used the masses and accretion rates for AGNs given by Bian and Zhao (2002). In their Table 1, accretion rates are given in units of Eddington accretion rate: $\dot{m} = \frac{1.578\dot{M}_{26}}{3.88M_8}$, and we used them to determine the effective temperature distribution. According to Bian and Zhao (2002), we assumed the central black hole with mass $M = 10^8 M_\odot$ and accretion rate $\dot{m} = 0.4$ units of Eddington accretion rate. The variations of normalized line flux and normalized continuum are calculated for different positions of the point-like microlens with ERR = 10 R_g and for a disk in both, Schwarzschild and Kerr metrics. Normalization is made by dividing the perturbed flux by its unperturbed value.

Concerning possible dimensions of the X-ray line and continuum sources, the three cases were considered:

1. The radii of both continuum and line emission region are the same; $R_{in} = R_{rms}$ and $R_{out} = 20\ R_g$,

2. The radus of the continuum emission region is smaller than that for line emission, but the inner part of accretion disk emits in the line as well as in the continuum. In this case for continuum accretion disk we choose the inner and outer radii $R_{in} = R_{rms}$ and $R_{out} = 20\ R_g$, respectively. The corresponding radii for line emission accretion disk are $R_{in} = R_{rms}$ and $R_{out} = 80\ R_g$,

3. The dimension of the line emitting region is larger than continuum one, and they are separated. The radii of continuum emission accretion disk are $R_{in} = R_{rms}$ and $R_{out} = 20\ R_g$ and those of the line emission disk are $R_{in} = 20\ R_g$ and $R_{out} = 80\ R_g$.

As one can see from Fig. 1., in the first case, there is a very high correlation between line flux variation and continuum variation.

In the second case (Fig. 2), the correlation is less but still significant. The main reason for such significant correlation could be that continuum emission region coincides with the inner part of line emission region

Both of cases are not in good agreement with observations of gravitationally lensed quasar MG J0414+0534. Chartas et al. (2002) found that the continuum emission component does not follow the enhancement of the iron line. Considering the third case (Fig. 3) one can say that this case may be compared with observed variation due to MLE observed by Oshima et al. (2001), Chartas et al. (2002) and Dai et al. (2003), where the amplification is observed only in the Fe Kα line. As one can see in

Fig. 3, the microlensing effect is strong in X-ray continuum, but when the microlens crosses the outer region, the amplification of Fe Kα line flux stays stronger, while continuum is also amplified, but stays nearly constant during the MLE. These results also follow the explanation given in Chartas et al. (2002) that non-enhancement of the continuum suggests that the continuum emission region is concentrated closer to the center of the accretion disk than the iron line emission region, and that the microlens does not reach close enough to the continuum region to amplify it.

4. CONCLUSION

In order to investigate the influence of microlensing on the variations of X-ray continuum and Fe Kα line profile, we used the ray tracing method and considered the standard black body radiation model for a relativistic accretion disk around a supermassive black hole in both, Schwarzschild and Kerr metrics.

From our investigation we can conclude that the satisfactory explanation for the fact that we observe only Fe Kα line flux amplification (the absence of corresponding

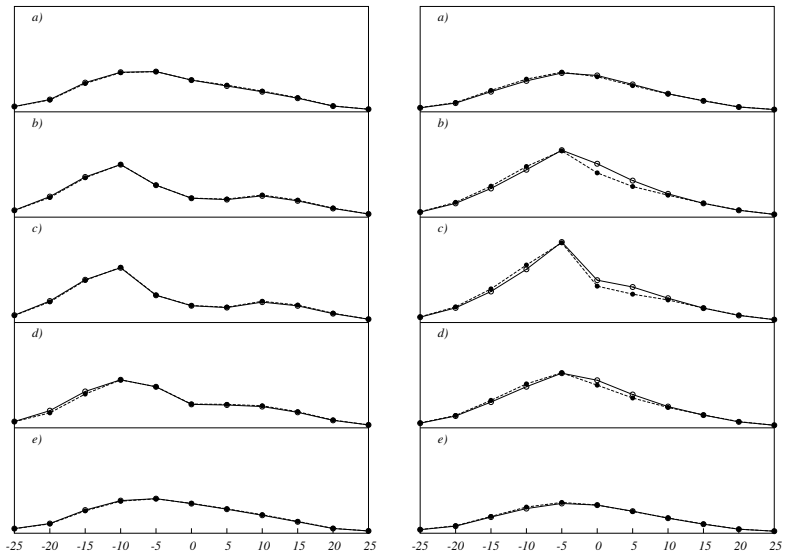

Fig. 1: The variations of normalized line flux (dashed line with full circles) and normalized continuum (solid line with open circles) for a disk in the Schwarzschild metric (left) and Kerr metric (right) with $i = 35^o$ and for different positions of the point-like microlens with ERR = 10 R_g. The radii of continuum and line emission regions of disk are $R_{in} = R_{rms}$ and $R_{out} = 20\ R_g$ in both cases. The central BH mass is $10^8 M_\odot$ and the accretion rate is 0.4 units of Eddington accretion rate. Case a) corresponds to the postion of MLE $Y_0 = 10$, case b) to $Y_0 = 5$, case c) to $Y_0 = 0$, case d) to $Y_0 = -5$, case e) to $Y_0 = -10$. The normalized flux is presented in range from 1 to 2.5.

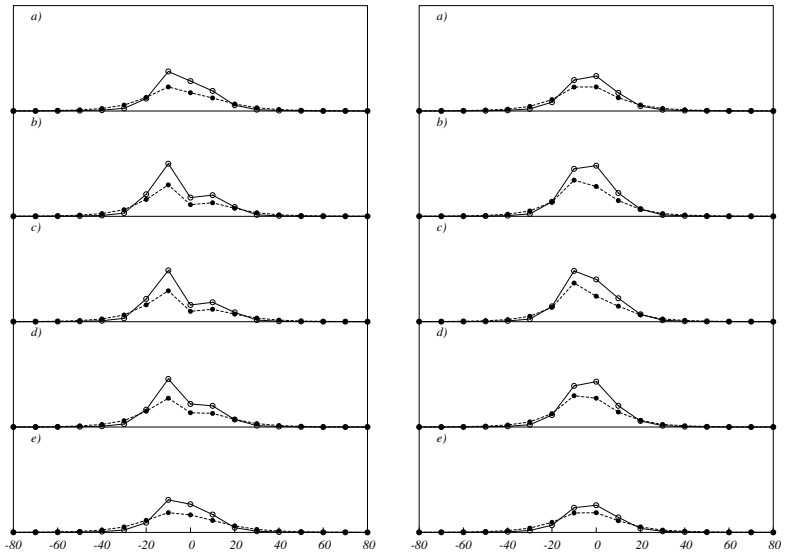

Fig. 2: The same as in Fig. 1, but the radii of continuum emission region are $R_{in} = R_{rms}$ and $R_{out} = 20\ R_g$ and the radii of line emission region are $R_{in} = R_{rms}$ and $R_{out} = 80\ R_g$.

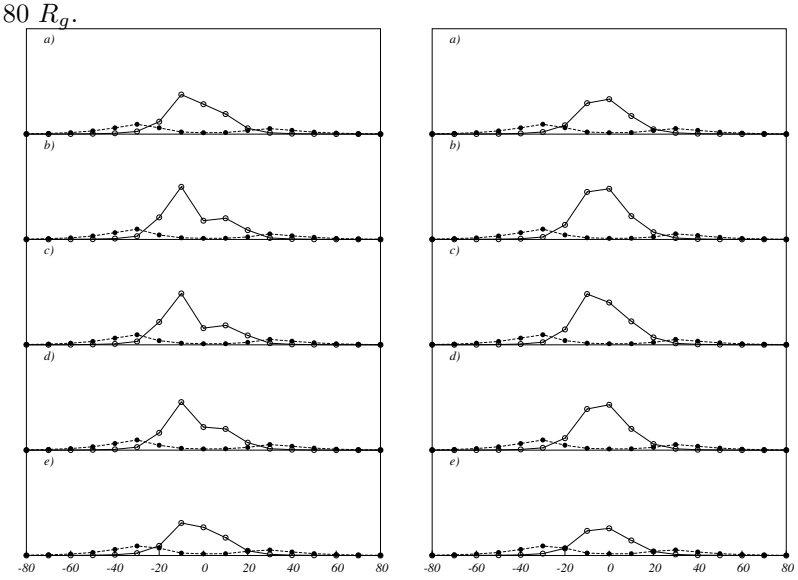

Fig. 3: The same as in Fig. 1, but the radii of continuum emission region are $R_{in} = R_{rms}$ and $R_{out} = 20\ R_g$ and the radii of line emission region are $R_{in} = 20\ R_g$ and $R_{out} = 80\ R_g$.

continuum variations) is that the Fe Kα emission region has different dimension than continuum one.

The more detailed discussion will be given in Jovanović et al. (2003).

Acknowledgments. This work is a part of the project GA 1196 "Astrophysical Spectroscopy of Extragalactic Objects" supported by the Ministry of Science, Technologies and Development of Serbia.

References

Bao, G., Hadrava, P., Ostgaard, E.: 1994, *Astrophys. J.*, **435**, 55.
Bian, W., Zhao, Y.: 2002, *Astron. Astrophys.*, **395**, 465.
Bromley, B.C., Chen, K., Miller, W.A.: 1997, *Astrophys. J.*, **475**, 57.
Chartas, G., Agol, E., Eracleous, M., Garmire, G., Bautz, M.W., Morgan, N.D.: 2002, *Astrophys. J.*, **568**, 509.
Čadež A., Fanton, C., Calvani, M.: 1998, *New Astronomy*, **3**, 647.
Dai, X., Chartas, G., Agol, E., Bautz, M.W., Garmire, G.P.: 2003, *Astrophys. J.*, **589**, 100.
Fanton, C., Calvani, M., Felice, F., Čadež, A.: 1997, *Publ. Astron. Soc. Japan*, **49**, 159.
Jovanović, P., Popović, L.Č., Mediavilla, E., Muñoz, J.A.: 2003, *Astron. Astrophys.*, in preparation.
Manners, J., Almaini, O., Lawrence, A.: 2002, *Mon. Not. Roy. Astron. Soc.*, **330**, 390.
Marshall, N., Warwick, R.S., Pounds, K.A.: 1981, *Mon. Not. Roy. Astron. Soc.*, **194**, 987.
Narayan, R., Bartelmann, M.: 1999, *Formation of Structure in the Universe* (Eds. A. Deker, J.P. Ostriker), Cambridge University Press, 360.
Oshima, T., Mitsuda, K., Fujimoto, R., Iyomoto, N., Futamoto, K., et al.: 2002, *Astrophys. J.*, **563**, L103.
Popović, L.Č., Mediavilla, E.G., Jovanović, P. and Muñoz, J.A.: 2003, *Astron. Astrophys.*, **398**, 975.
Shalyapin, V.N., Goicoechea, L.J., Alcalde, D., Mediavilla E., Muñoz J.A., Gil-Merino, R.: 2002, *Astrophys. J.*, **579**, 127.
Takahashi, R., Yonehara, A., Mineshige, S.: 2001, *Publ. Astron. Soc. Japan*, **53**, 387.
Turner, T.J., George, I.M., Nandra, K., Turcan, D.: 1999, *Astrophys. J.*, **524**, 667.
Zakharov, A.F., Popović, L.Č., Jovanović, P.: 2003, *Astron. Astrophys.*, submitted.

Publ. Astron. Obs. Belgrade No. 76 (2003), 211-214 *Contributed paper*

PEAK PARAMETERS DETERMINATION USING FRACTIONAL DERIVATIVE SPECTROMETRY

S.S. KHARINTSEV, M.Kh. SALAKHOV

Department of Physics, Kazan State University
Kremlevskaya str., 16, Kazan, Russia, 420008
E-mail: red@ksu.ru, msalakh@ksu.ru

Abstract. In this paper we propose a simple mathematical tool in terms of fractional derivative spectrometry (DS) to determine the overlapping bands spectral parameters. It is possible due to several positive effects of DS connected with the behavior of its zero-crossing and maximal amplitude. For acquiring a stable and unbiased FD estimate we utilize the statistical regularization method. Along with the well-known distributions such as Lorentzian, Gaussian and their linear combinations the Tsallis distribution is used as a model to correctly indentify overlapped bands.

The derivative spectrometry (DS) method is a simple and attractive instrument in analytical spectroscopy that provides a score of positive effects such as separating overlapping peaks, background noise suppression. It is possible due to the considerable increase in contrast to the derivative spectrum compared to original one. Even small changes of monotonicity in the initial spectrum are clearly recorded by its derivatives. Traditionally, DS has been successfully applied to the determination of a number of completely unresolved peaks and their positions (Salakhov and Kharintsev, 2001).

However, the application of integer-order derivatives is not always sufficient, since shapes of n-th and $(n+1)$-th differentiation curves are not close to each other in a qualitative sense and, therefore, some information on the data under study can be lost. On the other hand, as the differentiation order increases a high-frequency color noise amplifies strongly, so that the signal-to-noise ratio decreases sharply. This circumstance does not allow to utilize higher order derivatives for studying spectra. In order to weaken these restrictions and to make DS more flexible for processing and interpretation of the data it is necessary to generalize the DS method for non-integer (fractional) orders, that will be refered to as *fractional* derivative spectrometry (FDS). A fractional derivative (FD) provides information "gain" allowing one to follow the smooth variation in the analyzed data (Schmitt, 1998; Salakhov and Kharintsev, 2001). This redundancy can be rather useful when studying the behavior of non-simple points, for example, zero-crossing, extremum value, etc.

This paper demonstrates some effects of FD to be used to extract such spectral parameters as half-width, amplitude, shape, etc. and for further assigning overlapping peaks. Here we will not concern the determination of a number of individual components and their positions that have been the subject of intensive study (Salakhov and Kharintsev, 2001).

Traditionally, we will use the finite-difference expression known as Grunwald and Letnikov formulation of FD (Oldham and Spanier, 1974; Miller and Ross, 1993)

$$D_c^{\nu}\left[f\left(x\right)\right] \equiv \frac{d^{\nu} f\left(x\right)}{d\left(x-c\right)^{\nu}} = \lim_{N\to\infty} \Delta x_N^{-\nu} \sum_{k=0}^{N-1} c_k^{\nu}\ f\left(x-k\Delta x_N\right), \qquad (1)$$

$$c_k^{\nu} = \frac{\Gamma\left(k-\nu\right)}{\Gamma\left(-\nu\right)\Gamma\left(k+1\right)},$$

where ν is a fractional exponent ($-\infty < \nu < \infty$), N is a number of samples, $\Delta x_N = \left(x-c\right)/N$, x variation range: $c \le x < \infty$.

In order to demonstrate the effects of FD let us consider the ordinary Gaussian peak centered at $\overline{x}$ with a half-width of σ and amplitude of A: $G(x) = A\exp\left[-\left(x-\overline{x}\right)^2 \big/ 2\sigma^2\right]$. Figure 1 shows variation of the Gaussian contour during its differentiation at different ν values as an example of applying the FD operator to spectral curves. The dynamics of a zero-crossing point is indicated with circles in Fig. 1. The peak parameters were $\overline{x} = 0$, $A = 1$ and $\sigma = 0.1$. A number of samples was equal to 200.

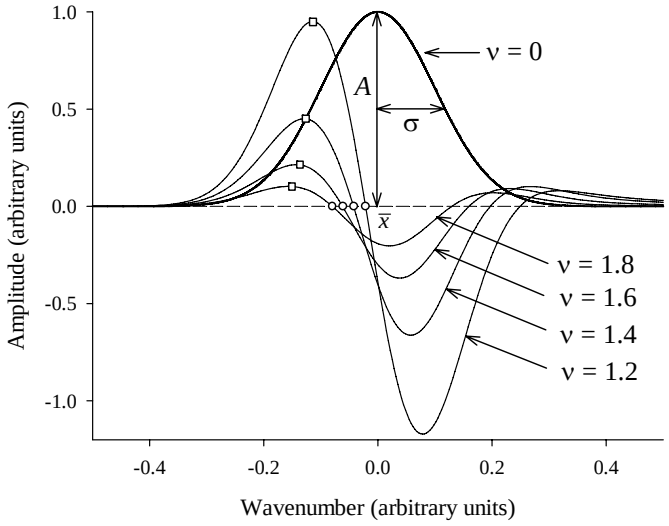

Fig. 1: Fractional derivatives of a Gaussian peak at various ν.

Interested in studying the behavior of the zero-crossing we need to solve the following equation

$$D^{\nu}\left[G(x)\right]\Big|_{x=x_0} = 0. \qquad (2)$$

Thus, we obtain the zero-crossing $x_0(\nu)$ as a function of ν:

$$x_0(\nu) = \bar{x} - (\nu - 1)\sigma. \tag{3}$$

From the obtained linear dependence such parameters as a position $\bar{x}$ and a half-width σ can be easily evaluated. This procedure will be referred to as estimator I.

The next step is to study the behavior of a maximal value of FD indicated by square boxes in Fig. 1. The position of this point $x_{\max}$ can be found by solving the equation

$$D^{1+\nu}\left[G(x)\right]\Big|_{x=x_{\max}} = 0. \tag{4}$$

Table 1. Estimators I^{*} and II^{**} for some types of distributions (see text).

	Gaussian	Lorentzian	Tsallis
	$A\mathrm{e}^{-\frac{(x-\bar{x})^2}{2\sigma^2}}$	$\frac{A}{(x-\bar{x})^2+\sigma^2}$	$A\left[1+\frac{q-1}{3-q}\cdot\frac{(x-\bar{x})^2}{\sigma^2}\right]^{-\frac{1}{q-1}}$
$x_0(\nu)^{*}$	$\bar{x}-(\nu-1)\sigma$	$\bar{x}-\frac{(\nu-1)}{\sqrt{3}}\sigma$	$\bar{x}-(\nu-1)\frac{\left(2q+3-q^2\right)^{1/2}}{(1+q)}\sigma$
$H(\nu)^{**}$	$\ln[F(\nu)]-\ln(\nu)$	$\ln[F(\nu)]-(3/2)\ln(\nu+2)$	$\ln[F(\nu)]+\frac{q}{q+1}\ln(\nu q-\nu+1)$
a	$-\ln(\sigma)-1$	$-\ln(\sigma)-\ln(2)$	$-\ln(\sigma)-\frac{1}{2}\ln(3-q)+\ldots$ $\ldots+\frac{3}{2}\ln(1+q)-\ln(2q-1)$
b	$\ln(A)+1/2$	$-2\ln(2)-2\ln(\sigma)+\ln(A)$	$\ln(A)-\frac{2-q}{q-1}\ln(1+q)+\ldots$ $\ldots+\frac{1}{q-1}\ln(2)-\ln(2q-1)$

After that we derive the maximal amplitude

$$F(\nu) \equiv D^{\nu}\left[G(x_{\max})\right] = A\nu\sigma^{-\nu}\,\mathrm{e}^{-(\nu-1/2)} \tag{5}$$

which contains the parameters of A and σ. It is convenient to linearize this relationship. After not complicated manipulations we rewrite Eq. (5) as:

$$H(\nu) = a\nu + b, \tag{6}$$

where we introduced the following denotations: $H(\nu) = \ln\left[F(\nu)\right] - \ln(\nu)$, $a = -\ln(\sigma) - 1$ and $b = \ln(A) + 1/2$. The magnitudes of a and b represent a slope and intercept, respectively. Note that these formulas are valid for the Gaussian peak only. We can interpret the magnitude of $H(\nu)$ as an eigencoordinate of a Gaussian peak. This approach will be referred to as estimator II. In contrast to estimator I, this permits to extract both the amplitude and the half-width.

Finally, we have two estimators based on features of FD that allow to determine, at least, the half-width in an independent way. There is no preference between them while a peak shape is *a priori* known. Otherwise the using of both is required.

By analogy with above stated, we can describe the behavior of nonsimple points for a peak having an arbitrary shape. In table 1 some types of distributions are considered. In particular, outputs of the estimators for the Tsallis (1999) distribution are given. In our case this approach enables to generalize the well-known distributions such as Gaussian and Lorentzian ones by varying a nonextensivity parameter q in the range of $0 < q < 3$. The Tsallis distribution recovers these when $q = 1$ and $q = 2$, respectively.

Tt was difficult before to say about a peak shape without additional research. Conventional nonlinear fitting methods based on the OLS approach are unsuitable to unambiguously assign the overlapped peaks. This implies that a composite band can be decomposed into elementary components of a given shape with the same integral reconstruction error in a large number of ways.

To avoid this uncertainty we suppose to use both the estimators in order to identify a peak shape in such a way that the half-widths obtained by these coincide. This fitness is accomplished by varying the nonextensivity parameter q in the range of $q \in [0,3]$. In the case of lack of coincidence for any q we conclude that the Tsallis model is unsuitable to fit the overlapping peaks.

Acknowledgment. This work has been supported by the CRDF (REC 007).

References

Miller, K.S., Ross, B.: 1993, *An Introduction to the Fractional Calculas and Fractional Differential Equations*, John Wiley & Sons, Inc.

Oldham, K., Spanier, J.: 1974, *The Fractional Calculus: Theory and Applications of Differentiation and Integration to the Arbitrary Order*, Academic Press, New York.

Salakhov, M.Kh., Kharintsev, S.S.: 2001, *Mathematical Processing and Interpretation of Spectroscopic Measurements*, Ed. Kazan St. Univ., Kazan, in Russian.

Schmitt J.M.: 1998, *Appl. Spectrosc.*, **52**, 840.

Tsallis, C.: 1999, *Brazilian J. Phys.*, **29**, 1.

Publ. Astron. Obs. Belgrade No. 76 (2003), 215-220 *Contributed paper*

IMPORTANCE OF COLLISIONS WITH CHARGED PARTICLES FOR STELLAR UV LINE SHAPES: Cd III

N. MILOVANOVIĆ, M.S. DIMITRIJEVIĆ, L.Č. POPOVIĆ, Z. SIMIĆ

Astronomical Observatory, Volgina 7, 11160 Belgrade, Serbia
E-mail: nmilovanovic@aob.bg.ac.yu, mdimitrijevic@aob.bg.ac.yu, lpopovic@aob.bg.ac.yu, zsimic@aob.bg.ac.yu

Abstract. Stark broadening parameters, widths and shifts, for 84 spectral lines of the doubly-ionized Cadmium (Cd III) have been calculated using modified semiemprical approach (MSE). Influence of collisions with charged particles on Cd III UV stellar lines along HR diagram has been discussed. Compared to the Doppler broadening, influence of Stark broadening mechanism is more important for deeper atmospheric layers and for larger values of log *g*. Influence of the Stark widths for standard models of DA and DB white dwarfs has been also discussed.

1. INTRODUCTION

Spectral lines of multiply charged heavy elements are present in the UV spectra of early-type stars, especially in spectra of chemically peculiar (CP) ones. Investigation of these lines is important for example for spectral lines synthesis, diagnostics and modelling of laboratory and stellar plasma, abundance determination and opacity calculation.

Stark broadening of spectral lines is the dominant pressure broadening mechanism in hot, early-type, stars and white dwarf atmospheres. Spectral lines of Cd I and Cd II are observed in stellar spectra of some CP stars, as e.g. χ Lupi (Leckrone *et al.,* 1999), so that Cadmium in various ionization stages is present in stellar atmospheres. With the development of space born telescopes, spectral instruments like Goddard High Resolution Spectrograph (GHRS) on Hubble Space Telescope provide good resolution spectra of stellar objects so that the need for trace element data, like Cadmium, increases.

2. METHOD OF CALCULATION AND RESULTS

Advanced calculation of the Stark broadening parameters using strong-coupling quantum-mechanical method (Baranger, 1958abc; Kolb and Griem, 1958; Griem, 1974; Dimitrijević *et al.,* 1981; Seaton, 1988; Ralchenko *et al.,* 1999; Zeng-xin *et al.,* 1999) are so complicated that only limited number of data for spectral lines originating from low laying transitions can be calculated in an adequate way. On the other hand, semiclassical method (Sahal-Bréchot, 1969ab; Dimitrijević *et al.,* 1991; see also a review of obtained results in Dimitrijević, 1997) need a set of large number of atomic data, energy levels and oscillator strengths. This method is not applicable in adequate way to the Stark broadening calculation of Cd III because there is no sufficient number of reliable atomic data.

We used the modified semiempirical approach (MSE, Dimitrijević and Konjević, 1980, Dimitrijević and Kršljanin, 1986). The accuracy of the MSE calculations for spectral line widths is around $\pm 50\%$ (Dimitrijević and Konjević, 1980). Error in obtained shifts with MSE calculations is within $\pm 50\%$ of the corresponding widths value.

Doubly-ionized cadmium (Cd III) belongs to Palladium isoelectronic sequence with the ground state electronic configuration $4d^{10}\ ^1S_0$ and ionization potential of 302200 ± 50 cm^{-1}. Atomic data needed for our MSE calculation were taken from Van Kleef *et al.* (1980). They observed Cd III spectra in UV spectral range from 50 to 210 nm with 6.65 and 10.7 meters normal-incidence vacuum spectrograph. Experimental values of energy levels were checked with the least-square level fitting of Hartee-Fock (HF) calculations of atomic parameters. They give more complete analysis of energy level values compared to the first observed spectra of Cd III presented in paper of Shenstone and Pittenger (1949). Van Kleef *et al.* (1980) estimated that the energy levels error for sharp lines is ± 0.5 cm^{-3} and several cm^{-3} for strong and asymmetric lines.

Even if coupling schemes slowly go from LS to jj coupling as we go throughout the isoelectronic sequence from Pd I to Sn V, most of energy levels, without loosing accuracy, can be represented with LS coupling (Van Kleef *et al.,* 1980). Consequently LS coupling scheme is adopted here.

The calculated Stark widths and shifts of Cd III spectral lines for 84 spectral lines, whereat 22 belong to $4d^9\ 5s–4d^9\ 5p$ and 62 to $4d^9\ 5p–4d^9\ 5d$ transition are given in Milovanović *et al.* (2003).

3. DISCUSSION

Behavior of Stark and Doppler spectral line widths in stellar atmospheres were calculated for Cd III $5p\ ^3F^o_3 – 5d\ ^3G_3$ (λ=144.754 nm), a strong spectral line in various atmospheric models. These calculations were performed for solar element abundance atmospheric models given in Kurucz (1979) and Kurucz's web site (http://kurucz.harvard.edu). Each model is characterized by the effective temperature $T_{\rm eff}$, logarithm of gravity log g and turbulent velocity v_t and each atmospheric layer within the model is characterized by electron density N and temperature T.

In hot stars atmospheres besides electron-impact broadening (Stark broadening) the important broadening mechanism is Doppler (thermal) one as well as the broadening due to the turbulence and stellar rotation. Other types of spectral line broadening, as Van der Waals, resonance and natural broadening, are usually negligible.

Importance of Stark broadening in hot stars atmospheres is illustrated in Figs. 1-3. In Fig. 1 Stark (FWHM) and Doppler widths for Cd III $5p\ ^3F^o_3 – 5d\ ^3G_3$ (λ=144.754 nm) spectral line as a function of atmospheric layer temperatures are shown. Stark widths are shown for 8 atmospheric models with effective temperatures $T_{\rm eff}$=7000 - 30000 K, corresponding to spectral classes (Sp) from F0 to B0, logarithm of surface gravity log g=4 and turbulent velocity v_t=0 km/s. In Fig. 1 one can see that Stark widths are larger than Doppler ones for stars with lower effective temperatures. For stars with higher effective temperatures Stark broadening is more important than Doppler one for deeper atmospheric layers (higher layer temperature T). For example, for stars with effective temperature $T_{\rm eff}$=30000 K (B0 stars) Stark and Doppler widths are equal for layer temperature $T \approx 35000$ K and for stars with $T_{\rm eff}$=7000 K (F0 stars) they are equal for $T \approx 5000$ K.

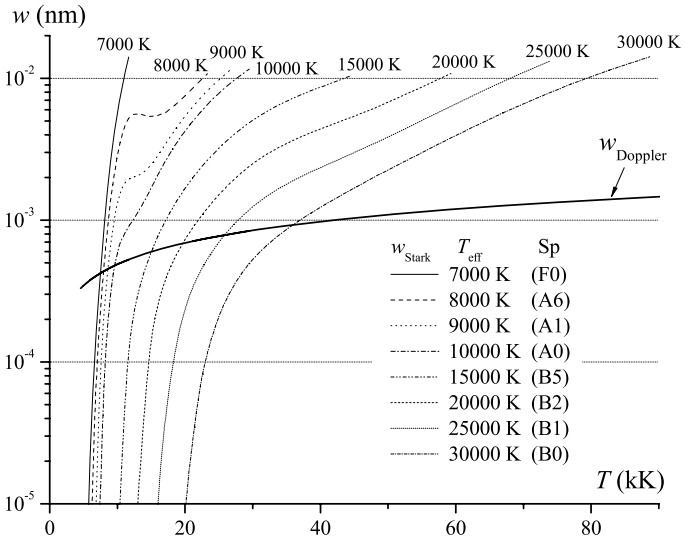

Fig. 1: Stark widths (FWHM) (thinner lines) and Doppler width (thicker line) for Cd III 5p $^3F^o_3$ – 5d $^3G_3$ (λ=144.754 nm)spectral line as a function of atmospheric layer temperatures. Stark widths are shown for 8 atmospheric models with effective temperatures $T_{\rm eff}$ =7000 - 30000 K, corresponding to spectral classes (Sp) from F0 to B0, log g=4 and turbulent velocity v_t=0 km/s.

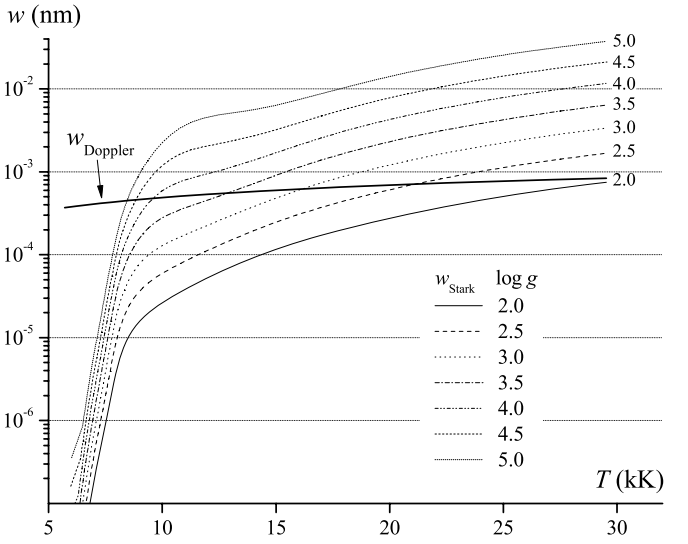

Fig. 2: Same as in Fig. 1 but Stark widths are shown for 7 values of model gravity log g= 2 - 5, $T_{\rm eff}$=10000 K and v_t=0 km/s.

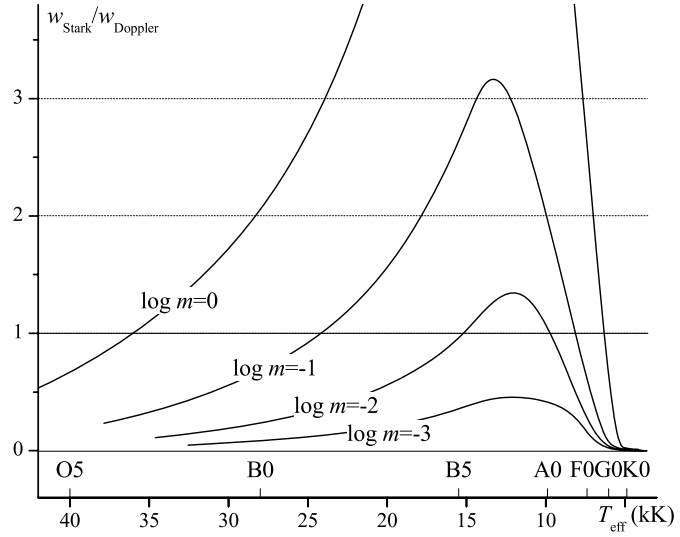

Fig. 3: Ratio of Stark and Doppler widths $w_{Stark}/w_{Doppler}$ as a function of the model effective temperature $T_{\rm eff}$ (upper part of horizontal axis is spectral class). Dependence is shown for 4 values of logarithm of the column mass at temperature minimum log m from 0 to -3, log g=4 and velocity v_t=0 m/s.

Dependence of Stark and Doppler broadening on atmospheric layer temperature for 7 values of surface gravity is shown in Fig. 2. Model used here has $T_{\rm eff}$ =10000 K and v_t=0 km/s. Stark broadening in stellar atmospheres with higher values of surface gravity is significantly larger than Doppler broadening. For stars with surface gravity log g=2 Stark broadening is comparable to Doppler widths only for deeper hot atmospheric layers. For upper parts of stellar atmospheres (T<10000 K) Stark widths rapidly decrease and for layer temperature T≈6000 - 7000 K Stark widths are several magnitudes lower than Doppler ones for all shown values of surface gravity log g.

Ratio of Stark and Doppler widths along Hertzsprung-Russell diagram, from K0 to O5 spectral class, and within the range of the column mass at temperature minimum log m from -3 up to 0 are shown in Fig. 3. In deeper parts of atmospheres, e.g. log m=0, Stark broadening is larger than Doppler one for stars of G, F, A and B spectral type. For log m=-3 (upper atmospheric parts) Doppler widths are comparable (approximately one-half) with Stark widths for spectral classes A0 to B5.

In order to compare Stark and Doppler broadening we have calculated spectral line widths for Cd III λ=144.754 nm for DA and DB white dwarfs atmospheres. Models were taken from Wickramasinghe (1972). DA dwarfs are helium and metal underabundant and DB white dwarfs are helium and metal overabundant compared to hydrogen.

As one can see in Figs. 4 and 5 Stark broadening is by one or two order of magnitudes higher than Doppler one. Consequently, with the increases of the pressure, electron density or effective temperature in DA and DB white dwarf models the importance of Stark broadening increases as well.

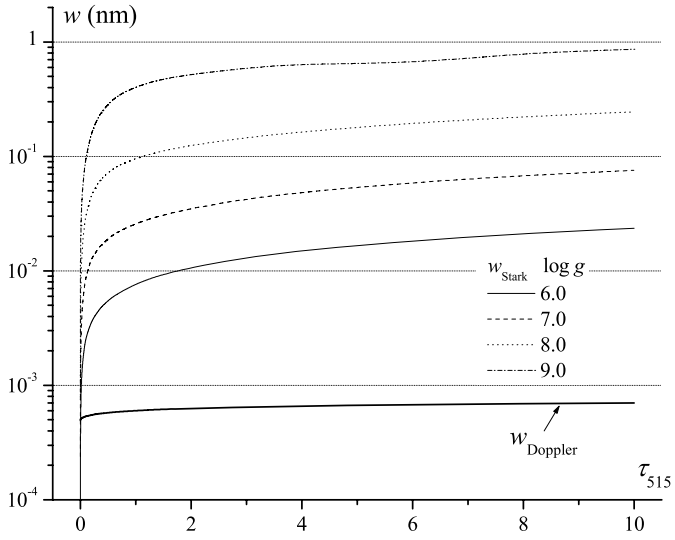

Fig. 4: Stark and Doppler widths for Cd III λ=144.754 nm spectral line as a function of optical depth for standard wavelength λ_{st}=505 nm for DA white dwarfs. Widths are given for 4 values of logarithm of surface gravity log g=6 - 9. Effective model temperature is $T_{\rm eff}$=10000 K.

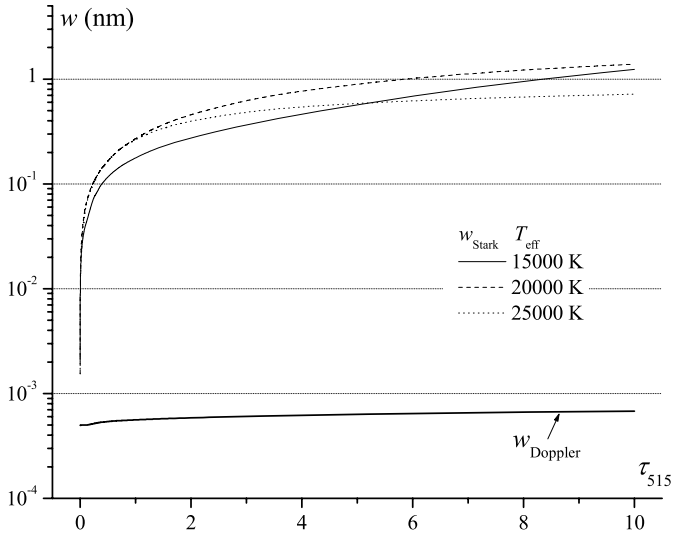

Fig. 5: Same as in Fig. 4 but for DB white dwarfs. Widths are given for $T_{\rm eff}$=10000, 20000 and 25000 K and log g=8.

Here we should mention that the comparison of Stark and thermal Doppler contributions to the line widths is calculated for one line of Cd III (λ=144.754 nm), and that we can expect a similar contribution of the Stark broadening for all UV Cd III lines. The contribution of the Stark effect to line widths increases with the principal quantum number (Vince and Dimitrijević, 1985) and also one should take into account that in some cases, due to close perturbing levels, Stark widths might also be large. In some cases the Stark broadening may significantly contribute to the line widths as well as to the line shapes (see e.g. Dimitrijević *et al.,* 2003, analogous results having been obtained from our similar investigations for Zr II and Zr III in Popović *et al.,* 2001a and Nd II in Popović *et al.,* 2001b).

Acknowledgements. This work is a part of the projects "Influence of collisional processes on astrophysical plasma lineshapes" (GA 1195) and "Astrophysical Spectroscopy of Extragalactic Objects" (GA 1196) supported by the Ministry of Science, Technologies and Development of Serbia.

References

Baranger, M.: 1958a, *Phys. Rev.*, **111**, 481.
Baranger, M.: 1958b, *Phys. Rev.*, **111**, 494.
Baranger, M.: 1958c, *Phys. Rev.*, **112**, 855.
Dimitrijević, M.S.: 1997, *Astrophys. Space Sci.*, **252**, 415.
Dimitrijević, M.S., Konjević, N.: 1980, *J. Quant. Spect. Rad. Transfer*, **24**, 451.
Dimitrijević, M.S., Kršljanin, V.: 1986, *Astron. Astrophys.*, **165**, 269.
Dimitrijević, M.S., Feautrier, N., Sahal-Bréchot, S.: 1981, *J. Phys.*, **B14**, 2559.
Dimitrijević, M.S., Sahal-Bréchot, S., Bommier, V.: 1991, *Astron. Astrophys. Suppl. Series*, **89**, 581.
Dimitrijević, M.S., Ryabchikova, T., Popović, L.Č., Shulyak, D., Tsymbal, V.: 2003, *Astron. Astrophys.*, **404**, 1099.
Griem, H.R.: 1974, *Spectral Line Broadening by Plasmas*, Academic Press, New York and London.
Kolb, A.C., Griem, H.R.: 1958, *Phys. Rev.*, **111**, 514.
Kurucz, R.L.: 1979, *Astron. Astrophys. Suppl. Series*, **40**, 1.
Leckrone, D.S., Proffitt, C.R., Wahlgren, G.M., Johansson, S.G., Brage, T.: 1999, *Astron. J.*, **117**, 1454.
Milovanović, N., Dimitrijević, M.S., Popović, L.Č., Simić, Z.: 2003, *Astron. Astrophys.*, submitted.
Popović, L.Č., Milovanović, N., Dimitrijević, M.S.: 2001a, *Astron. Astrophys.*, **365**, 656.
Popović, L.Č., Simić, S., Milovanović, N., Dimitrijević, M.S.: 2001b, *Astrophys. J. Suppl. Series*, **135**, 109.
Ralchenko, Yu.V., Griem, H.R., Bray, I., Fursa, D.V.: 1999, *Phys. Rev. A*, **59**, 1890.
Sahal-Bréchot, S.: 1969a, *Astron. Astrophys.*, **1**, 91.
Sahal-Bréchot, S.: 1969b, *Astron. Astrophys.*, **2**, 322.
Seaton, M.J.: 1988, *J. Phys. B*, **21**, 3033.
Shenstone, A.G., Pittenger, J.T.: 1949, *J. Opt. Soc. Am.*, 39, 219.
Van Kleef, Th.A.M., Joshi, Y.N., Uijlings, P.: 1980, *Phys. Scr.*, **22**, 353.
Vince, I., Dimitrijević, M.S.: 1985, *Publ. Obs. Astron. de Belgrade*, **33**, 15.
Wickramasinghe D. T.: 1972, *Mem. R. Astron. Soc.*, **76**, 129.
Zeng-xin, Z., Jian-min, Y., Yong-sheng, S.: 1999, *Chin. Phys. Lett.*, **16**, 885.

Publ. Astron. Obs. Belgrade No. 76 (2003), 221 - 224 *Contributed paper*

DIAGNOSTIC OF PHYSICAL CONDITIONS IN AGN BROAD EMISSION LINE REGIONS

L.Č. POPOVIĆ[1,2], G. RICHTER[2]

[1] *Astronomical Observatory, Volgina 7, 11160 Belgrade 74, Serbia*

[2] *Astrophysikalisches Institut Potsdam, An der Sternwarte 1, D-14482 Potsdam, Germany*

Abstract. Using a well known method for laboratory plasma diagnostic, the Boltzmann-plot, we discuss the physical properties in Broad Line Region (BLR) of Active Galactic Nuclei (AGNs). We apply the Boltzmann-plot method to Balmer lines on a sample of 14 AGN, finding that it may indicate the existence of "Case B" recombination or Partial Local Thermodynamical Equilibrium (PLTE).

1. INTRODUCTION

The emission lines of Active Galactic Nuclei (AGN) are produced over a wide range of distances from the central continuum source, and under a wide range of physical and kinematical conditions (see Osterbrock, 1989; Krolik, 1999 and references therein). The line strengths, their widths and shapes are powerful tools for emitting gas diagnostics in different parts of the emitting region of an AGN. The physics in the Broad Line Region (BLR) is more complicated than in the Narrow Line Region (NLR). The photoionization, recombination and collisions can be considered as relevant processes in BLRs.

Different types of the physical conditions and processes can be assumed in order to use the emission lines for diagnostic of emission plasma (Osterbrock, 1989; Griem, 1997; Ferland et al., 1998). Although "in many aspects the BLRs are physically as closely related to stellar atmospheres as traditional nebula" (Osterbrock, 1989), the plasma in the BLR probably does not come close to being in complete Local Thermodynamical Equilibrium (LTE). However, there may still be the Partial Local Thermodynamical Equilibrium (PLTE) in the sense that populations of sufficiently highly excited levels are related to the next ion's ground state population by Saha-Boltzmann relations, or to the total population in all fine-structure levels of the ground-state configuration (see Griem, 1968, 1997).

The aim of this work is to test the existence of PLTE, and discuss the possibility of estimation of the relevant physical processes and plasma parameters in BLRs using the Boltzmann-plot of Balmer lines.

2. THEORETICAL REMARKS

As a simple case let us consider the optically thin plasma. In the case of plasma of the length ℓ along the line of sight, spectrally integrated emission line intensity (I_{lu}) is given as (see e.g. Griem, 1997; Konjević, 1999)

$$I_{lu} = \frac{hc}{\lambda} g_u A_{ul} \int_0^{\ell} N_u dx \approx \frac{hc}{\lambda} A_{ul} g_u \ell \frac{N_0}{Z} \exp(-E_u/kT_e), \quad (1)$$

where λ is transition wavelength, g_u statistical weight of the upper level, A_{ul} transition probability, Z the partition function, N_0 the total number density of radiating species, E_u the energy of the upper level, T_e electron temperature and h, c, k are the well known constants (Planck, speed of light and Boltzmann constant, respectively).

If the plasma is in PLTE, the population of the parent energy states belongs to a Boltzmann distribution uniquely characterized by their excitation temperature (T_e in Eq. (1)), and this temperature may be obtained from a Boltzmann-plot when the transitions within the same spectral series are considered

$$\log(I_n) = \log \frac{I_{ul} \cdot \lambda}{g_u A_{ul}} = B - AE_u, \quad (2)$$

where I_{lu} is relative intensity of transition from upper to lower level ($u \rightarrow l$), B and A are constants, while A indicates temperature and we will call it the temperature parameter.

If we can approximate the $\log(I_n)$ as a linear decreasing function of E_u then: a) it indicates that PLTE may exist at least to some extent in the BLR; b) if PLTE is present, the population belonging to a Boltzmann distribution is uniquely characterized by its excitation temperature. Then we can estimate the electron temperature from Eq. (2), $T_e = 1/(kA)$, where $k = 8.6171 \cdot 10^{-5}$eV/K is the Boltzmann constant; c) if PLTE is present we can roughly estimate the minimal electron density in BLR. Here, we should mention that "Case B" recombination of Balmer lines can bring the $\log(I_n)$ *vs* E_u as linear decreasing function (Osterbrock, 1989). But, regarding the physical conditions (electron densities and temperatures) in BLRs in this case the constant A is too small ($A < 0.2$) and the Boltzmann-plot cannot be applied for diagnostics of electron temperature even if PLTE exists (see discussion in Sec. 4). Moreover, in this case Boltzmann-plot method can be used as an indicator of "Case B" recombination in BLRs of some AGN.

Taking into account that the Balmer lines originate from the same series, we can use the Boltzmann-plot relation for testing the existence of PLTE or "Case B" recombination. Also, here we should mention that we will assume that ℓ, the length of the Balmer line formation region, is the same for all Balmer lines.

3. REDUCTION OF THE DATA

In order to test the existence of PLTE in BLR, we use HST observations obtained with the Space Telescope Imaging Spectrograph (STIS) and Faint Object Spectrograph (FOS), covering the wavelength ranges 2900-5700 Å and 6295-6867 Å (rest wavelength). From the very large data base of AGN spectra at HST archive we selected the objects using following selection criteria: a) the observations covered the

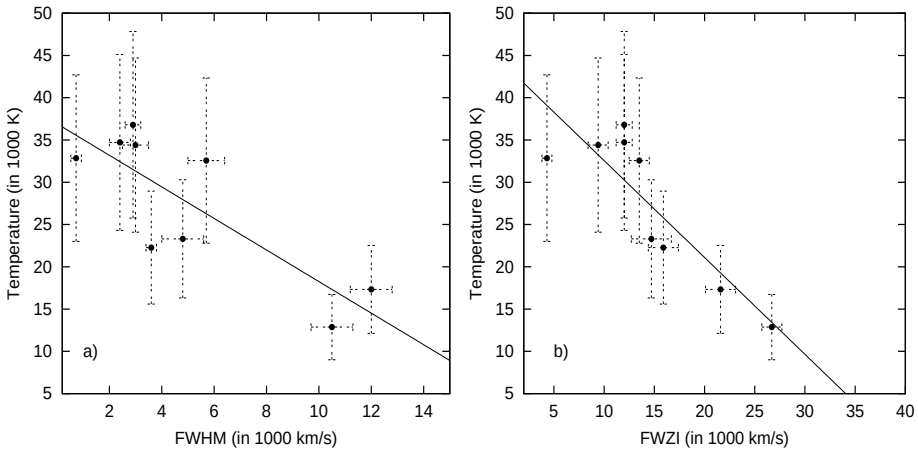

Fig. 1: The measured electron temperature using by Boltzmann-plot (only for the AGN where A$>$ 0.3 indicates the PLTE presence) as a function of velocities measured at: a) Full Width at Half Maximum; b) Full Width at Zero Intensity of an averaged profile from Hα and Hβ ones.

Balmer series line wavelength region; b) the observations were performed on the same day; c) all the lines from Balmer series can be recognized and all have relatively well defined shapes; d) we considered only low red-shifted objects.

The spectra were reduced by the HST team. We transformed the wavelength scale to zero red-shift taking into account the cosmological red-shift of the objects (Véron-Cetty and Véron, 2000). Thereafter that we estimated and subtracted the continuum. Estimated error of 5% - 10% due to subtraction of the continuum is included in the cumulative error. The fluxes of the lines were measured by using the DIPSO software.

To perform a test we subtracted the narrow and satellite lines from Balmer lines. To estimate the contribution of these lines we used a multi-Gaussian analysis (see Popović 2003).

On the other hand, the reddening effect can influence the Balmer lines ratio (see e.g. Crenshaw and Kraemer, 2001; Crenshaw et al., 2002 and references therein) and consequently temperature parameter obtained by Boltzmann-plot. Here the Galactic reddening was taken into account using the data from NASA's Extragalacitc Database (NED). In order to test the total (Galactic + intrinsic) reddening influence we have considered the case of Akn 564, where the reddening data are given by Crenshaw et al. (2002). We estimated that the reddening effect can contribute to the Boltzmann-plot slope around 30%-40% .

4. RESULTS

Using the fact that the Balmer lines belong to the same spectral series, we apply the Boltzmann-plot method to test the presence of PLTE in BLR and discuss the relevant physical processes in a sample of 14 AGN. The more detailed discussion will be given in Popović (2003), here we give the main conclusions from this test:

1) From the 14 selected AGN, we found that in 9 AGN Boltzmann-plot indicated

the existence of PLTE in BLR, while in the case of 4 of them the Boltzmann-plot indicated "Case B" recombination in BLR. In remaining 1 AGN the Boltzmann-plot cannot be applied.

2) The estimated BLR electron temperatures using Boltzmann-plot where PLTE exists are within a range (1.3 - 3.7)·10^4 K (within 30% accuracy). They are in good agreement with the previous estimations.

The electron densities in BLR have been considered for optically thin and optically thick plasma and we found that:

i) For optically thin plasma, the electron density in the case of PLTE, at least in some parts of BLR, should be higher than conventionally accepted for BLR.

ii) For optically thick plasma, the electron density in the case of PLTE is in agreement with the one conventionally accepted for BLR.

On the other hand, the electron temperatures estimated by using Boltzmann-plot tend to be velocity dependent as a linear decreasing function of random velocities measured at FWHM as well as at FWZI (see Fig. 1).

Although, an alternative of PLTE in some AGN may be very high intrinsic reddening effect, the Boltzmann-plot method may be used for fast insight into physical processes in BLR of an AGN prior to applying more sophisticated physical models.

Acknowledgments. This work was supported by the Ministry of Science, Technologies and Development of Serbia through the project "Astrophysical Spectroscopy of Extragalacitc Objects". Also, the work was supported by Alexander von Humboldt Foundation through the program for foreign scholars. We thank Prof. S. Djeniže, Prof. M.S. Dimitrijević and Prof. N. Konjević for useful discussion and suggestions.

References

Crenshaw, D.M., Kraemer, S.B.: 2001, *Astrophys. J.*, **562**, L29.

Crenshaw, D.M., Kraemer, S.B., Bruhweiler, F.C., Ruiz, J.R.: 2001, *Astrophys. J.*, **555**, 633.

Ferland, G.J., Korista, K.T., Verner, D.A., Ferguson, J.W., Kingdon, J.B., Verner, E.M.: 1998, *Publ. Astr. Soc. Pacific*, **110**, 761.

Griem, H.R.: 1968, *Plasma Spectroscopy*, McGraw-Hill, New York.

Griem, H.R.: 1997, *Principles of Plasma Spectroscopy*, University of Maryland at College Park, Cambridge University Press.

Konjević, N.: 1999, *Phys. Reports*, **316**, 339.

Krolik, J.H.: 1999, *Active Galactic Nuclei: From the Central Black Hole to the Galactic Environment*, Princeton University Press, Princeton, New Jersey.

Osterbrock, D.E.: 1989, *Astrophysics of Gaseous Nebulae and Active Galactic Nuclei*, Mill Valle, University Science Press.

Popović, L.Č.: 2003, *Astrophys. J.*, accepted (astro-ph/0304390).

Véron-Cetty, M.-P., Véron, P.: 2000, *A Catalogue of Quasars and Active Galactic Nuclei*, Sci. Report 19.

Publ. Astron. Obs. Belgrade No. 76 (2003), 225 - 228 *Contributed paper*

EXPERIMENTAL STARK SHIFTS IN THE F II 3s' - 3p' TRANSITION

A. SREĆKOVIĆ, S. BUKVIĆ

Faculty of Physics, University of Belgrade,
Studentski trg 14, 11 000 Belgrade, P.O.B. 368, Serbia
E–mail: srecko@ff.bg.ac.yu

Abstract. Stark shifts (d) of four singly ionized fluorine (F II) spectral lines (410.917 nm, 354.177 nm, 429.918 nm and 320.274 nm) in $2p^3 3s'$ – $2p^3(^2D^0)3p'$ transition have been measured in a linear, low–pressure, pulsed arc discharge created in SF6 plasma at 33 600 K electron temperatures and at 2.80×10^{23} m^3 electron densities. The measured Stark widths are compared with the existing experimental values.

1. INTRODUCTION

Atomic data such as Stark shift (d) are useful for plasma diagnostical purposes in a wide range of electron temperatures (T) in the case of astrophysical and laboratory plasmas. Three experiments (Platiša el al., 1977; Djeniže et al., 1991; Blagojević et al., 1999), known to the authors (Lesage and Fuhr, 1999; Konjević at al., 2002), have dealt with investigations of Stark broadening parameters (widths and shifts) of singly ionized fluorine lines. Only one experiment (Djeniže et al., 1991) has dealt with investigations of Stark shift of singly ionized fluorine lines. No calculated F II d values for 3s'-3p' transition existing, to the knowledge of the authors. The aim of this paper is to present the measured Stark shifts values at 33 600 K electron temperatures and at 2.80×10^{23} m^3 electron densities for 4 F II spectral lines belonging to the $2p^3 3s'$ – $2p^3(^2D^0)3p'$ transition. The measured Stark shifts are compared with existing experimental values.

2. EXPERIMENT

The linear, low–pressure, pulsed arc used as a plasma source, operated in SF_6, was described in detail in earlier publications (Djeniže et al., 1992, 2002; Srećković et al., 2001ab). Applied experimental set–up system, recording procedure and diagnostics methods are presented in our earlier publication (Djeniže et al., 2002). Here we present only necessary information related to the plasma parameters considered in this paper. Stark shift data (d) are taken at electron temperature T = 33 600 K and electron density $N = 2.80 \times 10^{23}$ m^3.

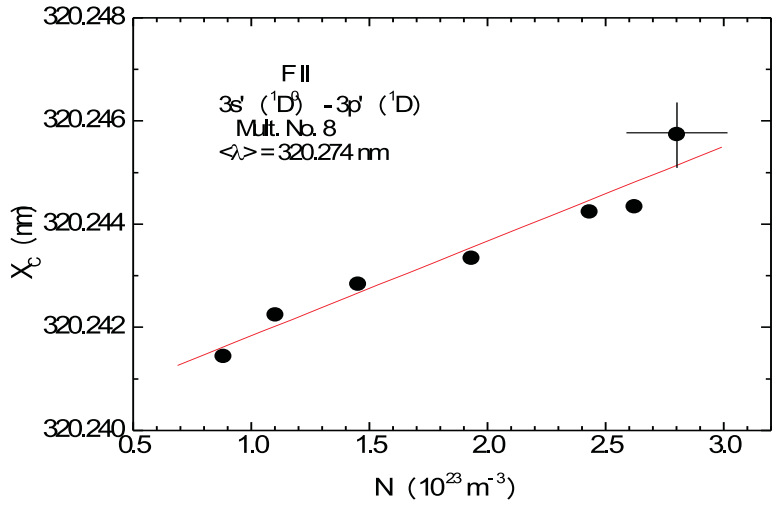

Fig. 1: The observed line center (X_C) position dependence on the electron density (N) during the plasma decay

3. STARK SHIFT MEASUREMENT

The measured profiles were of the Voigt type due to the convolutions of the Lorentzian Stark and Gaussian profiles caused by Doppler and instrumental broadening. For the electron density and temperature presented in our experiment, the Lorentzian fraction was dominant. Van der Waals (Griem, 1974) and resonance (Griem, 1974) broadening were estimated to be smaller by more than one order of magnitude in comparison to Stark, Doppler and instrumental broadening. The standard deconvolution procedure (Davies and Vaughan, 1963) has been computed using the least squares algorithm.

The Stark shifts were measured relative to the unshifted spectral lines emitted by the same plasma using a method established and applied first by Purić and Konjević (1972). According to that method the Stark shift of a spectral line can be measured experimentally by evaluating the position of the spectral line center (X_C) recorded at different electron density values during plasma decay (Srećković et al., 2000). In principle, the method requires recording of the spectral line profile at the higher electron density (N_1) that causes an appreciable shift and then, latter, when the electron concentration has dropped to a value (N_2) lower by at least an order of magnitude. The difference of the line center position in these two cases is Δd, so that the shift d_1 at the higher electro density N_1 is

$$d_1 = N_1 \Delta d/(N_2 N_1). \quad (1)$$

Our Stark shift values have been obtained for line center positions corresponding to the 15^{th} μs and 45^{th} μs after the beginning of the discharge. The observed line

Table 1: Our measured Stark shifts values (d_m in pm) at a given N and T.

Emiter	*Transition*	*Multiplet*	λ (nm)	T (10^4 K)	N (10^{23} m^{-3})	d_m (pm)
F II	$2p^3 3s'$ – $2p^3(^2D^0)3p'$	$^3D^0$ – ^3D (5)	410.917	3.36	2.80	-1.8±1.2
		$^3D^0$ – ^3P (6)	354.177	3.36	2.80	-1.7±0.5
		$^1D^0$ – ^1F (7)	429.918	3.36	2.80	-0.6±1.6
		$^1D^0$ – ^1D (8)	320.274	3.36	2.80	5.0±0.6

center (X_C) position dependence on the electron density (N) during the plasma decay of investigated 320.650 nm F II spectral line, as an example, is presented in Fig. 1. The Stark shift data are corrected for the electron temperature decay (Popović et al., 1992). Stark shifts data are determined with ±0.8 pm error at a given N and T. Measured (d_m) Stark shifts are presented in Table 1.

4. RESULTS AND DISCUSSION

Our experimental Stark shifts (d_m) values at a given electron temperature (T) and density (N) are given in Table 1. The necessary atomic data were taken from NIST (2003).

The measured d_m values are generally negative and very small. The positive Stark shift values are obtained in the $^1D^0$ - ^1D multiplet . The positive shift is toward the red. Our measured Stark shift values agree well with earlier experimental data at 45 000 K (Djeniže et al., 1991) except in case of the multiplet No. 8. where our d values overvalue the earlier data.

Acknowledgments. This work is a part of project Determination of the atomic parameters on the basis of the spectral line profiles supported in part by the Ministry of Science, Technologies and Development of the Republic of Serbia.

References

Blagojević, B., Popović, M.V., Konjević, N.: 1999, *Physica Scripta*, **59**, 374.
Davies, J.I., Vaughan, J.M.: 1963, *Astrophys. J.*, **137**, 1302.
Djeniže, S., Labat, J., Srećković, A., Labat, O., Platiša, M., Purić, J.: 1991, *Physica Scripta*, **44**, 148.
Djeniže, S., Srećković, A., Labat, J.: 1992, *Astron. Astrophys.*, **253**, 632.
Djeniže, S., Srećković, A., Jelisavčić, M., Bukvić, S.: 2002, *Astron. Astrophys.*, 389, 1086.
Griem, H.R.: 1974, *Spectral Line Broadening by Plasmas*, Academic Press, New York.
NIST: 2003, *Atomic Spectra Data Base Lines* (Wavelengths ordered), http://www.physics.nist.gov.
Konjević, N., Lesage, A., Fuhr, J.R., Wiese, W.L.: 2002, *J. Phys. Chem. Ref. Data*, **31**, No. 3, 819.
Lesage, A., Fuhr, J.R.: 1999, *Bibliography of Atomic Line Shapes and Shifts* (April 1992 though June 1999), Observatoire de Paris.

Platiša, M., Dimitrijević, M.S., Popović, M., Konjević, N.: 1977, *Astron. Astrophys.*, **64**, 837.
Popović, L.Č., Srećković, A., Djeniže, S.: 1992, *Proceed. of the 11th ICSLS*, **A25**, Carry de Rouet, France.
Purić, J., Konjević, N.: 1972, *Z. Physik*, **249**, 440.
Srećković, A., Drinčić, V., Bukvić, S., Djeniže, S.: 2000, *J. Phys*, **33**, 4873.
Srećković, A., Dimitrijević, M.S., Djeniže, S.: 2001, *Astron. Astrophys.*, **371**, 354.
Srećković, A., Drinčić, V., Bukvić, S., Djeniže, S.: 2001, *Phys. Scripta*, **63**, 306.

Publ. Astron. Obs. Belgrade No. 76 (2003), 229 - 232 *Contributed paper*

MEASURED STARK SHIFTS OF SEVERAL Ar III SPECTRAL LINES

A. SREĆKOVIĆ, S. BUKVIĆ, S. KALEZIĆ

Faculty of Physics, University of Belgrade, POB 368, Serbia
E–mail: srecko@ff.bg.ac.yu

Abstract. Stark shifts of five doubly ionized argon (Ar III) spectral lines have been measured in 3d-4p and 3d-4p transitions in a mixture of Ar (72%) and He (28%) plasma created in the linear, low pressure, pulsed arc discharge at about 30 150 K electron temperature and 1.47 10^{23} m^3 electron density. They are the first published data in this field.

1. INTRODUCTION

Atomic data such as Stark shifts (d) are useful for plasma diagnostical purposes. The d values for the doubly ionized argon (Ar III) ions are poorly known. Only one work deals with their measurements (Kobilarov and Konjević, 1990). No calculated Ar III d values exist, to the knowledge of the authors (Lesage and Fuhr, 1999; Konjević et al., 2002). The aim of this work is to present 5 Ar III d values measured in optically thin argon-helium discharge. They are the first data in this field.

2. EXPERIMENT

The modified version of the linear low pressure pulsed arc (Djeniže et al., 2002ab; Srećković et al., 2000, 2001) has been used as an optically thin plasma source. A pulsed discharge was performed in a pyrex discharge tube of 5 mm inner diameter and plasma length of 14 cm. The working gas was Ar (72%) and He (28%) mixture at 130 Pa filling pressure in flowing regime.

The capacitor of 14 μF was charged up to 2.8 kV. The spectral line profile recording procedure is described in Djeniže et al. (2002a,b). The averaged photomultiplier signal (five shots at the same spectral range) was digitized using an oscilloscope, interfaced to a computer. A sample output, as an example, is shown in Fig. 1.

The electron temperature (T) was determined (from the 1^{st} μs up to the 60^{th} μs) from the ratios of the relative intensities (Saha equation) of Ar III (330.186 and 331.124 nm) and Ar II (329.364 and 330.723 nm) spectral lines with an estimated error of ±8 %, assuming the existence of LTE, according to the criterion in Griem (1974). Also, the electron temperature has been obtained on the basis of the Boltzmann–plot method (from the 20^{th} μs up to the 60^{th} μs) using nine Ar III (330.186; 331.124; 348.055; 335.853; 336.131; 334.476; 333.618; 302.398 and 302.709 nm) relative line intensities within upper energy level interval of 4.42 eV (ΔE_u) with an estimated error of ±14%. All the necessary atomic data were taken from NIST (2003).

The electron density (N) decay was measured using a well–known single laser interferometry technique for the 632.8 nm He–Ne laser wavelength with an estimated error of ±6 % . Recorded interference fringe in argon–helium plasma is presented in Fig. 2. The electron density and electron temperature decay are presented in Fig. 3.

Table 1: Measured Ar III Stark shift (d_m) values at given electron temperatures (T) and densities (N). A negative shift is towards the blue.

Transition	*Multiplet*	λ (nm)	T (10^3 K)	N (10^{23} m^{-3})	d_m (pm)
$3p^3 3d'$ –	$^3F^0 - {}^3F$	248.411	30.15	1.47	-0.7
$3p^3(^2D^0)4p'$	(8uv)	250.891	30.15	1.47	-0.4
	$^3D^0 - {}^3D$	272.484	30.15	1.47	0.0
	(9uv)				
	$^3D^0 - {}^3P$	229.718	30.15	1.47	-2.5
	(10uv)				
$3d^3 3d''$ –	$^3P^0 - {}^3P$	347.129	30.15	1.47	-6.8
$3p^3(^2P^0)4p''$	(6)				

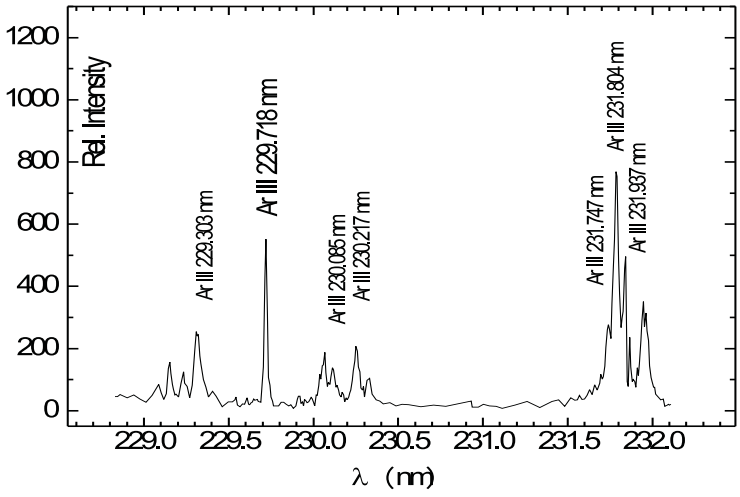

Fig. 1: Part of the recorded spectrum with several investigated Ar III spectral lines at the 20^{th} μs after the beginning of the discharge.

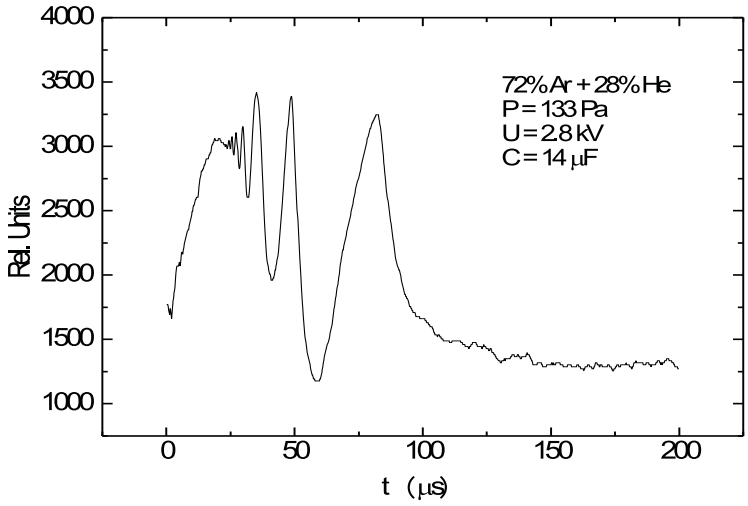

Fig. 2: Recorded interference fringe in argon-helium plasma

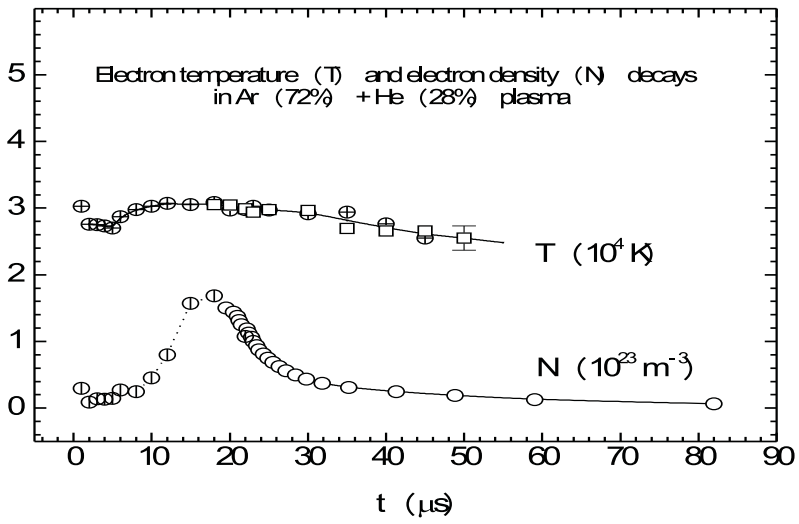

Fig. 3: Temporal evolution of the electron temperature (T) and electron density (N) during the plasma decay. $\bigoplus$, Saha equation; □, Boltzmann–plot.

3. STARK SHIFT MEASUREMENT

The stark shifts were measured relative to the unshifted spectral lines emitted by the same plasma (Srećković et al., 2000; Djeniže et al., 2002b and references therein). The Stark shift of the spectral line can be measured experimentally by evaluating the position of the spectral line center recorded at two electron density values during the plasma decay. In principle, the method requires recording of the spectral line profile at the higher electron density (N_1) that causes an appreciable shift and then, latter, when the electron concentration has dropped to a value (N_2) lower by at least an order of magnitude. The difference of the line center position in these two cases is Δd, so that the shift d_1 at the higher electro density N_1 is

$$d_1 = N_1 \Delta d/(N_2 N_1). \quad (1)$$

Stark shift data are determined with ± 0.8 pm error at a given N and T. Measured (d_m) Stark shifts are presented in Table 1.

4. CONCLUSION

We have obtained d values with negative sign.

Acknowledgments. This work is a part of project Determination of the atomic parameters on the basis of the spectral line profiles supported in part by the Ministry of Science, Technologies and Development of the Republic of Serbia.

References

Djeniže, S., Srećković, A., Bukvić, S.: 2002a, *Eur. Phys. J. D*, **20**, 11.
Djeniže, S, Dimitrijević, M.S, Srećković, A., Bukvić, S.: 2002b, *Astron. Astrophys.*, **396**, 331.
Srećković, A., Drinčić, V., Bukvić, S., Djeniže, S.: 2000, *J. Phys. B. At. Mol. Opt. Phys.*, **33**, 21, 4873.
Srećković, A., Djeniže, S., Bukvić S.: 2002, *Physica Scripta*, **65**, 359.
Griem, H.R.: 1974, *Spectral Line Broadening by Plasmas* ,New York, Academic Press.
NIST: 2003, Atomic Spectra Data Base Lines (Wavelengths ordered) http: //www.physics.nist.gov
Lesage, A., Fuhr, J.R.: 1999, *Bibliography of Atomic Line Shapes and Shifts (April 1992 though June 1999)*, Observatoire de Paris.
Kobilarov, R., Konjević, N.: 1990, *Phys. Rev. A*, **41**, 6023.
Konjević, N., Lesage, A., Fuhr, J.R., Wiese, W.L.: 2002 *J. Phys. Chem. Ref. Data*, Vol. **31**, No. 3, 819.

Publ. Astron. Obs. Belgrade No. 76 (2003), 233-236 *Contributed paper*

THE EFFECT OF CARBON CONCENTRATION ON ROTATIONAL PLASMA TEMPERATURE OF CARBON ARC IN HELIUM

B. TODOROVIĆ-MARKOVIĆ[1], Z. MARKOVIĆ[1], Z. NIKOLIĆ[2], T. NENADOVIĆ[1]

[1] *"Vinča" Institute of Nuclear Sciences, P.O.B. 522, 11001 Belgrade, Yugoslavia*

[2] *Faculty of Physics, University of Belgrade, P.O.B. 368, 11001 Belgrade, Yugoslavia*
E-mail:biljatod@vin.bg.ac.yu

Abstract. In this work, we present the results of a spectroscopic investigation of the emission from C_2 radicals of carbon arc in inert gas-helium. The rotational temperature of C_2 radicals was determined in dependence of electrode-anode- diameter. It was found that the rotational temperature of diatomic carbon molecules decreased when electrode diameter decreased. The pressure dependence on rotational temperature has shown that the rotational temperature of C_2 decreased with the increase of gas pressure.

1. INTRODUCTION

Since the fullerenes were discovered by Kroto and co-workers in 1985, they attracted a lot of interest of researchers because of their excellent properties (Kroto *et al.,* 1985). There are a few methods for fullerene synthesis: they are obtained by burning hydrocarbons, by resistive and rf heating of graphite in atmospheres of inert gases and in the so-called contact-arc (Withers *et al*., 1997). In order to understand the phenomena related to fullerene formation and to increase the fullerene yield, it is essential to study the role of parameters of carbon plasma. Kinetic model of fullerene formation in plasma arc reactor was developed previously (Marković *et al*., 1998). The fullerenes were formed in a hot jet of an inert gas that expanded from the interelectroede space. Based on the kinetic model, it was found that fullerene yield depended on four physical parameters simultaneously: carbon concentration, the velocity of carbon-helium jet from the interelectrode space, axial temperature and temperature gradient between the arc channel and chamber walls (Marković *et al*., 2002).

In this article, the results of spectroscopic measurement of emission molecular spectra of C_2 radicals are presented. We focus our attention on the determination of rotational temperature of C_2 radicals as a function of electrode diameter and the influence of gas pressure on the rotational temperature as well.

2. EXPERIMENTAL

The experimental used in this study was the plasma reactor for fullerene synthesis with minor modifications including two additional quenched glass windows for spectroscopy. All experiments were carried out under helium atmosphere, using electrodes with different diameters (D_{el}=12, 9, 7, 6, 5, 4 mm). The soot produced during the discharge was collected and the fullerene content was measured by the method described before (Marković *et al*., 2002). The gas pressure was in the range of 200-600 mbar. The current intensity had values of 50, 70 and 100 A.

The emission molecular spectra were recorded using the plane grating spectrograph of Ebert design (RSV). The light emitted from the carbon arc gap and the entrance slit of the spectrograph was fixed on 20 cm. The emission spectra of the carbon arc in helium were registered by CCD digital camera (Camedia-Olympus C700 ultra zoom). The spectra of Swan molecular bands of C2 radicals ((0,0) at 516.5 nm) were recorded with resolution of 150000 and reciprocal dispersion of 0.45 nm/mm which is enough to resolve rotational structure of emission spectra. The apparatus function was 0.02 nm. The spectrograph entrance slit was 15 μm. During the experiment, the expansion of carbon vapor from the interelectrode space was monitored on calibrated screen.

3. RESULTS AND DISCUSSION

The carbon vapor was formed in C/He arc plasmas under conditions favoring formation of fullerenes. In the spectra, intensive lines of CI, CII, HeI and Swan bands of C_2 radicals were detected.

The determination of gas temperature in the arc is performed by measurements of the rotational temperature of C_2 radicals. Owing to a small energy separation between the rotational levels of the molecules, the populations of the rotational states correspond more closely to the translational gas temperature in the arc column. Inelastic electron-molecule collisions excite C_2 radicals without altering their angular momentum. Hence the excited states have the same rotational distribution as the ground state. The C_2 ($d^3\Pi_g$) lifetime of the order of 1μs is much longer than the mean time between collisions at the atmospheric pressure which can be evaluated as less than 1 ns. Since rotational equilibrium typically requires ≈10 collisions, rotation-translation equilibrium does prevail for all emitting species.

Typical emission spectrum of C_2 ($d^3\Pi_g \rightarrow a^3\Pi_u$) recorded at the center of arc discharge is presented in Fig. 1. The rotational temperature of C_2 molecules was determined by Boltzman plot method. The obtained values should be considered to be average values over the spatial region. We assumed the plasma is optically thin.

The rotational temperature of C_2 radicals was measured as a function of carbon concentration on and around the arc axis. The carbon concentration was changed in the wide range by varying the electrode-anode-diameter and the gas pressure. In Fig. 2, the rotational temperature of C_2 radicals is presented as a function of electrode diameter. As can be seen from the diagram, the temperature decreases with the decrease of electrode diameter. For electrode diameter of 12 mm (carbon concentration is small), the rotational temperature is in the range of

5500-7000 K. For electrode diameter of 5 mm (carbon concentration is high), the rotational temperature of diatomic carbon molecules is varied from 2500-3000 K.

When the carbon concentration is small (D_{el}=12 mm), the carbon vapor is mainly located between the electrodes. The dominant mechanism for the excitation of C_2 is the collisions among electrons and C_2 radicals. In the case of high carbon concentration (D_{el}=5 mm), carbon vapor was located in the wide region: between and around the electrodes. Then, chemiluminiscent excitation of C_2 is dominant excitation mechanism. Particularly, this effect is very strong in the case of carbon arc discharge under conditions favoring the fullerene formations.

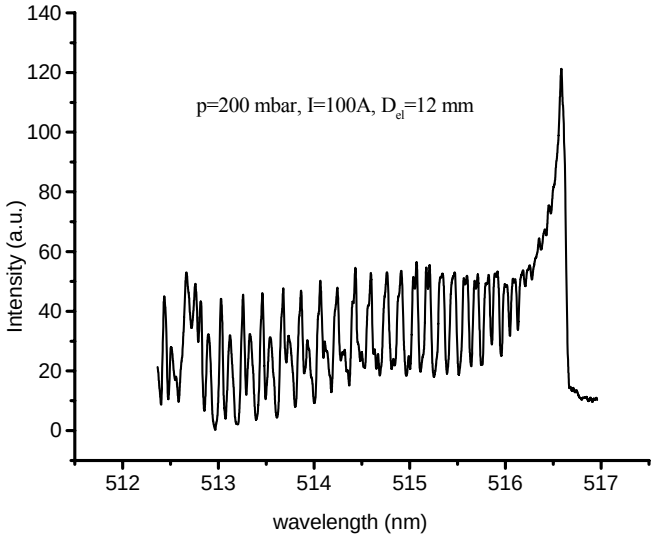

Fig.1: Emission molecular spectrum of C_2 radicals.

By changing the gas pressure (200-600 mbar), the rotational temperature of C_2 decreases with the increase the pressure of buffer gas. It was found that T_{rot}=7000 K was nearly constant when the anode diameter of 12 mm was applied. In the case of anode of 6 mm, significant changes of T_{rot} were detected. Rotational temperature was in the range of 4500-3500 K as the gas pressure increased. By increasing of buffer gas pressure, jet velocity from the interelectrode space decreases (Ramakrishnan *et al*., 1978). Then, the concentration of C_2 increases. Therefore, T_{rot} will decrease.

The obtained values of T_{rot} have different dependence on carbon concentration than vibrational temperature. While T_{rot} decreases with electrode diameter decreases, T_{vib} increases with carbon concentration increases (Marković *et al*., 2003).

It is worth mentioning that the highest yield of fullerene produced under He atmosphere was determined to be about 13 %.

4. CONCLUSION

In this work, the influence of carbon concentration and gas pressure on rotational temperature of C_2 radicals was studied. The rotational temperature was determined from the emission molecular spectra of the 0-0 band of $d^3\Pi_g \rightarrow a^3\Pi_u$ electronic transition of C_2. It was found that the rotational temperature of C_2 decreased as carbon concentration increased.

The difference between the rotational and vibrational temperatures of C_2 radicals indicates that there is no thermal equilibrium between rotational and vibrational population.

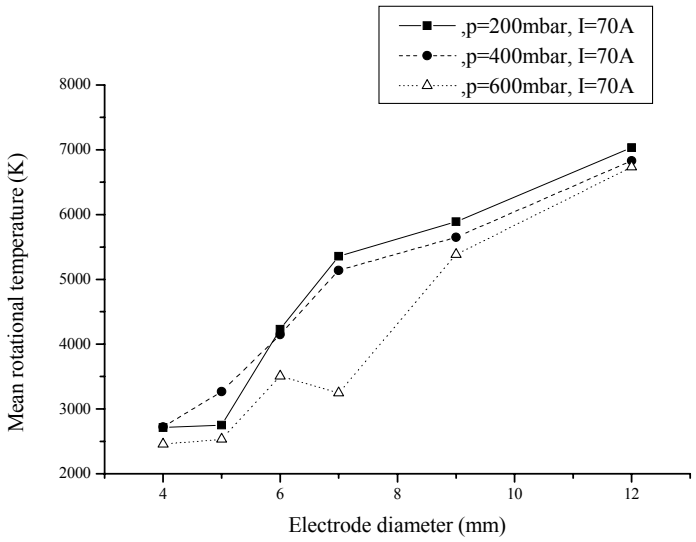

Fig. 2: Rotational temperature of C_2 radicals as a function of electrode diameter.

References

Kroto, H.W., Heath, R., O'Brien, S.C., Curl, R.F., Smalley, R.E.: 1985, *Nature*, **318,** 162.

Withers, J.C., Loutfy, R.O., Lowe ,T.P.: 1997, *Full. Sci.and Technol*., **5**, 1.

Marković, Z., Todorović-Marković, B., Jokić, T., Pavlović, P., Stefanović, P., Blanuša, J., Nenadović, T.: 1998, *Full. Sci. and Technol*. **6**, 1057.

Marković, Z., Todorović-Marković, B., Nenadović, T.: 2002, *Full.Nanotubes and Carbon Nanostructures*., **10,** 81.

Ramakrishan, S., Stokes, A., Lowke, J.: 1978, *J. Phys. D:Appl. Phys*., **11**, 2267.

Marković, Z., Todorović-Marković, B., Marinković, M., Nenadović, T.: 2003, *Carbon*, **41**, 369.